MATHEMATICAL MODELING OF CHAIN BRANCHING REACTIONS IN
OLEFIN COORDINATION POLYMERIZATIONS

Amanda Lemette Teixeira Brandão

Tese de Doutorado apresentada ao Programa de
Pós-graduação em Engenharia Química, COPPE,
da Universidade Federal do Rio de Janeiro, como
parte dos requisitos necessários à obtenção do
título de Doutor em Engenharia Química.

Orientadores: José Carlos Costa da Silva Pinto
André Luis Alberton
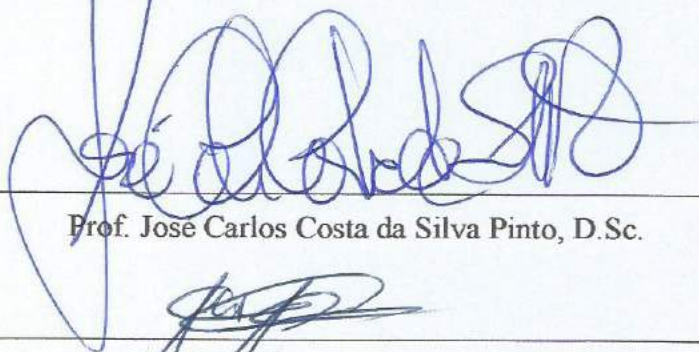João Batista de Paiva Soares

Rio de Janeiro
Fevereiro de 2017

MATHEMATICAL MODELING OF CHAIN BRANCHING REACTIONS IN OLEFIN COORDINATION POLYMERIZATIONS

Amanda Lemette Teixeira Brandão

TESE SUBMETIDA AO CORPO DOCENTE DO INSTITUTO ALBERTO LUIZ COIMBRA DE PÓS-GRADUAÇÃO E PESQUISA DE ENGENHARIA (COPPE) DA UNIVERSIDADE FEDERAL DO RIO DE JANEIRO COMO PARTE DOS REQUISITOS NECESSÁRIOS PARA A OBTENÇÃO DO GRAU DE DOUTOR EM CIÊNCIAS EM ENGENHARIA QUÍMICA.
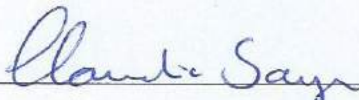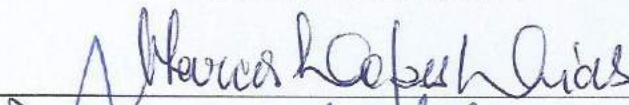
Examinada por:

_____

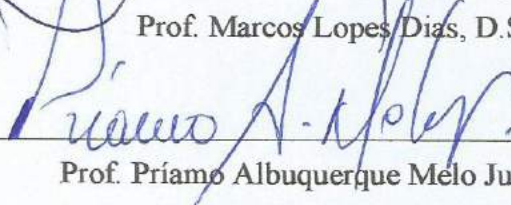Prof. José Carlos Costa da Silva Pinto, D.Sc.

_____

Prof. André Luis Alberton, D.Sc.

_____

Prof. Claudia Sayer, D.Sc.

_____

Prof. Marcos Lopes Dias, D.Sc.

_____

Prof. Príamo Albuquerque Melo Junior, D.Sc.

RIO DE JANEIRO, RJ – BRASIL

FEVEREIRO DE 2017

Agradecimentos

Eu agradeço a Deus por ter me guiado nesta trajetória e me abençoado sempre.

A minha mãe, eu agradeço por todo apoio e compreensão durante toda a minha vida. Obrigada por tudo - essa tese é sua também. Eu te amo muito.

Ao Prof. Luiz Bevilacqua, eu agradeço por ter me apresentado ao PEQ. Obrigada pelo seu exemplo no compromisso com a ciência.

Ao Prof. André Alberton, por no fim de 2011 ter me incentivado a me inscrever para o mestrado na COPPE. Agradeço muito por ter me acompanhado desde então, por ter me orientado no projeto final, no mestrado e agora no doutorado. Muito obrigada por todas as conversas, pelas inúmeras segunda-feiras na UERJ. A sua orientação foi essencial para o meu crescimento acadêmico e pessoal. Serei eternamente grata por ter sido tão presente. Obrigada pelo professor e amigo que se tornou!

Ao Prof. Zé, não tenho nem palavras para descrever o quanto sou grata por você ter aceitado ser meu orientador. Obrigada por me mostrar o mundo dos polímeros, por abrir meus olhos para tanta coisa que antes passava despercebida. Por acreditar em mim, me incentivar sempre, por todas as vezes que me fez rir quando estava tão preocupada, por me atender mesmo depois das 18 horas na COPPE. Obrigada por inspirar tantos alunos. Você, Zé é um exemplo para mim de pessoa, de pai e de professor. Obrigada!

Ao Prof. João Soares, eu agradeço por me fazer me sentir tão em casa mesmo estando em outro país. Por trazer essa cultura do cuidado, do acolhimento tão típicos dos brasileiros em nossas reuniões. Agradeço por ter acreditado em mim e ter me dado grandes oportunidades, como no artigo de Monte Carlo e agora no livro em produção. Muito obrigada pela orientação e amizade.

Agradeço a Bruno, pelas conversas, desabafos, risadas e todo o trabalho duro. Bruninho, obrigada - a sua amizade foi um grande presente que a COPPE me deu.

A Luciana, agradeço pela convivência no Engepol e LMSCP, a nossas conversas e aos planos futuros de trabalho! Que a nossa parceria e amizade dure para sempre!

A Kese Alberton, obrigada pela nossa amizade e por todo apoio que me deu.

MODELAGEM MATEMÁTICA DA CINÉTICA DE RAMIFICAÇÃO EM POLIMERIZAÇÕES DE OLEFINAS POR COORDENAÇÃO

Amanda Lemette Teixeira Brandão

Fevereiro/2017

Orientadores: José Carlos Costa da Silva Pinto
André Luis Alberton
João Batista de Paiva Soares

Programa: Engenharia Química

A frequência de ramos de cadeias longas em polietilenos produzidos por catalisadores de coordenação pode ser aumentada substancialmente por meio da copolimerização de etileno com pequenas quantidades de dienos não conjugados. Neste trabalho, investiga-se a cinética da copolimerização de etileno com 1,9-decadieno, utilizando um catalisador de geometria constrita em um processo em solução e reator semi-batelada, e propõe-se um novo modelo matemático para descrever os resultados das distribuições de massas molares e massas molares médias. O mecanismo proposto inclui a etapa de reincorporação do macromonômero por intermédio das ligações duplas pendentes resultantes da incorporação do dieno. Uma abordagem híbrida, combinando o método de otimização de enxame de partículas, procedimentos de identificabilidade de parâmetros e o método Gauss-Newton, foi aplicada para estimar os parâmetros do modelo. Para a predição das distribuições de massas molares, os métodos de Monte Carlo e colocação ortogonal com completa adaptação foram utilizados. Em particular, mostra-se que os modelos propostos são capazes de descrever dados reais de ramificações obtidos em uma unidade de laboratório, usada para conduzir copolimerizações de etileno e 1,9-decadieno.

Abstract of Thesis presented to COPPE/UFRJ as a partial fulfillment of the requirements for the degree of Doctor of Science (D.Sc.)

MATHEMATICAL MODELING OF CHAIN BRANCHING REACTIONS IN
OLEFIN COORDINATION POLYMERIZATIONS

Amanda Lemette Teixeira Brandão

February/2017

Advisors: José Carlos Costa da Silva Pinto

André Luis Alberton

João Batista de Paiva Soares

Department: Chemical Engineering

The frequency of long chain branching in polyethylenes made with coordination catalysts can be substantially increased by copolymerizing ethylene with small amounts of non-conjugated dienes. In this work, the kinetics of copolymerization of ethylene and 1,9-decadiene is investigated, using a constrained geometry catalyst in a solution polymerization semi-batch reactor. A novel mathematical model is also proposed to describe the resulting molecular weight distributions and average molecular weights. The proposed mechanism includes macromonomer reincorporation through pendant double bonds that result from the diene incorporation. A hybrid approach, combining Particle Swarm Optimization, parameter identifiability procedures and the Gauss-Newton method, was applied to estimate the model parameters. For MWD predictions, the Monte Carlo and complete adaptive orthogonal collocation methods were used. It is shown that the proposed model can accurately describe actual ethylene/ 1,9-decadiene copolymerization data collected in a lab-scale polymerization unit.

Contents

List of Figures

List of Tables

1 Introduction

The development of a modern society is unthinkable without polymer technologies. Regarding the relationship between the materials and the level of humanity development, some authors allude to the ages of the stone (ceramics), the bronze and iron (metals) and nowadays the age of polymers (KARAK, 2009). In fact, polymer formulations can lead to countless different materials and properties, which can be developed and applied to almost all human activities. Detailed overviews of the historical development of polymers can be found in different published materials (GNANOU and FONTANILLE, 2008, POLYMEREXPERT, 2002).

Polymers can be obtained from natural sources (such as cellulose, natural rubber and polysaccharides) or produced artificially (or through synthetic chemical routes); be organic or inorganic nature; and usually consist of a mixture of macromolecules, which results from chemical combination of a large number of much smaller molecules. These smaller molecules are known as *monomers* and reactions that promote the combination of the monomers are called *polymerizations*. One macromolecule can contain hundreds, thousands or even more monomer molecules that are kept together by covalent bonds (ODIAN, 2004). In the polymer backbone, the building unit formed from the monomer reaction is known as *mer*.

Nowadays, one of the most important classes of polymers comprises α-olefin based polymers. α-Olefins are molecules that contain a vinyl group at the extremity, i.e., the double bound is positioned at the primary position α, as illustrated in Figure 1.1. Among the many α-olefin based polymers, polyethylene (PE) and polypropylene (PP) must be highlighted, since these two polyolefins concentrate almost two-thirds of the world thermoplastic market (LIU et al., 2016). It is expected the annual growth rate of 4.3 % for PE, with global demand rising from 88.1 million m. t. / year[1] in 2015 to 108.8 million m.t./ year in 2020. PP represented 26 % of the global consumption of polymers in 2015 (CHEMWEEK, 2016).

---

[1] m. t. / year means metric ton per year. A metric ton is a unit of mass equal to 1000 kilograms (2205
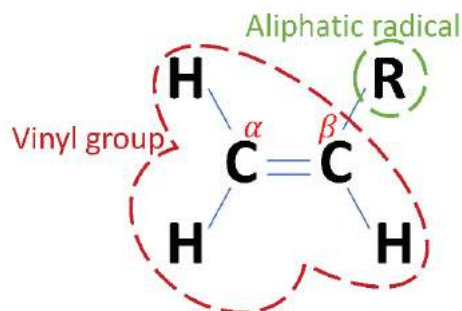
Figure 1.1 – Illustration of an α-olefin (a vinyl terminated chain).

An important advantage of polyolefins is the fact that these materials can be recycled easily due to their intrinsic thermoplastic properties (MARQUES et al., 1998). This is one of the reasons why polyolefins have replaced many other materials and become the most important polymer commodity.

The starting point for the commercial use of polyolefins took place in 1937, with the registration of the patent entitled *High Pressure – Low Density Polyethylene* (HP-LDPE) by ICI (Imperial Chemical Industries). However, the polymerization process used for production of this polyolefin through free-radical mechanism at high pressures and temperatures had already been discovered in 1933 by E. W. Fawcett and R. O. Gibson in the ICI laboratories (KRESSER, 1969).

Nevertheless, the most important advances in the polyolefin field were made with the advent of Ziegler-Natta (ZN) catalysts in the early 1950s. The use of Ziegler-Natta catalysts made possible the synthesis of stereospecific polymers at high rates; depending on the catalyst type and experimental conditions, isotactic and/or syndiotactic PP polymers could be produced (SOARES and MCKENNA, 2013). With the advent of metallocenes, new products with enhanced properties started challenging existing ZN based polymer markets. Metallocenes usually present higher activity when compared with ZN catalysts. Besides, polyolefins formed from metallocene based catalysts present more uniform molecular properties, narrower molecular weight distributions (MWD) and more uniform comonomer compositions (CHUM and SWOGGER, 2008).

The formation of chain branches was one of the key points for advance of the α-olefins polymerization technology. In the early 90s, Dow Company introduced the Constrained-Geometry Catalyst (CGC), leading to improvement of the physical

2

properties of polyolefins, also avoiding the falloff in processability, which occurs when the MWD is narrowed and the lower-molecular weight "tails" are not formed (CHUM and SWOGGER, 2008). This was possible because of the formation of long-chain branches (LCB) in the polymer chains, since CGC can incorporate α-olefins of high molecular weights and unsaturated macromolecules into the polymer chains. For example, during ethylene polymerization, α-olefins terminated chains, as illustrated previously in Figure 1.1, can be formed by transfer to ethylene or spontaneous transfer (SOARES, 2004). Such α-olefin chains are indeed macromonomers and can be incorporated into a living growing chain by the CGC, generating a long-chain. In most cases, the excessive formation of branches is undesirable, but the low frequency long-chain branching can partially compensates the absence of low-molecular-weight chains normally present in conventional ZN based polyolefins, increasing shear thinning, enhancing processability, improving melt elasticity of the material and, consequently, leading to desirable mechanical, adhesive and viscosity properties (KOLODKA et al., 2002; CHUM and SWOGGER, 2008; YANG et al., 2010). Furthermore, these polymers still present narrow molecular weight distributions and uniform comonomer composition distributions, as in resins manufactured with regular metallocenes. Figure 1.2 illustrates a branched polyolefin chain.
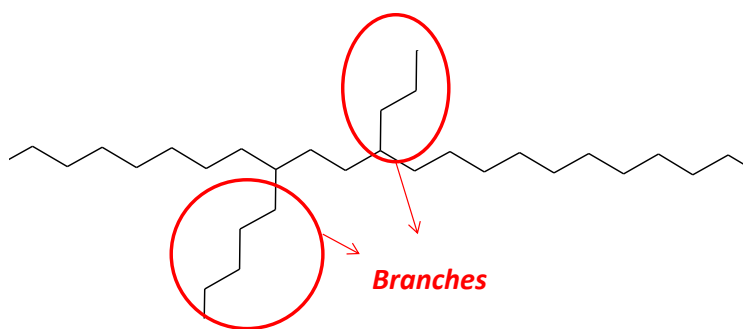
Figure 1.2 – Illustration of long-chain branches.

Despite the successful synthesis of branched polyolefins with CGCs, the fraction of LCBs in these polymers is usually low. It is hard to increase the LCB frequency in these polymers because each macromonomer contains a single branching point, which substantially reduces the probability of LCB formation in high molecular weight polymers. For this reason, the use of two distinct metallocene catalysts and the copolymerization of α-olefin and non-conjugated dienes with CGC are strategies devised to increase the LCB frequency in polyolefins under mild polymerization

conditions (WANG et al., 1998; BEIGZADEH et al., 2001; SIMON and SOARES, 2002; SERNETZ et al., 1997; UOZUMI et al., 2000; NAGA and TOYOTA, 2004).

The low LCB frequency of polyolefins made with CGC catalysts makes LCB quantification challenging. As a consequence, mathematical models that can predict the frequency and topology of LCBs in these materials are desirable. One possible approach is to build kinetic models that include steps for formation of LCBs, so that the final molecular architecture of the polymer chains can be obtained after simulations performed with the model.

In the polymerization field, one can usually classify the proposed kinetic models as hybrid empirical-phenomenological models, since they combine phenomenological aspects, like proposed mechanisms, with many empirical propositions and assumptions. As pointed out by other authors (PINTO et al., 2011; ALBERTON, 2010), most kinetic models rely on assumptions that are often weak when compared to reality; as a consequence, models are frequently oversimplified and empirical corrections must be proposed, conferring an empirical nature to the models.

Kinetic polymerization models can vary significantly in complexity and numerical difficulty. Generally, as the output information increases, more complex and hard to solve the models become, requiring additional efforts for model implementation and numerical solution. Besides, almost always some of the needed model parameters are unknown, which imposes the estimation of model parameters. The parameter estimation problem consists of an optimization method that leads to the most appropriate values for the unknown parameters, based on available reference experimental data. However, during the execution of this optimization process, the proposed mathematical model has to be simulated many times. Thus, the selection of the numerical method to solve the optimization problem depends on the simulation time required to solve the mathematical model. As a consequence, there is not an ideal numerical technique for the numerical solution of the model or the estimation of model parameters, as all the existing methods present advantages and drawbacks. It is up to the researcher to find the most appropriate method to be used in his/her particular work.

Two methods have been often applied to solve polymerization models: Monte Carlo and Orthogonal Collocation (BRANDÃO et al., 2015; PINTO and BISCAIA, 1996). This explains why these methods are explored and analyzed in the present work. In short, Monte Carlo methods describe the kinetics of polymerization as a series of

random events (SOARES and HAMIELEC, 1997), while orthogonal collocation techniques (PINTO and BISCAIA, 1996) assume that distributions can be approximated by polynomial fits.

Based on the previous comments, some questions that naturally arise are:

- In polymerization models with LCB generation, which apparent mechanisms seem to rule the reaction and which corresponding model can fit experimental data suitably?
- Regarding the distinct numerical approaches, what are their comparative performances? What are their relative advantages and disadvantages?

In order to answer these questions, the main objectives of the present PhD thesis can be summarized as follow:

- To investigate kinetic models for copolymerizations of ethylene and 1,9-decadiene using CGC-Ti catalyst, implementing and solving the mathematical models that derive from the proposed mechanisms;
- To perform the comparative evaluation of actual implementations of the Monte Carlo Method and of the Orthogonal Collocation Method for simulating the proposed models.

Some specific objectives that are pursued are:

- To perform experimental ethylene homopolymerization studies using the CGC-Ti catalyst;
- To perform experimental copolymerization studies of ethylene and 1,9-decadiene using the CGC-Ti catalyst;
- To propose kinetic mechanisms to describe the homo- and copolymerization of ethylene with a diene;
- To develop mathematical models to describe the solution homo- and copolymerization of ethylene with a diene in a semi-batch reactor;
- To estimate the homo- and copolymerization model parameters;
- To investigate and describe the relative advantages and disadvantages of the proposed stochastic and deterministic approaches used in the thesis, providing details to guide readers in implementation of other polymerization engineering problems.

1.1 Thesis Outline

The present PhD thesis consists of 11 chapters and is organized as follows:

- Chapter 1 presents the introduction, research goals and thesis outline.

- Chapter 2 contains a literature review on coordination polymerization. A brief review about the evolution of Ziegler-Natta catalysts is introduced and research works that use CGC catalysts are also presented.

- Chapter 3 presents a literature review on the deterministic methods applied in the present thesis. Detailed descriptions of the numerical procedures are also performed, with emphasis on reviewing deterministic methods applied to coordination polymerization problems with LCB formation.

- Chapter 4 introduces the Monte Carlo technique and presents some works that applied this approach to simulate coordination polymerizations. Different Monte Carlo methods are described and algorithms are also described and presented.

- Chapter 5 describes the adopted experimental procedure, including polymerization methods, apparatuses and polymer characterization techniques. The numerical methods employed in the present thesis are also outlined in this chapter.

- Chapter 6 shows the statistical procedures applied in the present thesis to estimate the parameters and evaluate the model predictions.

- Chapter 7 reports a brief literature review on the kinetics of ethylene copolymerization with non-conjugated dienes, considering the occurrence of LCBs. The complete development of the mathematical model is presented, including the proposed kinetic mechanism, the material balances, the parameter estimation procedure, the calculation of average properties and the computation of molecular weight distributions.

- Chapter 8 provides results for the estimation of model parameters and characterizes the predicted average molecular weights, long-chain branching frequencies and ethylene feed flow rates.

- Chapter 9 discusses in detail the model predictions for molecular weight distributions. Particularly, the experimental MWDs are compared with the simulated ones.

- Chapter 10 compares the predictions and efficiency of different implementations of Monte Carlo methods through 5 case studies that involve coordination polymerization.

- Chapter 11 summarizes the significant findings of the present research and presents recommendations for future works.

- Appendix A shows the material balances for all chemical species present in the polymerization mechanism used as example in Chapter 3. Additionally, Appendix A presents the flowcharts that describe how the polynomial roots were calculated in the orthogonal collocation procedure and how quadrature weights were computed.

- Appendix B describes of the experimental apparatuses used to perform the experiments.

- Appendix C shows the derivation of the objective function used in the parameter estimation process.

- Appendix D presents some convergence analyses performed during implementation of the complete adaptive orthogonal collocation methods, for all used experimental conditions.

The present PhD thesis was developed in EngePol (Laboratório de Engenharia de Polímeros) of PEQ (Programa de Engenharia Química) of COPPE (Instituto Alberto Luiz Coimbra de Pós-Graduação e Pesquisa de Engenharia) of UFRJ (Universidade Federal do Rio de Janeiro), in collaboration with GAME (Group of Applied Macromolecular Engineering) of UA (University of Alberta).

PART I- Literature Review

2 Polyolefins with LCB: catalysts and properties

First, it is convenient to describe some of the main structural polymer properties and how the catalyst types and operation conditions influence these properties.

2.1 Background of Structural Properties

The main structural properties described in the present text are those associated to distribution of chain sizes in polymers and tacticity.

2.1.1 Properties Associated with Molecular Weight Distributions (MWD)

The most relevant structural properties of polymer chains are associated with molecular weight distributions (MWD), which also define the number average molecular weight, the weight average molecular weight and the polydispersity index (PI).

Let us consider the distribution of sizes $P(i)$, where $P(i)$ is the number of chains of size i. If normalized, $P(i)$ can be understood as the probability of randomly selecting a chain of size i from the mixture of polymer chains. Then, $P(i)$ can be understood as a statistical distribution. One way to characterize this distribution is based on its moments. Each moment μ_n of order n of the distribution can be defined as:

$$\mu_n = \sum_i^\infty i^n \cdot P(i) \tag{2.1}$$

According with this definition, the zeroth, first and second moments of the distribution become:

$$\mu_0 = \sum_i^\infty i^0 \cdot P(i) = \sum_i^\infty P(i) \tag{2.2}$$

$$\mu_1 = \sum_i^\infty i \cdot P(i) \tag{2.3}$$

$$\mu_2 = \sum_i^\infty i^2 \cdot P(i) \tag{2.4}$$

If $P(i)$ is normalized, the moment μ_0 is equal to 1, since the sum of all probabilities must be equal to 1.

Now, one important question arises: what is the mean size of the chains in the distribution? The answer depends on the relative importance given to each size. For example, if one choses to weight the size in accordance with the number of chains of that size, then the mean (the number-average chain length $\bar{i}_n$) corresponds to:

$$\underbrace{\bar{i}_n}_{\substack{number-average\ chain\ length}} \cdot \underbrace{\sum_i^\infty P(i)}_{\substack{total\ number \\ of\ chains}} = \sum_i^\infty \left[i \cdot \underbrace{P(i)}_{\substack{number\ of \\ chains\ with \\ size\ i}} \right]$$

$$\bar{i}_n = \frac{\sum_i^\infty i \cdot P(i)}{\sum_i^\infty P(i)} = \frac{\mu_1}{\mu_0} \tag{2.5}$$

Otherwise, if one choses to weight the sizes in accordance with the mass concentrated in each size (the weight (mass) average chain length $\bar{i}_w$), one obtains:

$$\underbrace{\bar{i}_w}_{\substack{weight-average\ chain\ length}} \cdot \underbrace{\sum_i^\infty i \cdot P(i)}_{\substack{total\ weight \\ of\ chains}} = \sum_i^\infty i \cdot \underbrace{i \cdot P(i)}_{\substack{mass\ of \\ chains\ with \\ size\ i}}$$

$$\bar{i}_w = \frac{\sum_i^\infty i^2 \cdot P(i)}{\sum_i^\infty i \cdot P(i)} = \frac{\mu_2}{\mu_1} \tag{2.6}$$

In polymer science, M_n and M_w are defined as the number and weight average molecular weights, respectively. The molar mass of one specie is the mass of its molecule. If one admits that $\bar{i}_n$ or $\bar{i}_w$ are representative means of the whole distribution, then, the average molecular weights can be calculated as:

$$M_n = \bar{\iota}_n \, MM = \frac{\mu_1}{\mu_0} MM \tag{2.7}$$

$$M_w = \bar{\iota}_w \, MM = \frac{\mu_2}{\mu_1} MM \tag{2.8}$$

where MM is the average molecular weight of the structural units (mers). In most chain polymerizations, the average molecular weight of the structural mer is the molecular weight of the monomer. Figure 2.1 illustrates the distribution and the mean size values.
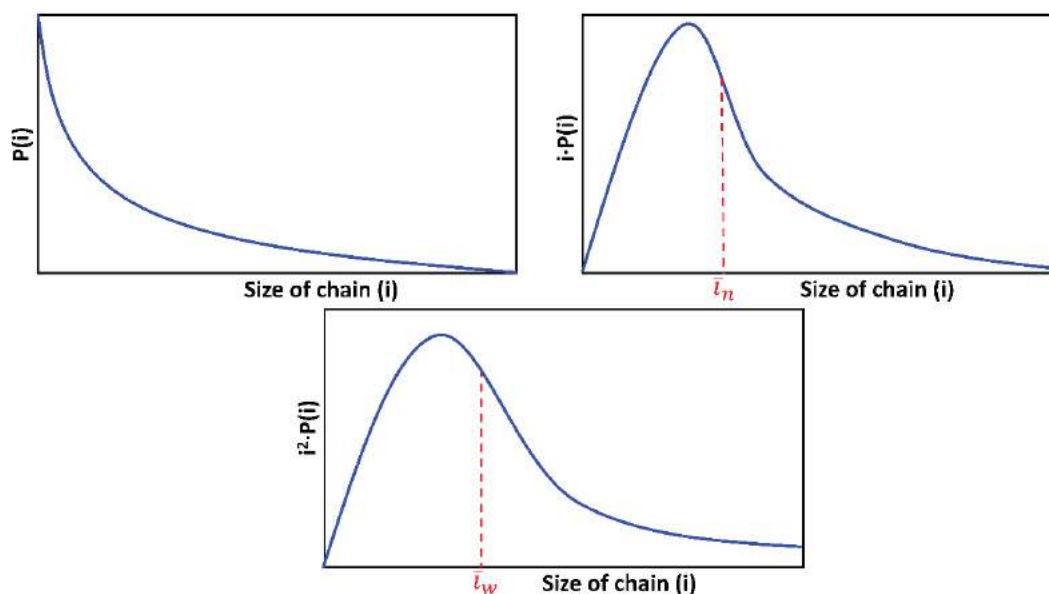
Figure 2.1 – Distributions and mean size values.

Since PI is defined as the ratio μ_2/μ_1, it can also be written as:

$$PI = \frac{\mu_2}{\mu_1} = \frac{M_w}{M_n} \tag{2.9}$$

It must be clear that PI is always greater than 1, being equal to 1 only when the distribution is concentrated in one singular chain size, characterizing a perfectly monodisperse polymer material. As PI increases, the chain size distribution becomes broader. So, the pairs (M_n, M_w) or (M_n, PI) or (M_w, PI) are often used to indicate polymer properties. However, they only provide information about the first moments (zeroth, first and second) and, consequently, they do not provide information about the full distribution.

The control of molecular weight and molecular weight distribution is usually performed to obtain and improve certain desired physical properties of the final polymer material. It is often desirable and necessary to characterize the full distribution of molecular weights, since there usually is a range of molecular weights for which a given polymer property is appropriate for a certain application (ODIAN, 2004).

There are many different PE commercial grades, including low molecular weight (MW) resins ($MW \approx 10^3 \ g \cdot mol^{-1}$), used as hot melt adhesives, and ultra-high MW PE ($MW \approx 10^6 \ g \cdot mol^{-1}$) applied where high draw ratio (gel-spinning) or high wear and fatigue resistance (hip prostheses) are required. Bimodal and multimodal MWD products, with exclusive mechanical and processing properties, can be applied for production of PE pipes of large diameter (SWALLOWE, 1999).

Analyzing the effects of MW and MWD on resin properties constitutes a long standing problem in the polymer field. Although the importance of MW and MWD on mechanical performance has been widely recognized, it has always been difficult to obtain quantitative correlations among these parameters. Additionally to MW and MWD, mechanical properties are also controlled by a large number of additional structural and external factors, such as chain orientation, crystalline structure and chain morphology. Only if these factors are held constant or kept within allowed ranges, it becomes possible to analyze the specific effects of MW and MWD on the mechanical performance of analyzed polymer samples (SWALLOWE, 1999).

2.1.2 Tacticity

One of the most important properties of α-olefin based resins is the tacticity. The different stereoisomerisms ("tacticity") are illustrated in Figure 2.2. In the macromolecular structure (-CH₂-CHX-), where X is different from hydrogen, the spatial position of X defines the tacticity and the material can be isotactic, syndiotactic or atactic (BRAUN et al., 2012). Obviously, this discussion does not make sense for polyethylene, since X=H for this polymer.

Polymerizations that yield tactic structures (isotactic or syndiotactic) are classified as stereoselective polymerizations. Stereoselective polymerizations that yield isotactic and syndiotactic polymers are named isoselective and syndioselective polymerizations, respectively (ODIAN, 2004).

Chain tacticity is the main factor that affects the crystallizability of polymers (SOARES and ANANTAWARASKUL, 2005). Isotactic polypropylene is a crystalline thermoplastic product with a melting point close to 188 °C, whereas atactic PP is an amorphous gummy material (MADJOUR and MARK, 1998). Isotactic PP is often used in several injection molding and extrusion processes due to its excellent rigidity and temperature resistance. Due to its irregular structure, atactic PP has low crystallinity, resulting in a sticky, amorphous material used mainly for adhesives and roofing tars (MAIER and CALAFUT, 2008), it has little commercial value (HAMIELEC and SOARES, 1996). Syndiotactic PP with a crystallinity of 30 % has a melting point of 130 °C (MAIER and CALAFUT, 2008) and it is less stiff than isotactic PP but has better impact strength and clarity. Syndiotactic PP possesses excellent properties to be applied as insulator in power cables (YOSHINO et al., 2003).
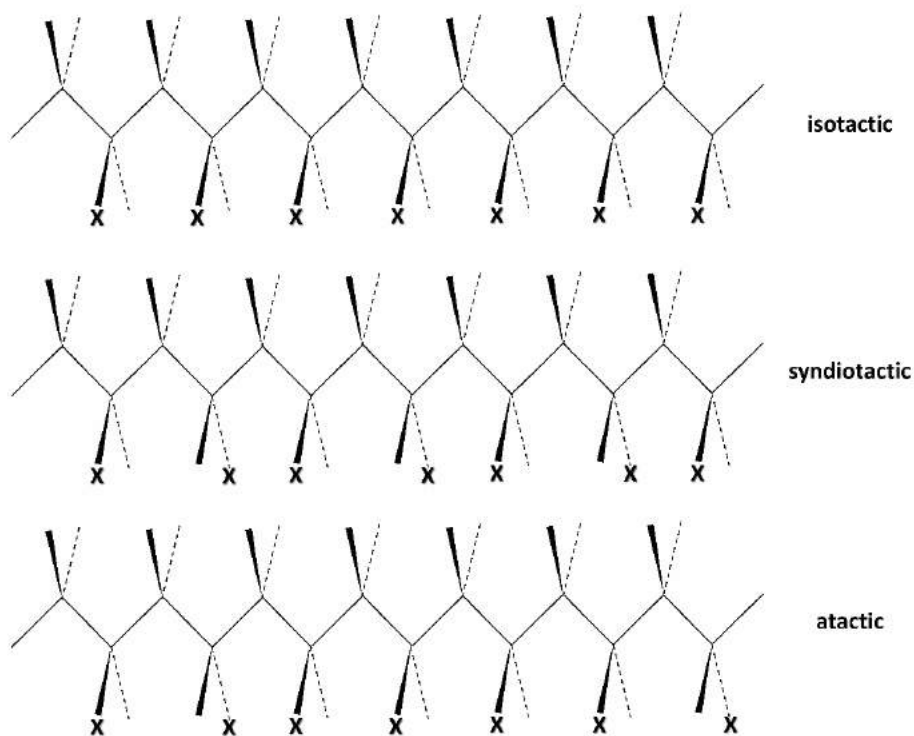
Figure 2.2 – Tacticity of substituted vinyl polymers (Natta Projection) (adapted from BRAUN et al., 2012).

The differences among the distinct forms of PP, assuming similar MWD and branching frequencies, are outstanding, as one can see in Table 2.1 (SINN and KAMINSKY, 1980).

Table 2.1 – Some characteristics of polypropylene

Characteristic	Isotactic PP	Syndiotactic PP	Atactic PP
Melting point (°C)	165 – 171	125 – 131	< 0
Crystallinity (%)	55 – 65	50 – 75	0
Tensile strength (kP cm^{-3})	320 – 350		

Besides the three classic PP configurations, new structures can also be synthesized with different catalysts such as the ones shown in Figure 2.3. Particularly, isotactic-atactic stereoblock PP presents interesting thermoplastic elastomeric properties. This PP can be synthesized using a metallocene catalyst that is able to isomerize between achiral and chiral coordination geometries (MADJOUR and MARK, 1998).
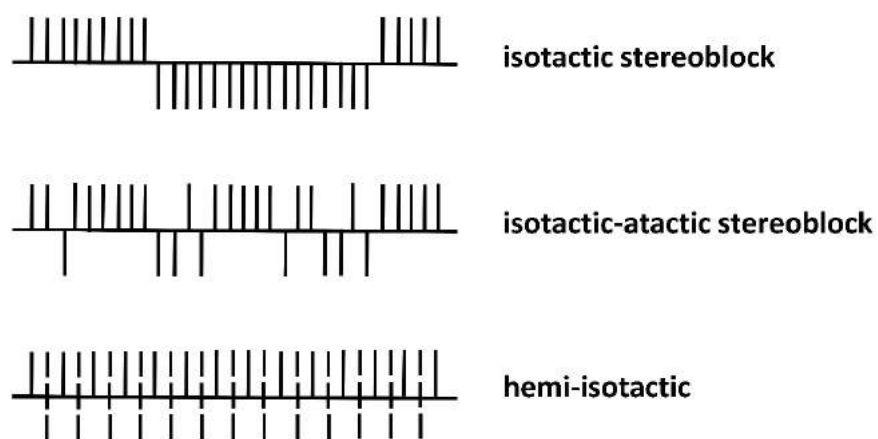
Figure 2.3 – Some types of PP chain configurations produced with metallocene catalysts (adapted from SOARES and HAMIELEC, 2012).

2.1.3 Long-Chain Branching

The rheology, processability and mechanical properties of a polymer are affected by the branching structure, which can be roughly divided into two groups: short-chain branched (SCB) and long-chain branched (LCB) polymers. What differentiates LCB from SCB is the branch length or branch molecular weight. LCB corresponds to a branch molecular weight above the critical molecular weight M_c of the respective polymer, which is an indicator of entanglement. One way to measure M_c is through the molecular weight dependence on the zero-shear viscosity (CHO et al., 2004). Other way to identify a branch as long is through the entanglement molar mass M_e. The usual

concept is that M_c is approximately twice as large as M_e (CHO et al., 2004). Branches can be considered long-chain branches if their length exceeds the entanglement molar mass. For PE, M_e is approximately 1300 g mol^{-1}. Branches below M_e are SCB and do not influence most rheological properties very significantly, although can affect other important properties, such as flexibility and transparency (STADLER et al., 2006).

SCB significantly affects the formation of the crystal structure and mechanical and thermal properties of the polymer, whereas LCBs exert a significant effect on the melt rheological behavior of the melt. Even very small quantities of LCB can affect the polymer processing properties considerably (KOKKO, 2002), improving melt strength and melt processability of narrow PI polymers (ODIAN, 2004), which make these polymers very attractive commercially. Additionally, LCB governs die swell, environmental stress crack resistance in blow molding operations, bubble stability and lamellae orientation in films, and sag resistance in pipe and geomembranes (YANG et al., 2010).

CARELLA et al. (1986) observed considerably enhanced zero-shear viscosities in LCB resins when compared to linear polymers with similar molecular weights, in star-branched hydrogenated polybutadienes (HPBs). LAI et al. (1993a) produced PE with long-chain branching densities (LCBD) in the range 0.01 – 3 carbons/ 1000 carbons. These LCBD PEs were compared to their Ziegler-Natta counterparts. The authors observed that at narrow PIs, the shear tinning of PE could be increased by adding more LCB. CHUM et al. (2000) also concluded that increasing LCB content would lead to the increase of shear thinning.

As one can see, the presence of LCBs in polymer chains is very desirable, so that controlling the LCB formation constitutes a major objective of commercial catalyst research. However, in order to achieve this purpose, it is first necessary to understand how the formation of LCBs occurs.

2.1.3.1 *Kinetic Mechanisms of LCB Formation*

Many researches attempted to demonstrate how LCBs are formed by proposing feasible kinetic mechanisms. The mechanism most widely accepted in literature is terminal branching. In the presence of the adequate catalyst and reaction conditions, polymer chains with terminal vinyl unsaturations, called macromonomers, can polymerize, generating LCBs (WOO et al., 1997; BEIGZADEH et al., 1999 & 2001;

COSTEUX et al., 2002; SOARES, 2001, 2002 & 2004; NELE and SOARES, 2002; NELE et al., 2003; SIMON and SOARES, 2005; YANG et al., 2010). The macromonomers are formed through β-hydride elimination or transfer to ethylene (SOARES et al., 2001). Figure 2.4 illustrates this mechanism for homopolymerization of ethylene with a Ti-catalyst. Macromonomer reincorporation can only be expected when the employed catalyst has high activity to polymerize long α-olefin monomers.

FERREIRA JR. et al. (2010) extended the macromonomer concept to macromolecules that present terminal vinyl unsaturations and pendant double bonds. Thus, the generation of LCBs is possible by macromonomer reincorporation through its terminal unsaturation, generating one LCB, or by one of its pendant unsaturations, producing two LCBs, as shown in Equations (2.10) to (2.12). BRANDAO et al. (2016) also used this approach to justify the formation of LCBs in copolymers made of ethylene and 1,9-decadiene using a coordination catalyst.

$$P_{i,b} + D_{j,c}^{=} \longrightarrow P_{i+j,b+c+1} \tag{2.10}$$

$$P_{i,b} + D_{j,c}^{=} \longrightarrow P_{i+j,b+c+2} \tag{2.11}$$

$$P_{i,b} + D_{j,c} \longrightarrow P_{i+j,b+c+2} \tag{2.12}$$

where $P_{i,b}$ is a living chain with size i and b LCBs; $D_{j,c}^{=}$ is a dead chain with terminal vinyl unsaturation of chain length j and with c LCBs; and $D_{j,c}$ is a dead chain that only contains pendant unsaturations, with size d and c LCBs.
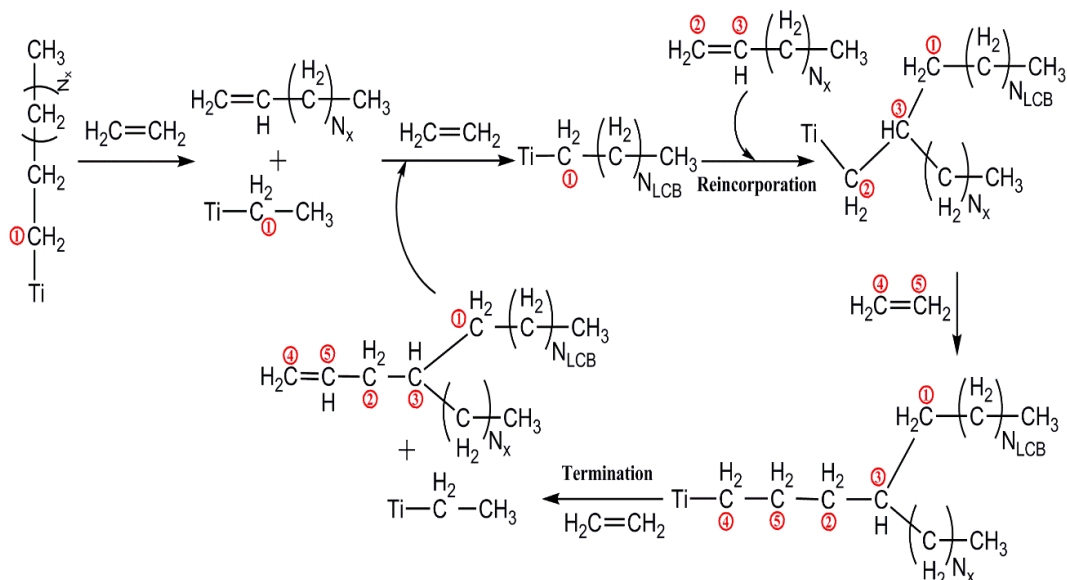
Figure 2.4 – Terminal branching mechanism (adapted from WOO et al., 1997).

YANG et al. (2010) proposed a new mechanism of LCB formation. The authors described their new mechanism as the intramolecular incorporation of macromonomer, as shown in Figure 2.5. According with this mechanism, initially the growing chain is coordinated with an active catalyst site. When the chain stops growing, it remains coordinated with the same site, even when a new chain starts growing in this active site. The macromonomer starts growing again when it gets covalently connected to the growing chain, generating one LCB.
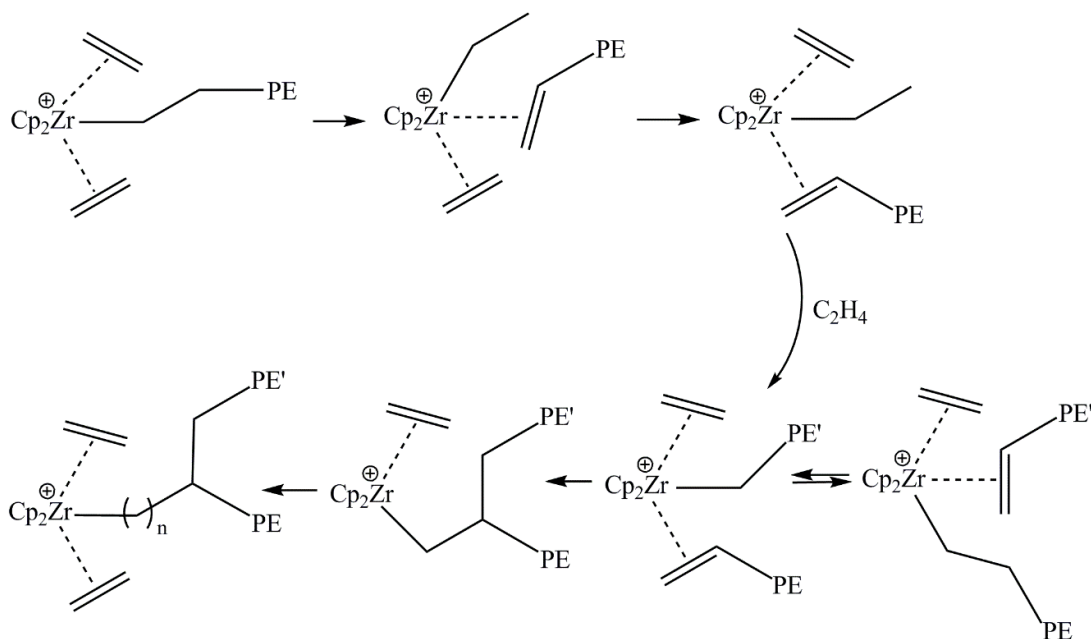
Figure 2.5 – Intramolecular incorporation of macromonomer (adapted from YANG et al., 2010).

17

According with YANG et al. (2010), the conventional mechanism (terminal branching) cannot explain some experimental results, such as the constant LCB frequencies with the increase of temperature for all tested metallocenes. According with the conventional mechanism, it might be expected that the decrease of the polymer molecular weight would elevate the concentration of vinyl terminal groups. Additionally, the vinyl groups would present higher mobility in the amorphous polymer regions, which would elevate LCB frequencies. However, the authors did not observe these effects experimentally. On the other hand, the intramolecular incorporation of macromonomer mechanism seems to be more adequate to explain LCB formation in polymerization processes conducted in the gas phase and in slurry, where the macromonomer is entangled in the polymer matrix (in solution polymerizations, the polymer chains certainly present higher mobility).

2.2 Catalysts for Polyolefins Formation

The main commercial processes for production of polyolefins are based on coordination polymerizations (HAMIELEC and SOARES, 1996). The term Coordination polymerization is related to the monomer addition step, when a *coordination complex*[2] is formed around the catalyst active center (KURAN, 2001).

For simple olefins, the formation of the coordination complex can be explained according to the Dewar-Chatt-Duncadson model, which proposes that the olefin π-bonded filled orbital donates its electrons to an empty *d*-orbital of the metal, with reciprocal backdonation of π-backbonding into an empty π^* orbital on the ethylene molecule (KURAN, 2001, TOREKI, 2015), as illustrated in Figure 2.6. Then, a covalent coordination complex is formed.

---

[2] A *coordination complex* is a complex where atoms are bounded to a center atom by "coordinate covalent bounds".
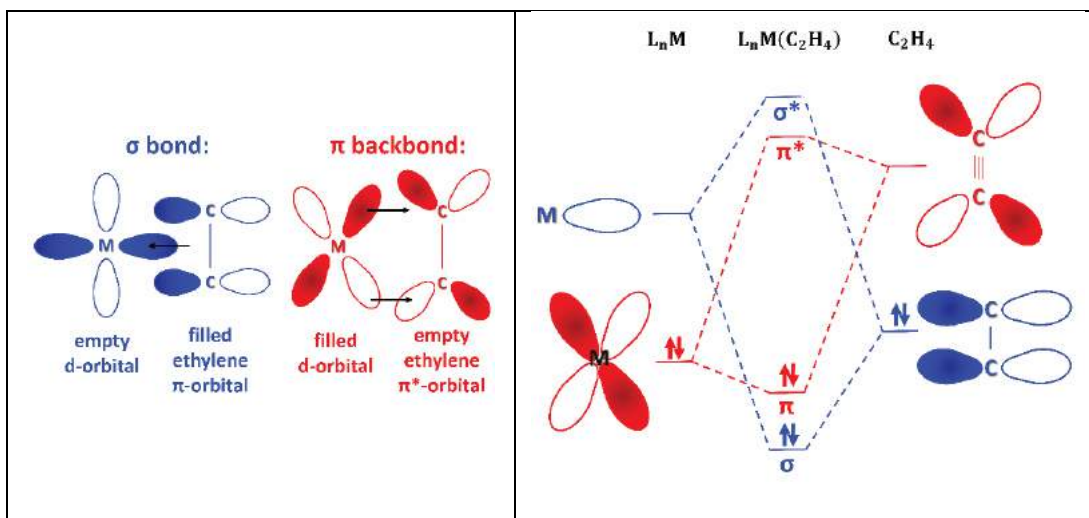
Figure 2.6 – Chemical bonds in metal-ethylene, according to the Dewar-Chatt-Duncanson model (adapted from TOREKI, 2015).

The important commercial catalysts used to perform coordination polymerization are organometallics, such as the Phillips and Ziegler-Natta catalysts. With these catalysts, a wide window was opened to perform stereoselective polymerizations. Depending on the catalyst and experimental conditions, innumerable types of polymers can be produced with these catalysts. Coordination polymerization processes and catalysts are described in details in the next sections.

2.3 Phillips Catalysts

Coordination processes for polyolefins production started with the discovery of the Phillips catalysts in the early 1950s by J. P. Hogan and R. L. Banks from "Phillips Petroleum Co". They discovered that ethylene could be converted, when submitted to relatively low pressures and with the use of chromium oxide supported on silica, into a solid polymer called HDPE (high density polyethylene) (WANG et al., 1991). The application of this catalyst was extended to copolymerizations of ethylene with α-olefins $C_4 - C_8$ afterwards, generating new grades of branched polymers known as LLDPE (linear low-density polyethylene).

HDPE presents few or none short-chain branches and does not present any long-chain branches. This type of polymer is often employed in structural applications due to its characteristic high rigidity. The crystallinity of the HDPE falls in the range of 70 to 90 %, with densities ranging from 0.94 to 0.96 g cm^{-3} (ODIAN, 2004).

19

The copolymerization of ethylene with α-olefins (generally 1-butene, 1-hexene or 1-octene) disturbs the order of linear polyethylene chains through the insertion of comonomer units and, consequently, of SCBs. As a consequence, the density, rigidity and crystallinity of LLDPE are lower than those of HDPE (HAMIELEC and SOARES, 1996). Figure 2.7 illustrates typical HDPE and LLDPE molecular structures.
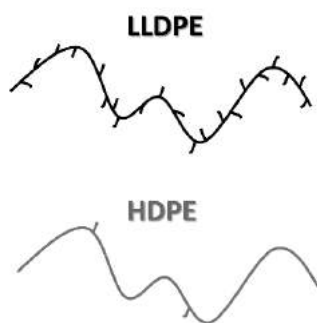
Figure 2.7 – Schematic representation of HDPE and LLDPE molecular structures.

Phillips catalysts achieved great commercial success because of the diversity of uses and products: more than 40 different types of HDPE or LLDPE could be produced with Phillips catalysts (WECKHUYSEN and SCHOONHEYDT, 1999). As a matter of fact, Phillips catalysts are used to manufacture one-quarter to one-third of all HDPE and LLDPE produced worldwide, but is not useful for homopolymerization of propene and other α-olefins, and does not yield stereoselective polymerization (ODIAN, 2004).

2.4 Ziegler-Natta Catalysts

The greatest milestone in the history of polymerization processes was the advent of Ziegler-Natta catalysts for olefin polymerization reactions. The use of these catalysts allowed for structural and steric control of the polymer chains, generating polyolefins with completely different properties than those of the materials produced before by other chemical routes (MACHADO and PINTO, 2011).

Generally, Ziegler-Natta catalysts present high activity, which results in the expressive reduction of catalyst residues and problems related to toxicity, corrosion and premature aging of the final pieces. Besides, ZN catalysts can be used to control many of the final properties of the polymer, such as transparency, rigidity and tensile strength (MACHADO and PINTO, 2011).

Besides tacticity, ZN catalysts have also allowed for control of other microstructural (like the molecular weight distribution) and macrostructural (like porosity, morphology and particle-size distribution) properties of the polymer material. As a consequence, ZN allowed for reduction of the investments and process operation costs.

ZN catalysts have been applied in solution, colloidal or heterogeneous forms to produce diverse types of polyolefins. Nevertheless, before the 1980, isotactic crystalline polyolefins were produced only through heterogeneous systems. The heterogeneous Ziegler-Natta catalyst systems brought important innovations in the manufacture of polyolefins such as the synthesis of HDPE, LLDPE and highly isotactic and syndiotactic polypropylene. For industrial applications, most Ziegler-Natta catalysts are based on titanium salts and aluminum alkyls (HAMIELEC and SOARES, 1996).

2.4.1 Composition

A ZN catalyst type is characterized by the combination of metallic compounds of two different classes, which are:

❖ Transition metal salts in the groups IV and VIII of the periodic table, usually titanium, zirconium or vanadium;

❖ Organometallic compounds of metals from groups I to III of the periodic table, often linked to alkyl groups (typically the metal is aluminum). These compounds are called cocatalysts.

The high reactivity depends on the presence of both catalyst and cocatalyst; in the absence of any of them, reaction will not occur. However, when both compounds are present, they interact chemically and promote the generation of active centers that are efficient enough to lead to stereospecific polymerizations of dienes and α-olefins (SEVERN et al., 2005).

2.4.2 Evolution of Ziegler-Natta Catalysts

The Ziegler-Natta catalysts were discovered by Karl Ziegler and Giulio Natta in the early fifties of the 20th century, in 1953, with the production of PE with high molecular weight at low temperatures (50 – 100 °C) and low pressures (10 – 15 atm). This polymer was much less branched and presented better mechanical properties, when compared with PE resins generated by free-radical polymerization (ODIAN, 2004). This discovery generated a patent in november of the same year called "*Process for the*

synthesis of high molecular poly(ethylene)s", causing a revolution in the chemical industry, since unexpectedly the polymerization of alkenes became feasible under mild conditions, when compared to previous techniques (FRIEBE et al., 2006).

Exactly 10 years after the discovery of the Ziegler-Natta catalysts, Karl Ziegler and Giulio Natta received the Nobel Prize for this achievement. The development of this class of catalysts was characterized by distinct stages, classified as new generations of Ziegler-Natta catalysts, as summarized in Table 2.2 and Figure 2.8.

Table 2.2 – Summary of the evolution of ZN catalysts (+ is high and – is low) (according to CERRUTI, 1999)

Generation	Year	Innovation			Result		
		Catalyst	Co-Catalyst	Support	Activity	Stereo-activity	Morphology
1st	1957	TiCl$_3$ purple phases	AlEt$_2$Cl			+	
	1964		Lewis bases added		-	+	
2nd	1973	TiCl$_3$ purple phases at ↓T			+		
3rd	1980			Activated MgCl$_2$	++		+
4th	1991	TiCl$_3$ purple phases at ↓ T		Silica gel		+	-
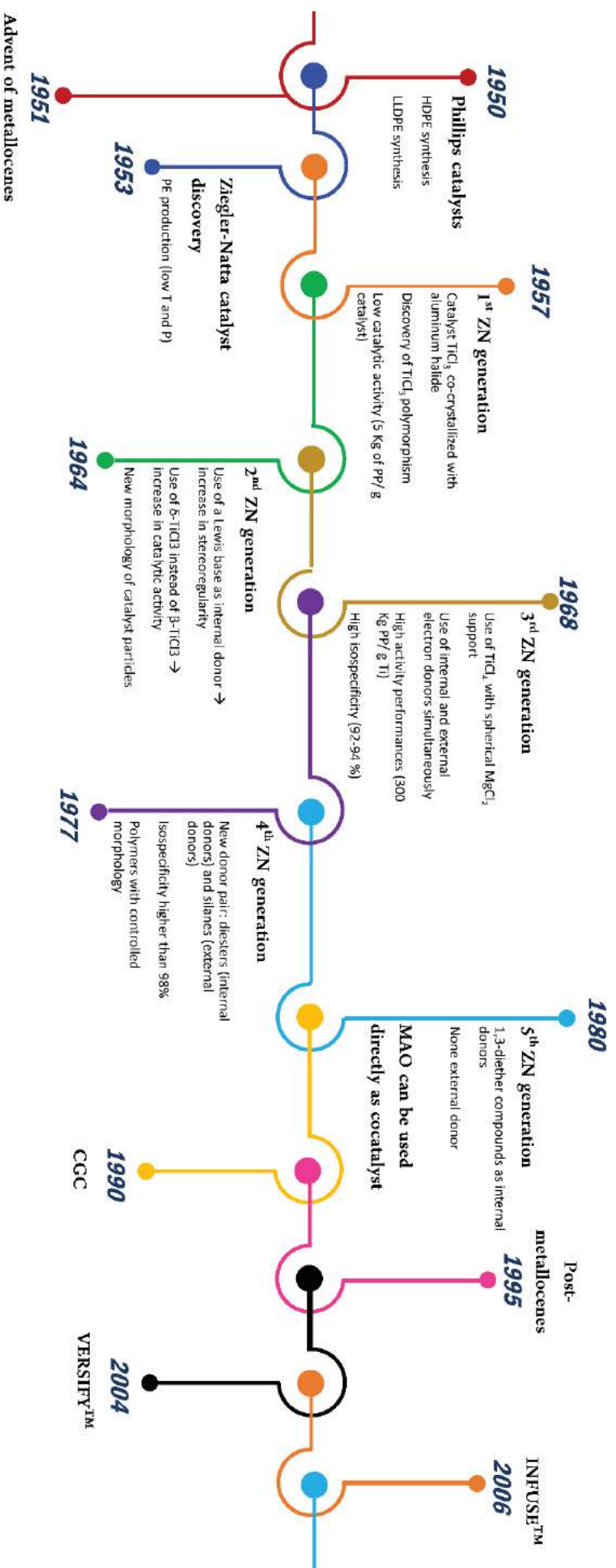
Figure 2.8 – Timeline of the evolution of coordination catalysts.

1950
Phillips catalysts
HDPE synthesis
LLDPE synthesis

1951
Advent of metallocenes

1953
Ziegler-Natta catalyst discovery
PE production (low T and P)

1957
1st ZN generation
Catalyst TiCl₃ co-crystallized with aluminum halide
Discovery of TiCl₃ polymorphism
Low catalytic activity (5 Kg of PP/ g catalyst)

1964
2nd ZN generation
Use of a Lewis base as internal donor → increase in stereoregularity
Use of δ-TiCl3 instead of β-TiCl3 → increase in catalytic activity
New morphology of catalyst particles

1968
3rd ZN generation
Use of TiCl₄ with spherical MgCl₂ support
Use of internal and external electron donors simultaneously
High activity performances (300 Kg PP/ g Ti)
High isospecificity (92-94 %)

1977
4th ZN generation
New donor pair: diesters (internal donors) and silanes (external donors)
Isospecificity higher than 98%
Polymers with controlled morphology

1980
5th ZN generation
1,3-diether compounds as internal donors
None external donor

MAO can be used directly as cocatalyst

1990
CGC

1995
Post-metallocenes

2004
VERSIFY™

2006
INFUSE™

According to CERRUTI (1999), the first generation of ZN catalysts started in 1957. The first catalyst generation, also known as conventional ZN catalyst, is basically formed by solid titanium trichloride ($TiCl_3$) co-crystallized with an aluminum halide ($AlCl_3$). This system was generated by reduction of titanium tetrachloride ($TiCl_4$) with an organoaluminum compound, as diethylaluminum chloride (DEAC – $AlClEt_2$) or triethylaluminum (TEAL – $AlEt_3$). Natta noted that $TiCl_3$ presented polymorphism, forming four different crystalline structures (α-hexagonal, β-linear, γ-cubic and δ-intermediate) and three of them (α, γ, δ) were stereoselective for α-olefin polymers, which explains the choice of Natta and Ziegler for $TiCl_3$ (CERRUTI, 1999). In comparison with $TiCl_4$, the crystalline forms α and γ of $TiCl_3$ have lower catalytic activity. The β structure has low stereospecificity and only produces amorphous polymer. On the other hand, the δ structure is the most active crystalline form to generate isotactic polypropylene (ODIAN, 2004). Particularly, Natta sought to synthesize the catalytic system outside the reaction environment and managed to produce $TiCl_3$ by reducing $TiCl_4$ with H_2 at high temperatures (SEYMOUR and CHENG, 1986).

The synthesis of crystalline polymers with high configurational regularity from polymerization of α-olefins and dienes became possible with the advent of the first generation of ZN catalysts. The stereoselectivity of the 1st generation of catalytic systems is low, with isotactic levels ranging from 20 to 40 % for polypropylene (ODIAN, 2004), which turns indispensable the process step responsible to remove atactic fractions from the polymer product.

The catalyst activity of the 1st ZN generation is also considered low: approximately 5 Kg of PP by g of catalyst (SOGA and SHIONO, 1997). According to ODIAN (2004), these catalytic systems were inefficient, with less than 1 % of active Ti during polymerization. Since the catalytic activity was considerably low, it was necessary to purify the polymer in order to remove residual metals through treatment with bases or acids (CERRUTI, 1999).

2.4.2.2 Second Generation of ZN Catalysts

Since 1964, a Lewis base (internal donor) was added to the catalyst in order to improve the polymer stereoregularity. Nevertheless, the increase in stereoregularity,

which actually means the increase in isotacticity, did not correspond to a similar increase in catalytic activity (CERRUTI, 1999). As a matter of fact, improvement of stereoregularity was obtained through poisoning of atactic sites, leading to reduction of catalyst activity.

However, according to CERRUTI (1999), the second ZN generation was really initiated in 1973 with the procedure to transform β-TiCl$_3$ in δ-TiCl$_3$ under mild temperatures (lower than 100 °C) and in the presence of TiCl$_4$. This innovation was responsible to quintuplicate the catalytic activity. The stereospecificity, due to the use of internal donors, was also increased to 95 %. This improvement was so significant that the removal of atactic fractions from the final polymer became dispensable.

The second ZN generation was also marked by the new morphology of the catalyst particles: they became smaller, due to reduction of temperature from 160 – 200 °C to 65 °C, and porous, as the result of the catalyst pretreatment with ether in order to extract AlCl$_3$.

2.4.2.3 Third Generation of ZN Catalysts

In 1960, the Shell company patented a catalyst system for the polymerization of propylene which used TiCl$_4$ supported on MgCl$_2$. In 1968, the companies Montecantini and Mitsui, independently, patented catalysts prepared from TiCl$_4$, MgCl$_2$ and an electron donor, activated by a mixture of trialkylaluminum and a second electron donor. In the early 1980s, industrial plants based on this latter type of catalyst started to operate (CERRUTI, 1999).

Some researchers assume that the beginning of 3rd ZN generation occurred in the 60's, while others consider that the 3rd ZN generation was started in the 80's (CERRUTI, 1999). Regardless, it can be said that the third generation of Ziegler-Natta catalyst is characterized by the use of TiCl$_4$ with spherical MgCl$_2$ supports and the use of internal and external electron donors simultaneously, with a trialkylaluminum as a catalytic system.

Catalyst supports comprise hydroxides, carbonates, halides, oxides or alkoxides of magnesium, manganese, iron, nickel, silicon and cobalt. Some of them originated catalyst systems with high activity, but low stereospecificity. However, magnesium chloride is able to polymerize propylene with very high stereoregularity (MONJI et al., 2009).

The catalyst support activation was initially performed over long grinding times in the presence of a Lewis base, such as ethyl benzoate, which acted as an internal electron donor. After activating the support, it was brought into contact with $TiCl_4$ and washed with hydrocarbons to remove soluble titanium complexes. During polymerization, an external electron donor was added with the aluminum alkyl compound (CERRUTI, 1999).

The usual electron donors include amines, ethers and esters (HUANG and REMPEL, 1995). The 3rd ZN generation typically combines ethylbenzoate (EB), as internal donor, with EB or para-substituted benzoate as external donor. The internal donor is responsible to (SOGA and SHIONO, 1997): prevent the coagulation of $MgCl_2$ particles during the milling process, enhancing the effective surface area; prevent the generation of non-specific sites on the $MgCl_2$ surface, where $TiCl_4$ is supported to generate non-stereospecific sites; promote the formation of highly isospecific sites; and be replaced by the external electron donors, forming even more isospecific catalyst sites. On the other hand, the roles of the external electron donors are: selectively poison non-stereospecific catalyst sites; convert non-stereospecific sites into highly isospecific sites; convert isospecific sites into even more highly isospecific catalyst sites; and enhance the reactivity of the isospecific catalyst sites.

The third generation of Ziegler-Natta catalysts achieved very high activity performance, being capable to produce 300 Kg of PP per g of Ti. Moreover, these catalyst systems achieved high isospecificity (92 – 94 %), with atactic content approximately between 6 and 10 wt % (CERRUTI, 1999).

2.4.2.4 *Fourth Generation of ZN Catalysts*

In 1977, the extraction process for poorly isotactic content was finally eliminated through use of a catalyst system prepared with new donor combination: diesters (as internal donor) and silanes (as external donor). This new pair of donors (phthalate/alkoxysilane) became part of the fourth generation catalyst, comprising $TiCl_4$/ $MgCl_2$/ phthalate and AlE_3/ alkoxysilane, and has been employed for the industrial production of PP since its discovery. The 4th ZN generation is capable to achieve isospecificity above 98 % (KAMINSKY, 2013).

Additionally, the 4th generation of Ziegler-Natta catalysts was marked by the production of polymers with controlled morphology (WANG et al., 2006). This

achievement was possible by using spherical $MgCl_2$ supports and chemical activation steps. In this case, $MgCl_2$ and $TiCl_4$ are usually mixed in alcoholic solutions and dried in spray-driers, where spherical particles are produced.

2.4.2.5 *Fifth Generation of ZN Catalysts*

Although not unanimously accepted, the fifth ZN generation was born between the late 1980s and initial 1990s, when a series of 1,3-diether compounds were proposed and used as internal donors (PARODI, 1982). Catalysts prepared with 1,3-diether as internal donor present quite high activities (almost two times higher than the activity achieved by the 4th ZN generation) and appropriate isospecificity without the use of external donors. Moreover, these new catalysts are more sensitive to hydrogen, allowing for production of PP with narrower molecular weight distribution (PI around 4), when compared with PPs produced with former generations of catalysts. In the following years, many researches tried to find new donors that would allow broadening the MWD without sacrificing the activity and isospecificity achieved by the fourth ZN generation. This eventually led to the development of heteroatom-containing donors (KAMINSKY, 2013).

Based on this discussion, several nitrogen-containing external donors were introduced. Although these donors led to unique polymer properties, the absence of the highest molecular weight tail in the MWD of PP and typical odor problems, among others, limited the application of the 5th ZN generation to some special grades. Despite that, the fifth and fourth ZN generations are still the most modern catalyst systems employed industrially to produce PP (PATERN et al., 2002).

The catalyst that uses succinate as the internal donor is often classified as a *sixth generation* Ziegler-Natta catalyst. Since the third generation, the evolution of heterogeneous Ziegler-Natta catalysts is related to finding new donors, since they can modify not only the catalyst activity, but also physical properties of PP, by changing isotacticity, MWD and comonomer incorporation. However, it is important to remark that the essential catalyst structure is not only influenced by donors, but also by the chemical preparation routes. Thus, the *seventh generation* might appear as the combination of new electron donors and new catalyst preparation techniques (KAMINSKY, 2013).

2.4.2.6 Metallocenes

Metallocenes constitute a special class of Ziegler-Natta catalysts. Metallocenes are organometallic complexes containing a transition metal, from groups IV to VII of the periodic table, usually zirconium, titanium or hafnium, bonded to at least one aromatic ring, such as cyclopentadienyl (Cp), indenyl (Ind) or fluorenyl (Flu), which can be substituted or not by π-type bonds formed by an electron of the transition metal and another electron shared by all carbon atoms in the ring (η^5). For these complexes to act as catalysts, the presence of a cocatalyst is also required and methylaluminoxane (MAO) is the most employed cocatalyst nowadays (MARQUES et al., 1998).

The advent of metallocenes occurred in the early 1950s of the 20th century, when KEALEY and PAUSON (1951) and MILLER et al. (1952) synthesized the bis(cyclopentadienyl)Fe or ferrocene (Figure 2.9). The structure of ferrocene was elucidated in 1952 by WILKINSON et al. (1952). These findings stimulated scientific research in the field of organometallic chemistry and, as a result, in 1973, Wilkinson and Fischer received the Nobel Prize for their scientific contributions in the field (COLLMAN et al., 1987).
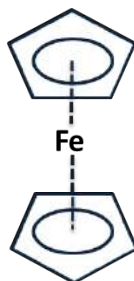
Figure 2.9 – Ferrocene.

BRESLOW and NEWBURG (1957, 1959) are in the group of the first researchers to employ metallocene catalysts in the polymerization of ethylene. They used soluble bis(cyclopentadienyl)titanium derivatives as catalysts and alkylaluminums as cocatalysts. Several other researchers also followed these footsteps, including Natta. Nevertheless, these catalytic systems presented low activities and stabilities to polymerize ethylene, synthesizing only low molecular weight polymers. Besides, these catalytic systems were not active for polymerization of propylene (HAMIELEC and SOARES, 1996).

REICHERT and MEYER (1973), using the catalytic system $Cp_2TiEtCl/AlEtCl_2$, observed that, through the controlled addition of water in the polymerization reactor, it becomes possible to considerably increase the activity of reaction due to the formation of alkylaluminoxane. This result was confirmed by other experimental tests using various catalyst systems and alkylaluminiums.

Based on experimental evidences, it is believed that aluminoxane acts as an alkylating agent, participates in the formation of active sites, prevents the deactivation of active sites by bimolecular processes, stabilizes the active species and removes impurities (HAMIELEC and SOARES, 1996).

UEYAMA et al. (1974) reported that an oligomeric alkylaluminoxane compound is produced by reacting a trialkylaluminum compound with water, such as methylaluminoxane, according with the following reaction:

$$nAl(CH_3)_3 + nH_2O \rightarrow [-O - Al(CH_3) -]_n + 2nCH_4 \qquad (2.13)$$
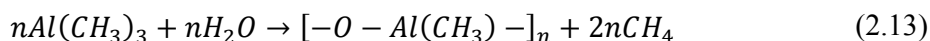
SINN and KAMINSKY (1980) proved that alkylaluminoxane could be used directly as cocatalyst, obtaining high reaction activities in the order of $40 \cdot 10^6$ g PE/ g Zr/ h. Furthermore, additional experiments showed that MAO exerts higher influence on metallocene activation than other alkylaluminoxanes. CIHLÁŘ et al. (1978, 1980) believed that this high catalytic activity, resulting from use of MAO as cocatalyst, occurs because of the significant increase of the propagation rate due to formation of aluminate anions. Since then, the use of MAO as cocatalyst has been highly indicated for polymerization of olefins.

This unique discovery led to the development of a new class of metallocene catalyst systems / methylaluminoxane, which is nowadays the most promising branch of the Ziegler – Natta catalyst family. However, until now, the composition, structure and chemical modifications imposed by MAO as a cocatalyst have not been fully elucidated. It is known that MAO is a mixture of oligomers of similar composition $(-Al(Me)O -)_n$ (MARQUES et al., 1998). According to GHIOTTO et al. (2013), one of the most important characteristics of MAO, responsible to gives its reactivity as a catalyst activator, is its trimethylaluminum content.

Although metallocenes present various advantages over conventional ZN catalysts (higher activity; more uniform physical properties; narrower MWD; more precise and uniform comonomer incorporation; among others), today they find limited applications in the polyolefins industry. One of the reasons is the fact that polymerizations conducted by metallocenes are carried out in solution, requiring large amounts of solvent and preventing the appropriate control of the polymer morphology. The polymer is typically obtained as a fine powder after precipitation, which results in the increase of the system viscosity and causes significant *reactor fouling*. Besides, the high cocatalyst/ metallocene ratios required impose high operational costs and generate metallic residues in the polymer mass that must be removed (MARQUES et al., 1998).

For industrial applications, metallocene catalysts must be heterogenized (ALT, 1999). As an attempt to respond to this fundamental requirement, metallocenes have been supported on a variety of inorganic and organic compounds, such as SiO_2, $MgCl_2$, Al_2O_3, MgF_2 and CaF_2 (HAMIELEC and SOARES, 1996). However, this constitutes a big challenge, since heterogenization usually causes significant loss of catalyst activity, when compared with the homogeneous metallocenes.

In 1990, Exxon started the commercialization of its EXACT LLDPE resin, made through metallocene/single-site technology. In the early 90s, Dow claimed to take single-site technology a step further, through enhancement of the physical properties. The strategy adopted by Dow was to avoid the falloff in processability that occurs because of the low polydispersity of the polymer (low PI) and the absence of the lower-molecular weight "tails" of the MWD. This strategy was possible through employment of a constrained-geometry catalyst (CGC) technology in a solution process that was capable to sustain the polymer processability through generation of long-chain branches (LCB). This occurs through incorporation of macromolecules by a constrained geometry ligand attached to a transition metal center (PAUL, 2015).

2.4.2.6.1 A Special Metallocene Class: Constrained Geometry Catalysts (CGC)

The constrained geometry catalyst is also known as the monocyclopentadienyl catalyst or the *half sandwich*. Figure 2.10 illustrates an example of a CGC. The absence of a second cyclopentadienyl ring facilitates the access of the active site to bulkier α-olefin comonomers. Consequently, polymer chains with a terminal vinyl group (SOARES, 2002) or pendant unsaturations (FERREIRA et al., 2010), known as

macromonomers or macromers (WANG et al., 1998), can be copolymerized with ethylene and other α-olefins to form LCBs (SOARES and HAMIELEC, 1996).
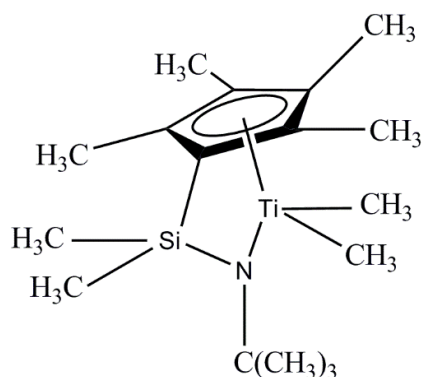
Figure 2.10 – Example of constrained geometry catalyst (CGC).

The low frequency of long-chain branches in the polyolefin chains synthesized with the CGC partially compensates the absence of low-molecular-weight components, increasing shear thinning, enhancing processability and improving melt elasticity of the material (SOARES and MCKENNA, 2012). Furthermore, these polymers continue to present narrow molecular weight distributions and uniform comonomer composition distributions, as those made by regular metallocenes.

2.4.2.6.1.1 Polymerization of Ethylene

LAI et al. (1993a,b) were the pioneers to synthesize PEs with long-chain branches using a constrained geometry catalyst at high-temperature homogeneous CSTR. The advantages of high-temperature homogeneous CSTR processes for long-chain branches include the high concentration and low diffusion barrier of macromonomers in the polymerization medium (SOARES and HAMIELEC, 1996). SWOGGER and KAO (1993) and SUGAWARA (1994) applied the procedure proposed by Lai and coworkers and produced polyethylenes with various branching degrees. WANG et al. (1998) produced polyethylenes with LCBs in a high-pressure and high-temperature CSTR system. The same group characterized LCB PEs and linear PEs prepared with the CGC through gel permeation chromatography (GPC) coupled with laser light scattering (LS), differential refractive index (DRI) and viscosity (CV) detectors. Using the Zimm-Stockmayer equation (ZIMM and STOCKMAYER, 1949), they could estimate the distributions of long-chain branch frequency (LCBF) and density (LCBD) as functions of the molecular weight of the chain. The authors showed

that LCBDF increased with the increase of molecular mass. While LCB affected the viscosity of the system, it did not improve the processing characteristics of the resin (WANG et al., 2004).

BEIGZADEH et al. (1999) polymerized ethylene with a mixture of two catalysts in a semi-batch reactor. One catalyst was a CGC, able to polymerize monomers and macromonomers, incorporating LCBs, while the second catalyst (regular metallocene) could only polymerize monomers and generate macromonomers. The combination selected was: CGC-Ti/Et[Ind]$_2$ZrCl$_2$. The authors showed that an optimum ratio of CGC-Ti/Et[Ind]$_2$ZrCl$_2$ can be found to maximize the amount of LCB of the formed PE.

YOUNG and MA (2002) investigated the kinetics of ethylene polymerization with CGC. They reported that the increase of monomer concentration caused the increase of the polymer yield and that the MAO/CGC ratio did not influence the polymer yield significantly.

MEHDIABADI and SOARES (2009) studied the polymerization of ethylene in a semi-batch reactor at 120 °C under distinct monomer pressures and catalyst concentrations. Two different types of catalysts were used: rac-Et(Ind)$_2$ZrCl$_2$ and CGC-Ti, both activated by MAO. The authors described the kinetics of ethylene polymerizations performed with rac-Et(Ind)$_2$ZrCl$_2$ as a first order polymerization, in presence of catalyst deactivation. On the other hand, with the CGC-Ti the authors observed second order polymerization kinetics, in presence of catalyst decay. Three years later, the same authors investigated the influence of ethylene concentration, temperature, MAO and catalyst concentrations on ethylene polymerization kinetics performed with the CGC-Ti and proposed a novel mathematical model to explain the polymerization kinetics and molecular weight response. They proposed the occurrence of reversible activation and deactivation steps with MAO and spontaneous thermal deactivation of the catalyst for the model to be able to capture the measured polymerization rates (MEHDIABADI and SOARES, 2012).

2.4.2.6.1.2 *Copolymerization of Ethylene with α-Olefins*

SOGA et al. (1996) and XU and RUCKENSTEIN (1998) produced ethylene/1-octene copolymers using CGC catalysts activated with MAO. SOGA et al. (1996) also copolymerized ethylene with oligoethylene. Several studies on copolymerization of ethylene/propylene with CGC have been published (WANG et al., 2004; KOLODKA et

al., 2002; KOLODKA et al., 2003; GALIMBERTI et al., 1999; SOGA et al., 1991; SOGA et al., 1994). Particularly, WANG and ZHU (2000) studied the chain structures of ethylene/propylene copolymers made in solution in a CSTR and using CGC. The authors observed that the increase of propylene feed composition increased the sequences of one and two methylene units and decreased the sequences of six and more consecutive methylene units. On the other hand, they also observed that the uninterrupted methylene sequence distributions did not suffer much influence from reaction temperature. In another work, the same group produced ethylene/propylene copolymers with low propylene ratios with CGC and rac-Et(Ind)$_2$ZrCl$_2$ (EBI). The authors concluded that CGC was more active for propylene incorporation than EBI and that LCB were formed through terminal vinyl macromonomer incorporation (WANG et al., 2000). GALIMBERTI et al. (1999) performed ethylene/propene copolymerizations in solution using a single centre catalyst system (CGC titanium dichloride) and MAO. The authors determined the reactivity ratios for ethene and propene based on rigorous statistical treatment of the polymerization data and concluded that this catalyst system promoted an almost random distribution of ethene and propene in the chains, providing similar reactivity ratios for both monomers, which is unusual.

2.4.2.6.1.3 *Copolymerization of Ethylene with Diene*

Despite the successful production of branched polyolefins with CGCs, the fraction of LCBs in these polymers is usually quite low (NELE et al., 2003; WANG et al., 1998). It is hard to increase the LCB frequency in these polymers because each macromonomer has only one branching point – a terminal vinyl group, which substantially reduces the probability of LCB formation in high molecular weight polymers. For this reason, some chemical routes used to increase the LCB frequency in polyolefins under mild polymerization conditions have been devised. One of them involves the simultaneous use of two metallocenes (BEIGZADEH et al., 1999, 2001; SIMON and SOARES, 2002; MEHDIABADI et al., 2008). Another strategy is to copolymerize an α-olefin and a non-conjugated diene with a metallocene (SERNETZ et al., 1997; NAGA and TOYOTA, 2004; SARZOTTI et al., 2005; MEHDIABADI and SOARES, 2011). In this case, only one double bond of the diene participates in the copolymerization reaction, producing polymer backbones with pendant double bonds. These unreacted double bonds can then be used to attach functional groups, form LCBs or build cyclic structures (PIETIKÄINEN et al., 1999). Besides, these strategies open

possibilities for the development of new products with improved mechanical properties and processability.

Despite the previous discussion, dienes do not have the same efficiency for induction of LCBs. The use of 1,5-hexadiene, for example, generates five-carbon rings in the polymer chains and does not form any considerable amount of coupling between two distinct polymer chains (PIETIKÄINEN et al., 1999). Longer dienes are less vulnerable to cyclization. For instance, the use of 1,9-decadiene generates LCBs without producing cycles that can be detected by nuclear-magnetic resonance (NMR) analyses (UOZUMI et al., 2000).

NAGA and TOYOTA (2004) investigated the copolymerization of ethylene and 1,7-octadiene (OD) with a CGC and found a unique insertion mode of OD units in the penultimate position, after the ethene insertion step, forming a cyclic structure (1,5-disubstituted cyclononane unit). SARZOTTI et al. (2005) copolymerized ethylene with 1,7-octadiene using CGC/MAO. They reported that the vinyl content of the copolymers increased when the concentration of diene in the reactor was increased. They also observed that more LCBs were formed due to the incorporation of macromonomers with pendant or terminal vinyl groups.

MEHDIABADI and SOARES (2011) produced ethylene/ α-olefin/ 1,9-decadiene copolymers, using rac-Et(Ind)$_2$ZrCl$_2$ (EBI) in a first polymerization step and CGC-Ti in a second polymerization step. With EBI, macromonomers with pendant and terminal vinyl groups were generated and copolymerized with ethylene and 1-butene or 1-octene using a CGC-Ti. This procedure allowed for production of branched polymers containing three main fractions: high-crystallinity fractions (macromers), low-crystallinity or amorphous fractions (α-olefin copolymer) and a cross-product (cross-linking of the two previous fractions).

BRANDAO et al. (2016) produced ethylene/ 1,9-decadiene copolymers under semi-batch operation using a CGC catalyst. The authors showed that the increase of the 1,9-decadiene content in the feed caused the decrease of the intrinsic viscosity (for the same molecular weight), since additional LCBs were formed. According with their experimental results, the use of higher catalyst concentrations led to higher concentrations of living polymer chains and macromonomers, increasing the probability of LCB formation. They proposed a novel mathematical model, which included macromonomer reincorporation through pendant double bonds resulting from the diene

incorporation. Experimental average molecular weights and ethylene feed flow rates were successfully predicted with help of the proposed model.

2.4.2.7 Post-metallocenes

Even after 50 years of the discovery of the Ziegler-Natta catalysts, the evolution of these catalysts continues nowadays. There is the commercial desire to design and produce polymers with well-defined properties through selective choice of the initiator, including branched, hyperbranched and block polymers, for example. Additionally, commercial interests require the continuing search for new initiators that have not yet been patented (ODIAN, 2004).

In 1995, Brookhart and coworkers reported a new family of late transition metal catalysts with unique chain architectures and capable to polymerize α-olefins, producing dendritic polymers (with includes dendrimers and hyperbranched polymers) (DONG and YE, 2012). These catalysts are much less oxophilic than conventional Ziegler-Natta, Phillips or metallocene catalysts, allowing the copolymerization of olefins with polar comonomers. In this new catalyst group, Ni(II) (JOHSON et al., 1995; KILLIAN et al., 1996), Co(II) (BROOKHART et al., 1995), Pd(II) (JOHSON et al., 1995; RIX and BROOKHART, 1995) and Fe(II) (SMALL and BROOKHART, 1998) are very active for polymerization of olefins (Figure 2.11). This discovery opened new possibilities to produce polyolefins with short- and long-chain branches simultaneously (BRITOVSEK et al., 2003). Additionally, these catalysts can also be used to synthesize diblock and triblock poly(α-olefins) (KILLIAN et al., 1996).
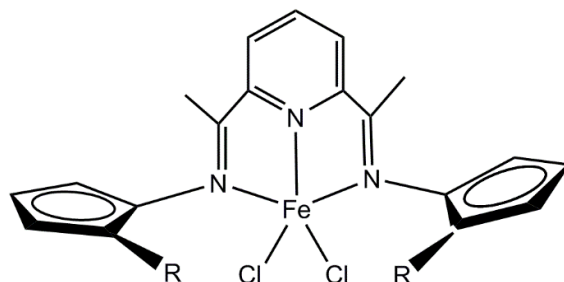
Figure 2.11 – Iron based catalyst for oligomerization of ethylene to linear α-olefins (R = Me, Et, *i*-Pr).

In 2004, Dow, in partnership with Symyx Techonologies, launched the plastomers and elastomers VERSIFY[TM], which constitute a new family of copolymers based on ethylene and propylene, produced with a new post-metallocene system called

pyridyl amine catalyst (STEVENS and VANDERLENDE, 2005; TAU et al., 2005). Plastomers and elastomers VERSIFY[TM] present very narrow molecular weight distributions and broad chemical composition distributions, when compared to materials produced by other single-site catalysts. These new polymers present higher transparency and are easier to process than the analogous ethylene based polymers.

In 2006, Dow announced a new family of block copolymers based on ethylene and octene: INFUSE[TM]. In order to produce this new polymer, two catalysts must be employed: one forms high density PE with high melting point, while the other generates elastomers with high octene incorporation. An external agent (diethyl zinc) is responsible for switching the catalyst systems while the polymer chain is growing (CHUM and SWOGGER, 2008).

2.5 Kinetic Studies on Olefin Polymerizations Performed with Metallocenes

The knowledge of the polymerization kinetics is essential for process scale-up and optimization. It is also important for development of new products with novel properties (MEHDIABADI and SOARES, 2009). Intense experimental investigations have been made about olefin homo- and copolymerizations with metallocenes. Consequently, studies were done to understand the polymerization kinetics of these systems and mechanisms were proposed as attempts to explain the collected experimental results. In these works, some proposed reaction steps are common and for this reason will be described in the next sections.

2.5.1 Catalyst Activation

The activation mechanism has not been clearly established. The need to use high excess of MAO and its role during polymerization are not well understood (MANDAL, 2013). MAO performs two main functions: alkylation of a metal-chloride bond and abstraction of the second chloride, to yield a metallocenium cation with a vacant coordination site (ODIAN, 2004):
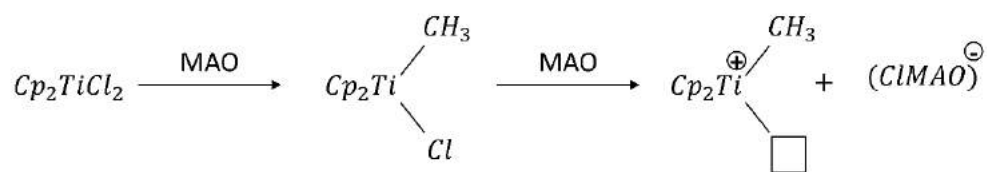
Figure 2.12 – Activation mechanism of Ti metallocene precatalyst (adapted from ODIAN, 2004).

The mechanism illustrated in Figure 2.12 can be summarized as shown in Equation (2.14):

$$C + MAO \xrightarrow{k_a} C^*$$
(2.14)

Usually, the catalyst activation step is assumed to be very fast and to occur instantaneously, especially for CGC catalysts of high activity. This hypothesis has been adopted in many works: WANG et al. (1998), NELE and SOARES (2002), SOARES (2002), MEHDIABADI and SOARES (2009), FERREIRA Jr. et al. (2010), MOGILICHARLA et al. (2014), KONSTANTINOV et al. (2016).

2.5.2 Chain Initiation

The chain initiation step is characterized by the first monomer insertion, producing a living polymer chain with length 1 (P_1^*) as shown in Figure 2.13.
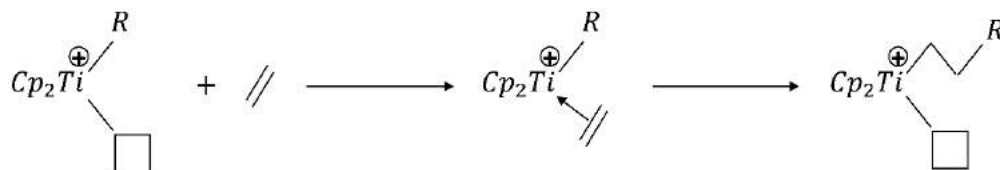
Figure 2.13 – Chain initiation mechanism using a Ti metallocene catalyst (adapted from ODIAN, 2004).

2.5.3 Monomer Propagation

Monomer propagation consists of successive monomer insertions into the living and growing polymer chain, increasing its length to *2, 3, …, r* until a chain transfer reaction occurs or the catalyst active site deactivates, as illustrated in Figure 2.14.
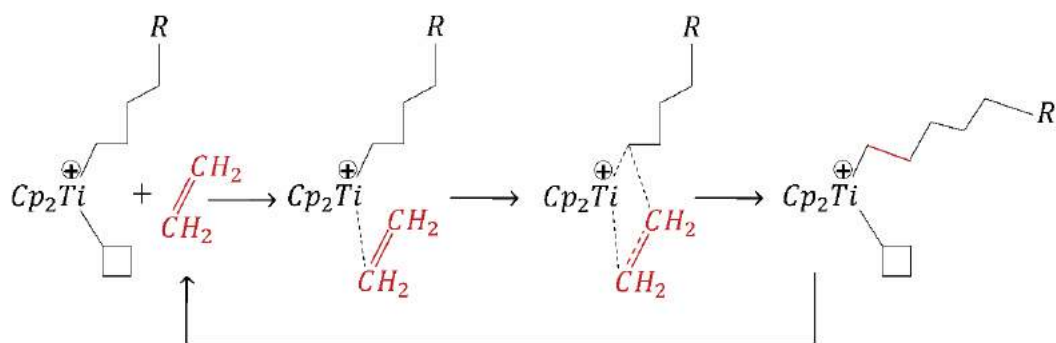
Figure 2.14 – Monomer propagation mechanism using a Ti metallocene catalyst (adapted from ODIAN, 2004).

2.5.4 Chain Transfer Reactions

Chain transfer reactions control the polymer average molecular weights and can occur spontaneously through transfer to hydrogen, monomer, cocatalyst and through β-hydride elimination.

2.5.4.1 Chain Transfer to Hydrogen

Hydrogen is the chain transfer agent used most often during olefin polymerization, since metallocene and late transition metal catalysts are normally very sensitive to hydrogen (SOARES and HAMIELEC, 2012). Chain transfer to hydrogen is illustrated in Figure 2.15:
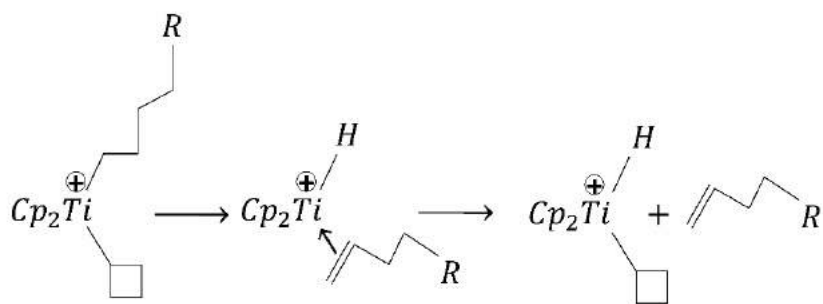
Figure 2.15 – Chain transfer to hydrogen (adapted from ODIAN, 2004).

The metal hydride site generated after transfer to hydrogen may also initiate other growing chain, according to the mechanism shown in Figure 2.16. The active species from Figure 2.16 differs from the active species in Figure 2.13 because of the

hydrogen atom placed at the chain end. This slight difference can be associated to the decrease in the overall ethylene polymerization rate that is normally observed in the presence of hydrogen (SOARES and HAMIELEC, 2012).
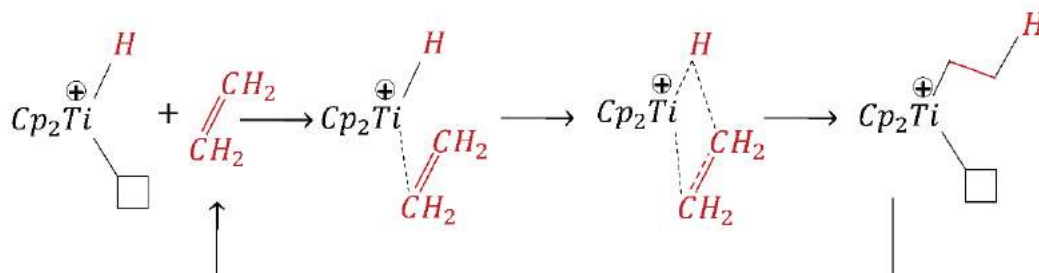
Figure 2.16 – Initiation of a metal hydride site (adapted from ODIAN, 2004).

2.5.4.2   Chain Transfer to Monomer

In the case of ethylene polymerization, chain transfer to ethylene forms a dead chain containing a terminal unsaturation (a vinyl-terminated chain) and a living chain with length 1, as one can see in Figure 2.17.
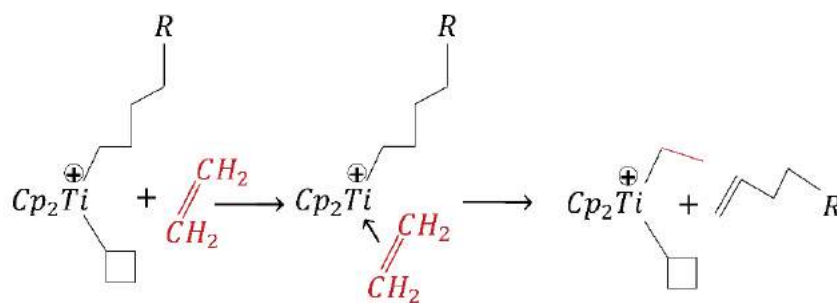
Figure 2.17 – Chain transfer to ethylene (adapted from ODIAN, 2004).

2.5.4.3   Chain Transfer to Cocatalyst

The cocatalyst can also act as a chain transfer agent, according to the mechanism illustrated in Figure 2.18.
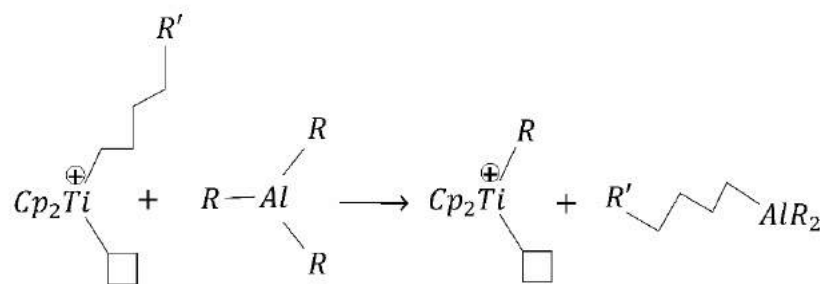
Figure 2.18 – Chain transfer to cocatalyst (adapted from ODIAN, 2004).

2.5.4.4 Spontaneous Transfer

β-Hydride elimination, usually called spontaneous transfer, forms a vinyl-terminated chain, in ethylene polymerizations, as shown in Figure 2.19. For propylene polymerizations, after spontaneous transfer, a vinylidine-terminated chain is generated.
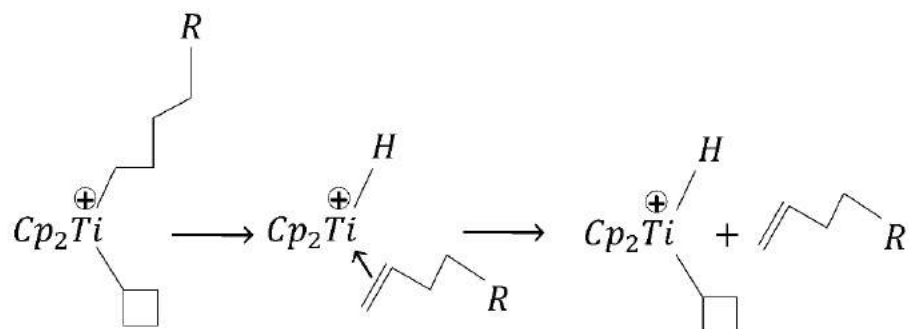
Figure 2.19 – β-Hydride elimination (adapted from ODIAN, 2004).

2.5.5 Catalyst Deactivation

After yielding a maximum polymerization activity, most coordination catalysts deactivate, following a dynamic deactivation profile that depends on catalyst type, polymerization temperature and levels of impurities present in the reaction medium. WANG et al. (1998) concluded that a first order catalyst decay was not appropriate to predict the results obtained from ethylene homopolymerizations performed with CGC in a CSTR. MEHDIABADI and SOARES (2009) concluded that the catalyst decay in polymerizations of ethylene performed with CGC-Ti catalyst and MAO could be described by a second order kinetics, while the order of polymerization changed from 2 to 1 with the increase of ethylene pressure. In other work, MEHDIABADI and

SOARES (2012) proposed the occurrence of reversible activation and deactivation steps with MAO with the simultaneous thermal deactivation of the catalyst to explain their experimental results, obtained during ethylene polymerizations carried out with CGC in a semi-batch reactor. Recently, BRANDÃO et al. (2016) successfully used a second order deactivation step to explain how living chains deactivate in ethylene polymerizations performed with CGC-Ti and MAO under semi-batch mode operation.

2.6 Concluding Remarks

Based on the information provided in Chapter 2, it can be said that the presence of long-chain branches in the polymer backbone may be desired since it can affect the polymer processing properties considerably, improving melt strength and melt processability of polymers with narrow PI, making these polymers very attractive commercially.

Given the positive effects that LCB cause on rheology, processability and mechanical properties of a polymer resin, many studies have been done to understand the mechanism responsible to form LCBs. As shown in this chapter, the mechanism most widely accepted is terminal branching, which was extended to include the incorporation of the macromonomer through pendant double bonds.

It can also be said that the evolution of the Ziegler-Natta catalysts did not stop until nowadays. The commercial desire to design and produce polymers with well-defined properties is one of the reasons that stimulate the search for new catalyst types.

3 Deterministic Numerical Methods

3.1 Summary

This chapter presents an overview of some deterministic numerical procedures used for model solving. Herein, the method of moments and MWD interpolation methods, such as the Orthogonal Collocation method and Polynomial Approximations based on the Moments of the Distributions, are described.

In order to illustrate the central idea of each method, a simple example can be proposed based on a simple living polymerization scheme:

$$C \xrightarrow{k_a} C^* \; (activation)$$

$$C^* + M \xrightarrow{k_{p11}} P_1^* \; (initiation)$$

$$P_i^* + M \xrightarrow{k_{p11}} P_{i+1}^* \;\; (propagation)$$
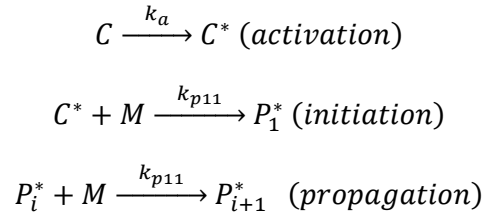
The material balance equations for the species present in the proposed mechanism can be written as:

$$C = C(0) \cdot \exp(-k_a \cdot t) \tag{3.1}$$

$$C^* = C(0) \cdot (1 - \exp(-k_a \cdot t)) \tag{3.2}$$

$$\frac{dM}{dt} = 0 \tag{3.3}$$

$$\frac{dP_1^*}{dt} = k_{p11} \cdot \frac{M}{V} \cdot V \left(\frac{C^*}{V} - \frac{P_1^*}{V} \right) \tag{3.4}$$

$$\frac{dP_i^*}{dt} = k_{p11} \cdot \frac{M}{V} \cdot V \cdot \left(\frac{P_{i-1}^*}{V} - \frac{P_i^*}{V} \right) \tag{3.5}$$

In this example, the monomer concentration is kept constant during the polymerization, as the monomer is supplied on demand to maintain the constant reactor pressure. The only distributed species in this proposed example is the living chain P_i^*, which can have length ranging from unity to infinity (or a large natural number).

Thus, the most difficult problem associated with the solution of the EDO system is the balance of species P_i^*, since $i \in (1, \infty)$. Even if infinity is limited to a feasible sufficiently large natural number (for example, 300000), the CPU time required to numerically integrate the equations using traditional ODE solvers, such as Runge-Kutta (CARTWRIGHT and PIRO, 1992), BDF (Backward differentiation formula) (PETZOLD, 1982), among others, would be impracticable. Therefore, in order to avoid solving infinite balance equations, which actually is impossible, strategies were developed to overcome this limitation and each method will deal with this problem in some peculiar manner. Among the deterministic approaches, one can emphasize the relevance of the method of moments and the methods that propose functional approximations of the MWD. For MWD approximation, the orthogonal collocation method and polynomial approximations based on moments of the distribution are described here. In Chapter 7 these methods will be applied to more complex cases that were investigated in this thesis both theoretically and experimentally.

3.2 Method of Moments

The method of moments allows for resolution of a finite number of balance equations, instead of the originally infinite set of balance equations that constitute the original problem. As previously described in Section 2.1.1, the distribution of sizes $P(i)$, where $P(i)$ is the number of chains of size i, can be interpreted as a statistical distribution (after normalization). Thus, one way to characterize this distribution is through its moments. For simple models, the model can be rearranged in terms of the moments of the distribution, making the implementation and simulation relatively simple. Usually, the first three moments are regarded as the most important ones, since the number and weight average molecular weights (and, consequently, the polydispersity index) can be calculated with them, as described in Section 2.1.1 (GALVAN and TIRREL, 1986).

For the example represented in Section 3.1, the balance equations for P_i^*, with $i \in (1, \infty)$, can be replaced by the following set of equations (derivation in Appendix A):

$$\frac{d\mu_0}{dt} = k_{p11} \cdot \frac{M}{V} \cdot V\left(\frac{C^*}{V}\right) \tag{3.6}$$

$$\frac{d\mu_1}{dt} = k_{p11} \cdot \frac{M}{V} \cdot C^* + k_{p11} \cdot \frac{M}{V} \cdot \mu_0 \tag{3.7}$$

$$\frac{d\mu_2}{dt} = k_{p11} \cdot \frac{M}{V} \cdot (C^* - P_1^*) + k_{p11} \cdot \frac{M}{V} \cdot (2 \cdot \mu_1 - \mu_0) \tag{3.8}$$

When the polymerization mechanism leads to moment closure problems, when the ith–moment balance equation requires the definition of the $(i+1)^{th}$ moments, the balance equation cannot be solved, unless one can propose the use of a closure method. HULBURT and KATZ (1964) developed a closure method that can be written in the form of algebraic expressions, using a distribution approximation procedure.[3] This approach has been applied successfully to eliminate closure problems in many different polymerization systems (PLADIS and KIPARISSIDES, 1998; IEDEMA and HOEFSLOOT, 2002; BRANDOLIN et al., 2007; BRANDÃO et al., 2016).

3.3 MWD Approximation Functions

The obtainment of molecular weight distributions through numerical solution of mathematical models is essential when one investigates nonlinear polymerizations. In these cases, the MWD may present multimodalities or high molecular weight tails and, consequently, molecular average weights may not be representative of the resin characteristics (NELE and SOARES, 2003; SAYER et al., 2001).

The calculation of distributions as described by mechanistic models constitutes a hard task, since the computation of these distributions is characterized by the solution of an infinite number of nonlinear differential-difference equations, turning the reduction of the dimension of these models fundamental for the study of the system dynamics and for optimization analyses (PINTO and BISCAIA Jr., 1988; NELE et al., 1999).

Order reduction techniques that preserve the discrete nature of the original system usually belong to the family of discrete weighted residual methods (DWRMs) (CANU and RAY, 1991). One of the best known methods from this group is orthogonal collocation. This method approximates the dependent variables by polynomial functions

---

[3]The closure expressions for μ_3, μ_4 and μ_5 were obtained as approximate algebraic equations in the form (IEDEMA and HOEFSLOOT, 2002): $\mu_3 = \frac{\mu_2}{\mu_0\mu_1}(2\mu_2\mu_0 - \mu_1^2)$, $\mu_4 = \frac{-(2\mu_1^2 - 3\mu_2\mu_0)(3\mu_1^2\mu_2 - 6\mu_2^2\mu_0 + 4\mu_0\mu_1\mu_3)}{\mu_0^2\mu_1^2}$,

$\mu_5 = -\frac{(12\mu_1^4\mu_2 - 42\mu_1^2\mu_2^2\mu_0 + 36\mu_0^2\mu_2^3 + 20\mu_1^3\mu_0\mu_3 - 30\mu_1\mu_0^2\mu_2\mu_3 + 5\mu_1^2\mu_0^2\mu_4)}{\mu_0^2\mu_1^2}$

of the independent variables, so that the equations must be satisfied at certain interpolation points called collocation points. These points are the roots of a certain family of orthogonal polynomials (PINTO and BISCAIA Jr., 1988). Comprehensive discussions regarding this method can be found in VILLADSEN and MICHELSEN (1978) and FINLAYSON (1981a; 1981b).

Many workers have employed orthogonal collocation methods to different chemical engineering processes. WONG and LUUS (1980) were the first to use orthogonal collocation procedures for order reduction and solution of discrete models used to describe staged separation systems. STEWART et al. (1985) proved that better and more reliable reduced models can be obtained through discrete orthogonal polynomials. PINTO and BISCAIA (1988) also employed orthogonal collocation to solve models of discrete staged separation systems. ALVAREZ and ALVAREZ (1987; 1989) used collocation methods to solve summation-difference equations. Particularly, the authors applied employed examples of staged processes and polymerization reactors to illustrate the technique. CANU and RAY (1991) reviewed the basic concepts of DWRMs and highlighted the relative advantages of the collocation and Galerkin formulations. The authors applied DWRM to simulate discrete chain length distributions in polymerization reaction problems. RIBEIRO et al. (2015) presented a technique to reduce the order of staged separation systems based on the sum of moment-weighted residuals. The performance of the classical method of orthogonal collocation on a discrete domain was compared with the performance of the proposed technique, and the last method was shown to present better performance for the investigated cases. The authors showed that the points where the residuals are canceled are fixed in the orthogonal collocation method, while the proposed technique would lead to moving interpolation points, providing an adaptive characteristic to the proposed technique.

Despite the successful applications in a large number of problems, some questions remain unanswered, regarding how one should select weighting functions and how the approximation function should be designed. PINTO and BISCAIA (1996) improved the robustness of polynomial approximation techniques by proposing a complete adaptation procedure; in other words, the authors employed the approximate solution as the new weighting function during the iterative numerical scheme. Thus, the weighting function was continuously updated, allowing to incorporate instantaneous

changes of the MWD. This new approach avoided some of the pitfalls of classical orthogonal collocation methods. NELE et al. (1999) and SAYER et al. (2001) applied the adaptive orthogonal collocation technique to successfully compute MWDs in nonlinear polymerization reactions, reinforcing the appropriateness of the proposed approach.

3.3.1 Orthogonal Collocation Method

Consider the initial boundary condition problem:

$$\frac{\partial u}{\partial t} = G(u(t,i),t) \qquad u(0,i) = u_i \tag{3.9}$$

The basic idea behind discrete weighted residual methods is the proposal of an approximating function $\tilde{u}(t,i)$ to represent the sought solution $u(t,i)$. Assuming that $\tilde{u}(t,i)$ is the proposed approximation in Equation (3.9), a function called residue R can be obtained.

$$R(t,i) = \frac{\partial \tilde{u}(t,i)}{\partial t} - G(\tilde{u}(t,i),t) \tag{3.10}$$

If the approximation $\tilde{u}(t,i)$ is exact, the residue is identically equal to zero at all points of the analyzed interval, which obviously does not demand a numerical solution. A typical function used as the approximating function for $\tilde{u}(t,i)$ is:

$$\tilde{u}(t,i) = \theta(i) \cdot \sum_{j=1}^{N} a_j(t) \cdot l_j(i) \tag{3.11}$$

where $\theta(i)$ is a reference or weighting function. $\theta(i)$ is a strictly positive function, summable over the whole analyzed interval. $a_j(t) \; \forall \, j \in (1,N)$ are the coefficients that must be determined to achieve the best approximation $\tilde{u}(t,i)$ of $u(t,i)$ and $l_j(i) \; \forall \, j \in (1,N)$ are the Lagrange interpolating polynomials, defined in the form of Equation (3.12), with the properties defined in Equation (3.13):

$$l_j(i) = \prod_{\substack{k=1 \\ k \neq j}}^{N} \frac{i - s_k}{s_j - s_k} \tag{3.12}$$

$$l_j(s_k) = \begin{cases} 0 & if \;\; j \neq k \\ 1 & if \;\; j = k \end{cases} \tag{3.13}$$

where $s_1, s_2, \ldots, s_N$ are the nodal interpolation points.

One possible way to improve the accuracy of proposed solution $\tilde{u}(t, i)$ is to choose nodal points $s_j, \forall\, j \in (1, N)$, as roots of a certain orthogonal polynomial of order N, considering the reference function $\theta(i)$ as the weighting function (PINTO and BISCAIA Jr., 1988).

The reference function $\theta(i)$ should be as close as possible to the true solution $u(t, i)$ in order to improve the accuracy of the method (PINTO and BISCAIA Jr., 1988). The polynomial coefficients can be calculated by making the residues at each collocation point $s_1, s_2, \ldots, s_N$ is equal to zero; in other words, by obliging the approximate equation to be satisfied at the nodal interpolation points. So:

$$\begin{aligned} R(t, s_j) &= 0 \\ \frac{\partial \tilde{u}(t, s_j)}{\partial t} &= G(\tilde{u}(t, s_j), t) \end{aligned} \qquad \forall\, j \in (1, N) \tag{3.14}$$

Inserting Equation (3.11) into Equation (3.14):

$$\theta(s_j) \cdot \frac{\partial\left(\sum_{k=1}^{N} a_k(t) \cdot l_k(s_j)\right)}{\partial t} = G(\tilde{u}(t, s_j), t) \quad \forall\, j \in (1, N) \tag{3.15}$$

As $\sum_{k=1}^{N} a_k(t) \cdot l_k(s_j) = a_j(t)$, due to the fundamental property of Lagrange interpolating polynomials, when applied to the nodal points and defined in Equation (3.13), Equation (3.15) becomes:

$$\frac{\partial a_j(t)}{\partial t} = \frac{G(\theta(s_j) \cdot a_j(t), t)}{\theta(s_j)} \quad \forall\;\; j \in (1, N) \tag{3.16}$$

Hence, Equation (3.16) leads to a system of N differential equations. One should note that, by making the residual null at all nodal points, the functions to be integrated

in time are the coefficients $a_j(t), \forall j \in (1, N)$ of the proposed approximation. The numerical procedure implemented to calculate the nodal points is presented in Appendix A.

When this methodology is applied to the example shown in the beginning of this chapter, the living chains P_i^* can be approximated as:

$$P_i^* = P(t, i) = \theta(t, i) \sum_{k=1}^{N} a_k(t) \cdot l_k(t, i) \tag{3.17}$$

But if one considers the values of P_i^* only at the nodal points, Equation (3.17) becomes:

$$P(t, s_j) = \theta(t, s_j) \sum_{k=1}^{N} a_k(t) \cdot l_k(t, s_j) \tag{3.18}$$

Inserting Equation (3.18) into Equations (3.4) and (3.5), the following equations can be obtained:

$$
\begin{aligned}
\frac{da_1(t)}{dt} &= \frac{k_{p11} \frac{M}{V} \left(\frac{C^*}{V} - \frac{\left[\theta(t, s_1) \sum_{k=1}^{N} a_k(t) l_k(t, s_1) \right]}{V} \right) V}{\theta(t, s_1)} \\
&= \frac{k_{p11} \frac{M}{V} \left(\frac{C^*}{V} - \frac{\left[\theta(t, s_1) a_1(t) \right]}{V} \right) V}{\theta(t, s_1)}
\end{aligned}
\tag{3.19}
$$

$$\frac{da_j(t)}{dt} = k_{p11} \frac{M}{V} \left\{ \frac{\left[\theta(t, s_j - 1) \sum_{k=1}^{N} a_k(t) l_k(t, s_j - 1) \right]}{V} - \frac{\left[\theta(t, s_j) a_j(t) \right]}{V} \right\} V \tag{3.20}$$

where j ranges from 2 to N.

As commented before, the reference function $\theta(i)$ should be as close as possible to the true distribution in order to improve the precision of the solution. As the investigation regards the application of the adaptive orthogonal collocation method in

polymerization problems, the reference function is frequently admitted to be the Flory distribution, which depends on the parameter q, calculated as:

$$q = (\mu_1 - \mu_0)/\mu_1$$

$$\theta(i) = (1 - q)\left[q^{(i-1)}\right] \qquad (at\ t = 0) \qquad (3.21)$$

The ODE system (Equations (3.19) and (3.20)) must be integrated in time interval $[t_0, t_1]$, resulting in new values for a_j ($\forall\ j = 1, N$). Thus, if $\left|a_j(t_1) - a_j(t_0)\right| > tol, \forall\ j \in (1, N)$, the collocation points, Lagrange polynomial, reference function and coefficients a_j have to be updated. The assumption is that the MWD (and, therefore, the approximating coefficients) should not be allowed to vary too much before adaptation, to keep the numerical approximation sufficiently accurate.

Possible ways to update the reference function includes (i) update parameters of the weighting function (admitted to be the distribution of Flory); or (ii) take the distribution calculated so far as the new reference function (*leading to the complete adaptive orthogonal collocation procedure*). Thus:

$$q^n = \frac{\mu_1(t) - \mu_0(t)}{\mu_1(t)}$$

$$\theta^n(i) = (1 - q^n)\left[q^{n(i-1)}\right] \qquad \left(\begin{array}{c} Alternative\ (i):\\ update\ the\ parameters\ of\ the\ weighting\ function \end{array}\right)$$

or

$$\theta^n(i) = \theta(i) \cdot \sum_{j=1}^{N} a_j(t) \cdot l_j(i) \qquad \left(\begin{array}{c} Alternative\ (ii):\\ update\ the\ full\ weighting\ function \end{array}\right)$$

Obviously, if one believes that the Flory distribution is not appropriate (and in this problem it is not, because the known analytical solution is the Poisson distribution (HINES et al., 2003)), then alternative (ii) should be chosen. In practice, a usual procedure is to define some critical time t_c below which alternative (i) is chosen, and above which alternative (ii) is selected.

Even so, regardless whether either alternative (i) or alternative (ii) has been chosen, every time the reference function is updated, new nodal points must be

calculated, also imposing the adaptation of the approximation coefficients in the form of Equation (3.22).

$$a_j^n = \frac{\theta(s_j^n) \sum_{k=1}^{N} a_k l_k(s_j^n)}{\theta^n(s_j^n)}$$ (3.22)

When alternative (ii) is chosen, the new coefficients will naturally be equal to 1 at the new nodal points, i.e., $a_j^n(t) = 1 \, \forall \, j \in (1, N)$, since the new approximating function must coincide with the old approximating function at the new nodal points:

$$\tilde{u}^n(t, s_j^n) = \tilde{u}(t, s_j^n)$$
$$\varepsilon^n(t, s_j^n) = \varepsilon(t, s_j^n)$$
$$\theta^n(s_j^n) \cdot \sum_{k=1}^{N} a_k^n(t) \cdot l_k^n(s_j^n) = \theta(s_j^n) \cdot \sum_{k=1}^{N} a_k(t) \cdot l_k(s_j^n)$$ (3.23)
$$\theta^n(s_j^n) \cdot a_j^n(t) = \underbrace{\theta(s_j^n) \cdot \sum_{k=1}^{N} a_k(t) \cdot l_k(s_j^n)}_{\theta^n(s_j^n)}$$
$$a_j^n(t) = 1$$

After calculating the new nodal points, coefficients and reference function, they become the new state variables ($\forall \, j, k \in (1, N)$):

$$a_k = a_k^n$$ (3.24)
$$s_j = s_j^n$$ (3.25)
$$\theta(s_j) = \theta^n(s_j)$$ (3.26)

∗ The reference function just need to be calculated at nodal points

Then, Equations (3.19) and (3.20) can be integrated again along the next time interval $[t_1, t_2]$. If $|a_j(t_2) - a_j(t_1)| > tol, \forall \, j \in (1, N)$, then nodal points, reference function and coefficients should be updated once more. The process must be repeated until the simulation reaches the final polymerization time. An algorithm for this numerical procedure is presented in Figure 3.1.
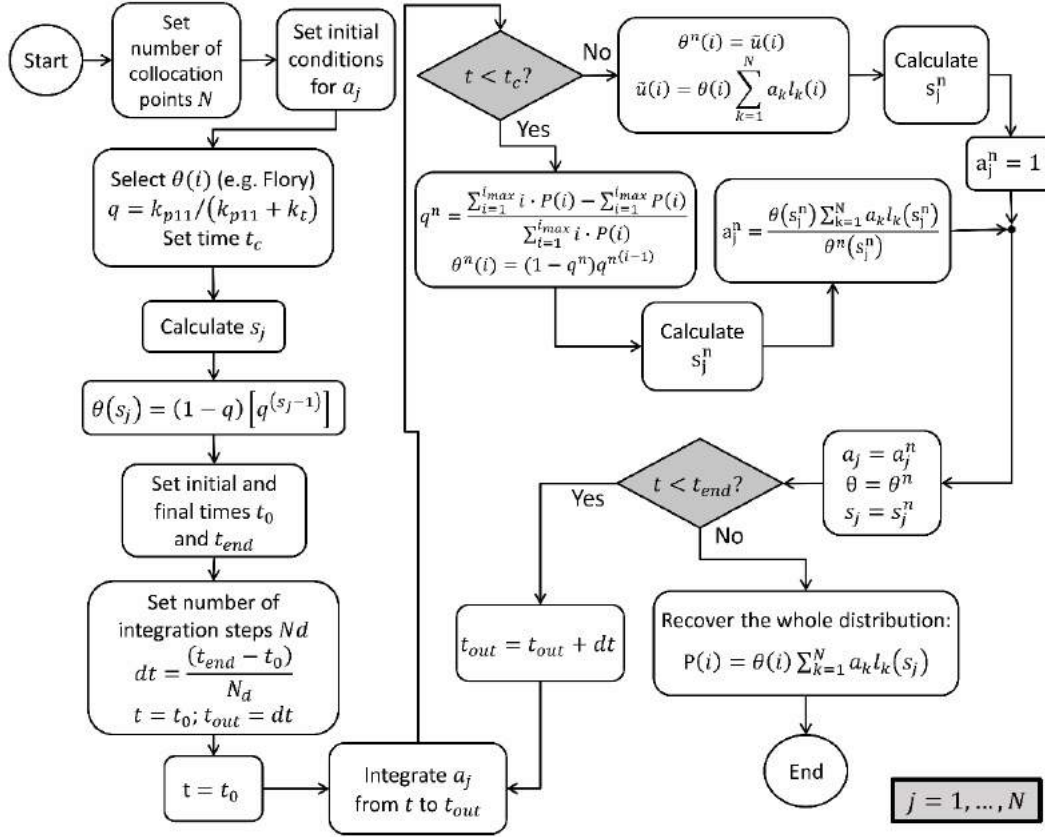
Figure 3.1 – Flowchart of the complete adaptive orthogonal collocation procedure.

3.3.2 Polynomial Approximation based on the Moments of the Distributions

When the polymerization mechanism does not lead to moment closure problems, the MWD can be calculated with the reference integration collocation procedure based on the moments of the distributions (NELE et al., 1999).

The true distribution $P(i)$ is unknown. Then, according to this method, the approximation for $P(i)$ can be written as:

$$P(i) = \theta(i) \cdot \sum_{k=1}^{N} a_k \cdot i^{k-1} \tag{3.27}$$

Again, the reference function $\theta(i)$ should be as close as possible to the true solution for improved accuracy. However, since the true solution is unknown, it is usual to admit that $\theta(i)$ follows a classical analytical distribution, such as the Schultz-Flory distribution function (Equation (3.21)).

51

The moment equations of the living chains are represented by Equations (3.6) to (3.8). Expanding P_i according to its definition, as shown in Equation (3.27), the following expressing can be obtained:

$$\mu_j = \sum_{i=1}^{\infty} i^j \cdot P(i) = \sum_{i=1}^{\infty} i^j \cdot \left(\theta(i) \sum_{k=1}^{N} a_k i^{k-1} \right) = \sum_{k=1}^{N} a_k \cdot \sum_{i=1}^{\infty} i^{j+k-1} \cdot \theta(i) \qquad (3.28)$$

In Equation (3.28), the inner sum is nothing more than the moment of order $j + k - 1$ of the reference function $\theta(i)$:

$$\mu_{\theta(j+k-1)} = \sum_{i=1}^{\infty} \theta(i) \cdot i^{(j+k-1)} \qquad (3.29)$$

Then, the moment of order j of $P(i)$ can be written as:

$$\mu_j = \sum_{k=1}^{N} a_k \, \mu_{\theta(j+k-1)} \qquad (3.30)$$

Writing Equation (3.30) for the first $N - 1$ moments of the distribution:

$$\underbrace{\begin{bmatrix} \mu_{\theta 0} & \mu_{\theta 1} & \cdots & \mu_{\theta N-1} \\ \mu_{\theta 1} & \mu_{\theta 2} & \cdots & \mu_{\theta N} \\ \mu_{\theta 2} & \mu_{\theta 3} & \cdots & \mu_{\theta N+1} \\ \cdots & \cdots & \cdots & \cdots \\ \mu_{\theta N-1} & \mu_{\theta N} & \cdots & \mu_{\theta\,2N-2} \end{bmatrix}}_{\mu_\theta} \cdot \underbrace{\begin{bmatrix} a_1 \\ a_2 \\ a_3 \\ \cdots \\ a_N \end{bmatrix}}_{a} = \underbrace{\begin{bmatrix} \mu_0 \\ \mu_1 \\ \mu_2 \\ \cdots \\ \mu_{N-1} \end{bmatrix}}_{\mu} \qquad (3.31)$$

which can be written in matrix form as:

$$\boldsymbol{\mu} = \boldsymbol{\mu_\theta} \cdot \boldsymbol{a} \qquad (3.32)$$

Now, as previously seen in Section 3.2, the method of moments can also be applied to allow for computation of moments for both the reference function $\theta(i)$ and

the proposed approximation $P(i)$. With the obtained solution, one can compute the coefficients $\boldsymbol{a}$ as:

$$\boldsymbol{a} = \boldsymbol{\mu}_\theta^{-1}\boldsymbol{\mu} \tag{3.33}$$

For better comprehension of the method, let the moments be defined in the proposed example as:

$$\frac{d\mu_k}{dt} = k_{p11} \cdot \frac{M}{V} \cdot C^* - k_{p11} \cdot \frac{M}{V} \cdot \mu_k + k_{p11} \cdot \frac{M}{V} \cdot \sum_{i=1}^{\infty}(i+1)^k P_i^* \tag{3.34}$$

Selecting four moments to be used in the polynomial approximation ($N = 4$), an additional expression for the third moment is needed, as described in Equations (3.6) to (3.8).

$$\frac{d\mu_3}{dt} = k_{p11} \cdot \frac{M}{V} \cdot C^* + k_{p11} \cdot \frac{M}{V} \cdot (3\mu_2 + 3\mu_1 + \mu_0) \tag{3.35}$$

Thus, after integrating the EDO system comprising Equations (3.6) to (3.8) and Equation (3.35) until the final polymerization time t_f, the first four moments of the distribution will be known at t_f. Then, the Flory coefficient q can be calculated as:

$$q = \frac{\mu_2 - \mu_1}{\mu_2} \tag{3.36}$$

Finally, matrix $\boldsymbol{\mu}_\theta$ can be build as shown in the following equation:

$$\boldsymbol{\mu}_\theta = \begin{bmatrix} \sum_{i=1}^{\infty} i^0(1-q)q^{i-1} & \sum_{i=1}^{\infty} i^1(1-q)q^{i-1} & \sum_{i=1}^{\infty} i^2(1-q)q^{i-1} & \sum_{i=1}^{\infty} i^3(1-q)q^{i-1} \\ \sum_{i=1}^{\infty} i^1(1-q)q^{i-1} & \sum_{i=1}^{\infty} i^2(1-q)q^{i-1} & \sum_{i=1}^{\infty} i^3(1-q)q^{i-1} & \sum_{i=1}^{\infty} i^4(1-q)q^{i-1} \\ \sum_{i=1}^{\infty} i^2(1-q)q^{i-1} & \sum_{i=1}^{\infty} i^3(1-q)q^{i-1} & \sum_{i=1}^{\infty} i^4(1-q)q^{i-1} & \sum_{i=1}^{\infty} i^5(1-q)q^{i-1} \\ \sum_{i=1}^{\infty} i^3(1-q)q^{i-1} & \sum_{i=1}^{\infty} i^4(1-q)q^{i-1} & \sum_{i=1}^{\infty} i^5(1-q)q^{i-1} & \sum_{i=1}^{\infty} i^6(1-q)q^{i-1} \end{bmatrix} \tag{3.37}$$

Then matrix $\boldsymbol{\mu}_\theta$ is inverted, originating matrix $\boldsymbol{\mu}_\theta^{-1}$. The polynomial coefficients are then calculated with Equation (3.33). Finally, the full MWD can be calculated by using Equation (3.27).

3.4 Deterministic Methods Applied in Coordination Polymerization Problems with LCB

Several works dedicated efforts to understand how LCBs are formed in ethylene and propylene homopolymerizations (HAMIELEC and SOARES, 1997; BEIGZADEH et al., 1999; YIANNOULAKIS et al., 2000; IEDEMA et al., 2004a, 2004b; MEHDIABADI and SOARES, 2012; MOGILICHARLA et al., 2014). YIANNOULAKIS et al. (2000) developed a dynamic model for calculation of the molecular weight and long chain branching distributions in ethylene polymerizations performed with metallocene catalyst. The authors used a numerical fractionation method (PLADIS and KIPARISSIDES, 1998) to simulate the MWD of the branched polymer. The numerical fractionation method assumes that the final MWD is the sum of the MWD produced at each time interval, weighted by the respective polymer yields. However, the MWD is computed with help of analytical approximate solutions at each time interval (TEYMOUR and CAMPBELL, 1994). IEDEMA et al. (2004a) used a Galerkin finite element model to predict the bimodal size distribution of PE produced with a mixed metallocene system and also applied a Monte Carlo method to simulate the branched architectures of these types of polymers (IEDEMA et al., 2004b). MOGILICHARLA et al. (2014) proposed a model to describe propylene polymerizations with LCB formation using a twin catalyst system. Their model successfully predicted the experimental evolution of molecular weights and grafting density.

FERREIRA Jr. et al. (2010) developed a mathematical model that simultaneously considered the generation of LCBs through macromonomer reincorporation and short-chain branches (SCB) by chain walking. The chain walking mechanism assumes that the active carbon site of the living chain can change (or walk) during the chain growth (SIMON et al., 2000). The authors also assumed that the rate of macromonomer incorporation increased with the number of pendant double bonds present in the macromonomer. Model predictions were compared with experimental data for ethylene polymerizations performed with a nickel catalyst and for 1,3-butadiene

polymerizations performed with a neodymium catalyst. The authors assumed a dual site system, but their model could be extended to catalysts with a higher number of sites. The authors claimed that the model fitted the experimental data adequately, but their model was complex, with 4 independent dimensions (chain length, LCBs, unsaturated double bonds, and active center placed at moving carbons on the polymer chain), and several kinetic reaction steps.

Nevertheless, only few publications proposed mathematical models to describe the polymerization kinetics and microstructure of olefin-diene branched copolymers (NELE et al., 2003; DIAS and COSTA, 2007; GUZMÁN et al., 2010). NELE et al. (2003) investigated the evolution of MWD and LCB distributions for olefin-diene copolymerizations performed in semi-batch reactors with help of a mathematical model. The authors included ring and LCB formations in their mechanism, and assumed that the reactivity of the macromonomer was proportional to the number of double bonds in the polymer backbone. Their model showed that, when diene is copolymerized with ethylene and other α-olefins, highly branched polymers can be produced in a controlled manner, and suggested that low diene concentrations should be used to produce LCB polymers in industrial polymerization reactors. Their simulation studies, however, were not supported by experimental data. DIAS and COSTA (2007) studied the coordination polymerization of two mono-vinyl monomers and a non-conjugated diene under semi-batch operation. The authors proposed a kinetic method that took into account crosslinking and long-chain branching and used generating functions to solve the mathematical model. Their model was able to predict the microstructure and molecular size of non-linear terpolymers before and after gelation. Gelation regards the formation of a hyper-branched tri-dimensional structure that leads to polymer precipitation. Generally, gelation takes place when the average molecular weights grow significantly and approach infinity. GUZMÁN et al. (2010) developed an analytical model to simulate the onset of gel formation in ethylene/1-octene/1,9-decadiene terpolymerizations using CGC catalysts. They produced polymer resins in a continuous stirred-tank reactor and validated the model predictions for polymer properties, beginning of gel formation and reactor fouling. Their model was shown to be a useful tool to prevent unintended reactor fouling during the duration of the experimental campaign.

3.5   Concluding Remarks

Based on the information provided in Chapter 3, it can be said that efficient deterministic strategies were devised in order to avoid solving an excessively large number of equations. Among these strategies, Chapter 3 presented the method of moments and two MWD interpolation methods (Orthogonal Collocation and Polynomial Approximations based on the Moments of the Distributions).

The method of moments is very useful and popular in polymerization applications, but it can only provide average properties. On the other hand, MWD interpolation methods can build the whole molecular weight distribution, but require additional implementation and CPU time.

When the polymerization mechanism does not lead to moment closure problems, the use of polynomial approximation based on the Moments of the Distributions constitutes a good alternative since it is much simpler than Orthogonal Collocation.

Orthogonal Collocation is a very efficient method to model MWDs but it depends on the selection of the reference function to work properly. In some cases, it is required to update the reference function during the simulation, leading to the adaptive orthogonal collocation procedure.

4 Monte Carlo Methods

4.1 Summary

This chapter presents the basis of Monte Carlo methods and discusses works that applied this technique in problems of coordination polymer reaction engineering. Additionally, variations of Monte Carlo algorithms are presented and their implementations are discussed.

4.2 Introduction

Monte Carlo (MC) methods apply random numbers to select one event among a set of possible outcomes. Events are selected according with probabilities calculated from macroscopic or microscopic parameters. MC methods can be employed in most fields of the natural sciences and engineering. For instance, these methods find several applications in polymer science and engineering (MEIMAROGLOU and KIPARISSIDES, 2014), being used to simulate polymer microstructural properties that are difficult or impossible to obtain with other modeling techniques (SOARES and HAMIELEC, 2007; BANNISTER et al., 2009). This is arguably the most important advantage of the MC approach in polymer science and engineering.

In polymer reaction engineering, MC methods can be used to model the degree of polymerization, comonomer sequence length distribution, short and long-chain branching, crosslinking density, terminal group functionality, and other polymer microstructural features. These properties are usually hard to predict using other mathematical methods, and even harder to measure (MOHAMMADI et al., 2005). MC methods can be applied to multicomponent non steady-state copolymerizations, for which conventional modeling methods require a high level of sophistication, and often use questionable simplifying assumptions (NAJAFI et al., 2007). If sufficient computational power is available, the applications of MC simulation are limitless (MAAFA et al., 2007).

The principles of MC modeling are easy to grasp. Let us consider a rather simple example: the integration of the function $y = x^3$ in the interval [0,1]. In this case, the event is the generation of points in the x-y plane, and the decision to be made is whether

these points fall below or above the $y = x^3$ curve. Figure 4.1 shows a flowchart for this MC algorithm.
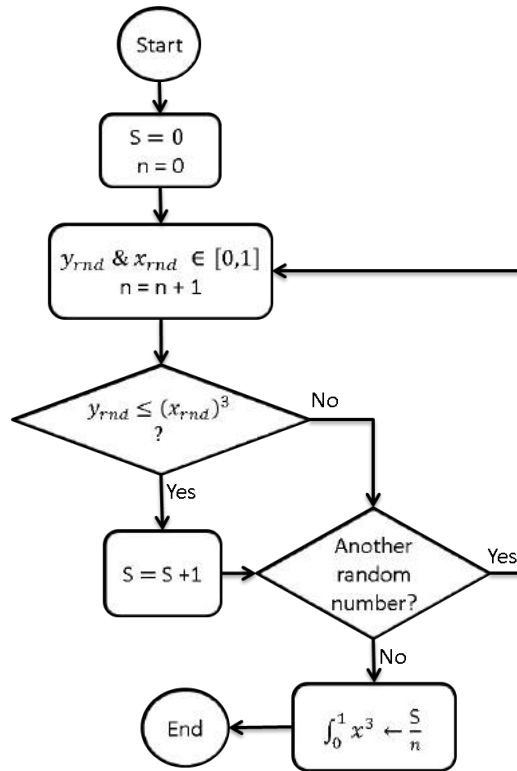
Figure 4.1 – Monte Carlo algorithm to estimate the value of $\int_0^1 x^3 dx$.

The variables y_{rnd} and x_{rnd} are random numbers generated from a uniform distribution in the interval [0,1]. When a point defined by the coordinates (x_{rnd}, y_{rnd}) is generated, the algorithm checks whether it falls below the $y = x^3$ curve. The variable n counts all points generated in the simulation, while the variable S sums how many of them fall under the $y = x^3$ curve. The integral is estimated as the ratio S/n. Figure 4.2 shows that the quality of the estimate depends on the number of generated points. When 50 random points are used, the estimate for $\int_0^1 x^3 dx$ is 0.129, far from the analytical value of 0.25; when 3000 points are used, however, the value estimated for the integral is 0.248, which is a good approximation of the analytical solution for this integral.

Even though this example is extremely simple, it demonstrates two of the defining features of all MC simulations: 1) events are selected based on the generation of random numbers, and 2) simulation results are better when more events are generated.

58
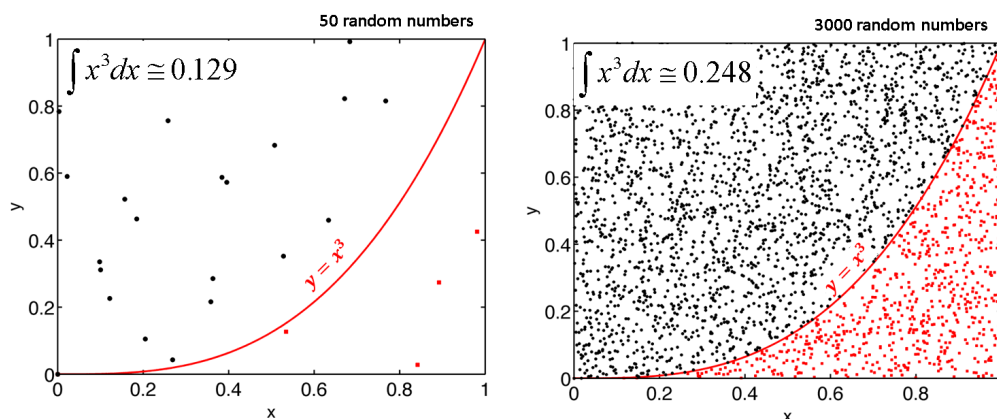
Figure 4.2 – Numerical Monte Carlo integration of $\int_0^1 x^3 dx$ with 50 (left) and 3000 (right) random points.

For polymerization, the events could be, for example, monomer propagation or chain transfer. By selecting propagation, the MC algorithm would build polymer chains, one monomer at a time, tracking the formation of a polymer population under a set of polymerization conditions. As the polymerization mechanism becomes more complex, for instance by including termination, long and short chain branch formation, and crosslinking steps, other probabilities must be associated with the additional events, but the rationale behind the MC model remains the same.

4.3 Steady-State Monte Carlo Methods

Steady-state polymerizations are easy to simulate with MC algorithms. Most of the steady-state MC models have been used to describe olefin polymerizations, as commercial polyolefins are produced in continuous reactors operated at steady state.

SOARES and HAMIELEC (1997) and BEIGZADEH et al. (1999a) developed the first MC models to describe the long chain branch (LCB) distribution of polyethylene made with single-site coordination catalysts. Even though their manuscripts applied constrained geometry catalysts (CGC), their approach is valid for any single-site catalyst that follows the same polymerization mechanism. In coordination polymerization, LCBs are formed by terminal branching: polymer chains with terminal double bonds (or macromonomers) are incorporated into growing polymer chains in a way that is similar to a copolymerization step (SOARES and HAMIELEC, 1996; WOO et al., 1997). SOARES and HAMIELEC (1996) used MC simulations to prove the analytical solution provided for the joint distribution of chain

length and LCB. BEIGZADEH et al. (1999a) extended their original model to classify the LCBs as comb or dendritic (or branches-on-branches), as illustrated in Figure 4.3. Particularly, BEIGZADEH et al. (1999a) showed that terminal branching can widen the chain length distribution (CLD) towards higher chain lengths, leading to significant deviations of the Schultz-Flory distribution. The authors also showed that, after a certain characteristic chain length, all chains have LCBs. After even higher size values, all chains have dendritic LCB topology. The authors suggested that the presence of hyper-branched, high molecular weight chains might be responsible for enhancing the rheological properties of polyethylene resins that contain LCBs.

(a)   (b)
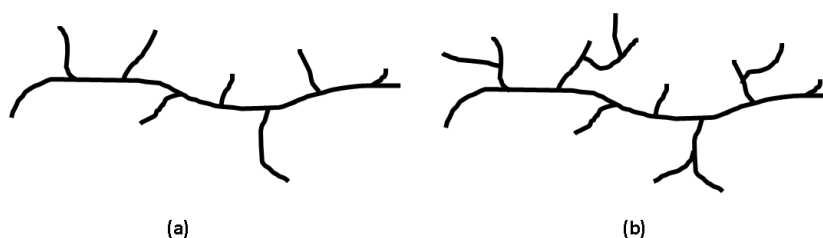
Figure 4.3 – LCB structures for polyethylene made with single-site catalysts: (a) comb, (b) dendritic (branches-on-branches) (adapted from BEIGZADEH et al., 1999a)**.**

SIMON and SOARES (2002) extended the MC model proposed by BEIGZADEH et al. (1999) to LCB formation when two catalysts are employed. They considered that one catalyst produced polyethylene with LCBs (branching catalyst) while the other one produced only linear chains (linear catalyst).

Later, BEIGZADEH (2003) modified the previous MC model (BEIGZADEH et al., 1999) to simulate the polymerization of ethylene with LCBs using different dual-site catalysts in a continuous stirred tank reactor (CSTR), including cases when both catalysts generated and reincorporated macromonomers.

HAAG et al. (2003) extended the model of SIMON and SOARES (2002) to describe the molecular structure of graft-block thermoplastic elastomers. These polymers are formed by the coordination copolymerization of amorphous backbones and semi-crystalline macromonomers. The LCBs, formed via macromonomer incorporation, create semi-crystalline domains that act as physical crosslinks between the amorphous backbones. They applied the model to map the branching topologies of polypropylene (isotactic polypropylene chains grafted onto atactic backbones, aPP-g-iPP) and ethylene/α-olefin (polyethylene chains grafted onto ethylene/α-olefin

amorphous copolymers, PEαO-g-PE) elastomers. The MC model predicted the length, number, and crystallizability of free arms and inner segments. Figure 4.4 illustrates some of the morphological details captured by their model.
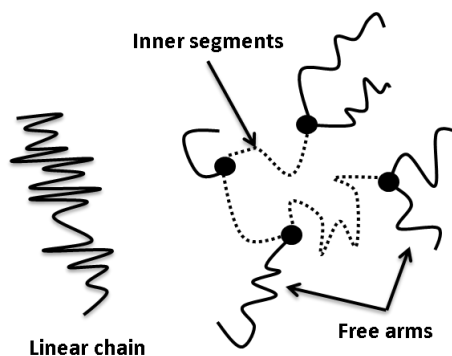
Figure 4.4 – Structural details of olefin branch-block elastomers (adapted from HAAG et al. 2003).

SIMON and SOARES (2005) further extended their model to classify polyolefin chains made with dual branching/linear catalyst systems into several distinct families. Chains were classified according to the number of LCBs: linear, 1LCB/chain, 2LCBs/chain and so on. Families with 3 LCB/chains or more were further subdivided into *members* with distinct LCB topologies

BEIGZADEH et al. (2001) applied a MC method to describe the fractionation of polyolefins by crystallization analysis fractionation (CRYSTAF). CRYSTAF fractionates semi-crystalline polymers according to their crystallizabilites in a batch solution process. The authors assumed that the longest crystallizable ethylene sequence in the chain determined when the chain would crystallize from solution. Copolymer chains generated with their MC algorithm were used to calculate the weight distribution of the longest crystallizable sequences in the sample. This distribution was then transformed into a crystallization temperature distribution using the Gibbs-Thompson equation.

COSTEUX et al. (2002) used a MC algorithm to simulate the polymerization of olefins with a single-site catalyst in a CSTR. They used two probabilities: propagation probability and monomer selection probability. These probabilities were calculated from the rates of four polymerization steps: monomer addition, macromonomer addition, transfer to a chain transfer agent or β-hydride elimination. Taking into consideration distinct chain segment types–linear chains, free arms and inner segments–the authors represented the topology of long-chain branched polyethylenes with help of an elegant

61

ternary diagram. The authors proposed a modification of the MC algorithm, by considering that the length of the segments between branch points obeys the Schultz-Flory distribution. Instead of adding one monomer at time during the simulation, segments that followed the Schultz-Flory distribution were added during the propagation events. This enhanced MC algorithm leads to results that are statistically equivalent to those obtained with the traditional MC method, but requires shorter computation times, since whole polymer segments between branching points are simulated in a single step.

COSTEUX (2003) extended this model for branched polyethylenes made with a mixture of single-site catalysts. The melt rheological behavior in shear and extensional flows were estimated qualitatively, using the topological information obtained via MC simulation. COSTEUX et al. (2002) also continued the investigation initiated by BEIGZADEH et al. (2001) to model CRYSTAF and temperature-rising elution fractionation (TREF) using MC techniques.

ALSHAIBAN and SOARES (2011) modified their previous MC model (ALSHAIBAN and SOARES, 2009) to describe the microstructure of polypropylene produced with single-site and Ziegler–Natta catalysts, including the reversible site transformation from the aspecific state to the stereospecific state by external electron donors (Do), as shown in Figure 4.5. The authors simulated propylene polymerization in steady-state and dynamic reactors. The MC model described how molecular weight distributions, average molecular weights and tacticity of the resins answered to changes in concentrations of hydrogen, external donors, and propylene during the polymerization. Interestingly, the developed model was used to predict the ^{13}C NMR spectra of polypropylene synthesized under different polymerization conditions.
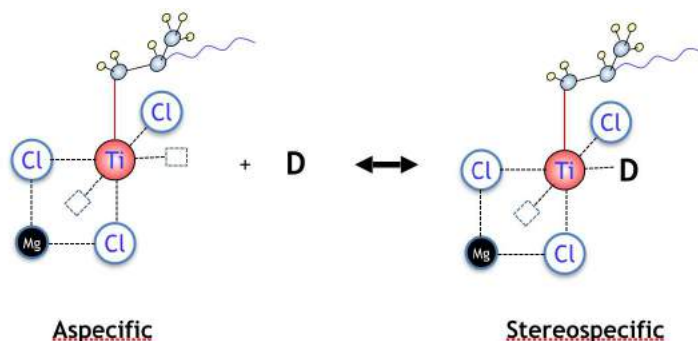
Figure 4.5 – Aspecific to stereospecific TiCl$_4$/MgCl$_2$ site transformation via reversible donor complexation (adapted from ALSHAIBAN and SOARES, 2009).

MADKOUR and MARK (1995) used MC simulations to model the stereoregularity and crystallinity of poly[methyl(3,3,3-trifluoropropyl)siloxane. The simulations generated representative monomer sequences that were used to study the packing of such sequences into crystalline regions. MADKOUR and MARK (1997) used MC algorithms to relate microstructure to polymer crystallinity for isotactic polypropylene. NELE et al. (2000) used the method of MADKOUR and MARK (1997) to relate crystallinity to polymerization conditions for polypropylene made with fluxional metallocene catalysts. In a later work (NELE et al., 2001), the same research group developed a general kinetic model for these systems, which was used to deduce the fundamental behavior of individual catalysts. MADKOUR and MARK (1998) also applied MC methods to model the microstructure of stereoblock polypropylene chains.

ANANTAWARASKUL et al. (2012) used MC methods to simulate the formation of linear olefin block copolymers (OBCs) via chain shuttling polymerization in steady-state and dynamic systems (TONGTUMMACHAT et al., 2016).

DRACHE and SCHMIDT-NAAKE (2007) studied styrene polymerization with benzyl dithiobenzoate as a RAFT agent. RAFT initialization included pre-equilibrium and main-equilibrium steps. In the pre-equilibrium step, a growing macroradical is inserted into the sulfur-carbon double bond of the initial dithioester compound (RAFT), producing a carbon-centered intermediate radical that suffers β-scission reactions to either yield back the reactants or to form an initiating radical $R^{\bullet}$ and a polymeric dithioester compound (polyRAFT). The main equilibrium consists of analogous reactions, in which a polymeric RAFT agent (polyRAFT) reacts with a growing macroradical, producing an intermediate radical that suffers subsequent β-scission reactions, either forming the reactants or generating a growing macroradical and a RAFT agent. These chain transfer events induce equilibrium between dormant and living chains (Figure 4.6) (DRACHE et al., 2005).

DRACHE et al. (2005) used two coefficients, C_{tr} ($C_{tr} = k_{tr}/k_p$) and C_{-tr} ($C_{-tr} = k_{-tr}/k_i$), to describe the reaction path of the propagating radical and the leaving group during the initialization of RAFT reaction. These coefficients were estimated by MC simulation, which could be regarded as a novelty, since MC simulations, due to their long computation times, are seldom used to estimate model parameters.
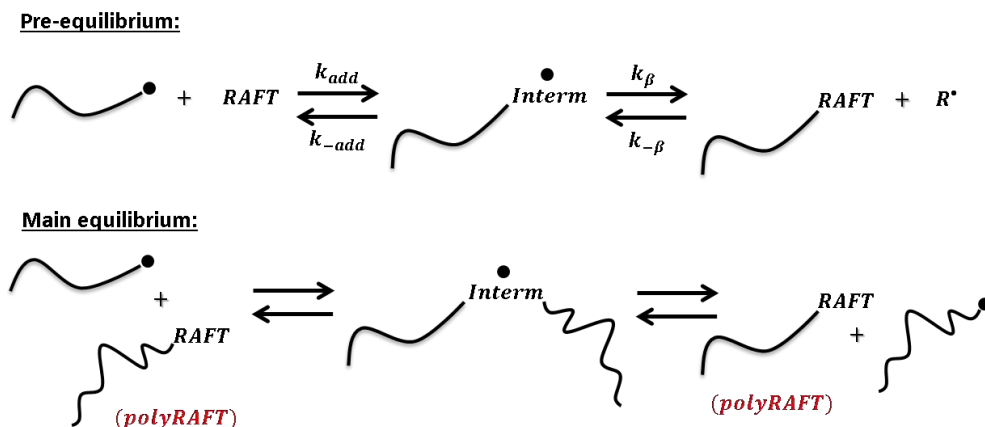
Figure 4.6 - Basic reaction steps during RAFT polymerization (adapted from DRACHE et al., 2005).

DRACHE and SCHMIDT-NAAKE (2008) also simulated the initialization period of RAFT agents with different leaving groups (benzyl dithiobenzoate (Bz-DB), 1-phenylethyl dithiobenzoate (PhEt-DB) and cumyl dithiobenzoate (C-DB)) for the bulk polymerization of styrene.

SANTOS et al. (2007) proposed a stochastic model to simulate the distribution of branches in poly(1-hexene)s synthesized with α-diimine nickel catalysts. Their model was able to predict the formation of methyl, butyl and longer chain branches. The information about polymer microstructure provided by their model can be useful in molecular simulation investigations to determine the conformational properties based on the Monte Carlo and molecular dynamics techniques.

4.4 The Chemical Master Equation (CME)

The chemical master equation (CME) is the starting point for the discussion of dynamic MC techniques. Even though the CME is usually hard to solve, most dynamic MC methods rely on the CME methodology to describe chemically reacting systems.

The number of molecules of each component in a homogeneous reacting chemical system defines its state. According to GILLESPIE (1992), the time evolution of this state cannot be treated as a deterministic problem because chemical reactions are intrinsically stochastic. The following assumptions are used to model the stochastic nature of chemically reacting systems (GILLESPIE, 1992; MACQUARRIE, 1967):

- The system is homogeneous, in thermal equilibrium, and has fixed volume.

- Considering N species {S_1, …, S_N}, the system is described by a set of states along time {$\mathbf{X}(t) = [X_1(t), …, X_N(t)]^T$}, where each $X_i(t)$ represent the number of molecules of specie S_i in the system at time t.

- There are *M* reaction types in the system, {R_1, R_2, …, R_M}.

- The dynamics of these *M* reactions are characterized by *M propensity functions* {$a_1(X)dt$,…, $a_M(X)dt$}.

- A state change vector $\mathbf{v}_j = \{v_{1j}, …, v_{Nj}\}$ is associated to each reaction type *j*. The parameter v_{ij} is the number of molecules of each species *i* that are formed or consumed by reaction path *j* in the analyzed time interval, considering the two possible states.

State changes are considered to be Markov processes (CAO and CHEN, 1997). The future state of a Markov process can be predicted based only on its present state, independently of anything that has happened in the past. *All polymerizations are Markov processes.*

Each *propensity function* is associated to one reaction type and is calculated as the product of the microscopic reaction rate constant and the number of feasible ways the reaction may occur (MCCOLLUM et al., 2006). Propensity functions are reaction frequencies for the elementary steps involved in a reaction mechanism.

The probability that the system will be at state **X** at time *t* is given by the CME:

$$\frac{\partial P(\mathbf{X}, t | \mathbf{X}_0, t_0)}{\partial t} = \sum_{j=1}^{M} \left[a_j(\mathbf{X} - \mathbf{v}_j) P(\mathbf{X} - v_j, t | \mathbf{X}_0, t_0) - a_j(\mathbf{X}) P(\mathbf{X}, t | \mathbf{X}_0, t_0) \right] \qquad (4.1)$$

The CME is a system of linear ordinary differential equations (ODE), with one ODE for each possible state. The function $P(\mathbf{X}, t | \mathbf{X}_0, t_0)$ is the probability that the system will be at state **X** at time *t*, starting from state $\mathbf{X}_0$ at time t_0. The state vector **X** may vary over a large set of discrete values (HIGHAM, 2008).

In order to illustrate the CME, let us consider a reaction mechanism involving only three elementary steps,

R_1: $\qquad S_1 \xrightarrow{k_1} S_2$

R_2: $\qquad S_1 + S_2 \xrightarrow{k_2} S_3$

R_3: $\qquad\qquad S_3 \xrightarrow{\ k_3\ } \emptyset$
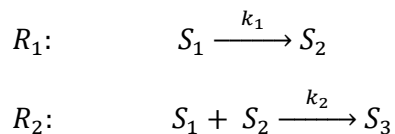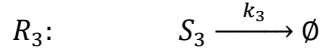
The state change vectors and the propensity functions for these reactions are shown in Table 4.1.

Table 4.1. **State change vectors and propensity functions for reactions R_1, R_2 and R_3.**

State Change Vectors	Propensity Functions[a]
$\mathbf{v}1 = [\text{-}1\ \ 1\ \ 0]T$	$a_1(X) = k_1 X_1$
$\mathbf{v}2 = [\text{-}1\ \ \text{-}1\ \ 1]T$	$a_2(X) = k_2 X_1 X_2$
$\mathbf{v}3 = [0\ \ 0\ \ \text{-}1]T$	$a_3(X) = k_3 X_3$

[a] k_i: microscopic reaction rate constants; X_i: number of reactant molecules in the system at a given state.

Let us start with K molecules of S_1 and no molecules of S_2 and S_3. The state vector at $t_0 = 0$ is,

$$X(0) = \begin{bmatrix} K \\ 0 \\ 0 \end{bmatrix} \qquad (4.2)$$

The state vector at time $t > t_0$ may assume many possible values, such as,

$$X(t) = \begin{bmatrix} K-1 \\ 1 \\ 0 \end{bmatrix}; \ X(t) = \begin{bmatrix} K-2 \\ 2 \\ 0 \end{bmatrix}; X(t) = \begin{bmatrix} K-2 \\ 1 \\ 1 \end{bmatrix}; X(t) = \begin{bmatrix} K-3 \\ 1 \\ 2 \end{bmatrix} \ldots \qquad (4.3)$$

Figure 4.7 illustrates this state transition process.
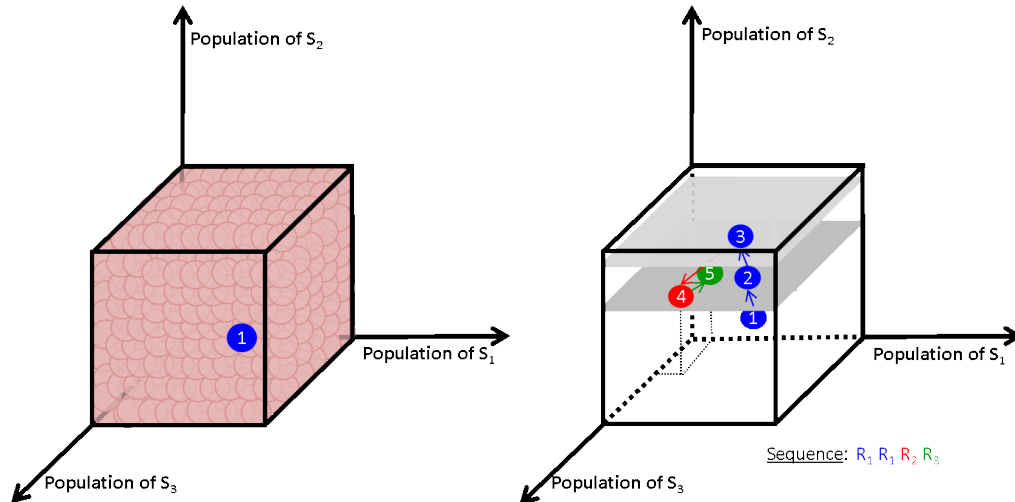
Figure 4.7 – Schematic representation of state changes due to chemical reaction.

The CME generates the entire probability distribution for a chemically reacting system. It is easy to compute a single realization of the state vector, but the complete solution of the CME can be very hard to obtain (GIBSON and BRUCK, 2000; DRAWERT et al., 2010). Monte Carlo algorithms offer a more efficient way to handle this problem, as described in the following sections.

4.5 Stochastic Simulation Algorithms (SSA)

GILLESPIE (1976; 1977) developed two exact stochastic simulation algorithms (SSA) that apply MC methods to simulate the Markov processes described by the CME: the Direct method (DM) and the First Reaction method (FRM). Instead of solving the CME to obtain the probability density function of the state vector $\mathbf{X}(t)$, the SSA obtains a random sample of $\mathbf{X}(t)$ (GILLESPIE, 2007). One finds results equivalent to solving the CME by averaging many realizations of the SSA (GILLESPIE, 2008).

The SSA simulates the time evolution of a chemically reacting system by updating the state vector according to the answers given to two questions (CAO et al., 2004):

➲ When will the next reaction occur?

➲ Which reaction will happen next?

In order to build the time trajectory for $\mathbf{X}(t)$, the following probability function has to be defined,

$p(\tau, j|X, t)d\tau$: probability that, given $X(t) = X$, the next reaction will occur within the time interval $[t + \tau, t + \tau + d\tau)$ and will be of type R_j. $\qquad$ (4.4)

If the system is at state X at time t, the probability density function in Equation (4.4) depends on two random variables: τ, the time when the next reaction will occur; and j, the index of the next reaction type. An exact formula for $p(\tau, j|X, t)$ was presented by Gillespie,

$$p(\tau, j|X, t) = a_j(X)exp(-a_0(X)\tau) \qquad (4.5)$$

where $a_0(X)$ is the sum of all propensity functions (or sum of all microscopic reaction rates),

$$a_0(X) = \sum_{j=1}^{M} a_j(X) \qquad (4.6)$$

Many exact MC methods can be applied to generate samples of the random variables τ and j. One of the simplest procedures is the *Direct Method*, as explained in the next section.

4.5.1 The Direct Method (DM)

In the *Direct Method* (DM), two random numbers r_1 and r_2, are sampled from a uniform distribution in the interval [0,1] to calculate the random variables τ and j,

$$\tau = \frac{1}{a_0(X)} \ln\left(\frac{1}{r_1}\right) \qquad (4.7)$$

$$\sum_{j'=1}^{j} a_{j'}(X) \geq r_2 a_0(X) \qquad (4.8)$$

where j is the smallest integer that satisfies Equation (4.8). Figure 4.8 is a graphical representation of how Equation (4.8) can be used.

$$a_1(X) < r_2 a_0(X) \leq \sum_{j'=1}^{2} a_{j'}(X)$$

$$0 \qquad a_1(X) \qquad a_1(X) + a_2(X) \qquad a_0(X) = \sum_{j=1}^{M} a_j(X)$$

(Reaction 2 is selected: j = 2)
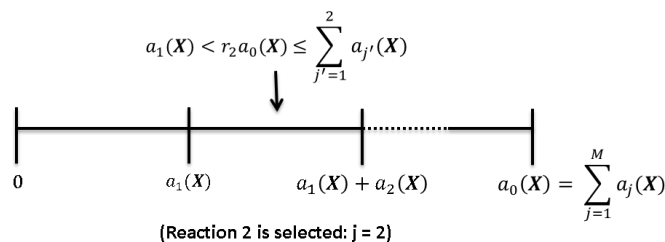
Figure 4.8 – Reaction selection in the SSA direct method.

The DM generates two random numbers: one to select the time increment τ, and the other to choose the reaction type j, that takes place within that time increment. The state vector is updated after each reaction step, and the process is repeated until the specified simulation time is reached. Figure 4.9 shows a flowchart for the DM.

1. Initialize time $t = t_o$ and system state $\mathbf{X} = \mathbf{X}_o$.

2. Calculate $a_j(\mathbf{X})$ $\{j = 1...M\}$ and their sum $a_o(\mathbf{X})$, Equation (4.6).

3. *Generate* values for τ using Equation (4.7), and for j using Equation (4.8).

4. *Execute* reaction j updating the state vector $\mathbf{X} \leftarrow \mathbf{X} + \mathbf{v}_j$ and $t \leftarrow t + \tau$.

5. *Record* $(\mathbf{X}, t)$ as desired. If t is lower than the final simulation time, return to step 2; else, stop simulation.
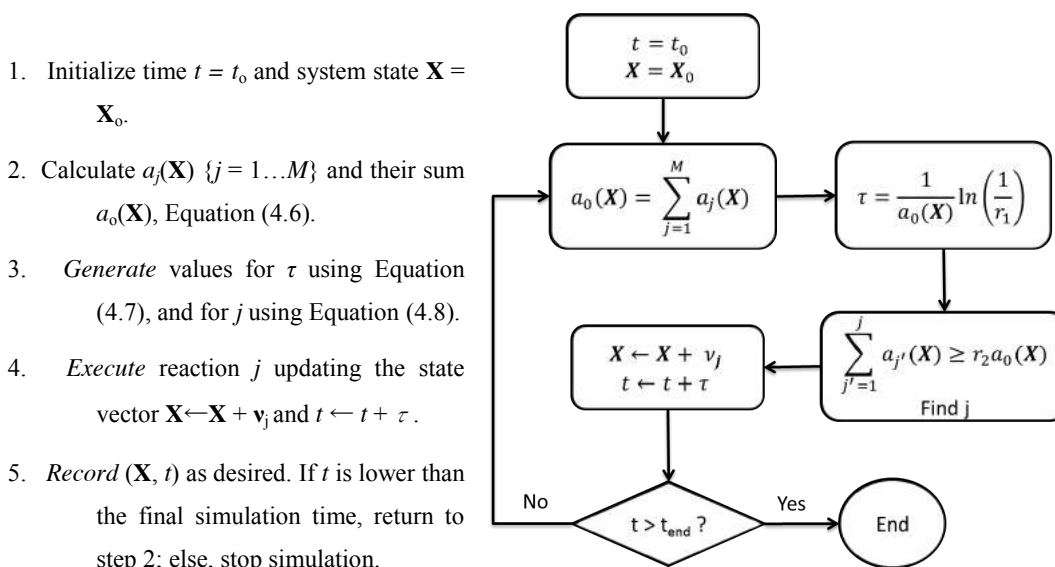
Figure 4.9 – Flowchart for the Direct Method.

The DM is simple to implement, even for reaction mechanisms with several elementary steps. Unfortunately, this method requires long computation times because of the term $\tau = 1/a_0(X)$, which can be very small when the number of at least one of the reactants is large (GILLESPIE, 2008). Simplicity is the main advantage of DM; long computational times is its biggest drawback.

4.6   Monte Carlo Reaction Rate Constants

Each polymerization step is assigned a MC reaction rate, also called propensity function, R_j^{MC}, with j varying from 1 to the total number of steps in the polymerization

69

mechanism. The MC reaction rates are defined with the help of microscopic rate constants, k^{MC},

$$R^{MC} = k^{MC} N_c \tag{4.9}$$

where N_c is the number of unique combinations between reactant molecules inside the control volume. The parameter N_c depends on how many molecules participate in the reaction, on the reaction order, and whether or not the reactants are of the same type (MAAFA et al., 2007).

The microscopic reaction rate constants k^{MC} can be calculated with the macroscopic reaction rate constants k^{exp}, as shown in Table 4.2 (MAAFA et al., 2007). Finally, Table 4.3 shows how to calculate MC reaction rates for unimolecular, bimolecular, and termolecular reactions for free-radical polymerization.

Table 4.2. **Conversion of macroscopic reaction rate constants into microscopic MC rate constants.**

Unimolecular reactions	$k^{MC} = k^{exp}$
Bimolecular reactions between different molecules	$k^{MC} = \dfrac{k^{exp}}{VN_A}$
Bimolecular reactions between equal molecules	$k^{MC} = 2\dfrac{k^{exp}}{VN_A}$
Termolecular reactions between equal molecules	$k^{MC} = 6\dfrac{k^{exp}}{V^2 N_A^2}$

N_A: Avogadro number.

Table 4.3. Definition of MC reaction rates.

Unimolecular reactions	$R^{MC} = k^{MC} X_i$
Bimolecular reactions between different molecules	$R^{MC} = k^{MC} X_i X_j$
Bimolecular reactions between equal molecules	$R^{MC} = k^{MC} X_i(X_i - 1)/2$
Termolecular reactions between equal molecules	$R^{MC} = k^{MC} X_i(X_i - 1)(X_i - 2)/6$

X_i, X_j: Number of molecules of reactants i and j in the control volume.

4.7 Control Volume Selection

Before starting the simulation, a suitable control volume, containing all reactants (monomer, free radicals, and living and dead polymer chains) must be selected. When the control volume is small, random fluctuations affect the accuracy of the simulation; when it is excessively large, computation times may be unacceptably long. Therefore, the size of the control volume has to be large enough to provide accurate results at acceptable computation times (AL-HARTHI et al., 2006), ensuring convergence of polymer properties (CHAFFEY-MILLAR et al., 2007).

4.8 SSA Applied in Coordination Polymerization Problems

The DM has been applied to several problems in polymer science and engineering, including free radical, living free radical and coordination polymerization systems. These investigations have broadened the understanding of these polymerization systems by predicting the dynamic evolution of several microstructural distributions under different polymerization conditions. A review on MC methods applied in polymer reaction engineering problems was presented by BRANDÃO et al. (2015). In the present work, focus will be given to discussion about MC techniques applied to coordination polymerization problems.

SOARES and HAMIELEC (2007) used MC simulations to validate a proposed analytical solution for the time evolution of the CLD of polyolefins made with coordination catalysts during short polymerization times. These conditions are encountered in stopped flow reactors (SFR), as the one shown in Figure 4.10. The authors assumed the polymerization mechanism described in Table 4.4 and used the algorithm shown in Figure 4.11. As the polymerization proceeds, the peak of the CLD of living chains moves towards higher chain lengths, "dragging" a tail with sorter chains produced by transfer reactions, as depicted in Figure 4.12.

Table 4.4. Polymerization mechanism proposed by SOARES and HAMIELEC (2007).

Elementary Step	Chemical Equations [a]	Reaction number
Initiation	$C^* + M \xrightarrow{k_p} P_1$	Reaction 1 (R1)
Propagation	$P_r + M \xrightarrow{k_p} P_{r+1}$	Reaction 2 (R2)
Transfer	$P_r + CTA \xrightarrow{k_t} C^* + D_r$	Reaction 3 (R3)
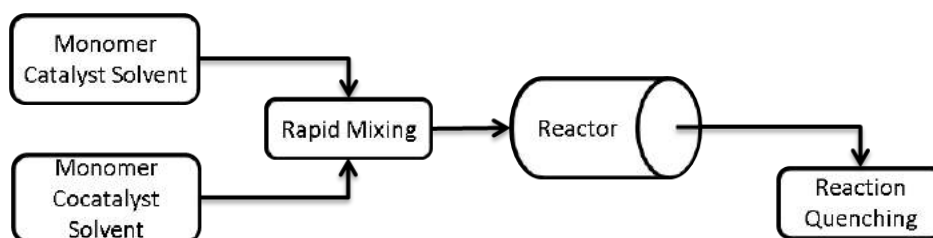
Figure 4.10 – Schematic diagram for a stopped-flow reactor.

The authors used dynamic CLDs to determine when the steady-state hypothesis became valid for chains of different lengths. Their MC model was extended to polymerizations with multiple-site catalysts under short polymerization times. They showed that the time required for the CLD to reach its fully developed shape depends on the types of active sites, even when the final CLD is the same.
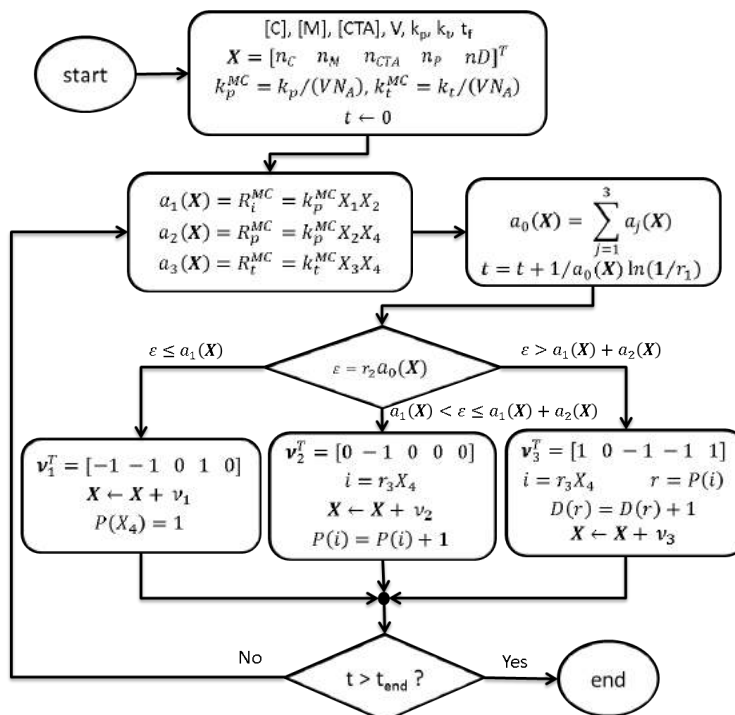
Figure 4.11 – **Monte Carlo simulation flowchart for dynamic olefin coordination polymerization. Vectors $P(i)$ and $D(i)$ store the length, r, of living and dead chains, respectively. The variables r_1, r_2, and r_3 are random numbers between [0,1] that follow a uniform distribution.**
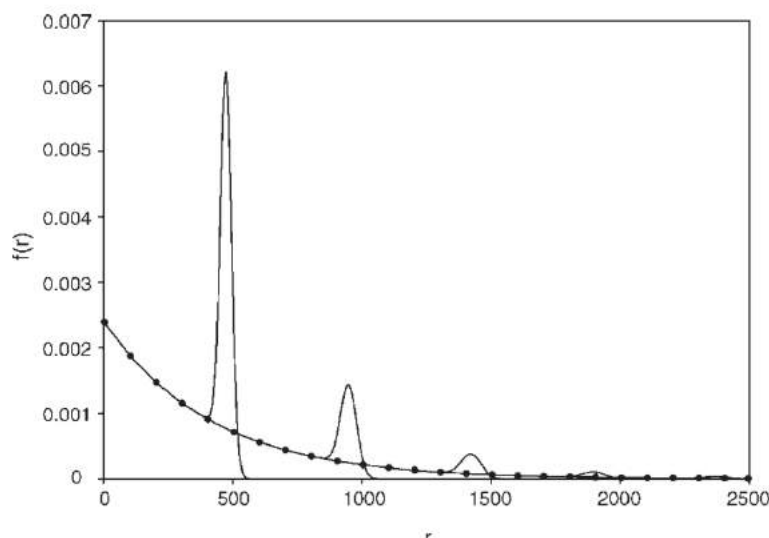
Figure 4.12 – **CLD of living polymer chains produced at 0.5, 1.0, 1.5, 2.0 and 2.5 s (from left to right). The Flory distribution is represented by the dotted line. Reproduced with permission from ref. (SOARES and HAMIELEC, 2007). Copyright 2007, John Wiley & Sons.**

SOARES and NGUYEN (2007) used a MC model to show how the common assumption of instantaneous catalyst activation, made in several articles that describe the use of SFR, could predict CLDs that were not observed experimentally. According to the authors, the non-instantaneous site activation could be associated to a slow (relatively to the residence time in the reactor) rate of site activation, although it could also be caused by mass transfer and mixing limitations. In a later article, SOARES and HAMIELEC (2008) investigated these effects in more details using MC models and analytical solutions.

SALAMI-KALAJAHI et al. (2009) used a MC model to describe how different active site types contributed to the polymerization of ethylene with a multiple site type Ziegler-Natta catalyst. They concluded that the molecular weight distribution of each active center follows a Schultz–Flory distribution. However, the total molecular weight distribution obtained by all catalyst centers together does not follow a Schultz–Flory distribution. The authors also concluded that the introduction of hydrogen does not mainly affect the polymerization kinetics.

KHORASANI et al. (2014) used a MC model to simulate the consecutive/simultaneous trimerization and polymerization of ethylene using two catalysts. Oligomers made by the oligomerization catalyst were copolymerized with ethylene by the polymerization catalyst. The authors applied their model to the reaction scheme suggested by ZHANG et al. (2008) and shown in Figure 4.13. Their model

predicted the instantaneous copolymer composition for several pre-trimerization times. Figure 4.14 shows that longer pre-trimerization times allowed for increase of the instantaneous 1-hexene consumption rates because 1-hexene was accumulated in the reactor before the onset of the copolymerization step. The copolymer also became more homogeneous due to the more uniform incorporation of 1-hexene molecules.
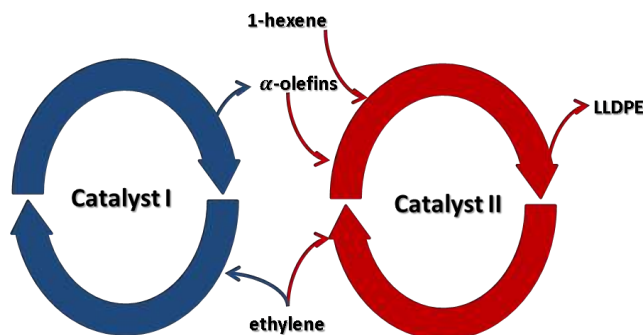
Figure 4.13 – LLDPE production by tandem catalysis: ethylene oligomerization to 1-hexene (Catalyst I) followed by copolymerization of ethylene and 1-hexene (Catalyst II).
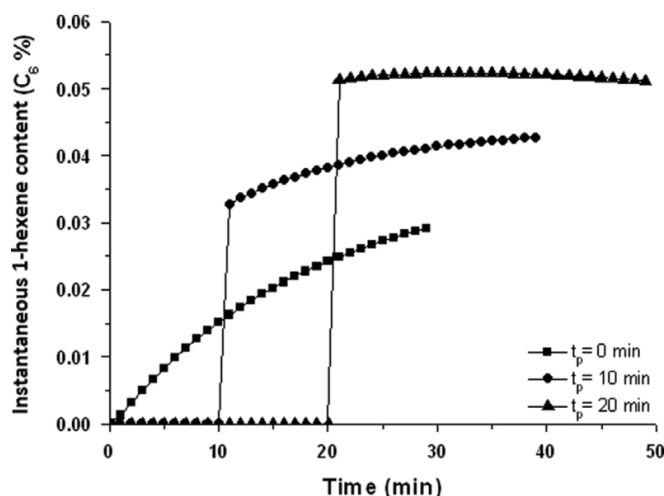
Figure 4.14 – **Instantaneous molar fraction of 1-hexene in the copolymer as function of the polymerization time at different pre-trimerization times (t_p). Reproduced with permission from ref. (KHORASANI et al., 2014). Copyright 2014, Elsevier.**

The pre-trimerization time also affected the average ethylene sequence length of the copolymer (Figure 4.15). Longer ethylene sequences were produced without pre-trimerization ($t_p = 0$), and significant copolymer composition drift was observed. The pre-trimerization time could, however, be used to control the average length of the ethylene sequences and uniformity of the copolymer composition.
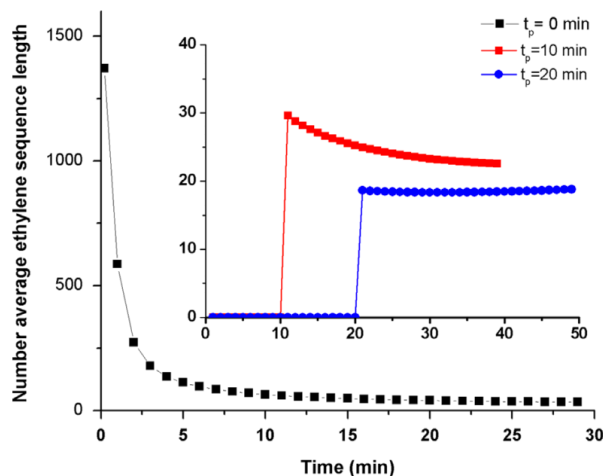
Figure 4.15 – **Evolution of the number average ethylene sequence length without (main plot) and with pre-trimerization (insert). Reproduced with permission from ref. (KHORASANI et al., 2014). Copyright 2014, Elsevier.**

ZHENGHONG et al. (2006) used MC simulations to investigate the polymerization of propylene and determine the effects of impurities on the polymerization kinetics. They found that the polymerization rate decreases with the increasing initial concentration of the impurity and after approximately 400 s of reaction, the impurity hardly affects the polymerization rate.

BRANDÃO et al. (2016) compared the performances of different dynamic MC methods to simulate olefin polymerization with coordination catalysts. These results will be discussed in Chapter 9 of the present thesis.

4.9 Variations of Monte Carlo Algorithms

As aforementioned, SSA is a specific class of exact MC methods and simulates one reaction event a time. For polymerizations, chains are built one monomer a time until chains stop growing through termination or transfer reactions. The first SSAs to be introduced in the literature were the Direct and the First Reaction methods (GILLESPIE, 1976). Although these methods are accurate, they also require long computational times. Attempts to improve the efficiency of the direct methods led to additional SSA techniques, such as the Next Reaction (GIBSON and BRUCK, 2000), Optimized Direct (CAO and PETZOLD, 2004), and Sorting Direct (MCCOLLUM et al., 2006) methods. Unfortunately, the computational times demanded by these methods may still make them unsuitable to simulate complex systems, such as polymerizations.

As a matter of fact, it may be necessary to sacrifice some of the accuracy of SSA methods to shorten the simulation time. One of these compromising techniques is the τ-Leaping method (CAO et al., 2005; 2006). Instead of moving from one reaction event to the next one, the τ-Leaping method 'leaps' during the system history from one time subinterval to the next, executing many reactions in the same subinterval as shown in Figure 4.16.
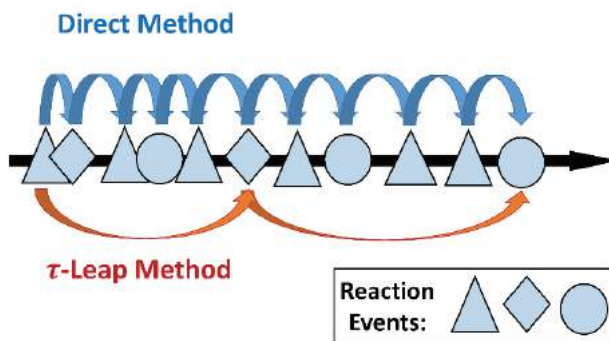
Figure 4.16 – Schematic comparison between the DM and τ-Leaping method.

The applications of DM, FRM, NRM and τ-Leaping methods will be explained below with the simple polymerization mechanism proposed by SOARES and HAMIELEC (2007) to simulate the polymerization of ethylene, using a single-site catalyst in a stopped-flow reactor (Table 4.4). However, the rate constant for chain initiation was assumed to be different from the rate constant for propagation.

4.9.1 Direct Method (DM)

The DM is the most straightforward method among all SSA techniques. A random number is used to select which reaction will take place at a given time interval (also determined at random), and the number of reactants and products are updated accordingly. The process is iterated until it reaches the final polymerization time.

Figure 4.17 shows the flowchart of the basic DM algorithm. Figure 4.18 lists the computation steps needed to simulate the polymerization mechanism presented in Table 4.4 using the DM.

Figure 4.17 – Flowchart for the Direct Method algorithm.

1 Initialize time: $t = t_o$.

2 Initialize the number of molecules of each species in the control volume, represented by the system state vector $(\mathbf{X} = \mathbf{X}_o)$ which represents the number of molecules in the control volume.

$$\begin{bmatrix} Monomer\ (M) \\ Chain\ transfer\ agent\ (CTA) \\ Living\ polymers\ (P) \\ Catalyst\ (C^+) \\ Dead\ polymers\ (D) \end{bmatrix} = \begin{bmatrix} X_1 \\ X_2 \\ X_3 \\ X_4 \\ X_5 \end{bmatrix}_0$$

Create vectors $\mathbf{P}$ and $\mathbf{D}$ to save the length of each chain. All positions in these two vectors receive value 0 because there are none living or dead chain at time t_o.

3 Convert the macroscopic reaction rate constants into microscopic MC rate constants:

MC rate constant for R1: $k_i^{MC} = \dfrac{k_i^{exp}}{VN_A}$

MC rate constant for R2: $k_p^{MC} = \dfrac{k_p^{exp}}{VN_A}$

MC rate constant for R3: $k_t^{MC} = \dfrac{k_t^{exp}}{VN_A}$

4 Calculate MC reaction rates, $a_j(\mathbf{X})$ $\{j = 1 \dots M\}$:

MC reaction rate for R1: $a_1(\mathbf{X}) = k_i^{MC} X_1 X_4$

MC reaction rate for R2: $a_2(\mathbf{X}) = k_p^{MC} X_1 X_3$

MC reaction rate for R3: $a_3(\mathbf{X}) = k_t^{MC} X_2 X_3$

5 Calculate the sum of all MC reaction rates $a_0(\mathbf{X})$:

$$a_0(\mathbf{X}) = a_1(\mathbf{X}) + a_2(\mathbf{X}) + a_3(\mathbf{X})$$

6 Generate a value for the time step τ:

$$\tau = \frac{1}{a_0(\mathbf{X})} \ln\left(\frac{1}{r_1}\right)$$

where r_1 is a random number sampled from a uniform distribution in the interval [0,1].

7 Select which reaction will be executed, finding the value for j in the equation:

$$\sum_{j\prime=1}^{j} a_{j\prime}(\mathbf{X}) \geq r_2 a_0(\mathbf{X})$$

where j is the smallest integer that satisfies the inequality above.

8 Execute reaction R_j updating the state vector $\mathbf{X} \leftarrow \mathbf{X} + \mathbf{v}_j$, where $\mathbf{v}_j$ is the stoichiometric vector for reaction j:

- If j equals 1, R1 (initiation) is executed: A new live chain is formed, vector $\mathbf{P}$ stores the length of this chain (1) in its last position $P(X_3 + 1) = 1$, and the state of the system is updated:

$$\begin{bmatrix} X_1 \\ X_2 \\ X_3 \\ X_4 \\ X_5 \end{bmatrix} = \begin{bmatrix} X_1 \\ X_2 \\ X_3 \\ X_4 \\ X_5 \end{bmatrix} + \begin{bmatrix} -1 \\ 0 \\ +1 \\ -1 \\ 0 \end{bmatrix}$$

- If j equals 2, R2 (propagation) is executed: A random number is generated ($r_3 \epsilon\ U[0,1]$) and multiplied by the total number of molecules of species X_3 (living polymer) to select a chain in vector $\mathbf{P}$ that will propagate, increasing its length by 1: $P(X_3 r_3) = P(X_3 r_3) + 1$. The state of the system is then updated:

$$\begin{bmatrix} X_1 \\ X_2 \\ X_3 \\ X_4 \\ X_5 \end{bmatrix} = \begin{bmatrix} X_1 \\ X_2 \\ X_3 \\ X_4 \\ X_5 \end{bmatrix} + \begin{bmatrix} -1 \\ 0 \\ 0 \\ 0 \\ 0 \end{bmatrix}$$

- If j equals 3, R3 (chain transfer) is executed: A random number is generated ($r_3 \epsilon\ U[0,1]$) and multiplied by the total number of molecules of species X_3 (living polymer) to select which chain in vector $\mathbf{P}$ will terminate. A dead chain is formed with length $D(X_5 + 1) = P(X_3 r_3)$. The state of the system is then updated:

$$\begin{bmatrix} X_1 \\ X_2 \\ X_3 \\ X_4 \\ X_5 \end{bmatrix} = \begin{bmatrix} X_1 \\ X_2 \\ X_3 \\ X_4 \\ X_5 \end{bmatrix} + \begin{bmatrix} 0 \\ -1 \\ -1 \\ +1 \\ +1 \end{bmatrix}$$

9 Update t: $t \leftarrow t + \tau$

10 Save $(\mathbf{X}, t)$ as desired. If t is lower than the final simulation time, return to step 4; else, stop simulation.

Figure 4.18 – Direct Method algorithm applied to the stopped-flow polymerization of ethylene with a single-site catalyst.

4.9.2 First Reaction Method (FRM)

Figure 4.19 shows a flowchart for the FRM. Figure 4.20 lists the sequence of steps needed to simulate the mechanism shown in Table 4.4 using the FRM. One can

notice that the only difference between the DM and the FRM regards how the next reaction is selected. In the DM, the sum of all rates of reaction is used to select the next reaction; while in the FRM, the reaction with the shortest characteristic time is the one that takes place next.
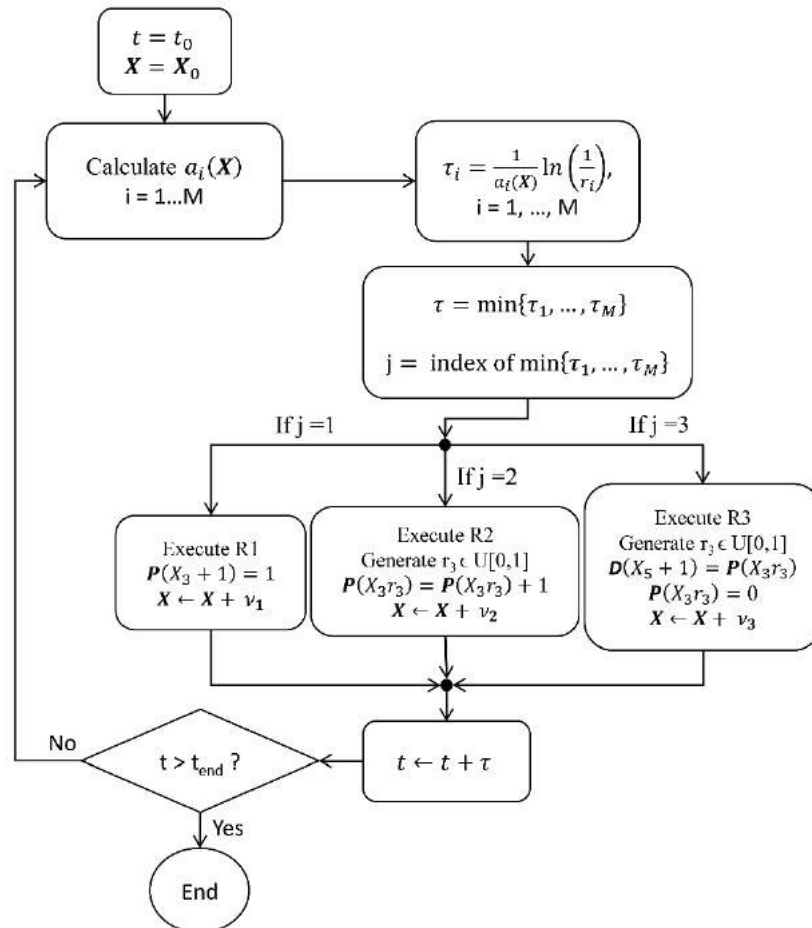
Figure 4.19 – Flowchart for the FRM algorithm.

The DM and FRM produce the same results (GILLESPIE, 1976;1977). They use the same distribution to generate the pair of simulation parameters τ and j. However, the DM is more efficient than the FRM because the FRM generates M times but discards M-1 times at each interaction, while the DM only generates two random numbers at each interaction (CAO and PETZOLD, 2004).

1 Initialize time: $t = t_0$.

2 Initialize the number of molecules of each species in the control volume, represented by the system state vector ($\mathbf{X} = \mathbf{X_o}$) which represents the number of molecules in the control volume.

$$\begin{bmatrix} Monomer\ (M) \\ Chain\ transfer\ agent\ (CTA) \\ Living\ polymers\ (P) \\ Catalyst\ (C^*) \\ Dead\ polymers\ (D) \end{bmatrix} = \begin{bmatrix} X_1 \\ X_2 \\ X_3 \\ X_4 \\ X_5 \end{bmatrix}_0$$

Create vectors **P** and **D** to save the length of each chain. All positions in these two vectors receive value 0 because there are none living or dead chain at time t_0.

3 Convert the macroscopic reaction rate constants into microscopic MC rate constants:

MC rate constant for R1: $k_i^{MC} = \dfrac{k_i^{exp}}{VN_A}$

MC rate constant for R2: $k_p^{MC} = \dfrac{k_p^{exp}}{VN_A}$

MC rate constant for R3: $k_t^{MC} = \dfrac{k_t^{exp}}{VN_A}$

4 Calculate MC reaction rates, $a_j(\mathbf{X})$ {$j = 1...M$}:

MC reaction rate for R1: $a_1(\boldsymbol{X}) = k_i^{MC} X_1 X_4$

MC reaction rate for R2: $a_2(\boldsymbol{X}) = k_p^{MC} X_1 X_3$

MC reaction rate for R3: $a_3(\boldsymbol{X}) = k_t^{MC} X_2 X_3$

5 Calculate the sum of all MC reaction rates $a_0(\mathbf{X})$:

$$a_0(\boldsymbol{X}) = a_1(\boldsymbol{X}) + a_2(\boldsymbol{X}) + a_3(\boldsymbol{X})$$

6 Compute the time step for each reaction type τ_i:

Time step for reaction R1: $\tau_1 = \dfrac{1}{a_1(X)} \ln\left(\dfrac{1}{r_1}\right)$

Time step for reaction R2: $\tau_2 = \dfrac{1}{a_2(X)} \ln\left(\dfrac{1}{r_2}\right)$

Time step for reaction R3: $\tau_3 = \dfrac{1}{a_3(X)} \ln\left(\dfrac{1}{r_3}\right)$

where r_1, r_2 and r_3 are random numbers sampled from a uniform distribution in the interval [0,1].

7 Chose the minimum value of τ_i as the time when the next reaction occurs:

$$\tau = \min\{\tau_1, \tau_2, \tau_3\}$$

The time steps not selected are discarded.

8 Use the index of the smallest τ to select the reaction type to be executed:

If τ is equal to τ_1, then $j = 1$.
If τ is equal to τ_2, then $j = 2$.
If τ is equal to τ_3, then $j = 3$.

9 Execute reaction R_j updating the state vector $\mathbf{X} \leftarrow \mathbf{X} + \mathbf{v_j}$, where $\mathbf{v_j}$ is the stoichiometric vector for reaction j:

- If j equals 1, R1 (initiation) is executed: A new live chain is formed, vector P stores the length of this chain (1) in its last position $\boldsymbol{P}(X_3 + 1) = 1$, and the state of the system is updated:

$$\begin{bmatrix} X_1 \\ X_2 \\ X_3 \\ X_4 \\ X_5 \end{bmatrix} = \begin{bmatrix} X_1 \\ X_2 \\ X_3 \\ X_4 \\ X_5 \end{bmatrix} + \begin{bmatrix} -1 \\ 0 \\ +1 \\ -1 \\ 0 \end{bmatrix}$$

- If j equals 2, R2 (propagation) is executed: A random number is generated ($r_3 \epsilon\ U[0,1]$) and multiplied by the total number of molecules of species X_3 (living polymer) to select a chain in vector **P** that will propagate, increasing its length by 1: $\boldsymbol{P}(X_3 r_3) = \boldsymbol{P}(X_3 r_3) + 1$. The state of the system is then updated:

$$\begin{bmatrix} X_1 \\ X_2 \\ X_3 \\ X_4 \\ X_5 \end{bmatrix} = \begin{bmatrix} X_1 \\ X_2 \\ X_3 \\ X_4 \\ X_5 \end{bmatrix} + \begin{bmatrix} -1 \\ 0 \\ 0 \\ 0 \\ 0 \end{bmatrix}$$

- If j equals 3, R3 (chain transfer) is executed: A random number is generated ($r_3 \epsilon\ U[0,1]$) and multiplied by the total number of molecules of species X_3 (living polymer) to select which chain in vector **P** will terminate. A dead chain is formed with length $\boldsymbol{D}(X_5 + 1) = \boldsymbol{P}(X_3 r_3)$. The state of the system is then updated:

$$\begin{bmatrix} X_1 \\ X_2 \\ X_3 \\ X_4 \\ X_5 \end{bmatrix} = \begin{bmatrix} X_1 \\ X_2 \\ X_3 \\ X_4 \\ X_5 \end{bmatrix} + \begin{bmatrix} 0 \\ -1 \\ -1 \\ +1 \\ +1 \end{bmatrix}$$

10 Update t: $t \leftarrow t + \tau$

11 Save ($\mathbf{X}$, t) as desired. If t is lower than the final simulation time, return to step 4; else, stop simulation.

Figure 4.20 – First Reaction Method algorithm applied to the stopped-flow polymerization of ethylene with a single-site catalyst.

4.9.3   Next Reaction Method (NRM)

GIBSON and BRUCK (2000) modified the FRM to make it more efficient, generating the Next Reaction Method (NRM). The NRM is faster than the FRM because the M-1 unused reaction times, determined with $\tau_i = \frac{1}{a_i(X)} \ln\left(\frac{1}{r_i}\right), (i = 1 \dots M)$, are modified and reused during the simulation. Moreover, the random parameter pair τ and j is calculated more efficiently with the use of data storage structures (dependency graph and indexed priority queue).

Figure 4.21 shows the flowchart for the NRM.

Figure 4.22 lists the steps needed for the NRM to simulate the polymerization mechanism presented in Table 4.4.

Figure 4.21 – Flowchart for the NRM algorithm.

1 Initialize time: $t = t_o$.

2 Initialize the number of molecules of each species in the control volume, represented by the system state vector $(\mathbf{X} = \mathbf{X}_0)$ which represents the number of molecules in the control volume.

$$\begin{bmatrix} Monomer\ (M) \\ Chain\ transfer\ agent\ (CTA) \\ Living\ polymers\ (P) \\ Catalyst\ (C^*) \\ Dead\ polymers\ (D) \end{bmatrix} = \begin{bmatrix} X_1 \\ X_2 \\ X_3 \\ X_4 \\ X_5 \end{bmatrix}_0$$

Create vectors $\mathbf{P}$ and $\mathbf{D}$ to save the length of each chain. All positions in these two vectors receive value 0 because there are none living or dead chain at time t_o.

3 Generate a dependency graph showing which reactions in the mechanism are affected after the execution of a certain reaction:

4 Convert the macroscopic reaction rate constants into microscopic MC rate constants:

MC rate constant for R1: $k_i^{MC} = \frac{k_i^{exp}}{VN_A}$

MC rate constant for R2: $k_p^{MC} = \frac{k_p^{exp}}{VN_A}$

MC rate constant for R3: $k_t^{MC} = \frac{k_t^{exp}}{VN_A}$

5 Calculate MC reaction rates, $a_j(\mathbf{X})$ $\{j = 1 \ldots M\}$:

MC reaction rate for R1: $a_1(\mathbf{X}) = k_i^{MC} X_1 X_4$

MC reaction rate for R2: $a_2(\mathbf{X}) = k_p^{MC} X_1 X_3$

MC reaction rate for R3: $a_3(\mathbf{X}) = k_t^{MC} X_2 X_3$

6 Calculate the sum of all MC reaction rates $a_o(\mathbf{X})$:

$$a_0(\mathbf{X}) = a_1(\mathbf{X}) + a_2(\mathbf{X}) + a_3(\mathbf{X})$$

7 Compute the time step for each reaction type τ_i:

Time step for reaction R1: $\tau_1 = \frac{1}{a_1(\mathbf{X})} \ln\left(\frac{1}{r_1}\right)$

Time step for reaction R2: $\tau_2 = \frac{1}{a_2(\mathbf{X})} \ln\left(\frac{1}{r_2}\right)$

Time step for reaction R3: $\tau_3 = \frac{1}{a_3(\mathbf{X})} \ln\left(\frac{1}{r_3}\right)$

where r_1, r_2 and r_3 are random numbers sampled from a uniform distribution in the interval [0,1].

8 Store the τ_i values in an indexed priority queue, which is a binary tree with M nodes (where M is the total number of reaction types in the mechanism; in the present case, $M = 3$). An indexed priority queue stores vertically ordered (i, τ_i) pairs, in which i is the reaction type and τ_i is the time when reaction i is executed. If $\tau_1 < \tau_2$ and $\tau_1 < \tau_3$, the indexed priority queue is: - - - - - - - - -

9 Let R_j be the reaction whose time (τ_j) stored in indexed priority queue is the lowest time (top of the tree).

10 Let τ be τ_j.

11 Execute reaction R_j updating the state vector $\mathbf{X} \leftarrow \mathbf{X} + \mathbf{v_j}$, where $\mathbf{v_j}$ is the stoichiometric vector for reaction j:

- If j equals 1, R1 (initiation) is executed: A new live chain is formed, vector $\mathbf{P}$ stores the length of this chain (1) in its last position $\mathbf{P}(X_3 + 1) = 1$, and the state of the system is updated:

$$\begin{bmatrix} X_1 \\ X_2 \\ X_3 \\ X_4 \\ X_5 \end{bmatrix} = \begin{bmatrix} X_1 \\ X_2 \\ X_3 \\ X_4 \\ X_5 \end{bmatrix} + \begin{bmatrix} -1 \\ 0 \\ +1 \\ -1 \\ 0 \end{bmatrix}$$

- If j equals 2, R2 (propagation) is executed: A random number is generated ($r_3 \in U[0,1]$) and multiplied by the total number of molecules of species X_3 (living polymer) to select a chain in vector $\mathbf{P}$ that will propagate, increasing its length by 1: $\mathbf{P}(X_3 r_3) = \mathbf{P}(X_3 r_3) + 1$. The state of the system is then updated:

$$\begin{bmatrix} X_1 \\ X_2 \\ X_3 \\ X_4 \\ X_5 \end{bmatrix} = \begin{bmatrix} X_1 \\ X_2 \\ X_3 \\ X_4 \\ X_5 \end{bmatrix} + \begin{bmatrix} -1 \\ 0 \\ 0 \\ 0 \\ 0 \end{bmatrix}$$

- If j equals 3, R3 (chain transfer) is executed: A random number is generated ($r_3 \in U[0,1]$) and multiplied by the total number of molecules of species X_3 (living polymer) to select which chain in vector $\mathbf{P}$ will terminate. A dead chain is formed with length $\mathbf{D}(X_5 + 1) = \mathbf{P}(X_3 r_3)$. The state of the system is then updated:

$$\begin{bmatrix} X_1 \\ X_2 \\ X_3 \\ X_4 \\ X_5 \end{bmatrix} = \begin{bmatrix} X_1 \\ X_2 \\ X_3 \\ X_4 \\ X_5 \end{bmatrix} + \begin{bmatrix} 0 \\ -1 \\ -1 \\ +1 \\ +1 \end{bmatrix}$$

12 Update t: $t \leftarrow t + \tau$

13 For each edge (j, α) (j is the index of the reaction that was executed, and α are the indices of each reaction affected by the execution of reaction j) in the dependency graph:

Store the old value of $a_\alpha(\mathbf{X})$ in a new variable and update $a_\alpha(\mathbf{X})$.

- If $\alpha \neq j$, set $\tau_{a_{\alpha \neq j}} \leftarrow \frac{a_{\alpha,old}(\mathbf{X})}{a_{\alpha,new}(\mathbf{X})} (\tau_\alpha - t) + t$

- If $\alpha = j$, generate a random number (r) and compute τ_α according to: $\tau_{a_{\alpha=j}} \leftarrow \frac{1}{a_j(\mathbf{X})} \ln\left(\frac{1}{r}\right) + t$

Update τ_α in in the indexed priority queue. Reorganize the indexed priority queue so that it saves on its root (top of the tree) the pair (i, τ_i) in which τ_i is the lowest.
In the present case according to the dependency graph shown above:
- If R1 is executed, all reaction rates have to be updated.
- If R2 is executed, $a_1(\mathbf{X})$ and $a_2(\mathbf{X})$ have to be updated.
- If R3 is executed, all reaction rates have to be updated.

14 Save $(\mathbf{X}, t)$ as desired. If t is lower than the final simulation time, return to step 9; else, stop simulation.

Figure 4.22 – Next Reaction Method algorithm applied to the stopped-flow polymerization of ethylene with a single-site catalyst.

4.9.4 τ-Leaping Method

All SSA methods described in the last two sections are exact simulation algorithms. They might have shorter simulation times than the DM, but still simulate one reaction at a time. Thus, they may not be fast enough for some practical applications. The τ-Leaping method was formulated to decrease simulation time, at the cost of lower accuracy.

Instead to proceeding one reaction at a time, the τ-leaping method *leaps* along the time axis from one subinterval to the next. The leap time τ is selected with help of a Poisson random variable, being small enough to satisfy the *leap condition* (GILLESPIE, 2008). The leap condition requires that the value of the propensity functions $a_j(X)$ remain approximately constant in the interval $[t, t + \tau]$,

$$a_j(X) \approx constant\ in\ [t, t + \tau], \forall j \tag{4.10}$$

If Equation (4.10) is satisfied, $a_j(\mathbf{X})\mathrm{d}t$ becomes the probability of reaction R_j occuring in every $\mathrm{d}t$ subinterval in $[t, t + \tau]$. By definition, the Poisson random variable $P(a_j(\mathbf{X})t)$ is the number of times reaction R_j will take place in the interval $[t, t + \tau]$. Therefore, the state at time $(t + \tau)$ is determined from the state $\mathbf{X}$ at time t with the expression,

$$X(t + \tau) = X(t) + \sum_{j=1}^{M} P\big(a_j(X)\tau\big)\mathbf{v}_j \tag{4.11}$$

Equation (4.11) is known as the *explicit τ-leaping formula*. Its accuracy depends on how well the leap condition is satisfied.

In the τ-leaping method originally proposed by GILLESPIE (2001), the algorithm initially selects a value for τ that would satisfy the leap condition. Then, the procedure would generate the Poisson random variable $P(a_j(\mathbf{X})t)$ and multiply this value by $\mathbf{v}_j$ for each reaction type. Finally, the algorithm would update the system state using Equation (4.11).

Selecting τ is the most sensitive step in the τ-leaping method. If τ is excessively small (with a value lower than a few multiples of $1/a_0(X)$, the time step expected in the exact solution of the SSA), the τ-leaping method becomes inefficient because too few reactions will take place during the time leap (GILLESPIE, 2008). If τ is excessively large, the system will also change excessively during the leap and the hypothesis that the propensity functions are nearly constant during the leap can no longer be valid. However, if τ is large but still compatible with the leap condition, the τ-leaping method will be faster than the exact SSA.

Many procedures have been proposed to guarantee that the leap condition is respected (GILLESPIE, 2001; CAO et al., 2006; GILLESPIE and PETZOLD, 2003). Particularly, the method proposed by CAO et al. (2006) is accurate, easier to code, and fast. This method assures that changes in all propensity functions remain bounded by an accuracy control parameter ε (0 < ε << 1),

$$\Delta_\tau X_i \leq max\{\varepsilon_i X_i, 1\}, \qquad \forall i \in I_{rs}, \qquad \varepsilon_i = \varepsilon_i(\varepsilon, X_i) \tag{4.12}$$

where $\Delta_\tau X_i = \sum_{j=1}^{M} P(a_j(X)\tau)v_j$, the term used to calculate the change in the system state in Equation (4.11), and I_{rs} is the set of indices of all reactant species.

The condition defined in Equation (4.12) requires that the relative change in X_i, $\Delta_\tau X_i$, be bounded by ε_i, assuring that the relative changes in all propensity functions are bounded by ε, and that X_i be changed by an amount larger than or equal to 1. To calculate ε_i, all reactions need to be analyzed individually before the simulation begins, as summarized in Figure 4.23.

Figure 4.23 – Procedure used to calculate values for ε_i in order to obtain relative changes in the propensity functions bounded by ε. Reproduced with permission from ref. (BRANDAO et al., 2015). Copyright 2015, John Wiley & Sons.

CAO et al. (2006) proposed a procedure for selecting proper values for ε_i in order to guarantee that the relative changes in the propensity functions will all be bounded by ε, thus satisfying the leap condition:

- For each $i \in I_{rs}$, determine the value of HOR(i), the highest order of reaction for which species i is a reactant. For instance, if species i is a reactant only in 1st order reactions, then HOR(i) = 1; if species i is a reactant in 1st and 2nd order reactions, then HOR(i) = 2.

- Determine ε_i using the relation: $\varepsilon_i = \varepsilon/g_i$.
  - If HOR(i) = 1, $g_i = 1$.
  - If HOR(i) = 2, $g_i = 2$ if only one molecule of i is involved in the reaction.
  - If HOR(i) = 2, $g_i = 2 + 1/(X_i - 1)$ if two molecules of i are involved in the reaction.
  - If HOR(i) = 3, see CAO et al. (2006).

The polymerization example in Table 4.4 will be used to clarify some of the features of the τ-leaping algorithm.

CAO et al. (2006) suggested setting ε to 0.03 and n_c between 2 and 20 (GILLESPIE, 2001; CAO et al., 2006). The next step is to determine $\varepsilon_i(\varepsilon, X_i)$ according to the procedure devised by CAO et al. (Figure 4.23). The main points of the τ-Leaping method are summarized in Figure 4.24.

The algorithm presented in Figure 4.24 should be applied to all non-distributed species in the system. In polymerizations, however, there are at least two distributed species: live and dead polymer chains. The algorithm can only update the number of molecules of live and dead polymers, but it cannot calculate how many chains of different lengths are present at a given time in the reactor. Thus, BRANDÃO et al. (2016) adapted the τ-leaping method to account for these chain populations just like done for the SSA algorithms. The algorithm presented in Table 4.5 describes the proposed adaptation for the polymerization mechanism described in Table 4.4.

Figure 4.24 shows the flowchart used to update the chain lengths of living and dead polymer chains after updating the state of the system with the τ-Leaping simulation method.

Table 4.5. Algorithm used to update the chain lengths of distributed species, applying the τ-Leaping method.

1. This algorithm starts after step 12 in Figure 4.24: • Set *Count₁*, *Count₂* and *Count₃* to zero. These variables count how many times reactions R1, R2 and R3 are executed during the current iteration.
2. Execute the DM procedure until reaction R1 is executed $\mathbb{P}(a_1(X)\tau)$ times, R2 is executed $\mathbb{P}(a_2(X)\tau)$ times, and R3 is executed $\mathbb{P}(a_3(X)\tau)$ times. The variable $\mathbb{P}$ refers to a Poisson random variable and $\boldsymbol{P}$ is the vector of live chains, containing at each vector position the length of the correspondent chain. This procedure ends when $Count_1 = \mathbb{P}(a_1(X)\tau)$, $Count_2 = \mathbb{P}(a_2(X)\tau)$ and $Count_3 = \mathbb{P}(a_3(X)\tau)$
3. Return to step 4 in Figure 4.24.

1 Initialize time: $t = t_o$.

2 Initialize the number of molecules of each species in the control volume, represented by the system state vector $(\mathbf{X} = \mathbf{X_o})$ which represents the number of molecules in the control volume.

$$\begin{bmatrix} Monomer\ (M) \\ Chain\ transfer\ agent\ (CTA) \\ Living\ polymers\ (P) \\ Catalyst\ (C') \\ Dead\ polymers\ (D) \end{bmatrix} = \begin{bmatrix} X_1 \\ X_2 \\ X_3 \\ X_4 \\ X_5 \end{bmatrix}_0$$

Create vectors **P** and **D** to save the length of each chain. All positions in these two vectors receive value 0 because there are none living or dead chain at time t_0.

3 Convert the macroscopic reaction rate constants into microscopic MC rate constants:

- MC rate constant for R1: $k_i^{MC} = \dfrac{k_i^{exp}}{VN_A}$
- MC rate constant for R2: $k_p^{MC} = \dfrac{k_p^{exp}}{VN_A}$
- MC rate constant for R3: $k_t^{MC} = \dfrac{k_t^{exp}}{VN_A}$

4 Calculate MC reaction rates, $a_j(\mathbf{X})$ {$j = 1 \ldots M$}:

- MC reaction rate for R1: $a_1(\mathbf{X}) = k_i^{MC} X_1 X_4$
- MC reaction rate for R2: $a_2(\mathbf{X}) = k_p^{MC} X_1 X_3$
- MC reaction rate for R3: $a_3(\mathbf{X}) = k_t^{MC} X_2 X_3$

5 Evaluate all $a_j(\mathbf{X})$ for state **X** at time t:

- Classify as *critical reaction* any R_j for which $a_j(\mathbf{X}) > 0$ and the number of molecules of any of one of its reactants is equal or less than n_c.

- Classify all other R_j as noncritical.

If the initial conditions set in step 3 is: $X_{1_0} > n_C$, $X_{2_0} > n_C$, $X_{3_0} = 0 < n_C$, $X_{4_0} > n_C$, $X_{5_0} = 0 < n_C$, R1 is noncritical but R2 and R3 are classified as critical reactions at initial time ($t = t_o$). But, during polymerization, live and dead chains are being formed and usually all reactions are classified as noncritical reactions during all polymerization.

6 Calculate τ' for each noncritical reaction:

$$\tau' = \min_{i \in I_{rs}} \left\{ \frac{max\{\varepsilon_i X_i, 1\}}{\left| \sum_{j \in J_{ncr}} a_j(\mathbf{X}) v_{ij} \right|}, \frac{max\{\varepsilon_i X_i, 1\}^2}{\sum_{j \in J_{ncr}} a_j(\mathbf{X}) v_{ij}^2} \right\}$$

Take the smallest τ' as the maximum leap time that satisfies the leap condition for the noncritical reactions. If there are no noncritical reactions set τ' to a very large number ($\tau' \to \infty$).

In the present case, the only τ' is from reaction R1 when $\underline{t = t_0}$:

$$\tau' = \min \left\{ \frac{max\{\varepsilon_1 X_1, 1\}}{|a_1(\mathbf{X}) v_{11}|}, \frac{max\{\varepsilon_1 X_1, 1\}^2}{a_1(\mathbf{X}) v_{11}^2} \right\}$$
$$= \min \left\{ \frac{max\{\varepsilon_1 X_1, 1\}}{|k_i^{MC} X_1 X_4 \cdot (-1)|}, \frac{max\{\varepsilon_1 X_1, 1\}^2}{k_i^{MC} X_1 X_4 \cdot (-1)^2} \right\}$$

7 Compute τ'' as the time when the next critical reaction would occur:

$$\tau'' = \frac{1}{a_{0c}(\mathbf{X})} \ln\left(\frac{1}{r_1}\right)$$

- For the present case, $a_{0c}(\mathbf{X}) = a_2(\mathbf{X}) + a_3(\mathbf{X})$ at t = t_0.
- If there are no critical reactions set τ'' to a very large number ($\tau'' \to \infty$).

8 Set the value of the actual leap time to:
$$\tau = \min(\tau', \tau'')$$

9 Update the state vector $\mathbf{X}(t + \tau)$:

$$\mathbf{X}(t + \tau) = \mathbf{X}(t) + \sum_{j \in J_{ncr}}^{M} \mathsf{P}\big(a_j(\mathbf{X})\tau\big) v_j$$

The equation above provides the new state of the system if no critical reaction fired during the current leap.
In $t = t_0$, $J_{ncr} = 1$ only for the present case discussed.

10 If $\tau'' \leq \tau'$, calculate j_c from

$$\sum_{j \in J_{cr}}^{j_c} a_j(\mathbf{X}) \geq r_2 a_{0c}(\mathbf{X})$$

In $t = t_0$, J_{cr} can be 2 and 3 only for the present case discussed.

11 Update again the state of the system considering this time the changes caused by one firing of reaction R_{j_c}:

$$\mathbf{X}(t + \tau) \leftarrow \mathbf{X}(t + \tau) + v_{j_c}$$

12 Update $t \leftarrow t + \tau$ and $\mathbf{X}(t) \leftarrow \mathbf{X}(t + \tau)$. If t is still less than the final time chosen, return to step 4, else stop simulation.

Figure 4.24 – τ-Leaping method algorithm.
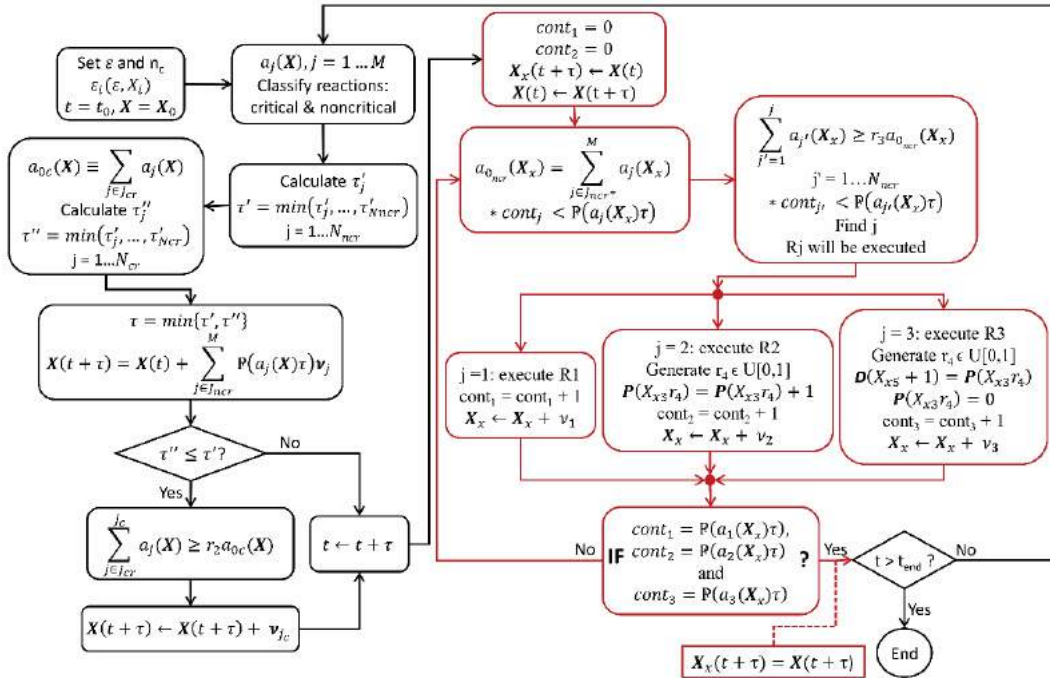
Figure 4.25 – Flowchart for the τ-Leaping method considering distributed species.

4.10 Concluding Remarks

As one can see, the Monte Carlo method may constitute an efficient tool when used in polymerization reaction engineering problems. Its simplicity is attractive, so that complex polymerization problems can be solved with MC algorithms without solving differential equations, allowing for simulation of molecular weight, chain composition and branching distributions. The main criticism against MC methods is related to the computational time required to solve the problems under investigation. However, the development of faster personal computers and the easier access to parallel computing and computer clusters is rapidly dismissing this criticism.

In the present work, a personal computer was used to run all the simulations performed in this thesis. MC method will be shown to constitute a very good alternative for numerical applications in olefin polymerization systems. However, it is important to comment that the experimental reactions carried out in this work lasted 10 to 15 minutes, facilitating the use of the MC direct method. Besides, it must be emphasized that the selection of the numerical method depends on many different aspects, including the skills of the researcher and the competitive advantages and disadvantages of each method.

PART II- METHODOLOGY

5 Experimental and Numerical Methods

5.1 Summary

This chapter describes the experimental and numerical methods adopted in the present work.

5.2 Experimental section

5.2.1 Materials

The following materials were used to perform the experiments:

- Methylaluminoxane (MAO, 10 wt % in toluene, Sigma-Aldrich, USA)
- Anhydrous Ethyl Alcohol ($\geq$ 99.5 %, Sigma-Aldrich, USA)
- Toluene anhydrous (99.8 %, Sigma-Aldrich, USA)
- Dimethylsily (N-tert-butylamido) (tetramethylcyclopentadienyl) titanium dichloride (CGC) (85.0 – 99.8 %, Boulder Scientific, USA)
- 1,9-Decadiene (98 %, Sigma-Aldrich, USA)
- Triisobutylaluminum (TIBA) (25 wt % in toluene, Sigma-Aldrich, USA)
- n-Butyllithium solution, 2.5 M in hexane (Sigma-Aldrich, USA)
- Sodium ($\geq$ 99 % , stored in mineral oil, Sigma-Aldrich, USA)
- Nitrogen ($>$ 99.998 %, Praxair, USA)
- Ethylene ($>$ 99 %, Praxair, USA)

Ethylene and nitrogen were purified by flowing through molecular sieves (3 and 4 Å) and CuO/Al_2O_3 packed beds to remove oxygen and water residues. Toluene was distilled over butyl lithium and metallic sodium to remove polar impurities and residual moisture, dried over molecular sieves, and purged with nitrogen. CGC was dissolved with purified toluene inside the glovebox (OMNI-LAB VAC 101965, Vacuum Atmospheres Company, USA) to make a solution with concentration of 1.02×10^{-4} g CGC/g toluene. MAO was used as received. 1,9-Decadiene was dried with molecular sieves and purged with nitrogen. All air sensitive compounds were handled under inert atmosphere in a glovebox.

90

5.2.2 Reaction unit

The reaction unit used in the present work is represented in Figure 5.1. Reactions were performed in a 300 mL Parr autoclave reactor operated in semi-batch mode (in the reaction, ethylene was continuously added to the reactor).
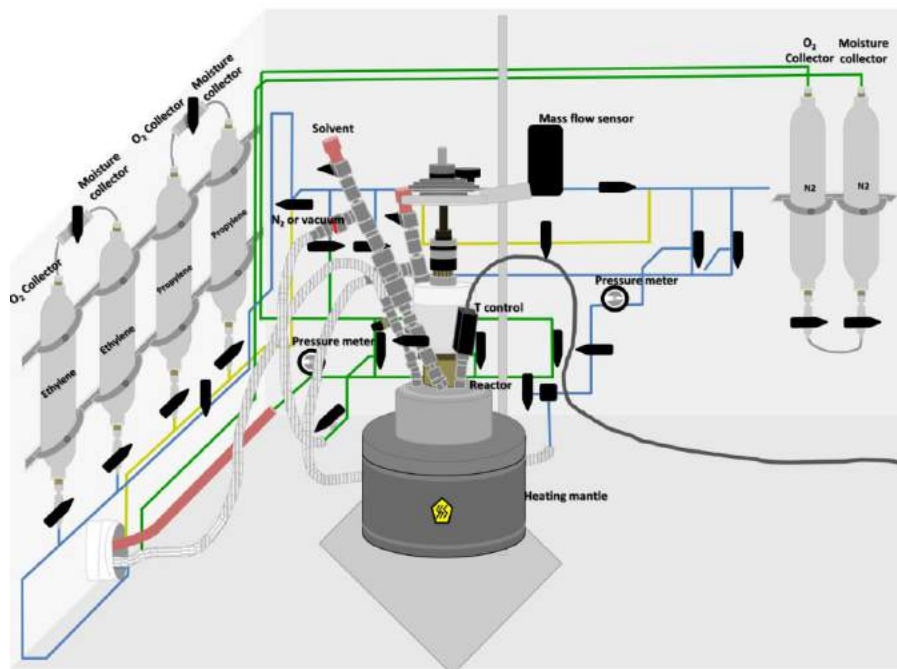
Figure 5.1 – Illustrative scheme of the experimental unit.

The polymerization temperature was controlled with an electrical band heater and internal cooling coils placed inside the reactor. Two independent proportional-integral derivative controllers were employed to control the cold water flow in the cooling coil and the power input to the electric heater, as shown in Figure B.1 of Appendix B. The reactor was also equipped with a stirrer (comprising a pitched blade turbine impeller connected to a magneto-driver stirrer, set to the agitation speed of 1200 rpm. The stirrer, cooling coil, reactor vessel and heating mantle used in the experiments are illustrated in Figure 5.2.

An in-line mass flow meter was installed in the gaseous ethylene feed line to supervise the monomer mass flow rate, monitored with help of the LabView software (National Instruments, USA)[4]. The temperature control calculations were also

---

[4] www.ni.com/labview; visited on january 1st, 2017.

performed with LabView. An in-line pressure regulator was installed in the ethylene feed line to regulate the reactor pressure.
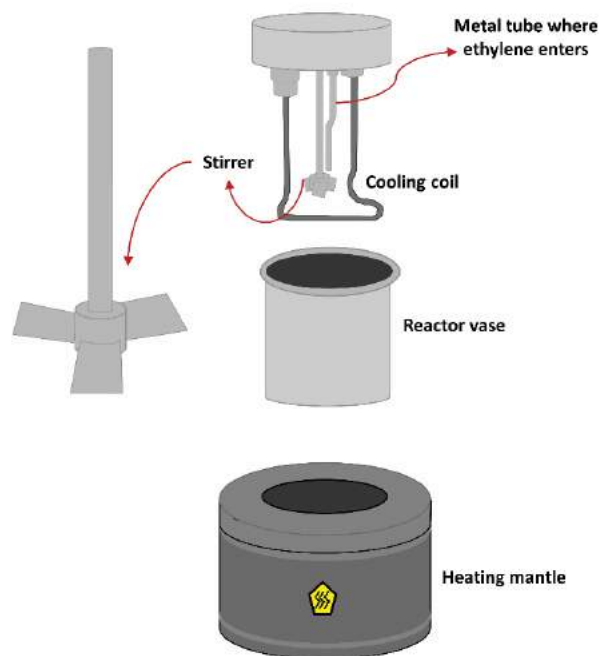
Figure 5.2 – Illustration of stirrer, cooling coil, reactor vessel and heating mantle used in this work.

5.2.3 Experimental procedure and related computations

Prior to polymerization, the reactor was submitted to reactor purging, applying six cycles of nitrogen venting and vacuum at 125 °C to remove oxygen from the reactor. Then, 150 mL of toluene and 0.5 g of triisobutylaluminum (impurity scavenger) were charged to the reactor. The reactor temperature was increased to 120 °C and kept constant during approximately 20 minutes.

5.2.3.1 *Homopolymerization Reactions*

After reactor purging, 150 mL of toluene were charged into the reactor at ambient temperature. A solution of MAO was prepared inside the glovebox by adding 2.0 g of MAO and a small volume of toluene in a 20 mL sampling cylinder, which was then sealed and removed from the glovebox. The MAO solution was transferred to the reactor with a cannula under nitrogen pressure.

The band heater was powered on to heat the reactor until reaching the desired polymerization temperature (120, 130 or 140 °C). Then, ethylene was added to the reactor in order to saturate the toluene solvent. After stabilizing the reactor temperature, the catalyst solution was fed into reactor with pressurized nitrogen. After starting the polymerization, a small temperature increase (1 – 2 °C) could be observed for about 1 minute, after which the temperature became constant throughout the polymerization, with variations of ± 0.15 °C from the set point. Ethylene was supplied on demand to keep a constant reactor pressure of 120 psig, and the ethylene flow rate was monitored with a mass flowmeter. After 15 minutes, the polymerization was interrupted by closing the ethylene valve, and immediately blowing out the reactor contents into a 1 L beaker filled with 100 – 250 mL of ethanol. The polymer was kept overnight in a beaker under constant stirring. Afterwards, the polymer powder was filtered and dried in an oven. Table 5.1 shows the homopolymerization conditions employed in the present work. The proposed experiments allowed for analysis of temperature and catalyst concentration effects on the final properties of the polymerization products. Triplicates were performed in order to evaluate the magnitude of the experimental variability.

Table 5.1. Homopolymerization Conditions

Sample ID	Catalyst ($\mu mol\ L^{-1}$)	Temperature (°C)	Polymerization Time (min)
A1	0.767	120	15
A2	0.767	120	15
A3	0.767	120	15
B1	0.767	130	15
B2	0.767	130	15
B3	0.767	130	15
C1	0.767	140	15
C2	0.767	140	15
C3	0.767	140	15
J1	0.271	120	10
J2	0.174	120	10

5.2.3.2 Copolymerization Reactions

The required amount of 1,9-decadiene was diluted in a small volume of toluene in a 20 mL sampling cylinder. The cylinder was sealed and removed from the glovebox. The copolymerization procedure was analogous to the homopolymerization procedure described previously. The only difference regards the fact that, after adding MAO to the reactor, the comonomer solution was injected into the reactor following the same procedure used to feed MAO. Table 5.2 presents the copolymerization conditions used

in the present work. The proposed experiments allowed for analysis of comonomer concentration, catalyst concentration and reaction time effects on the final properties of the polymerization products.

Table 5.2. Copolymerization Conditions.

Sample ID	Catalyst ($\mu mol\ L^{-1}$)	1,9-Decadiene (g)	Temperature (°C)	Polymerization Time (min)
D1	0.325	0.10	120	10
E1	0.325	0.20	120	10
F1	0.325	0.30	120	10
G1	0.271	0.30	120	2
G2	0.271	0.30	120	4
G3	0.271	0.30	120	6
G4	0.271	0.30	120	8
G5	0.271	0.30	120	10
H1	0.271	0.40	120	4
H2	0.271	0.40	120	6
H3	0.271	0.40	120	8
H4	0.271	0.40	120	10
I1	0.368	0.40	120	6
I2	0.174	0.40	120	6

5.2.3.3   Calculation of Ethylene Concentration in Toluene

For each experiment, the calculation of ethylene concentration in the liquid phase was performed with help of simple modeling procedure, since kinetic modeling requires knowledge of the ethylene concentration. The total volume of toluene inserted into the reactor at room temperature ($T_0 = 25$ °C) was 150 mL. This was assumed to be the total solution volume, since the other liquid compounds (MAO and diene) were present in much smaller amounts. When the reactor was heated up until the desired reaction temperature (T_f = 120, 130 or 140 °C), it can be assumed that the vessel operated as a flash reactor. Using the engineering software simulator Aspen Hysys (Aspen Technology)[5], it was possible to calculate the molar concentrations of toluene liquid and vapor in equilibrium at reaction temperature. The Peng–Robinson equation of state was used to calculate the fugacity coefficients in the gas phase, and UNIQUAC model was used to determine the activity coefficients (Equation (5.1)) in the liquid phase.

---

[5] https://www.aspentech.com/hysys/; visited on january 1st, 2017.

$$\tau_{ij} = exp\left[-\left(\frac{a_{ij} + b_{ij}T}{RT}\right)\right] \tag{5.1}$$

where a_{ij} is non-temperature dependent energy parameter between components i and j (cal gmol^{-1}), b_{ij} is temperature dependent energy parameter between components i and j (cal gmol^{-1} K^{-1}), T is the temperature in K and R is the ideal gas constant (in this case, R = 1.987 cal gmol^{-1} K^{-1}).

The parameters a_{ij} and b_{ij} employed to determine the activity coefficients of ethylene and toluene in the liquid phase are presented in Table 5.3.

Table 5.3. Parameters a_{ij} and b_{ij} of Equation (5.1) from UNIQUAC model provided by Aspen Hysys (ethylene = 1 and toluene = 2).

a_{ij}	Parameter value	b_{ij}	Parameter value
a_{11}	0	b_{11}	0
a_{12}	17.005	b_{12}	-0.399
a_{21}	-1404.117	b_{21}	-3.810·10^{-3}
a_{22}	0	b_{22}	0

By knowing the toluene vapor pressure at T_f and the total system pressure P_T, the toluene and ethylene molar fractions in the gas phase at T_f could also be calculated. Given the saturation condition and solving the flash equations, the toluene and ethylene molar fractions and concentrations in the liquid phase could also be determined. By multiplying the solution volume by the respective molar concentrations in the liquid phase, the total amounts of ethylene and toluene in both liquid and gas phases might be calculated. This procedure was performed for different reaction temperatures, T_f, as one can see in Table 5.4.

Table 5.4. Ethylene and toluene liquid compositions in equilibrium at P = 120 psig for 150 mL of toluene.

T (°C)	$x_{toluene}$	x_{C2H4}	$[C_2H_4]$(mol L^{-1})	n_{C2H4} (mol)
90	0.92228	0.07772	0.70090	0.10514
100	0.92973	0.07027	0.62355	0.09353
110	0.93626	0.06374	0.55644	0.08347
120	0.94237	0.05763	0.49472	0.07420

130	0.94816	0.05184	0.43732	0.06560
140	0.95395	0.04605	0.38141	0.05721

5.2.4 Polymer Characterization

5.2.4.1 High-Temperature Gel Permeation Chromatography (GPC)

Average molecular weights, molecular weight distributions and intrinsic viscosity of polymer samples were measured with a Polymer Char high-temperature gel permeation chromatography (GPC) unit coupled with three detectors (infra-red, light scattering and differential viscosimeter) and calibrated with polystyrene standards and using a universal calibration curve. The GPC was operated at 140 °C, using 1,2,4-trichlorobenzene (TCB) as solvent at flow rate of 1 mL min^{-1}.

High-temperature GPC, also known as high-temperature size-exclusion chromatography (SEC), is the most widely used technique for determination of polyolefins molecular weight distributions of polyolefins. High temperatures are required because most commercial polyolefins are only soluble at temperatures above 120 °C in chlorinated solvents (SOARES and MCKENNA, 2013).

In GPC, the separation is based on size exclusion. The columns are packed with particles of different pore sizes. The pore volume (V_p) of the gel particles is summed to the interstitial volume (V_0) (which is the volume occupied by the mobile phase circulating around the particles) to form the total volume available for the mobile phase (LUCAS et al., 2001). The GPC separation principle is illustrated in Figure 5.3.
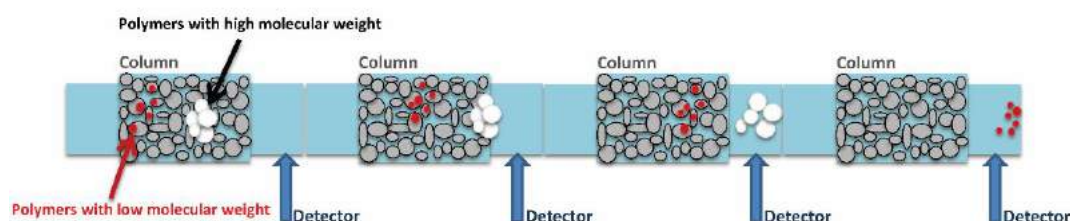

Figure 5.3 – GPC separation principle.

When a solution, containing polymer molecules of different sizes, is injected into the mobile phase, it flows through a series of packed columns. The elution time of a polymer chain depends on its *hydrodynamic* volume (its volume in solution). Chains with higher volumes elute first, as they penetrate into fewer pores. The elution time or

elution volume of larger polymer chains depends essentially on the interstitial volume (V_0). On the other hand, chains with very small volumes penetrate deeper into the pores, requiring larger amounts of solvent for complete removal from the column. The elution time of small molecules depends on the total mobile phase volume ($V_0 + V_p$) and they are eluted last. Finally, polymer chains with intermediate volumes diffuse only into few pores, presenting elution times between V_0 and $V_0 + V_p$ (GABORIEAU and CASTIGNOLLES, 2011). The mass detector monitors the polymer concentration exiting from the column. A calibration curve is required to relate the elution volume to the molecular weight of the chains, as shown in Figure 5.4. The hydrodynamic volume of polymer chains depends on the chain length, branching topology, solvent type and also temperature (SOARES and MCKENNA, 2012).
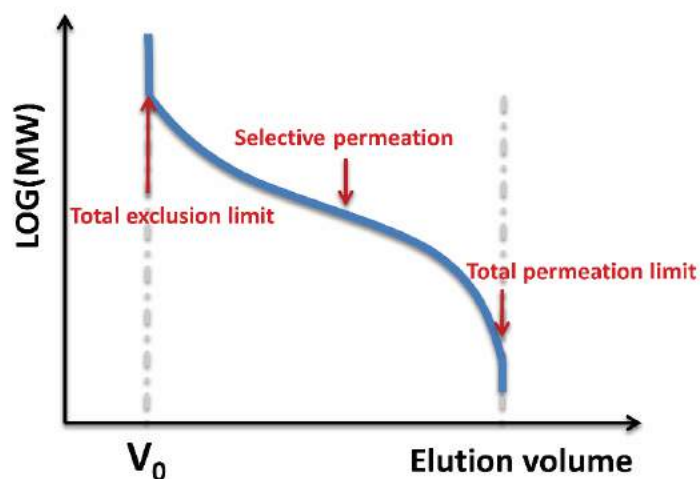
Figure 5.4 – Log(MW) as a function of the SEC elution volume.

When the GPC is coupled with specific functional detectors, the characterization of polymer chains can improve significantly, making possible not only the determination of molecular weight distributions but also branching distributions (TRIEBE et al., 2006).

5.2.4.2 *Gravimetric Analysis*

Gravimetric analysis consists in determining the reaction states based on sample weights. In order to achieve this, the weight of a filter paper was measured (m_0). Then, the filter was placed in a plastic funnel supported on an empty 1 L beaker. The reactor content plus ethanol (after staying approximately 12 hours under constant stirring) was poured into the funnel, separating the polymer from toluene and ethanol. The filter

paper with the filtrated polymer was placed in the oven to dry. When the polymer and the filter were completely dried, the weight of the filler was measured (m_1). The polymer weight (m_p) could be calculated by discounting m_0 from m_1 as: $m_p = m_1 - m_0$.

5.3 Numerical methods

In all problems investigated in the present thesis, the final model was written as a set of ordinary differential equations with well-defined initial conditions. A simple example of this type of model is presented in Equations (3.1)-(3.5). Different numerical approaches were employed to solve this type of models:

- Method of moments coupled with DASSL solver (Chapter 8) to predict average molecular weights of polymer samples and chemical species concentrations;
- Polynomial approximation based on the moments of the distributions to build the MWDs of the PE samples (Chapter 9).
- Adaptive Orthogonal Collocation Method and Monte Carlo Method for computation of the full MWD of polymer samples (Chapter 9)

These methods were chosen because they are commonly used to solve polymer reaction engineering problems. Besides, obtaining simulation results and executing statistical evaluation of different models, makes possible to compare the performances of the different numerical approaches used to solve the kinetic model proposed herein. Details of numerical implementations are presented in Chapter 7, where the main model developed in the present thesis is described.

6 Statistical Methods

6.1 Summary

This chapter describes the statistical procedures used in the present thesis to estimate model parameters and evaluate model performances. The parameter estimation procedure consists in finding parameters for a model so that model predictions become as close as possible to the available experimental data (SCHWAAB and PINTO, 2007), considering the experimental uncertainty. The parameter estimation problem can be divided into three parts:

1. definition of the objective function;
2. minimization of the objective function;
3. statistical analysis of parameter estimates and model quality.

6.2 Objective Function

In the present work, the objective function used in the parameter estimation process was the well-known weighted least-squares function (BARD, 1974) (see APPENDIX C):

$$F_{obj} = \sum_{i=1}^{NE} \sum_{j=1}^{NY} \frac{\left[y_{ij}^e - y_{ij}^m (\boldsymbol{x_i^e}, \boldsymbol{\theta}) \right]^2}{\sigma_{y_{ij}}^2} \tag{6.1}$$

where NE is the total number of available experiments, NY is the total number of dependent variables, y_{ij}^e is a dependent variable measured experimentally (variable j from experiment i), y_{ij}^m is a dependent variable calculated with the mathematical model (variable j from experiment i), $\boldsymbol{x_i^e}$ is a vector of independent variables measured experimentally (from experiment i), $\boldsymbol{\theta}$ is the vector of model parameters and $\sigma_{y_{ij}}^2$ is the variance of the experimental fluctuations of the dependent variable j in experiment i.

6.3 Parameter Estimation

In the present work, the computational package ESTIMA (SCHWAAB and PINTO, 2007) was used to solve the parameter estimation problem. ESTIMA employs a hybrid optimization scheme, combining particle swarm stochastic optimization

(KENNEDY and EBERHART, 1995) with the deterministic Gauss-Newton method (ANDERSON et al., 1978), with the accelerator of LAW and BAILEY (1963). Interested readers should refer to SCHWAAB (2005) and SCHWAAB et al. (2008).

The Gauss-Newton method frequently fails when dealing with ill-posed problems, making impossible the determination of parameter uncertainties (as the covariance matrix of parameter uncertainties cannot be obtained). In these cases, first, particle swarm optimization can be applied. Then, with the point of minimum obtained, an identifiability procedure (see Section 6.4.2) can be applied to determine which set of model parameters can have their uncertainties evaluated. Afterwards, ESTIMA can be applied to estimate the selected parameters and refine the minimum of the previously estimated model parameters. Figure 6.1 illustrates this process.

Figure 6.1 – Employed parameter estimation procedure.
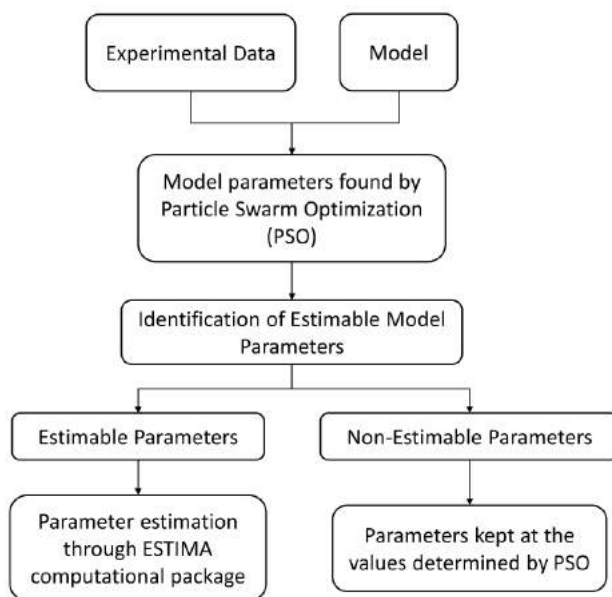
The experimental data used to estimate the parameters included the number and weight average molecular weights (M_n, M_w) of the polymer samples and the observed ethylene feed rates.

6.4 Statistical Analyses

Parameter estimation procedure should not be ceased when the optimization problem is solved. It is important to perform the statistical analysis of the obtained

results in order to calculate the confidence limits of the parameter estimates and to classify the quality of the model predictions (SCHWAAB and PINTO, 2007).

6.4.1 Parameter Uncertainty

The parametric uncertainty is normally characterized by the covariance matrix of parameter uncertainties $\boldsymbol{V_\theta}$, which can be obtained through the quadratic approximation of the objective function in respect to the model parameters, whose derivation can be found elsewhere (SCHWAAB and PINTO, 2007; BARD, 1974). First, the Fisher Information Matrix $\boldsymbol{FIM}$ and its inverse $\boldsymbol{V_\theta}$ can be obtained as:

$$\boldsymbol{FIM} = \boldsymbol{B^T V_y^{-1} B}$$
$$\boldsymbol{V_\theta} = \boldsymbol{FIM}^{-1} \tag{6.2}$$

where $\boldsymbol{B}$ is the sensitivity matrix:

$$\boldsymbol{B} = \left[\frac{\partial \boldsymbol{y^m(x^m, \theta)}}{\partial \boldsymbol{\theta}} \right] \tag{6.3}$$

Admitting that the parametric errors can be described by the t-Student distribution, the confidence intervals of estimated model parameters can be given by:

$$\theta_j + t_{DF}\left(\frac{1-\alpha}{2}\right)\sigma_{\theta,j} < \theta_j < \theta_j + t_{DF}\left(\frac{1+\alpha}{2}\right)\sigma_{\theta,j} \tag{6.4}$$

where the normalized variable t_{DF} follows the t-Student distribution, with DF degrees of freedom and confidence level α. $\sigma_{\theta,j}$ is the standard deviation associated with model parameter θ_j, placed at the main diagonal of matrix $\boldsymbol{V_\theta}$.

6.4.2 Parameter Identifiability Procedure

The matrix $\boldsymbol{FIM}$ can be readily obtained. However, depending on the model structure and/or available experimental data, $\boldsymbol{FIM}$ can be singular. In this case, the matrix $\boldsymbol{V_\theta}$ cannot be obtained, and the parameter uncertainties remain unknown. One possible alternative is to select a subset of model parameters that can be estimated with their respective uncertainties; the other parameters must be kept constant and equal to their original values. This procedure is called *parameter identifiability*.

In general, parameter identifiability procedures comprise two basic steps: (i) selection and (ii) ordering of model parameters, which are normally carried out simultaneously in most algorithms. The goal of the parameter selection step is to identify the model parameters that can be estimated from the available experimental data. Then, the selected parameters are classified as estimable parameters and must be estimated using an optimization method. The remaining parameters are classified as non-estimable parameters and an alternative solution must be searched to estimate their values. A conventional choice is to maintain the non-estimable parameter values at the original value (that can be obtained from literature, professional experience or arbitrated) (ALBERTON, 2013).

Probably, the invertibility of FIM is associated with linear independence of the columns of matrix B. The methodology proposed by YAO et al. (2003) is based on local sensibility analysis and is characterized by its simplicity to interpret the results and ease of implementation. This procedure analyzes the parameters estimability by evaluating the parameter sensitivity matrix in respect to the normalized model prediction obtained by the Gram-Schmidt orthogonalization method (RICE, 1966). The selection order of parameters values are based on the magnitude and correlation of the columns of the matrix $B,$ using a cut-off value previously specified as a stop criterion of selection. THOMPSON et al. (2009) replaced this criterion for the point where the parameter estimation problem becomes ill-posed. The algorithm developed by YAO et al. (2003) with the stop criterion proposed by THOMPSON et al. (2009) is presented next:

(1) Build the local sensitivity matrix **B** and normalize this matrix, generating matrix B_N (Figure 6.3).

(2) Calculate the sum of the squares of the elements of each column of B_N as shown next.

$$Nb = \left[\|b_{\theta_1}\| \quad \cdots \quad \|b_{\theta_{nP}}\|\right] = \left[\sum_{i=1}^{nY} B_N(i,1)^2 \quad \cdots \quad \sum_{i=1}^{nY} B_N(i,nP)^2\right] \qquad (6.5)$$

(3) Select the parameter for which the column of matrix **Nb** presents the largest value as the first identifiable parameter.

(4) Build the local sensitivity matrix for the selected parameters **B**$_{sel}$. When the first parameter is selected, k = 1, **B**$_{sel}$ has only one column. When the following parameters are selected, **B**$_{sel}$ has k columns.

(5) Calculate **B**$_{orth}$, which is the orthogonal correspondent matrix of the complete local sensitivity matrix **B**, according with:

$$B_{orth} = B_{sel}\left(B_{sel}^{T}B_{sel}\right)^{-1}B_{sel}^{T}B \tag{6.6}$$

where $B_{sel}^{T}B_{sel}$ is the FISHER information matrix (**FIM**) of the selected parameters.

(6) Calculate the residual matrix **R**:

$$R = B - B_{orth} \tag{6.7}$$

(7) Calculate the sum of the squares of the elements of each column of matrix **R**. The column that provides the highest value corresponds to the next identifiable parameter.

(8) Select, in matrix **B**, the correspondent column obtained in step (7) and add it to matrix **B**$_{sel}$.

(9) Repeat steps (4) to (8) until all parameters are selected or until singularity problems are found during the **FIM** inversion procedure.

Figure 6.2 – Normalized local sensitivity matrix B_N and sensitivity vectors of parameters (adapted from ALBERTON (2013)).

(a) 1st estimable parameter: θ_1 since $b_{\theta_1} > b_{\theta_3} > b_{\theta_2}$

(b) The next parameter to be selected has to present the lowest correlation with θ_1 → corresponds to the parameter whose orthogonal sensitivity vector in respect to b_{θ_1} has the longest length: θ_3 is the second parameter selected since $b_{ort\theta_3} > b_{ort\theta_2}$.

(c) Since b_{θ_2} is highly correlated with b_{θ_1}, parameter θ_2 can not be selected without making matrix **FIM** singular. Then, the procedure is ceased and parameters θ_1 and θ_3 are classified as estimable.

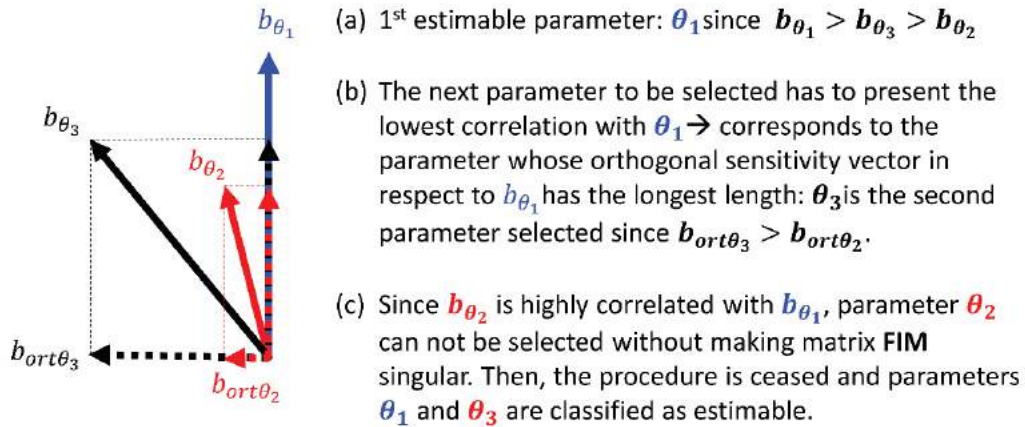**Figure 6.3 – Illustration of YAO et al. (2003) procedure for 3 parameters (adapted from ALBERTON (2013)).**

6.4.3   Confidence Region of the Model Parameters

In the present work, the confidence regions of the estimated model parameters were built according with the following expression:

$$F_{obj}(\boldsymbol{\theta}) \le F_{obj}(\hat{\boldsymbol{\theta}})\left[1 + \frac{NP}{(N - NP)}F^{\alpha}_{NP,N-NP}\right] \tag{6.8}$$

where, $F_{obj}(\boldsymbol{\theta})$ is the objective function value calculated with the estimated model parameters $\widehat{\boldsymbol{\theta}}$ and $F_{NP,N-NP}^{\alpha}$ is the upper limit from the Fisher distribution with degrees of freedom equal to $N - NP$ and confidence level α.

According to SCHWAAB and PINTO (2007), although Equation (6.8) can be obtained from the quadratic approximation of the objective function, the shape of the confidence region is not restricted to the elliptical shape. Elliptical confidence regions only occur when the experimental data follow the normal distribution and if the model is linear. Thus, in the case of nonlinear models, confidence regions that are closer to the real confidence region can be obtained with Equation (6.8). This can be done by using the particle swarm optimization method for objective function minimization, since this method naturally performs a high number of objective function evaluations.

6.4.4 Model Quality

After defining the objective function, considering the hypotheses presented in the last section, model predictions and objective function can be seen as variables that follow certain probability distributions. Thus, in the case of the maximum likelihood functions developed from the hypothesis that the fluctuations between the experimental and predicted values follow the normal distribution, the objective function is equivalent to the weighted sum of the squares of deviations weighted by the respective variances. This is the definition of the normalized variable chi-square (χ^2). Thus, the confidence limits of the objective function, at the point of optimum, can be calculated with the chi-square values, which depend on the confidence level α and the degrees of freedom DF.

$$\chi_{DF}^2 \left(\tfrac{1-\alpha}{2}\right) < F_{obj}(\theta^{est}) < \chi_{DF}^2 \left(\tfrac{1+\alpha}{2}\right) \tag{6.9}$$

where DF is calculated by:

$$DF = NE \cdot NY - NP \tag{6.10}$$

where NP is the number of estimated parameters.

When the objective function value lies between limits given by the χ^2 distribution, given the degrees of freedom and confidence level, the model can be considered adequate and describes well the experimental data. If the lower limit of the

χ^2 distribution is higher than the objective function, the model describes the experimental data with a precision that is higher than the precision given by the experimental errors, indicating that the model might be over-parameterized. On the other hand, if the upper limit of the χ^2 distribution is lower than the objective function, the model is not capable of describing the experimental data with the precision of the experimental measurements; consequently, the model can be considered inadequate.

6.4.5 Model Prediction Uncertainty

In order to be possible to analyze the quality of the model predictions, it is required to calculate how the parametric errors propagate through the model and become prediction errors. So, the prediction uncertainties are characterized by the prediction covariance matrix $\widehat{V}_y$, which can be described according with:

$$\widehat{V}_y = B^T V_\theta B \tag{6.11}$$

Therefore, the elements positioned at the diagonal of the prediction covariance matrix correspond to the prediction variances. Similarly, the confidence intervals of model prediction can be defined as:

$$y_j^m + t_{DF}\left(\frac{1-\alpha}{2}\right)\hat{\sigma}_{y_j} < y_j^m < y_j^m + t_{DF}\left(\frac{1+\alpha}{2}\right)\hat{\sigma}_{y_j} \tag{6.12}$$

6.5 Reparameterization

Parameter correlation is undesirable since it introduces numerical and interpretation difficulties into the problem. One well-known form that presents high parameter correlation is the Arrhenius expression $k = k_0 exp\left(-\frac{E}{RT}\right)$ (SCHWAAB and PINTO, 2007).

Reparameterization procedures propose that model expressions be written in different ways in order to reduce the parameter correlation. Several propositions for reparameterization have been proposed in the literature; the commonest ones use a T_r reference temperature to allow for reduction of parameter correlation in Arrhenius expressions, which can also lead to reduction of the computational effort required to

estimate the model parameters (ESPIE, 1988). SCHWAAB & PINTO (2007, 2008) showed that a more proper form to write the Arrhenius equation is:

$$k = exp\left[A + B\left(\frac{(T - T_r)}{T}\right)\right] \tag{6.13}$$

where

$$B = \frac{E}{RT_r} \tag{6.14}$$

$$A = ln(k_0) - \frac{E}{RT_r} = ln(k_0) - B \tag{6.15}$$

The reference temperature can be selected to reduce the correlation of the parameters.

Other typical reparameterization procedure is associated with the order of magnitude of model parameters. Since the parameters to be estimated can present different orders of magnitude, the following variable change has been proposed for some of the model parameters:

$$p = \log(\boldsymbol{\theta}) \tag{6.16}$$

where p represents the order of magnitude of the parameter estimates $\boldsymbol{\theta}$. Therefore, instead of estimating $\boldsymbol{\theta}$, one may estimate the order of magnitude of $\boldsymbol{\theta}$ (p). By doing this, the estimation of parameters with different orders of magnitude (for example, between 10^{-4} and 10^4) become much simpler, as the new parameters present the same orders of magnitude (for example, between -4 and 4).

7 Model Development

7.1 Summary

In this chapter a brief introduction is presented about works published in the literature that investigated the kinetics of ethylene polymerization and copolymerization with non-conjugated dienes and that consider the formation of LCBs. Based on literature and some assumptions, a model is proposed to describe the copolymerization of ethylene and 1,9-decadiene. Some details regarding the implementation of the numerical techniques are also given.

7.2 Introduction

As previously presented in Chapter 2, CGC catalysts can promote the chain incorporation of higher α-olefins and dead chains that contain terminal (SOARES, 2002) and/or pendant double bonds (FERREIRA Jr. et al., 2010), usually known as macromonomers (WANG et al., 1998). In the case of ethylene homopolymerization, the macromonomers are formed in-situ through β-hydride elimination or transfer to ethylene reactions. Particularly, macromonomers form LCBs when they are re-incorporated into the growing polymer chains.

Many experimental investigations have been devised to understand how LCBs are generated in ethylene and propylene homopolymerizations (WANG et al., 1998; KOKKO et al., 2000; WANG et al., 2004; STADLER et al., 2006, MEHDIABADI and SOARES, 2012). However, only few publications presented kinetic polymerization studies that included LCB generation steps in the copolymerization mechanism of olefins and dienes (WANG et al., 2000; KOKKO et al., 2001; SARZOTTI et al., 2005; MEHDIABADI and SOARES, 2011), as already mentioned in Chapter 2.
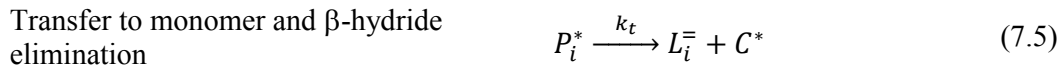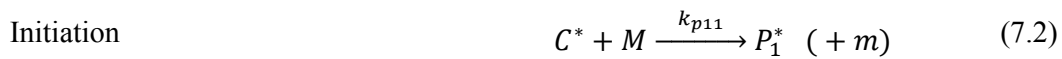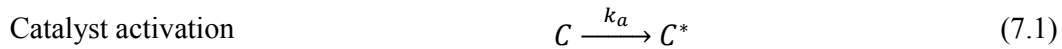
KOKKO et al. (2001) reported that the copolymerization of ethylene and 1,7-octadiene with metallocene catalysts presented higher selectivities for branch formation and could lead to formation of LCBs. NAGA and IMANISHI (2002) investigated the copolymerization of ethylene and 1,7-octadiene or 1,9-decadiene with different zirconocenes. According to these authors, one of the feasible propagation reactions of α,ω-non-conjugated dienes and ethylene takes place between the pendant double bond in the polymer backbone and a growing chain, generating a LCB. They reported the

presence of 1-hexenyl branches in ethylene/ octadiene copolymers, and of 1-octenyl branches in ethylene/ decadiene copolymers.

The low LCB frequency of polyolefins made with coordination catalysts makes the LCB quantification a considerable challenge. Therefore, the development of mathematical models that can predict the frequency and topology of LCBs in these materials is desirable. In this chapter, a mathematical model is proposed to describe the ethylene solution polymerization with a CGC in a semi-batch reactor. Then, the mechanism is adapted to simulate the copolymerization of ethylene with a non-conjugated diene, considering the formation of LCB through reincorporation of macromonomers presenting terminal or pendant double bonds. The model is solved with help of the method of moments and with Monte Carlo procedures to predict comonomer, catalyst, polymer concentration, polymer average molecular weights, and LCB frequencies as functions of time. The model can be eventually employed to select polymerization conditions that lead to production of branched polyethylenes with desired microstructures.

7.3 Kinetic Mechanism Proposed

The mechanism for the copolymerization of ethylene and diene is described by Equations (7.1) to (7.7). When diene propagation (Equation (7.4)) and reincorporation (Equation (7.7)) rate constants are set to zero, the model describes only ethylene homopolymerization.

Catalyst activation	$C \xrightarrow{k_a} C^*$	(7.1)
Initiation	$C^* + M \xrightarrow{k_{p11}} P_1^* \ (+m)$	(7.2)
Propagation (Ethylene)	$P_i^* + M \xrightarrow{k_{p11}} P_{i+1}^* \ (+m)$	(7.3)
Propagation (Diene)	$P_i^* + D \xrightarrow{k_{p12}} P_{i+1}^* \ (+d)$	(7.4)
Transfer to monomer and β-hydride elimination	$P_i^* \xrightarrow{k_t} L_i^= + C^*$	(7.5)
Living chain deactivation	$P_i^* + P_j^* \xrightarrow{k_{dP}} L_i + L_j + 2DC$	(7.6)
Macromonomer reincorporation	$P_i^* + L_j^= \xrightarrow{k_b K} P_{i+j}^* (+ 2 \ lcb)$	(7.7)

where C is the catalyst precursor; C^* is an active catalyst site; M is ethylene; D is diene; DC is a dead catalyst site; m and d are the total amounts of ethylene and diene inserted

into the growing polymer chains, respectively; lcb is the total number of long chain branches in the polymer; P_i^* is a living polymer chain with chain size i; $L_i^=$ is a dead polymer chain that contains a terminal unsaturation and has chain size i; and L_i is a dead polymer chain without a terminal unsaturation.

It is assumed that the initiation rate constant is equal to the propagation rate constant for ethylene (k_{p11}). Moreover, it is also assumed that diene-, ethylene-, and LCB-terminated living polymer chains present similar reactivities, meaning that propagation is controlled by the chemical nature of the monomer species. It is also important to emphasize that k_{p11}, k_{p12} and k_b are not assumed to be equal, meaning that rates of propagation are not equal for the different monomer species.

In the activation reaction step shown in Equation (1), the activation rate constant is equivalent to $k_{a0}[MAO]$. Since the cocatalyst is present in large excess, the product $k_a = k_{a0}[MAO]$ may be considered constant for these polymerizations (SOARES, and MCKENNA, 2012).

Since ethylene concentration is kept constant during the polymerization and does not vary from one experiment to another, transfer to ethylene and β-hydride elimination can be grouped into a single effective reaction rate constant, represented as $k_t = k_{tm}[M] + k_\beta$, as shown in Equation (7.5).

It is assumed the catalyst decay follows the second-order mechanism described in Equation (7.6), since a first order decay rate could not fit the experimental results adequately. Previous modeling results also show that a second order decay rate is more adequate for this catalyst system (MEHDIABADI and SOARES, 2012).

The step responsible for formation of LCBs is the macromonomer reincorporation reaction described in Equation (7.7), where a macromonomer, through one of its pendant vinyl groups, is reincorporated into a propagating chain, generating two LCBs, as illustrated in Figure 7.1. Since pendant vinyl groups in the polymer backbone are the *loci* for LCB formation, it is assumed that the reactivity of the macromonomer is proportional to the number of pendant double bonds in the chain. Thus, the reincorporation reaction rate constant k_b has to be multiplied by the factor K, defined as,

$$K = \varphi j = \frac{d}{(d+m)} j \qquad (7.8)$$

where φ is the average frequency of pendant double bonds in the polymer chains and j is the macromonomer chain length. Therefore, K is the total number of pendant unsaturations present in $L_j^=$ or L_j.

It is important to emphasize that reincorporation of macromonomer through terminal unsaturation is not taken into account in the mechanism. According to the obtained experimental data (Chapter 8), branches were not present in the homopolymer PE, indicating that reincorporation of macromonomer through terminal unsaturation did not occur at significant rates. Besides, when copolymerization is considered, the probability of macromonomer reincorporation through pendant diene double bonds is much higher than the probability of reincorporation through the terminal double bonds, given the relatively high amounts of decadiene incorporated into the polymer chains.
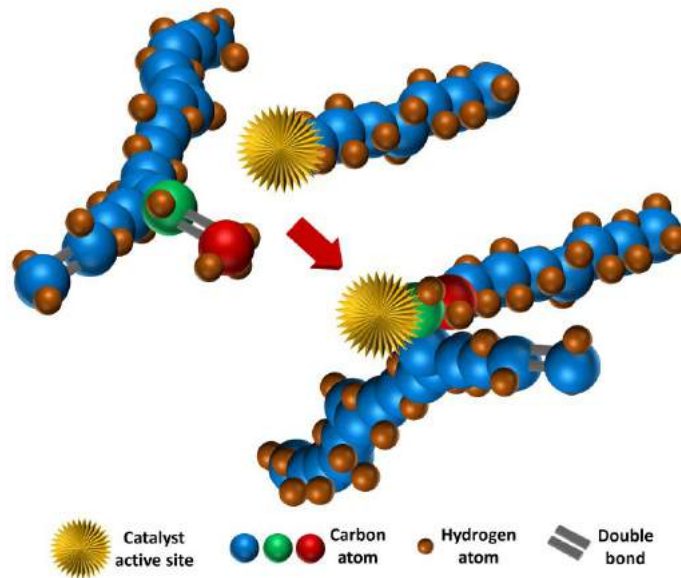

Figure 7.1 – Macromonomer reincorporation through pendant double bonds into a growing polymer chain.

7.4 Material Balances

The mass balance equation for an arbitrary species k can be represented by:

$$\frac{dN_k}{dt} = \dot{N}_k^{\,in} - \dot{N}_k^{\,out} + \int_V \left(\sum_{j \in Reactions} v_{k,j} \cdot r_j \right) dV \qquad (7.9)$$

111

where N_k is the number of mols of species k, $\dot{N}^{in}$ and $\dot{N}^{out}$ are the input and output molar flow rates respectively, $\nu_{k,j}$ is the stoichiometry coefficient for species k in reaction j and V is the system volume.

In the studied system, species k can be the catalyst precursor, active catalyst site, ethylene, diene, dead catalyst site and living or dead polymer chains $\{k \in \{C, C^*, M, D, P_i^*, L_i\}, i \in (1, \infty)\}$. For sake of simplicity, in Equations (7.10) to (7.20), the number of mols will be directly written in terms of the species variables. For example, for catalyst precursor C, instead of representing the number of mols of catalyst precursor as N_C, it will be written as C.

Since the important model variables are related to the liquid phase, the molar balances can be written in terms of the liquid phase. The following additional hypotheses are also assumed:

- The total number of mols of the monomer in the liquid phase remains practically constant during the reaction time, i.e., $\frac{dM}{dt} \approx 0$, since the monomer is constantly fed during the reaction by the feeding gaseous ethylene system;

- The liquid phase is homogeneous, since the mixing is efficient; then

$$\int_V \left(\sum_{j \in Reactions} \nu_{k,j} \cdot r_j \right) dV = V \cdot \sum_{j \in Reactions} \nu_{k,j} \cdot r_j$$

It is important to observe that the energy balance is not necessary, because the temperature was kept constant during the reaction time in all experiments.

Then, for the kinetic model described in Equations (7.1)-(7.7), the molar balances become.

For catalyst C

$$\frac{dC}{dt} = -k_a \left(\frac{C}{V} \right) V \tag{7.10}$$

For active sites C^*

$$\frac{dC^*}{dt} = k_a \left(\frac{C}{V} \right) V - k_{p11} \left(\frac{C^*}{V} \right) \left(\frac{M}{V} \right) V + k_t \sum_{i=1}^{\infty} \left(\frac{P_i^*}{V} \right) V \tag{7.11}$$

For dead sites DC

$$\frac{dDC}{dt} = k_{dP} \sum_{i=1}^{\infty} \left(\frac{P_i^*}{V}\right) \sum_{j=1}^{\infty} \left(\frac{P_j^*}{V}\right) V \tag{7.12}$$

For monomer M

$$\frac{dM}{dt} = 0 \tag{7.13}$$

For diene D (comonomer)

$$\frac{dD}{dt} = -k_{p12} \sum_{i=1}^{\infty} \left(\frac{P_i^*}{V}\right) \left(\frac{D}{V}\right) V \tag{7.14}$$

For the total amount of M added to polymer chains, m

$$\frac{d(m)}{dt} = \left[k_{p11} \left(\frac{C^*}{V}\right) + k_{p11} \sum_{i=1}^{\infty} \left(\frac{P_i^*}{V}\right) \right] \left(\frac{M}{V}\right) V \tag{7.15}$$

For the total amount of D added to polymer chains, d

$$\frac{d(d)}{dt} = k_{p12} \sum_{i=1}^{\infty} \left(\frac{P_i^*}{V}\right) \left(\frac{D}{V}\right) V \tag{7.16}$$

For the total amount of LCB added to polymer chains, lcb

$$\frac{d(lcb)}{dt} = 2 k_b \varphi \sum_{i=1}^{\infty} \left(\frac{P_i^*}{V}\right) \sum_{j=1}^{\infty} j \left(\frac{L_j^=}{V}\right) V \tag{7.17}$$

For the number of living polymer chains with size one P_1^*

$$\frac{dP_1^*}{dt} = k_{p11} \left(\frac{C^*}{V}\right) \left(\frac{M}{V}\right) V - k_{p11} \left(\frac{P_1^*}{V}\right) \left(\frac{M}{V}\right) V - k_{dP} \left(\frac{P_1^*}{V}\right) \sum_{i=1}^{\infty} \left(\frac{P_i^*}{V}\right) V$$

$$- k_t \left(\frac{P_1^*}{V}\right) V - k_b \varphi \left(\frac{P_1^*}{V}\right) \sum_{j=1}^{\infty} j \left(\frac{L_j^=}{V}\right) V - k_{p12} \left(\frac{P_1^*}{V}\right) \left(\frac{D}{V}\right) V \tag{7.18}$$

113

For the number of living polymer chains with size greater than one P_i^*, $i \in$

$$(2, \infty)$$

$$\frac{dP_i^*}{dt} = -k_{p11}\left(\frac{P_i^*}{V}\right)\left(\frac{M}{V}\right)V + k_{p11}\left(\frac{P_{i-1}^*}{V}\right)\left(\frac{M}{V}\right)V + k_{p12}\left(\frac{P_{i-1}^*}{V}\right)\left(\frac{D}{V}\right)V$$

$$- k_{dP}\left(\frac{P_i^*}{V}\right)\sum_{j=1}^{\infty}\left(\frac{P_j^*}{V}\right)V - k_t\left(\frac{P_i^*}{V}\right)V - k_{p12}\left(\frac{P_i^*}{V}\right)\left(\frac{D}{V}\right)V$$

$$- k_b\varphi\left(\frac{P_i^*}{V}\right)\sum_{j=1}^{\infty}j\left(\frac{L_j^=}{V}\right)V + k_b\varphi\sum_{j=1}^{i-1}j\left(\frac{P_{i-j}^*}{V}\right)\left(\frac{L_j^=}{V}\right)V$$

(7.19)

For the number of dead polymer chains LL_i, $i \in (1, \infty)$

$$\frac{dLL_i}{dt} = k_t\left(\frac{P_i^*}{V}\right)V + k_{dP}\left(\frac{P_i^*}{V}\right)\sum_{j=1}^{\infty}\left(\frac{P_j^*}{V}\right)V - k_b\varphi i\left(\frac{L_i^=}{V}\right)\sum_{j=1}^{\infty}\left(\frac{P_j^*}{V}\right)V$$

(7.20)

where $LL_i = L_i^= + L_i$

Equations (7.11) to (7.20) define a system of infinite discrete ordinary differential equations. As previously commented, the concentration of ethylene in the reaction mixture is practically constant throughout the polymerization, calculated as described before (Section 5.2.3.3).

7.5 Numerical Approach

As discussed in Section 5.3, the model was solved by using:

- the Method of Moments, coupled with the DASSL solver, for solving the system of differential equations;
- the Adaptive Orthogonal Collocation Method and the Monte Carlo Method, calculation of MWDs.

One must observe that Monte Carlo simulations do not require a traditional solver for solution of the discretized set of ODE.

7.5.1 Material Balances after Applying the Method of Moments

The material balances of Section 7.4 can be rewritten using the moments defined in Chapter 3. For the non-distributed species (Equation (7.11) to (7.17)), all summations

have to be replaced by a moment; the substitution is straightforward. For distributed species (living and dead chains), the molar balances must be replaced by zeroth, first and second moment balance equations, resulting in the following expressions (see APPENDIX D).

$$\frac{d\mu_0}{dt} = k_{p11}\left(\frac{C^*}{V}\right)\left(\frac{M}{V}\right)V - k_t\left(\frac{\mu_0}{V}\right)V - k_{dP}\left(\frac{\mu_0}{V}\right)^2 V \tag{7.21}$$

$$\frac{d\mu_1}{dt} = -k_t\left(\frac{\mu_1}{V}\right)V - k_{dP}\left(\frac{\mu_1}{V}\right)\left(\frac{\mu_0}{V}\right)V + k_{p12}\left(\frac{\mu_0}{V}\right)\left(\frac{D}{V}\right)V$$

$$+ k_{p11}\left[\left(\frac{\mu_0}{V}\right) + \left(\frac{C^*}{V}\right)\right]\left(\frac{M}{V}\right)V + k_b\varphi\left(\frac{\mu_0}{V}\right)\left(\frac{\lambda_2}{V}\right)V \tag{7.22}$$

$$\frac{d\mu_2}{dt} = -k_t\left(\frac{\mu_2}{V}\right)V - k_{dP}\left(\frac{\mu_2}{V}\right)\left(\frac{\mu_0}{V}\right)V + k_{p11}\left[2\left(\frac{\mu_1}{V}\right) + \left(\frac{\mu_0}{V}\right) + \left(\frac{C^*}{V}\right)\right]\left(\frac{M}{V}\right)V$$

$$+ k_{p12}\left[2\left(\frac{\mu_1}{V}\right) + \left(\frac{\mu_0}{V}\right)\right]\left(\frac{D}{V}\right)V \tag{7.23}$$

$$+ k_b\varphi\left[2\left(\frac{\mu_1}{V}\right)\left(\frac{\lambda_2}{V}\right) + \left(\frac{\mu_0}{V}\right)\left(\frac{\lambda_3}{V}\right)\right]V$$

$$\frac{d\lambda_0}{dt} = k_{dP}\left(\frac{\mu_0}{V}\right)^2 V + k_t\left(\frac{\mu_0}{V}\right)V - k_b\varphi\left(\frac{\lambda_1}{V}\right)\left(\frac{\mu_0}{V}\right)V \tag{7.24}$$

$$\frac{d\lambda_1}{dt} = k_{dP}\left(\frac{\mu_1}{V}\right)\left(\frac{\mu_0}{V}\right)V + k_t\left(\frac{\mu_1}{V}\right)V - k_b\varphi\left(\frac{\lambda_2}{V}\right)\left(\frac{\mu_0}{V}\right)V \tag{7.25}$$

$$\frac{d\lambda_2}{dt} = k_{dP}\left(\frac{\mu_2}{V}\right)\left(\frac{\mu_0}{V}\right)V + k_t\left(\frac{\mu_2}{V}\right)V - k_b\varphi\left(\frac{\lambda_3}{V}\right)\left(\frac{\mu_0}{V}\right)V \tag{7.26}$$

By using the method of moments, the problem to be solved changes from a system of infinite discrete-differential equations to a finite, and relatively small, set of differential equations.

Macromonomer reincorporation through pendant unsaturations gives rise to a moment closure problem. To solve this problem, the method of HULBURT and KATZ (1964) presented in Section 3.2 was used.

During the polymerization, the volume of the reacting system changes slightly because of the polymer formation. This effect was accounted for by using the following expression,

$$\frac{dV}{dt} = \left(\frac{d\lambda_1}{dt} + \frac{d\mu_1}{dt}\right)\frac{MM}{\rho_{PE}} \tag{7.27}$$

where ρ_{PE} is the specific volume of polyethylene.

Equation (7.11) to (7.17) and Equations (7.21) to (7.27) were solved with the backward differentiation formula, as available in DASSL code, with relative and absolute tolerances of 10^{-4} (PETZOLD, 1982).

After solving the model, the average polymer properties could be obtained. The weight and number average molecular weights and polydispersity index were calculated with the calculated moments as shown in Chapter 3. The equations are rewritten below.

$$M_n = \frac{\lambda_1 + \mu_1}{\lambda_0 + \mu_0} MM \tag{7.28}$$

$$M_w = \frac{\lambda_2 + \mu_2}{\lambda_1 + \mu_1} MM \tag{7.29}$$

$$PDI = \frac{M_w}{M_n} = \frac{\lambda_2 + \mu_2}{\lambda_0 + \mu_0} \tag{7.30}$$

The average molar mass of the repeating unit MM can be calculated as

$$MM = \varphi MM_D + (1 - \varphi)MM_M \tag{7.31}$$

where MM_D and MM_M are the molar masses of diene and ethylene, respectively, and φ is the average molar fraction of diene in the copolymer. Since the molar fraction of diene is very small for the copolymers studied in the present investigation, MM can be approximated to the molar mass of ethylene without much influence on the final numerical results.

The average LCB per 1000 carbon atoms and average LCB per chain can also be calculated with the help of the moments,

$$LCB/1000C \ atoms = 1000 \frac{lcb}{2(\lambda_1 + \mu_1)}$$ (7.32)

$$LCB/chain = \frac{lcb}{(\lambda_0 + \mu_0)}$$ (7.33)

7.5.2 Estimation of Homopolymerization Parameters

As already commented in Chapter 6, model parameters were estimated using the computational package ESTIMA (SCHWAAB et al., 2008). The method described by YAO et al. (2003) was used to verify which parameters could be estimated with their respective uncertainties. The non-estimable parameters were kept constant during the parameter estimation process. Figure 6.1 illustrates this process.

With the exception of the propagation rate constant, the homopolymerization rate constants were written using the following reparameterized form of the Arrhenius equation,

$$k = exp\left[A + B\left(\frac{(T - T_r)}{T}\right)\right]$$ (7.34)

where T and T_r are reaction and reference temperatures, respectively; and k is the reaction rate constant. The reference temperature is usually defined as a suitable average temperature for the analyzed experimental data (SCHWAAB et al., 2008). In this work, T_r was set to 130 °C.

Table 7.1 summarizes the parameters estimated for the homopolymerization reactions and shows how the pre-exponential factor k_0 and the activation energy E can be recovered.

It was assumed that the activation energy for propagation was equal to 20520 J mol^{-1}, based on a previous work performed with this very same catalyst system (MEHDIABADI, 2011). Thus, k_{p11} was represented by the traditional Arrhenius expression as:

117

$$k_{p11} = k_{0_p} exp\left(-\frac{20520}{8.314 \cdot T}\right) = 10^{k_7} exp\left(-\frac{20520}{8.314 \cdot T}\right)$$ (7.35)

Table 7.1. Kinetic reaction constants for the mechanism shown in Equation (7.1) to (7.7).

Reaction Step	Reparameterized Arrhenius Equation	Traditional Arrhenius Parameters	
Catalyst activation	$k_a = exp\left\{k_1 + k_2\left[\frac{(T - T_r)}{T}\right]\right\}$	$E_a = k_2 R T_r$	$k_{0_a} = e^{(k_1+k_2)}$
Monomer transfer & β-hydride elimination	$k_t = exp\left\{k_3 + k_4\left[\frac{(T - T_r)}{T}\right]\right\}$	$E_t = k_4 R T_r$	$k_{0_t} = e^{(k_3+k_4)}$
Living chain deactivation	$k_{dP} = exp\left\{k_5 + k_6\left[\frac{(T - T_r)}{T}\right]\right\}$	$E_{dP} = k_6 R T_r$	$k_{0_{dP}} = e^{(k_5+k_6)}$

For ethylene homopolymerizations, 7 parameters were defined $(k_1, k_2, ..., k_7)$. On the other hand, for copolymerization of ethylene and diene at 120 °C, two parameters were estimated (k_{p12}, k_b), and the other parameters were set equal to the values estimated for the homopolymerization reactions.

7.5.3 Adaptive Orthogonal Collocation Method

The adaptive orthogonal collocation method was used to build the molecular weight distributions and the final curves were compared with those obtained by simulation with the MC method and with the experimental MWDs provided by Polymer Char high-temperature gel permeation chromatography. As already mentioned in Chapter 3, it was initially assumed that the Flory distribution could be used as an appropriate reference function. Then, when a certain time was reached (t_c), the reference function was updated and made equal to the distribution of the last iteration, as shown in Figure 3.1.

Let ε represent either *P or L* in the balance equations. As commented in Chapter 3, for the orthogonal collocation method, the following approximation is proposed.

$$\varepsilon(i) = \theta^{\varepsilon}(i) \sum_{k=1}^{N} a_k^{\varepsilon} l_k^{\varepsilon}\left(s_j^{\varepsilon}\right)$$

(7.36)

where ε is equal to either P or L. It must be pointed out that the reference function and nodal points of P and L can be different. Based on this approach, the dependent variables are the Lagrange polynomial coefficients a_k^P and a_k^L. It is important to emphasize that the residue at the collocation points are equal to zero. Inserting Equation (7.36) into Equations (7.18) to (7.20), the material balances can be rewritten as shown in Equations (7.37)-(7.39). The first collocation point for the living polymer chain approximation is always equivalent to one in the present work. So, a separate ODE must be solved for the coefficient a_1^P:

$$\theta^P(s_1^P)\frac{da_1^P}{dt} = k_{p11}\left(\frac{C^*}{V}\right)\left(\frac{M}{V}\right)V - \left(k_{p11}\left(\frac{M}{V}\right) + k_t\right)\left(\frac{\theta^P(s_1^P)a_1^P}{V}\right)V$$

$$- k_{dP}\left(\frac{\theta^P(s_1^P)a_1^P}{V}\right)\left[\sum_{k=1}^{N} a_k^P \sum_{j=1}^{\infty}\left(\frac{\theta^P(s_j^P)l_k(s_j^P)}{V}\right)\right]V$$

$$- k_b\varphi\left(\frac{\theta^P(s_1^P)a_1^P}{V}\right)\left[\sum_{k=1}^{N} a_k^L \sum_{j=1}^{\infty} j\left(\frac{\theta^L(s_j^L)l_k(s_j^L)}{V}\right)\right]V$$

$$- k_{p12}\left(\frac{\theta^P(s_1^P)a_1^P}{V}\right)\left(\frac{D}{V}\right)V$$

(7.37)

The other $N - 1$ polynomial coefficients for the living polymer chain approximation are computed according with Equation (7.38), with j varying from 2 to N.

$$\theta^P(s_j^P)\frac{da_j^P}{dt}$$

$$= -\left(k_{p11}\left(\frac{M}{V}\right) + k_t\right)\left(\frac{\theta^P(s_j^P)a_j^P}{V}\right)V$$

$$+ k_{p11}\left(\frac{\theta^P(s_j^P - 1)\sum_{k=1}^{N} a_k^P l_k(s_j^P - 1)}{V}\right)\left(\frac{M}{V}\right)V$$

$$+ k_{p12}\left(\frac{\theta^P(s_j^P - 1)\sum_{k=1}^{N} a_k^P l_k(s_j^P - 1)}{V}\right)\left(\frac{D}{V}\right)V$$

$$- k_{dP}\left(\frac{\theta^P(s_j^P)a_j^P}{V}\right)\left[\sum_{k=1}^{N} a_k^P \sum_{jj=1}^{\infty}\left(\frac{\theta^P(s_{jj}^P)l_k(s_{jj}^P)}{V}\right)\right]V \qquad (7.38)$$

$$- k_{p12}\left(\frac{\theta^P(s_j^P)a_j^P}{V}\right)\left(\frac{D}{V}\right)V$$

$$- k_b\varphi\left(\frac{\theta^P(s_j^P)a_j^P}{V}\right)\left[\sum_{k=1}^{N} a_k^L \sum_{jj=1}^{\infty} jj\left(\frac{\theta^L(s_{jj}^L)l_k(s_{jj}^L)}{V}\right)\right]V$$

$$+ k_b\varphi\sum_{h=1}^{N} a_h^L \sum_{k=1}^{N} a_k^P \sum_{jj=1}^{s_j^P-1} jj\left(\frac{\theta^P(s_j^P - jj)l_k(s_j^P - jj)}{V}\right)\left(\frac{\theta^L(jj)l_h(jj)}{V}\right)V$$

The population balance for the dead polymer chains are similarly substituted by Equation (7.39).

$$\theta^L(s_j^L)\frac{da_j^L}{dt}$$

$$= k_t\left(\frac{\theta^P(s_j^L)\sum_{k=1}^{Nk} a_k^P l_k(s_j^L)}{V}\right)V$$

$$+ k_{dP}\left(\frac{\theta^P(s_j^L)\sum_{k=1}^{Nk} a_k^P l_k(s_j^L)}{V}\right)\left[\sum_{k=1}^{N} a_k^P \sum_{jj=1}^{\infty}\left(\frac{\theta^P(s_{jj}^P)l_k(s_{jj}^P)}{V}\right)\right]V \qquad (7.39)$$

$$- k_{b1}\varphi s_j^L\left(\frac{\theta^L(s_j^L)a_j^L}{V}\right)\left[\sum_{k=1}^{N} a_k^P \sum_{jj=1}^{\infty}\left(\frac{\theta^P(s_{jj}^P)l_k(s_{jj}^P)}{V}\right)\right]V$$

where $j = 1, \ldots, N$.

All balance equations for the non-distributed species that depend on P_j^* must also be modified, by replacing P_j^* by Equation (7.40):

$$\varepsilon(i) = \theta^\varepsilon(i) \sum_{k=1}^{N} a_k^\varepsilon l_k^\varepsilon \left(s_j^\varepsilon\right) \tag{7.40}$$

where $\varepsilon = P$ or L.

MWDs can be obtained from the number chain length distribution (CLD). While the number CLD is represented with respect to the chain length (polymerization degree), the MWD is represented as a function of the molecular weight (chain length multiplied by the molecular weight of the monomer unit) (SAYER et al., 2001). Thus, after running the complete adaptive orthogonal collocation (Figure 3.1), the MWD can be obtained as follows:

$$P_i^* \longrightarrow iP_i^* \longrightarrow i^2P_i^*$$

number CLD   weight CLD   GPC MWD
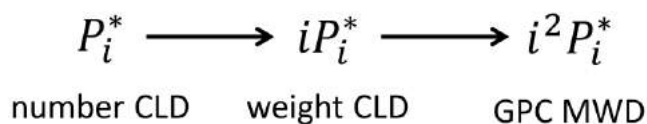
Figure 7.2– Scheme to obtain MWD from the number CLD.

7.5.4 Monte Carlo Technique

The Monte Carlo basic principles were described thoroughly in Chapter 4. As commented there, the number of molecules of each species present in the reaction system must be updated after each time increment and saved in a position of vector **X**. The set of initial conditions for each simulation are written in Table 7.2.

Table 7.2. Number of molecules of each species present in the system at the initial time.[a)]

	Species	Number of molecules at t = 0
C	X_1	$[C]_{sID}N_AV$
C*	X_2	0
DC	X_3	0
M	X_4	$[C_2H_4]_T N_AV$
D	X_5	$[D]_{sID}N_AV$
Living chains **P**	X_6	0
Dead chains **L**	X_7	0

[a)]sID is the experimental condition used to produce sample ID; N_A is the Avogadro number, and V is the control volume selected to run the simulation.

121

The most adequate control volume selected to perform all the MC simulations in the present work was $5 \cdot 10^{-15}$ L. Table 7.3 summarizes all MC reaction rate expressions and the implemented algorithm for Equations (7.10) to (7.20).

Then, the Monte Carlo steps could be implemented as follows:

- ⮑ **Step 1:** Define the initial time $t = t_0 = 0$ and initial conditions for all species (Table 7.2).
- ⮑ **Step 2:** Convert the macroscopic reaction rate constants into microscopic MC rate constants. For unimolecular reactions $k^{MC} = k^{exp}$; for bimolecular reactions between different molecules $k^{MC} = \frac{k^{exp}}{VN_A}$; for bimolecular reactions between equal molecules $k^{MC} = 2\frac{k^{exp}}{VN_A}$ (Table 4.2).
- ⮑ **Step 3:** Calculate all MC reaction rates, also called propensity functions (Table 4.3).
- ⮑ **Step 4:** Calculate the sum of all propensity functions and save the result in the variable $a_0(X)$,

$$a_0(X) = \sum_{k=1}^{NR} a_k(X)$$

where NR is the total number of reaction channels (in this case, 7).

- ⮑ **Step 5:** Calculate the time step τ for the current iteration,

$$\tau = \frac{1}{a_0(X)} \ln\left(\frac{1}{r_1}\right)$$

where r_1 is a random number sampled from a uniform distribution in the interval [0,1].

- ⮑ **Step 6:** Select the reaction that must be executed, finding the value for j in the equation,

$$\sum_{j\prime=1}^{j} a_{j\prime}(X) \geq r_2 a_0(X)$$

where j is the smallest integer that satisfies the inequality and r_2 is a random number sampled from a uniform distribution in the interval [0,1].

⮞ **Step 7:** Execute reaction R_j, updating the state vector $\mathbf{X} \leftarrow \mathbf{X} + \mathbf{v}_j$, where v_j is the stoichiometric vector for reaction j.

⮞ **Step 8:** Update time:

$$t = t + \tau$$

⮞ **Step 9:** Save $(\mathbf{P}, \mathbf{L}, \mathbf{X}, t)$ as desired. If t is lower than the final simulation time, return to Step 3; else, stop simulation.

The Monte Carlo method was implemented to simulate the polymerization mechanism described by Equations (7.1) to (7.7), but a few changes were made in some of the reaction steps in order to include the number of pendant double bonds and LCBs in the living and dead chains. Because of these modifications, it was not necessary to consider species m, d and lcb, since they can be calculated precisely for each chain. A structure (or matrix) called $\mathbf{L}$ was used to store all the information regarding the dead chains. Each position of $\mathbf{L}$ saved the chain length, number of double bonds and number of LCBs for a certain dead polymer chain, as illustrated in Figure 7.3.

The overall MC procedure employed to simulate the copolymerization of ethylene with 1,9-decadiene using CGC-Ti in semi-batch operation is illustrated in Figure 7.4.

Table 7.3. Monte Carlo computation steps for each chemical reaction and their respective MC reaction rates.[6]

Reaction Type	MC Reaction Rates
Catalyst activation $C \xrightarrow{k_a} C^*$	$a_1(X) = R_1^{MC} = k_a^{MC} X_1$
Initiation $C^* + M \xrightarrow{k_{p11}} P_{1,0,0}^*$	$a_2(X) = R_2^{MC} = k_{p11}^{MC} X_2 X_4$
Propagation $P_{i,j,k}^* + M \xrightarrow{k_{p11}} P_{i+1,j,k}^*$	$a_3(X) = R_3^{MC} = k_{p11}^{MC} X_4 X_6$
Propagation $P_{i,j,k}^* + D \xrightarrow{k_{p12}} P_{i+1,j+1,k}^*$	$a_4(X) = R_4^{MC} = k_{p12}^{MC} X_5 X_6$
Monomer transfer & β-hydride elimination $P_{i,j,k}^* \xrightarrow{k_t} L_{i,j,k}^= + P_1^*$	$a_5(X) = R_5^{MC} = k_t^{MC} X_6$
Living chain deactivation $P_{i,m,b}^* + P_{j,n,z}^* \xrightarrow{k_{dP}} L_{i,m,b} + L_{j,n,z} + 2DC$	$a_6(X) = R_6^{MC} = k_{dP}^{MC} \dfrac{X_6 X_6}{2}$
Macromonomer reincorporation $P_{i,m,b}^* + L_{j,n,z}^= \xrightarrow{k_b} P_{i+j,m+n-1,b+z+2}^*$	$a_7(X) = R_7^{MC} = k_b^{MC} X_6 \pi_t$ [a)]

[a)] where π_t corresponds to the total number of pendant double bonds in the dead chains.

---

[6] All dead chains were saved in $\mathbf{L}$: $L_{i,j,k}$ and $L_{i,j,k}^=$.
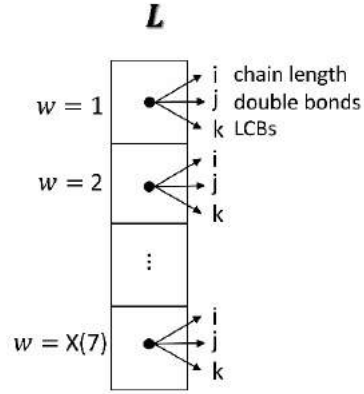
$$\pi_t = \sum_{w=1}^{X_7} j_{from\ L_{i,j,k}} = \left(j_{from\ L_{i,j,k}}\right)_{w=1} + \cdots + \left(j_{from\ L_{i,j,k}}\right)_{w=X_7}$$

Figure 7.3 – Calculation of the total number of pendant double bonds in dead chains (π_t).
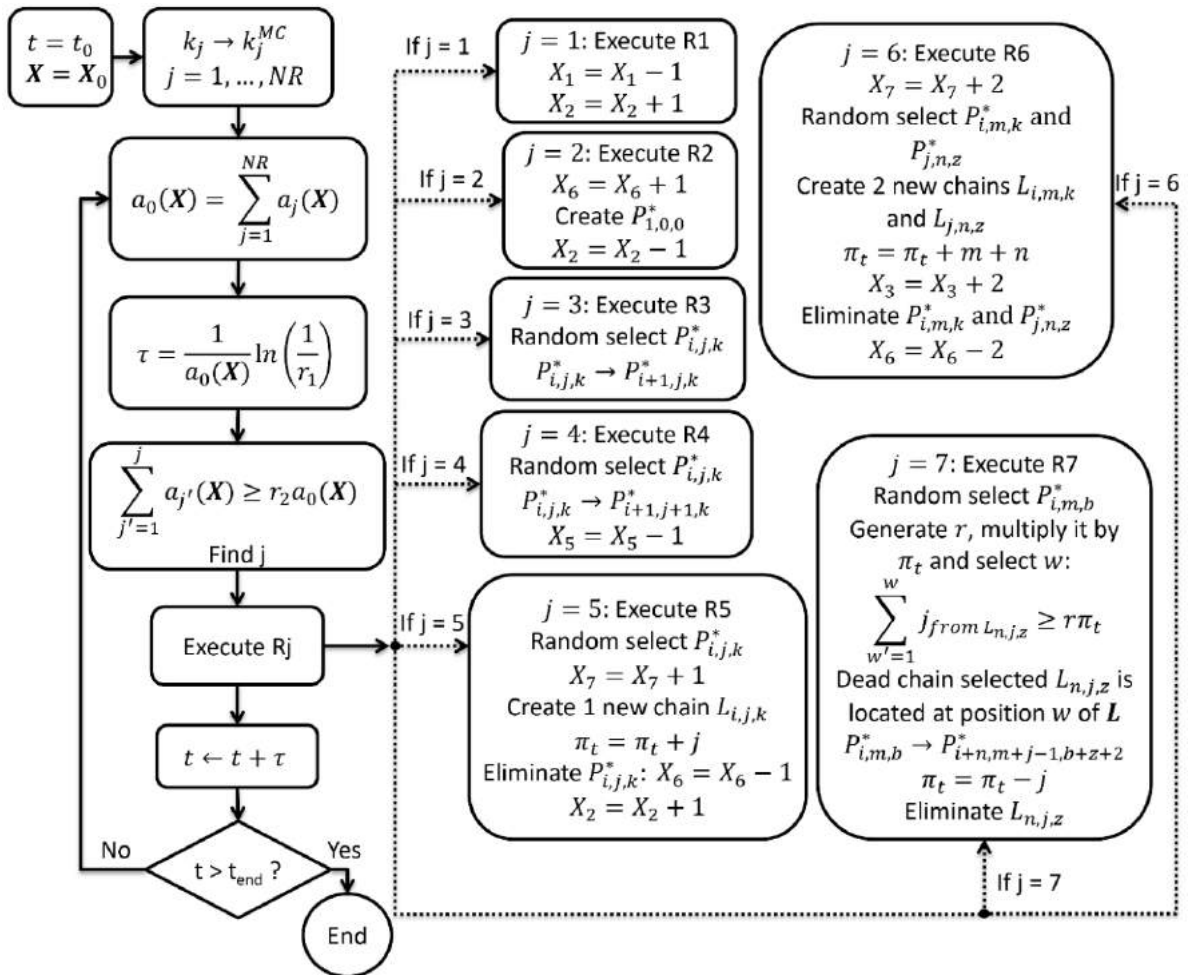

Figure 7.4 – Monte Carlo flowchart (r_1, r_2 and r are uniform random numbers in the interval [0,1]).

124

PART III- Results

8 Prediction of Average Molecular Weights and LCB Frequencies

8.1 Summary

In this chapter, the estimation results obtained for homo – and copolymerization reactions are presented and discussed. For the homopolymerization model parameters, not all of them could be estimated, as some of them were classified as non-estimable parameters. Nevertheless, the confidence region for the model parameters could be built according to the Particle Swarm Optimization method. The model predictions calculated with the method of Moments are also compared with the available experimental data. The simulation results for long-chain branching frequencies using the method of moments and using the method of Monte Carlo are compared with each other. Additionally, the MC technique is used to predict the MWD of the copolymers.

8.2 Ethylene Homopolymerization

As presented in the experimental section, the investigated conditions included different temperatures and catalysts concentrations, as shown in Figure 8.1.
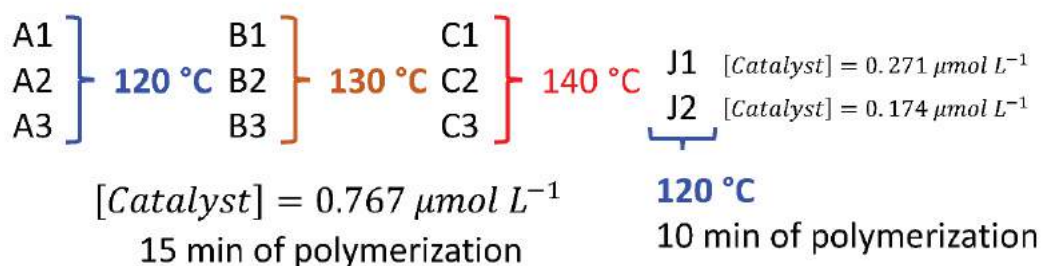
Figure 8.1 – Experimental conditions for homopolymerization reactions.

To facilitate reading, the proposed kinetic mechanism and the final expressions of the homopolymerization model reaction rate constants are rewritten as:

Catalyst activation	$C \xrightarrow{k_a} C^*$	(8.1)
Initiation	$C^* + M \xrightarrow{k_{p11}} P_1^* \ (+m)$	(8.2)
Propagation (Ethylene)	$P_i^* + M \xrightarrow{k_{p11}} P_{i+1}^* \ (+m)$	(8.3)
Propagation (Diene)	$P_i^* + D \xrightarrow{k_{p12}} P_{i+1}^* \ (+d)$	(8.4)
Transfer to monomer and β-hydride elimination	$P_i^* \xrightarrow{k_t} L_i^= + C^*$	(8.5)
Living chain deactivation	$P_i^* + P_j^* \xrightarrow{k_{dP}} L_i + L_j + 2DC$	(8.6)
Macromonomer reincorporation	$P_i^* + L_j^= \xrightarrow{k_b K} P_{i+j}^* (+ 2\ lcb)$	(8.7)
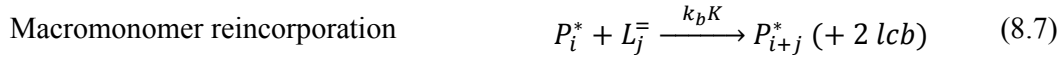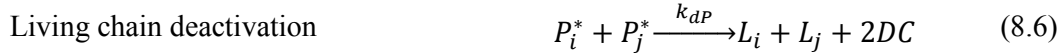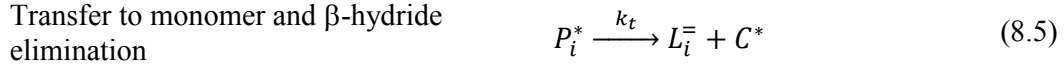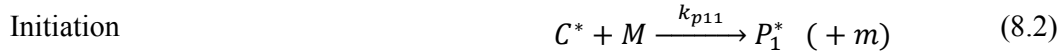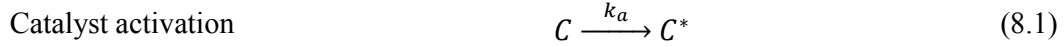
As commented in Section 6.5, the homopolymerization model parameters (k_a, k_{p11}, k_t and k_{dP}) were expressed in the form of reparameterized Arrhenius equations, with the exception of k_{p11}, since the activation energy is already known (20520 J mol^{-1} (MEHDIABADI, 2011)), resulting in seven parameters to be estimated which are shown in Table 8.1.

Table 8.1. Kinetic reaction constants for the mechanism shown in Equations (7.1) to (7.7).

Reaction Step	Final Expression for the model parameter
Catalyst activation	$k_a = exp\left\{k_1 + k_2 \left[\dfrac{(T - T_r)}{T}\right]\right\}$
Monomer transfer & β-hydride elimination	$k_t = exp\left\{k_3 + k_4 \left[\dfrac{(T - T_r)}{T}\right]\right\}$
Living chain deactivation	$k_{dP} = exp\left\{k_5 + k_6 \left[\dfrac{(T - T_r)}{T}\right]\right\}$
Ethylene propagation	$10^{k_7} exp\left(-\dfrac{20520}{8.314 \cdot T}\right)$

8.2.1 Parameter Estimation

The experimental data used to estimate the model parameters are the number and weight average molecular weights of the polymer samples and the observed ethylene feed rates. These experimental data and the fit of the model after the estimation procedure are shown in Section 8.2.2.

Initially, the seven parameters $(k_1, k_2, ..., k_7)$ defined for the homopolymerization reactions had their values determined stochastically by the PSO algorithm. The obtained values are presented in Table 8.2.

Table 8.2. Values of parameters from PSO

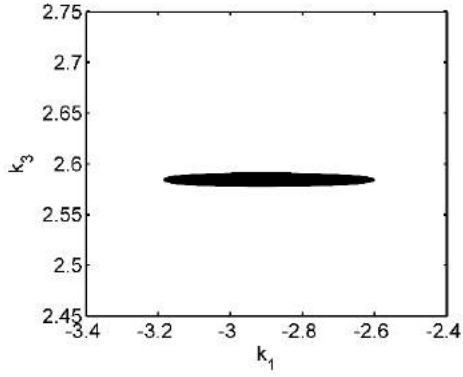| Parameter	
k_1	-2.92
k_2	25.2
k_3	2.58
k_4	17.2
k_5	10.91
k_6	30.12
k_7	7.56

It is very common in kinetic polymerization studies to take some parameters from the literature and estimate others. One can argue that this can lead to misleading confidence regions of parameters uncertainties, and this topic will be explored in more details here.

Figure 8.2 represents the confidence regions of parameter uncertainties obtained with the PSO and after random generation of model parameters values. In the left column, the confidence regions were represented for pair of parameters (keeping the others equal to the values presented in Table 8.2); in the right column, the confidence regions were generated considering all 7 parameters varying simultaneously, as obtained through the PSO.

Model parameters calculated with the PSO

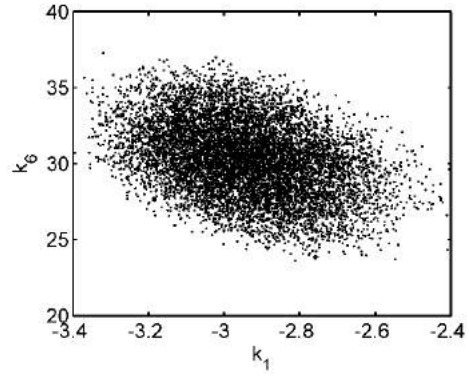(a) (b)
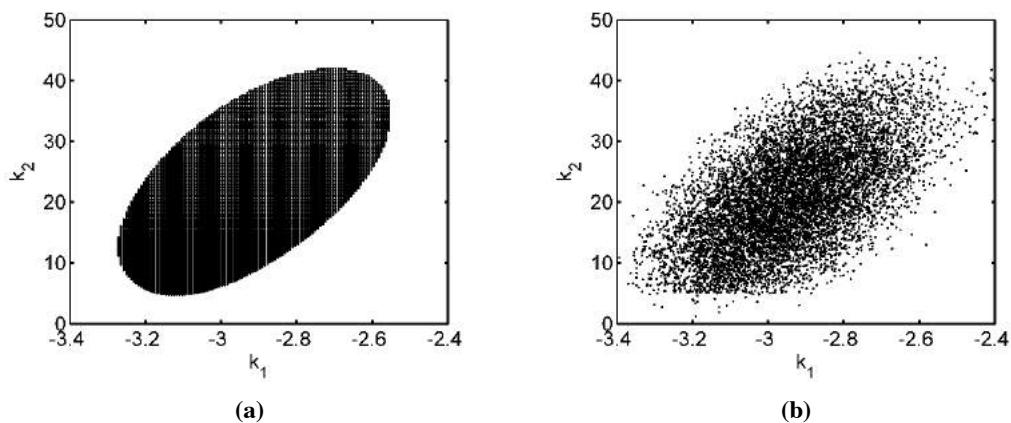
Model parameters calculated with the PSO
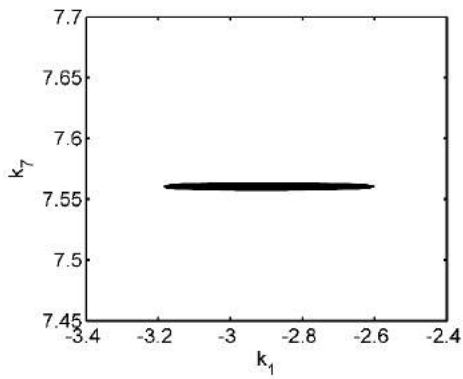

(c)
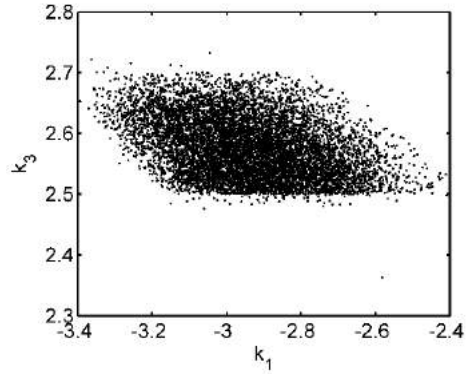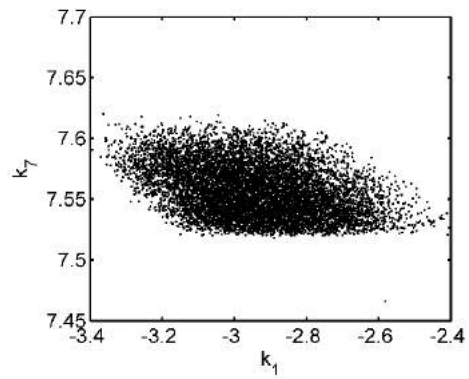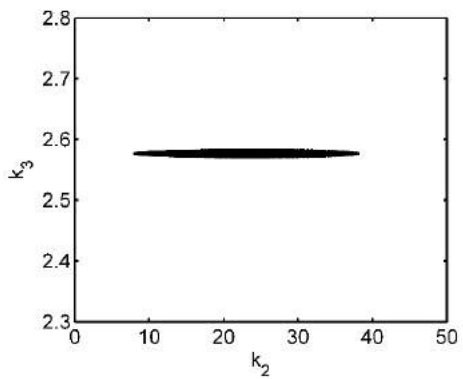
(d)
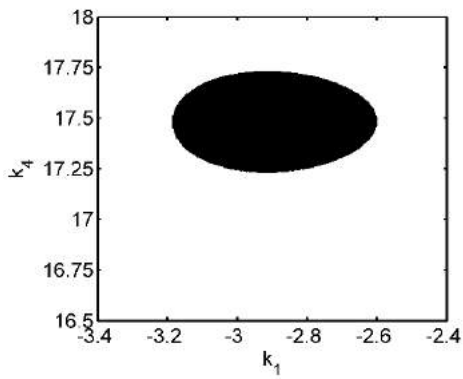
(e)
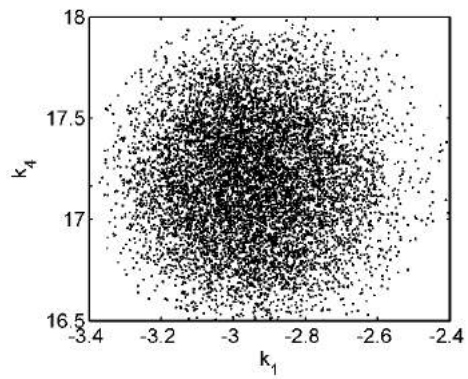
(f)
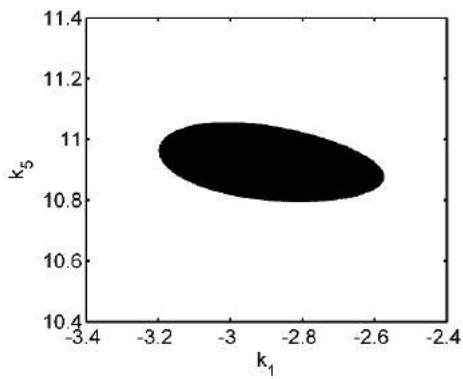
(g)
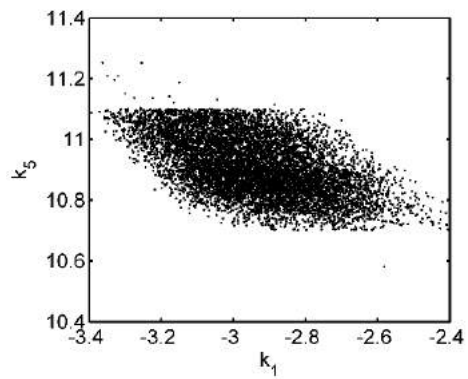
(h)

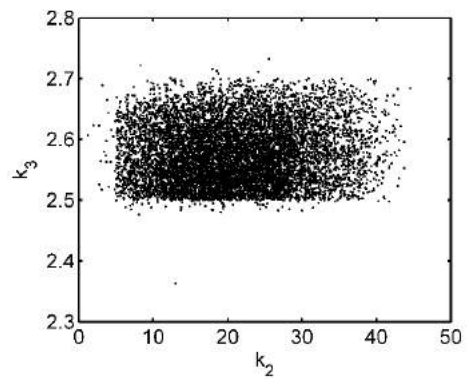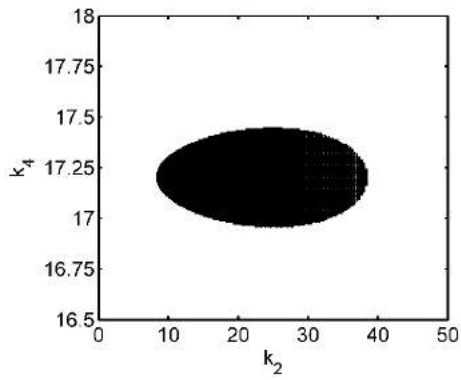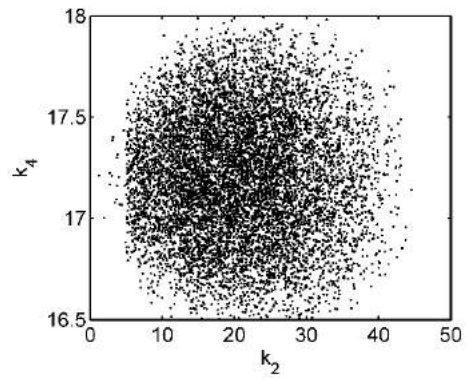# Model parameters calculated with the PSO
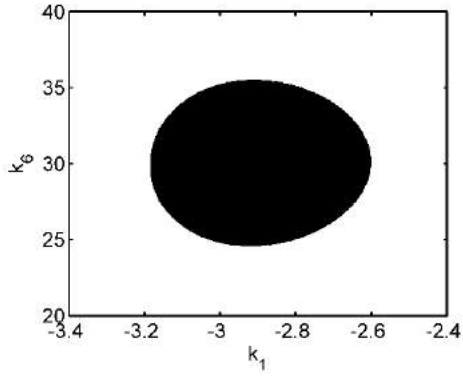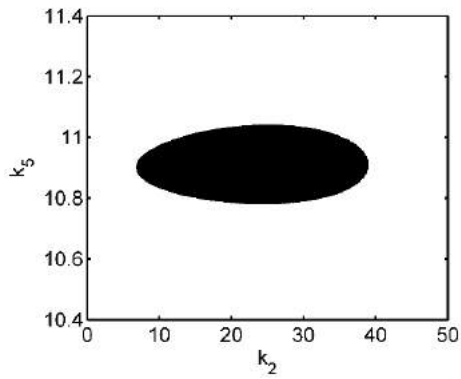

(i)
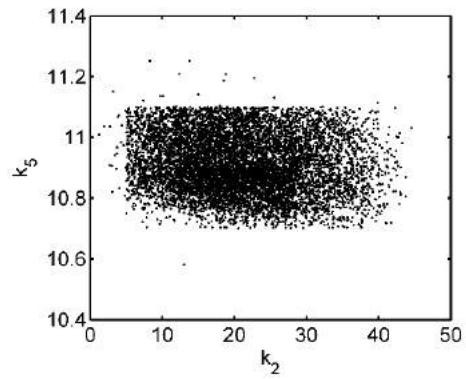
(j)

(k)

(l)

(m)

(n)

Model parameters calculated with the PSO

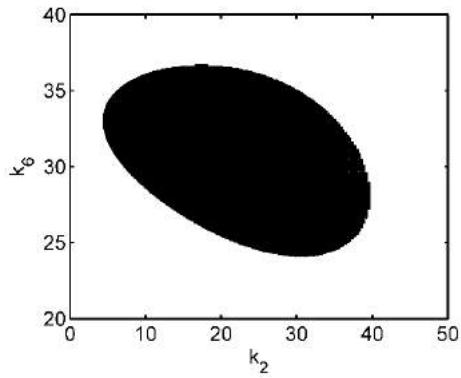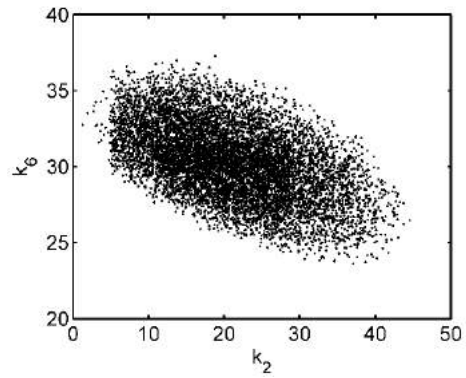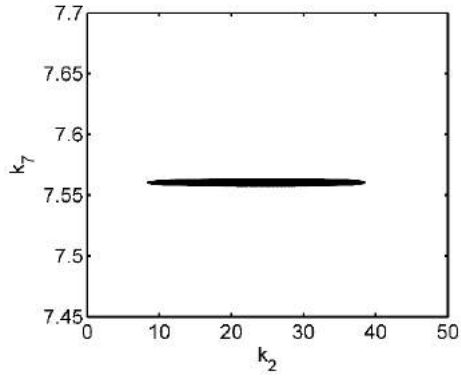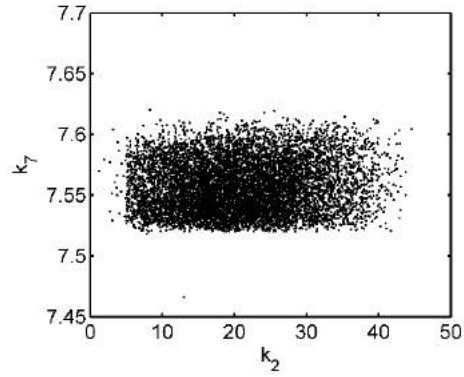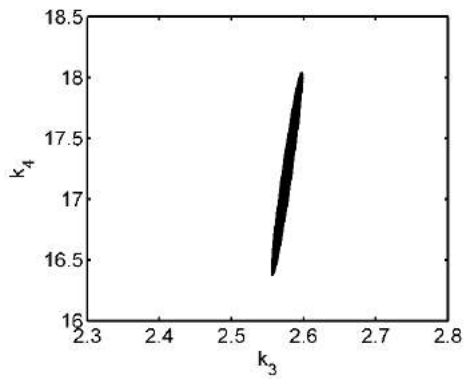(o)

(p)

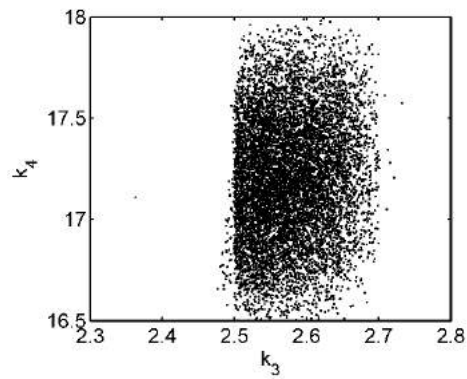
(q)

(r)

(s)

(t)

Model parameters calculated with the PSO

(u)

(v)

(w)

(x)

(y)

(z)

132
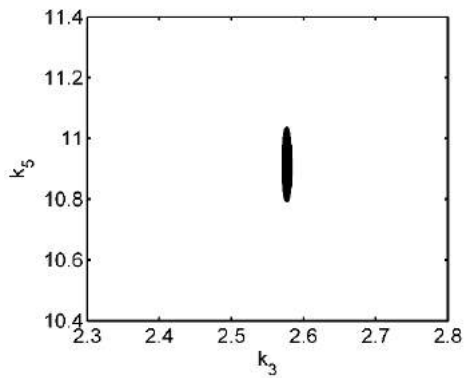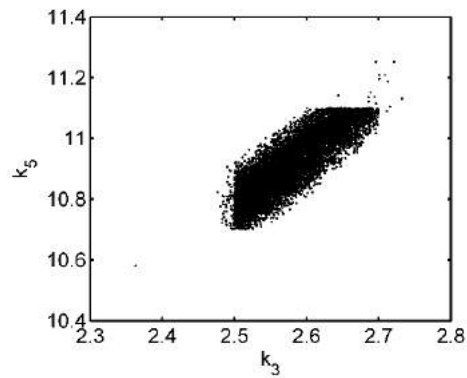
Model parameters calculated with the PSO

(aa)

(ab)

(ac)

(ad)

(ae)

(af)

133
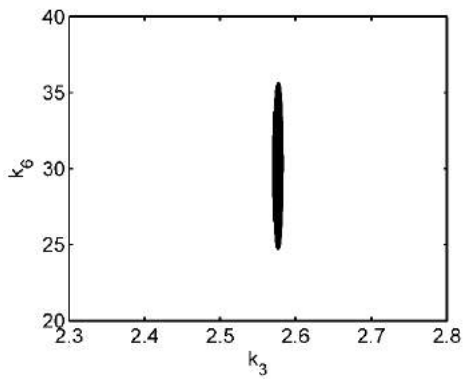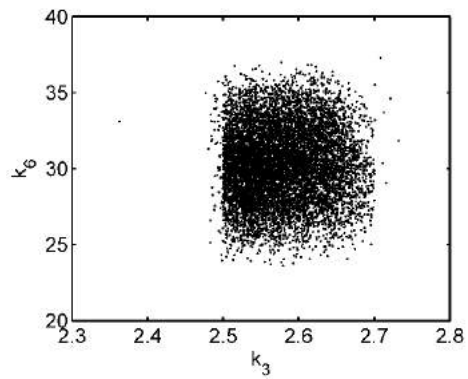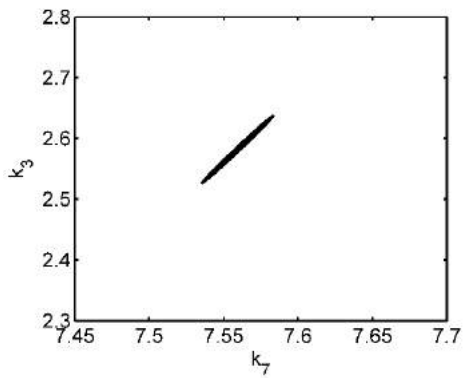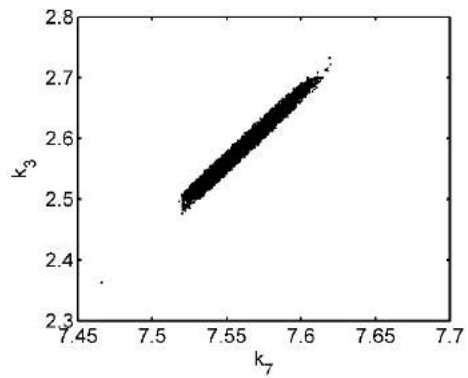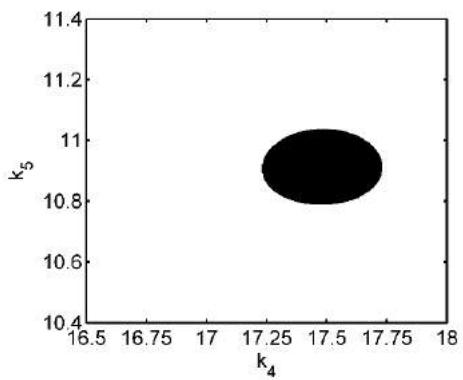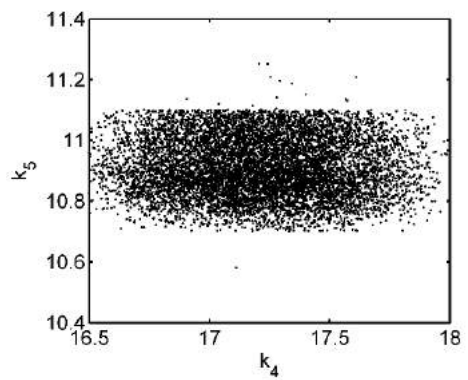
Model parameters calculated with the PSO
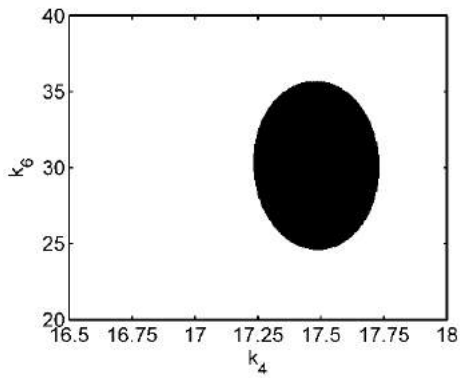
(ag)
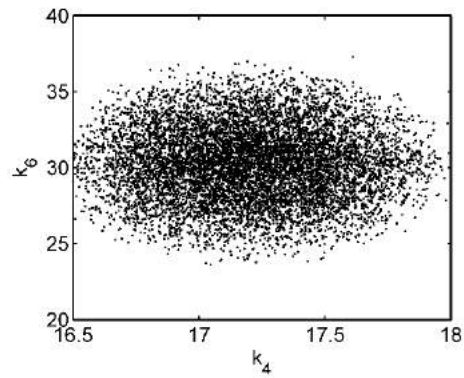
(ah)
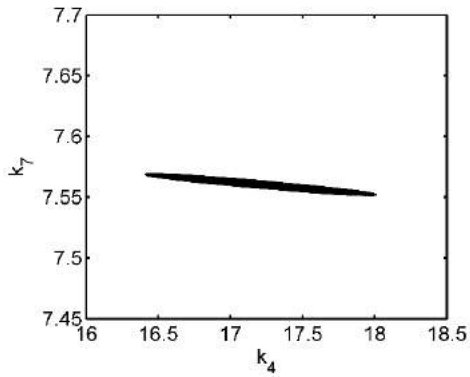
(ai)
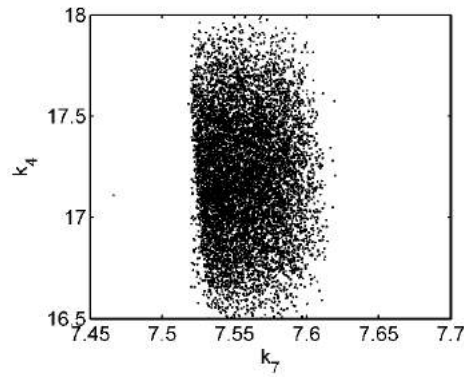
(aj)
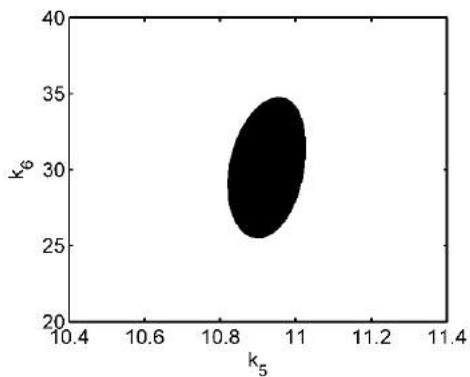
(ak)
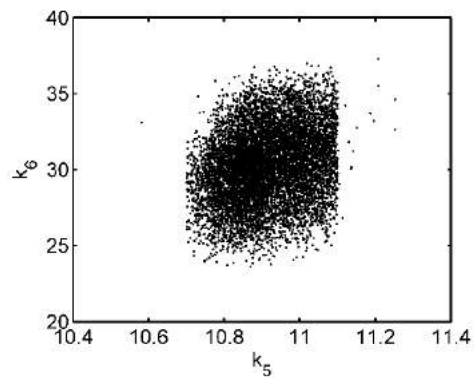
(al)

Model parameters calculated with the PSO
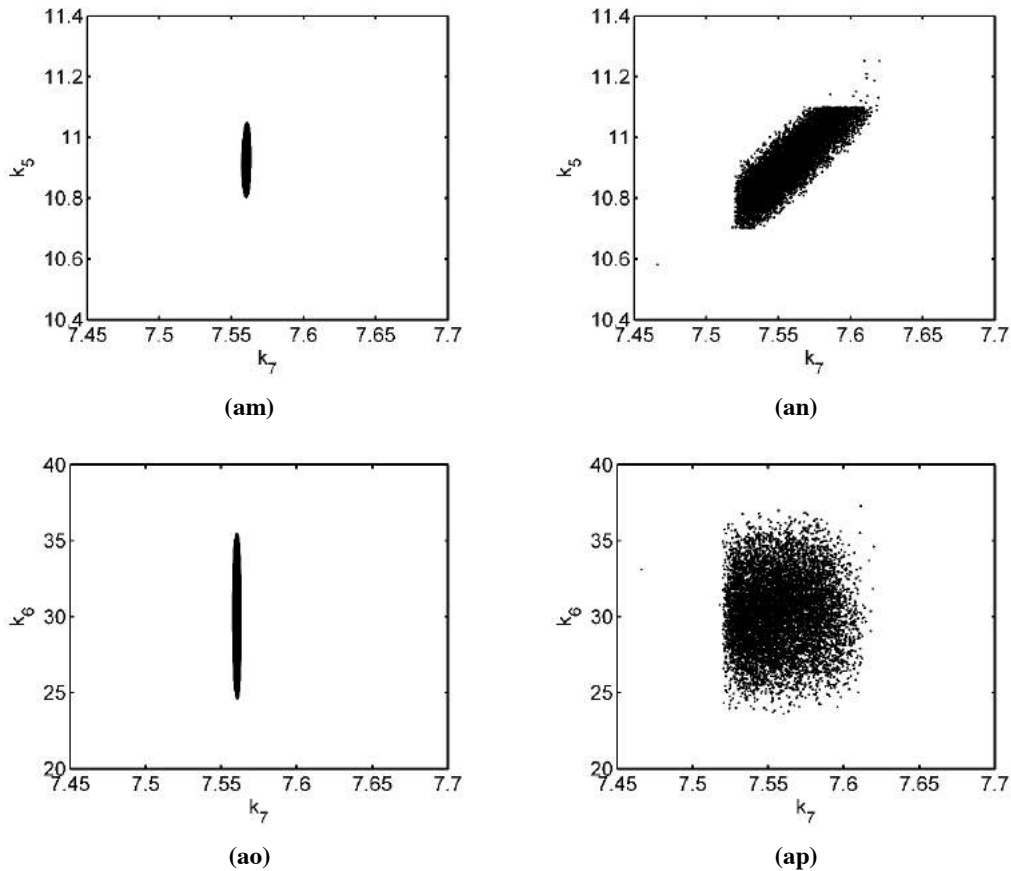
Figure 8.2 – Values of model parameters calculated with the PSO

As one can observe in Figure 8.2, pairs of parameters almost always lead to near elliptical confidence regions of parameter uncertainties. However, the inclusion of other parameters makes the confidence region of parameter uncertainties much bigger (remember that the reparameterization for k7 was performed in terms of 10 elevated to the original parameter values), also suggesting that the confidence region of parameters uncertainties become open (SWCHAAB et al., 2008), indicating estimability problems. In fact, the estimation of all parameter uncertainties simultaneously is infeasible, since the matrix *FIM* cannot be inverted. Thus, application of parameter identifiability procedure becomes essential. Additionally, the confidence regions located at the right were built by running the PSO algorithms for numerous set of parameter combinations. These combinations were generated using the Monte Carlo algorithm. For each parameter, a limit range was defined (lower and upper limit). For each region in Figure

8.2, 5,000,000 combinations of the 7 parameters were generated and tested with the PSO algorithm. Then, new parameter combinations were generated again, but extrapolating the previous considered interval. This time, 1,000,000 combinations were produced and run in the PSO method. That is the reason why some isolated points can be observed in the confidence regions positioned at the right column, indicating that these confidence regions possibly have open boundaries (SWCHAAB et al., 2008).

The details regarding the identifiability procedure used in the present thesis were presented in Section 6.4.2. After application of this procedure, the identifiability analysis indicated that only four parameters could be estimated simultaneously (k_3, k_5, k_6, k_7). The remaining parameters (k_1, k_2, k_4), although important for model computations, could not be estimated independently with the available experimental data; therefore, they were kept constant and equal to the values provided by the particle swarm optimization method and shown in Table 8.2. Then, the four selected parameters were estimated using the computational package ESTIMA. Table 8.3 lists the parameters estimated using ESTIMA.

Table 8.3. Parameter estimates for ethylene homopolymerization.

	Parameter
k_3	2.58 ± 0.08
k_5	10.91 ± 0.95
k_6	30.12 ± 2.10
k_7	7.56 ± 0.07

The confidence region for these parameters, keeping non-estimable parameters constant, are presented in Figure 8.3. In all confidence regions the parameter values from Table 8.3 are highlighted.

Keeping some parameters at constant values and estimating others is similar to applying an identifiability procedure. Identifiability procedures unavoidably neglect part of the uncertainty that cannot be assessed from data and model structure, reducing the uncertainty to a subset of parameters. Obviously the full uncertainty picture cannot be recovered, considering all model parameters. However, the procedure allows for quantification of the uncertainty of model parameters and model predictions that can be regarded as more significant and meaningful for model interpolation and interpretation.
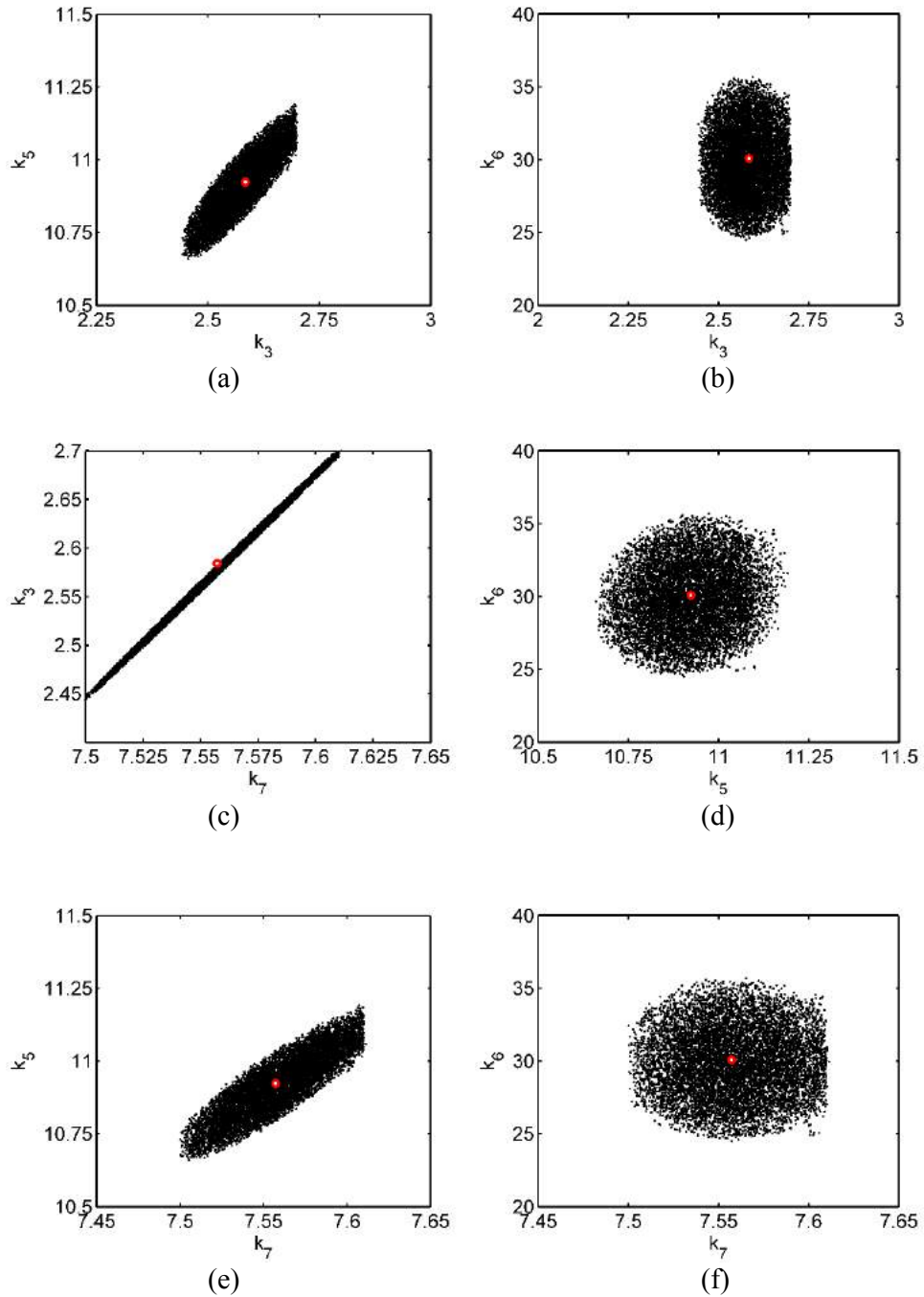
Figure 8.3 – Values of estimable parameters obtained with PSO.

8.2.2 Model Prediction and Statistical Evaluation

Table 8.4 presents the reaction rate constants for ethylene homopolymerization, as shown in Equation (8.1) to (8.3), (8.5) and (8.6).

Table 8.4. Ethylene homopolymerization reaction rate constants at different temperatures.

	120 °C	130 °C	140 °C	Unit
k_a	0.02847	0.05	0.10	s^{-1}
k_{p11}	67736.5	79150.0	91792.1	$L \cdot (mol \cdot s)^{-1}$
k_t	8.5	13.2	20.0	s^{-1}
k_{dP}	25456.3	54770.1	113549.2	$L \cdot (mol \cdot s)^{-1}$

The quality of the model fit was evaluated with the chi-square (χ^2) statistical test. According to this test, the model is admitted to be suitable if the final objective function F_{obj} lies between limits given by the χ^2 distribution, given the degrees of freedom. A 95% confidence degree was adopted. The final value of F_{obj} was equal to 156.6, with the lower and upper χ^2 of 149.2 and 224.5, respectively. According to the χ^2 statistical test, the proposed model fits the experimental data adequately.

Figure 8.4 shows the experimental data for ethylene feed flow rates used to estimate the model parameters in Table 8.3. The model predicted ethylene feed flow rates for all three polymerization temperatures and for experimental conditions J1 and J2 satisfactorily, given the experimental uncertainties.
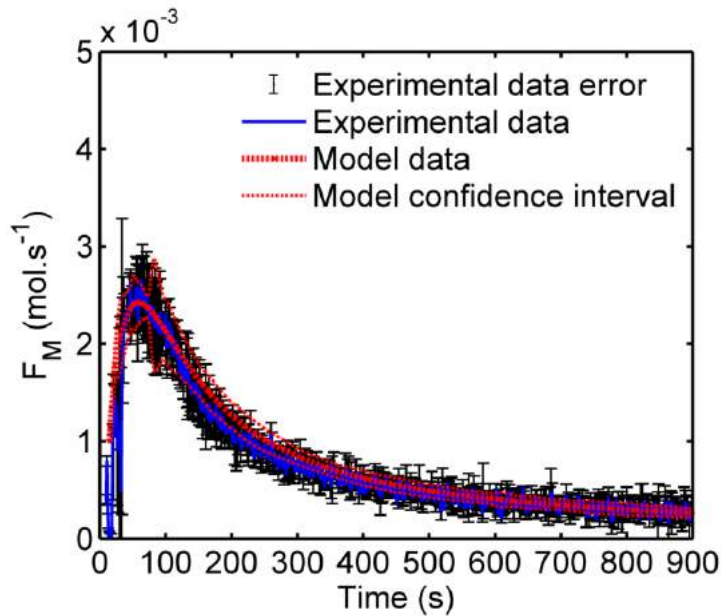
(a) **Experimental data and model predictions for $\dot{F}_M$ as a function of time at 120 °C.**
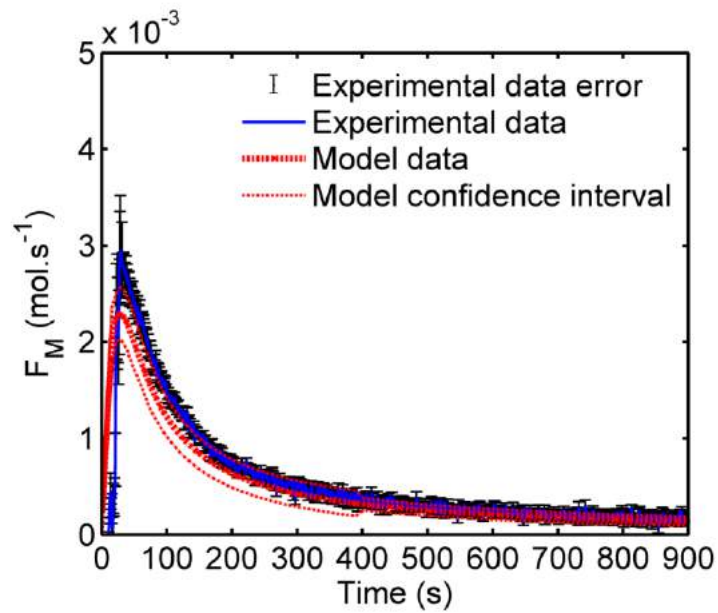
(b) Experimental data and model predictions for $\dot{F}_M$ as a function of time at 130 °C.
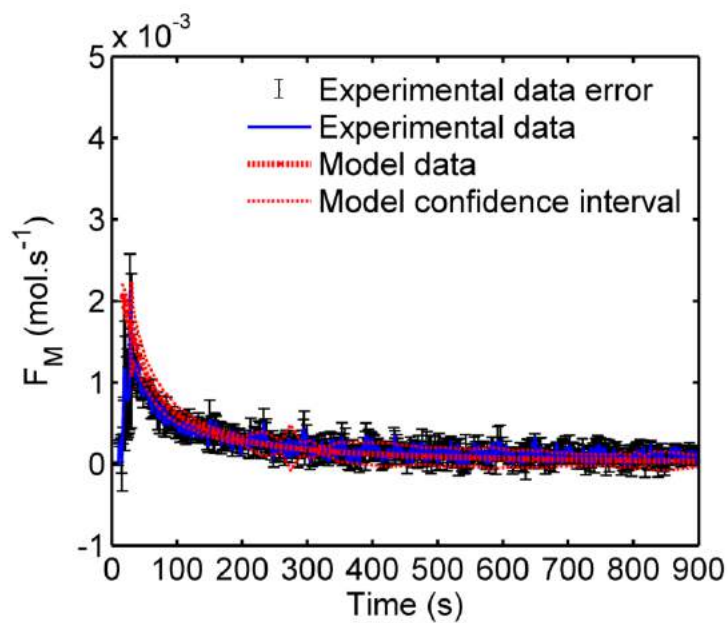
(c) Experimental data and model predictions for $\dot{F}_M$ as a function of time at 140 °C.
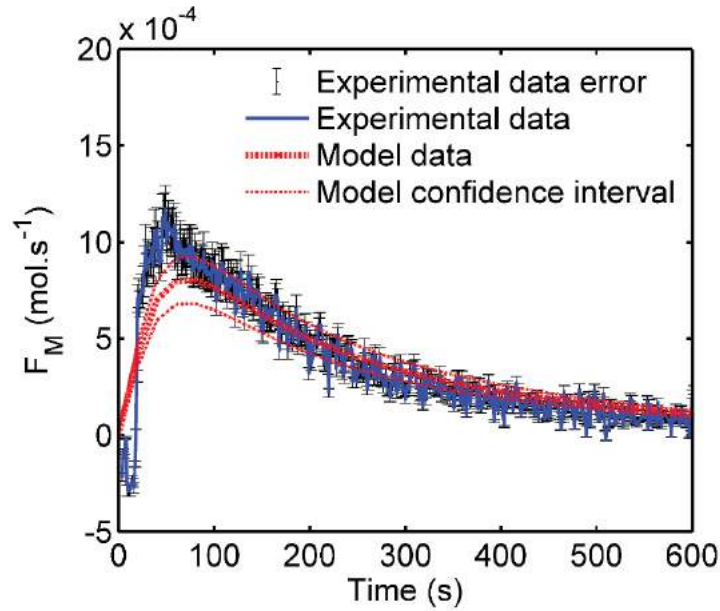
(d) Experimental data and model predictions for $\dot{F}_M$ as a function of time at 120 °C and with catalyst concentration equals to 0.271 μmol L^{-1}.
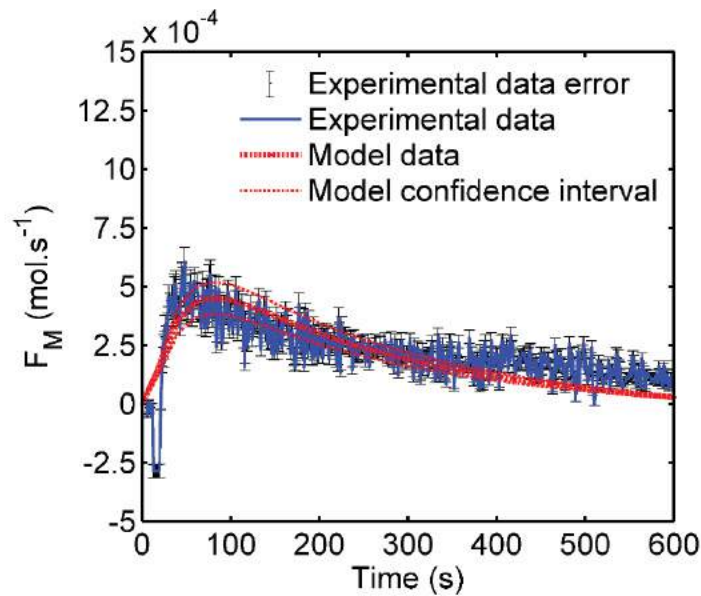
(e) Experimental data and model predictions for $\dot{F}_M$ as a function of time at 120 °C and with catalyst concentration equals to 0.174 μmol L^{-1}.

Figure 8.4 – Comparison between experimental data and model predictions for ethylene feed flow rate versus polymerization time at different temperatures: a) 120 °C, b) 130°C and c) 140 °C and with different catalyst concentrations: d) condition J1 and e) condition J2.

All experimental errors presented in the present work were calculated according with Equation (8.8):

$$y = \bar{y}_{exp} \mp \frac{t_{Student}\sigma_y}{\sqrt{N_{exp}}}$$

<div style="text-align: right;">(8.8)</div>

where $\bar{y}_{exp}$ is the average of the dependent measured variables y_{exp} (replicates) and σ_y is the standard deviation for each y_{exp} as measured from replicates.

Figure 8.5 and Figure 8.6 compare model predictions for M_n and M_w with experimental data, showing that the model can represent these averages adequately within the experimental uncertainties. Although the propagation kinetic constant increases with the increasing of temperature, both M_n and M_w decayed with the increase of temperature due to the more accentuate increase in the values of k_{dP} than the increase of k_{p11}, leading to a faster catalyst deactivation at higher temperatures and, consequently, lower M_n and M_w at higher temperatures. The transfer kinetic constant k_t also increases with the increasing of temperature, which contributes for decreasing the average molecular weights when the reaction temperature increases.
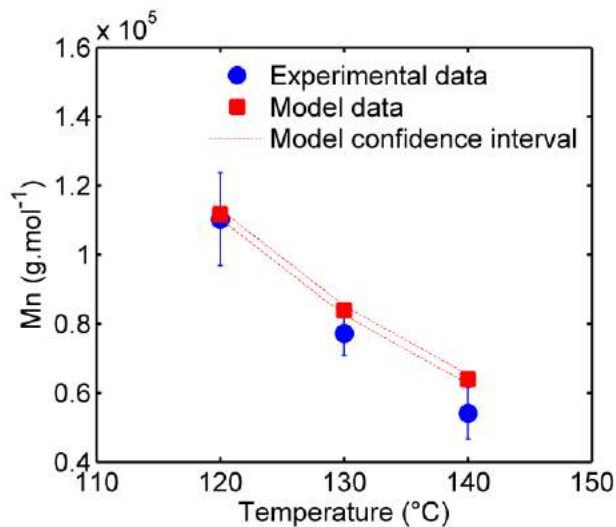
Figure 8.5 – Comparison between experimental data and model predictions of number average molecular weights at different temperatures: 120 °C, 130 °C and 140 °C.
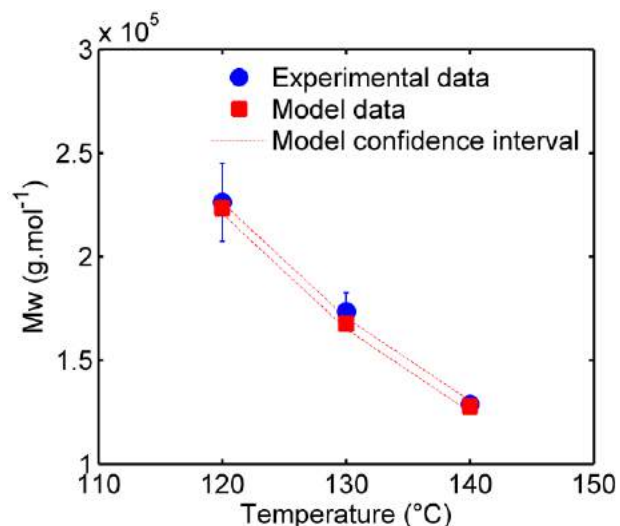
Figure 8.6 – Comparison between experimental data and model predictions of weight average molecular weights at different temperatures: 120 °C, 130 °C and 140 °C.

Figure compares model predictions for PI with experimental data. According to the model, PI does not vary with the increase of temperature, but as one can see the available experimental PI slightly increased when temperature was increased from 120 to 140 °C. Given the experimental uncertainties, fair agreement could be noted between experimental data and model predictions for PI.
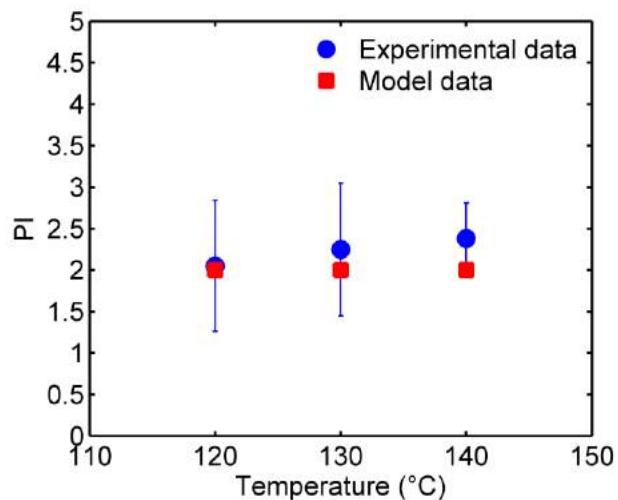
Figure 8.7 – Comparison between experimental data and model predictions of polydispersity indexes at different temperatures: 120 °C, 130 °C and 140 °C.

Figure 8.8 illustrates how M_n and M_w vary when the catalyst concentration increases. Increasing the amount of catalyst used leads to an increase in the catalytic

activity which affects directly in the increase of average molecular weights of the polymer. More catalyst in the system consumes more monomer and, consequently, more monomer is fed in the reactor in order to maintain constant the total pressure.

(a)

(b)
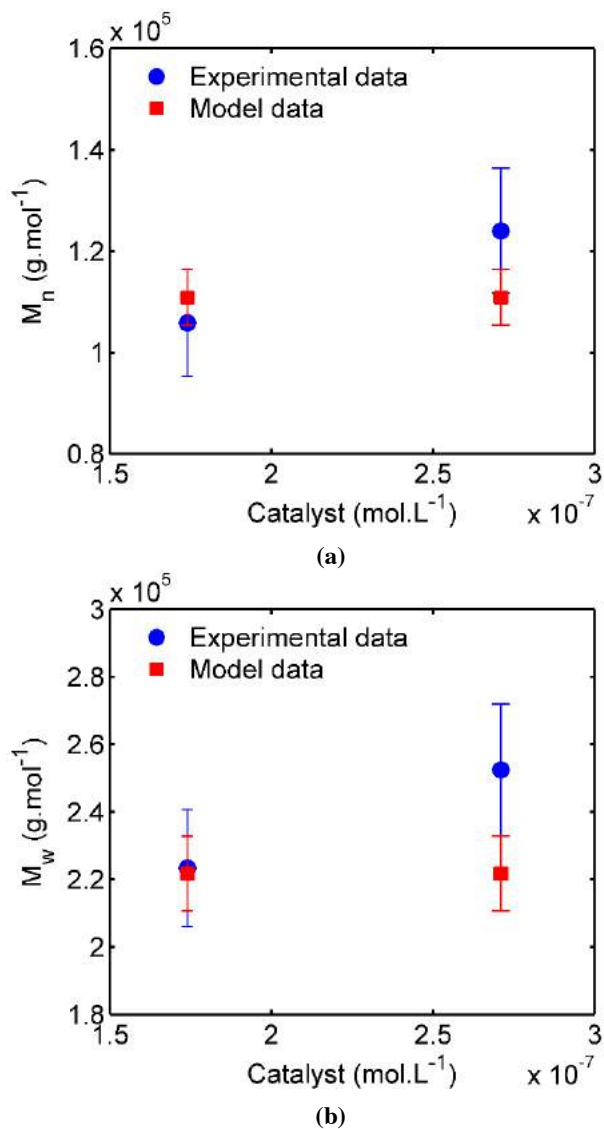
Figure 8.8 - Comparison between experimental data and model predictions of number and weight average molecular weights and polydispersity index for experimental conditions J2 and J1 (from left to right).

Figure 8.9 illustrates the comparison between experimental data and model predictions for PI of polymers synthesized with different catalyst concentrations. Very good agreement was obtained with experimental data and model predictions. As one can

see, the increase in the catalyst concentration did not change the polydispersity index of the polymers, as expected.
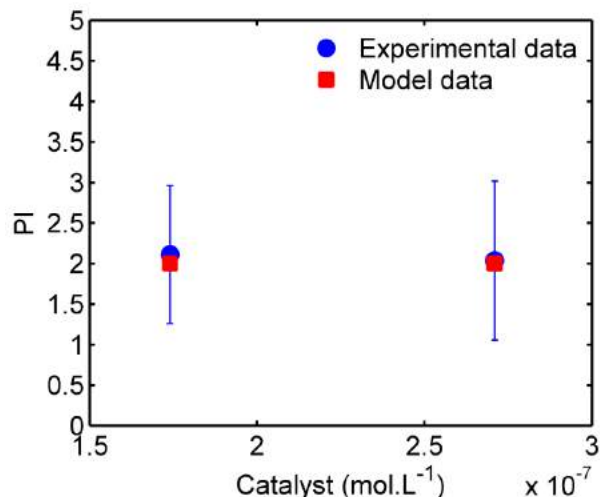
Figure 8.9 - Comparison between experimental data and model predictions for polydispersity indexes for experimental conditions J2 and J1 (from left to right).

Table 8.5 presents the polymer yields obtained in the homopolymerization reactions at different temperatures.

Table 8.5. Polymer yield for the homopolymerization runs at different temperatures.

Sample ID (120 °C)	Polymer weight (g)	Sample ID (130 °C)	Polymer weight (g)	Sample ID (140 °C)	Polymer weight (g)
A1	4.81	B1	2.95	C1	1.63
A2	3.87	B2	2.99	C2	1.74
A3	3.69	B3	3.02	C3	1.24
J1	2.05	J2	0.98		

From Table 8.5, it is clear that at the lowest temperature (120 °C) the highest amounts of polymer are produced, while at the highest temperature (140 °C) one can observe the lowest amounts of polymer. It is important to comment that the gravimetric analyses carry out high uncertainties, since it cannot be guaranteed that all polymer material is recovered from the reactor (for instance, some polymer can be sticked to the reactor). Thus, considering that the results in Table 8.5 can contain uncertainties that are

144

hard to quantify, one can conclude that smaller amounts of polymer are produced at high temperatures, because the catalyst deactivates much faster when the reaction is conducted at higher temperatures. This conclusion agrees with results presented by SOARES and MCKENNA (2012), as these authors also observed for a similar catalyst that the increase in the polymerization temperature would lead to the decrease of polymer yield. This can also be confirmed in Figure 8.10, where it is possible to see that at 120 °C it takes longer for the ethylene feed flow rate to reach its lowest value, when compared to results obtained at 130 °C and 140 °C.
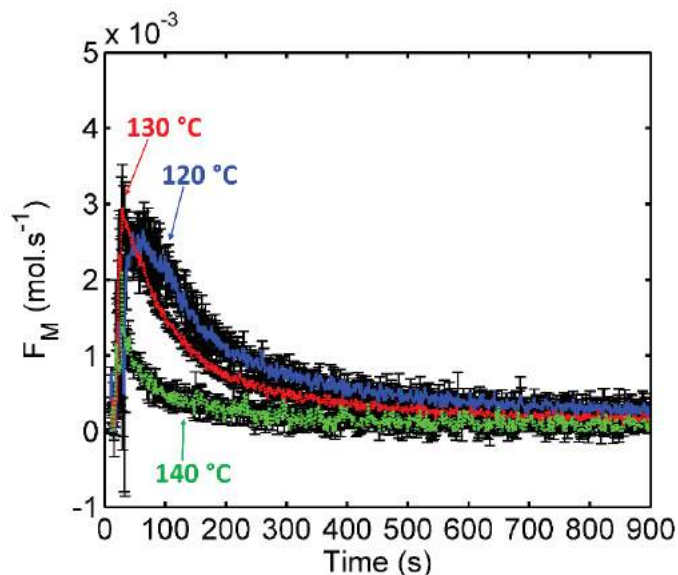
Figure 8.10 – Ethylene feed flow rate versus polymerization time at different temperatures: 120 °C, 130°C and 140 °C

8.3 Copolymerization of Ethylene with 1,9-Decadiene

As commented in Chapter 5, 14 copolymerization reactions were carried out, varying catalyst and diene concentration and also the total time of polymerization. Figure 8.11 summarizes these experimental conditions. All reactions were performed at 120 °C, temperature that catalyst activities were higher, and reactor pressure of 120 psig.
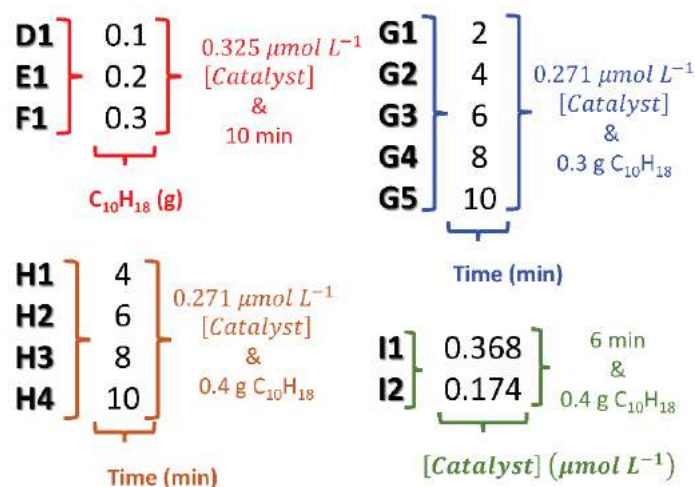
Figure 8.11 – Experimental conditions for copolymerization reactions.

Table 8.6 presents the polymer yields obtained in the copolymerization reactions at different experimental conditions.

Table 8.6. Polymer yield for the copolymerization runs.

Sample ID	Polymer weight (g)	Sample ID	Polymer weight (g)	Sample ID	Polymer weight (g)
D1	1.94	G4	1.91	I1	2.01
E1	1.71	G5	1.95	I2	0.76
F1	1.95	H1	1.39		
G1	1.15	H2	1.46		
G2	1.41	H3	1.50		
G3	1.62	H4	1.87		

As expected, it is possible to observe in Table 8.6 that the addition of more catalyst resulted in more polymer at the end of the reaction. This can be confirmed by comparing the polymer yields obtained for runs D1 and F1 with the polymer yields obtained for runs G5 and H4. However, the higher amounts of polymer produced in D1 and F1 can also be associated with the longer polymerization time (15 min). Sample E1 produced the lowest polymer amounts among samples produced with the same catalyst concentration. Later in this chapter, it will be shown that sample E1 may be an outlier and maybe this is the reason why it produces less polymer. Sample I1 produced more polymer than sample H2 and sample H2 led to more polymer than sample I2. All these three samples (I1, H2 and I2) were generated after 6 min of reaction and using 0.4 g of

146

1,9-decadiene. The only difference among them was the used catalyst concentration, as expected.

Comparing the polymer yields of sample J1 and samples G5 and H4, one can say that the increase of the diene concentration can cause the production of less polymer. This scenario can be explained by:

. the presence of contaminants in the diene solution, even after purification, as described in Chapter 5;

. the presence of the diene, which may act as a transfer agent or present lower reactivity, slowing down the rates of polymerization;

. experimental uncertainties, as it was not possible to quantity the experimental error of the gravimetrical analysis.

The copolymerization reaction mechanism differs from the homopolymerization mechanism by the addition of two additional reaction steps: the diene propagation, Equation (8.4), and the macromonomer reincorporation, Equation (8.7). The last reaction forms LCBs and, consequently, can substantially increase the molecular weight averages, due to incorporation of macromonomers of larger molecular weights into the growing chains. This increase can be confirmed when one plots the intrinsic viscosity of the samples as functions of the average molecular weight, as shown in Figure 8.12 and Figure 8.13.
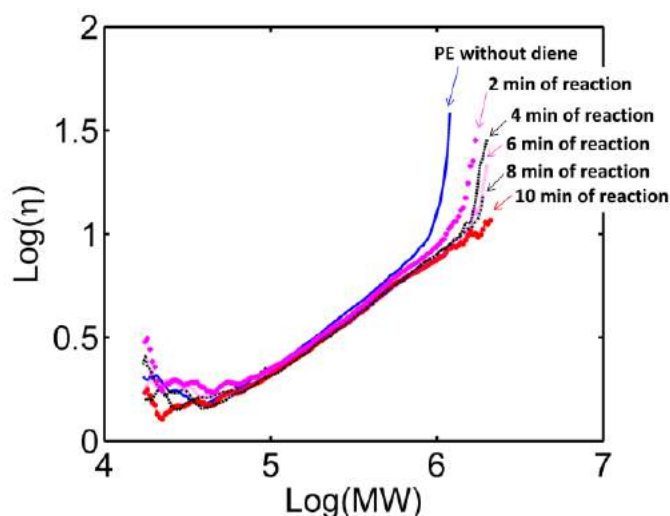
Figure 8.12 – Intrinsic viscosity for copolymers of ethylene and 1,9-decadiene when 0.3 g of diene is used (G1 to G5 and J1 in Figure 8.11).

(b)
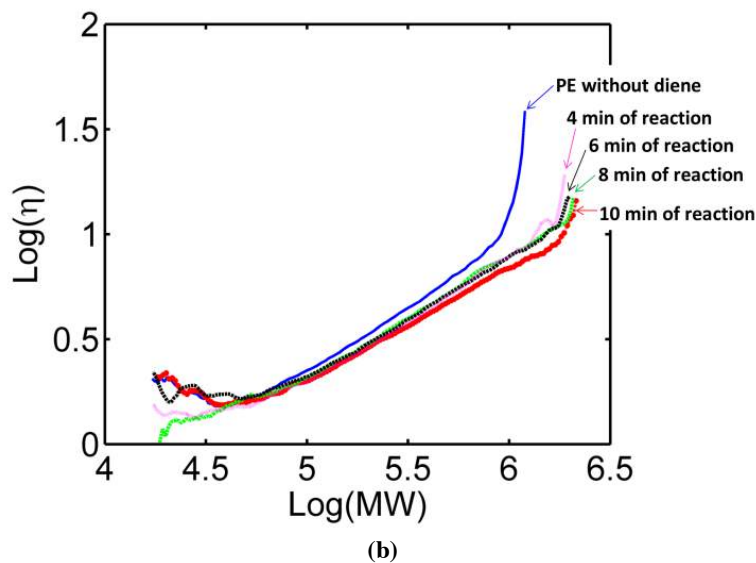
Figure 8.13 – Intrinsic viscosity for copolymers of ethylene and 1,9-decadiene when 0.4 g of diene is used (H1 to H4 and J1 in Figure 8.11).

Examining Figure 8.12 and Figure 8.13, it becomes evident that the intrinsic viscosity of ethylene/diene copolymers decreases for similar molecular weights. Besides, the intrinsic viscosity deviates from the linear relation with $\log(M_W)$, as expected for linear polymers, in the high molecular weight region (MEHDIABADI and SOARES, 2011). As the polymerization evolves, more macromonomers are reincorporated, forming more LCBs, magnifying this effect. When one compares Figure 8.12 with Figure 8.13, one can note that the intrinsic viscosity decreases slightly (for the same molecular weight) with the increasing diene concentration, since more LCB are formed in the latter case. Therefore, formation of LCBs is very likely in the analyzed system and increase with time and diene content. For similar molecular weights, intrinsic viscosities are usually smaller for branched polymer chains because of the smaller hydrodynamic volumes and entanglement frequency.

Similar deviations could be observed for copolymers prepared with similar amounts of diene, but with increasing catalyst concentrations. Figure 8.14 shows that the intrinsic viscosity of polymers produced with higher CGC concentrations deviates more from the PE curve, because higher catalyst concentration leads to higher concentrations of living polymer chains and macromonomers, increasing the probability of LCB formation.

148
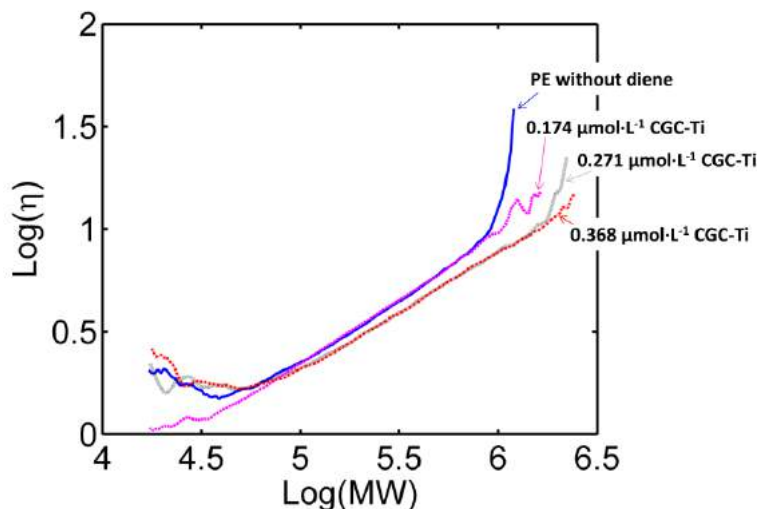
Figure 8.14 – Intrinsic viscosity for copolymers of ethylene and 1,9-decadiene when 0.4 g of diene is used (H1, I1 and I2 in Figure 8.11) and for pure PE (J1).

As one can see, in Figures 8.13 to 8.15, there is an upward deviation of the intrinsic viscosity in the region of high molecular weights and this deviation becomes less pronounced as the copolymerization time increases, this deviation is maximum when there is no diene present. This deviation, in fact, occurs due to the low concentration of chains with weight in this range of high molar masses and, therefore, the GPC cannot detect these chains, either because they are in very low concentrations or because they do not exist. What is really important in Figures 8.13 to 8.15 is to observe that the higher the amount of diene, the reaction time and the catalyst concentration, the more distant the intrinsic viscosity of the copolymer stays in relation to the intrinsic viscosity of PE without diene.

8.3.1 Parameter Estimation

The experimental data used to estimate the model parameters were the number and weight average molecular weights of the polymer samples. These experimental data and the fit of the model after the estimation procedure are shown in Section 8.3.2.

Table 8.7 lists the parameters estimated for the copolymerization model. The calculated F_{obj} was equal to 31.2, with lower and upper χ^2 of 16.8 and 47.0, respectively. Thus, according to the χ^2 statistical test, the proposed model fitted adequately the available experimental data, being suitable to predict average molecular weights of the copolymers made of ethylene/ 1,9-decadiene.

149

Table 8.7. Estimated parameter values for ethylene and 1,9-decadiene copolymerization with a CGC at 120 °C.

	Parameter
k_1^*	3.31 ± 0.34
k_2^*	2.96 ± 0.33

The copolymerization parameters k_{p12} and k_b can be calculated from the estimated values of k_1^* and k_2^* as shown in Table 8.8.

Table 8.8. Model parameters for ethylene and 1,9-decadiene copolymerization with a CGC at 120 °C.

	Parameter	Unit
$k_{p12} = 10^{k_1^*}$	2039.8	$L \cdot mol^{-1} \cdot s^{-1}$
$k_b = 10^{k_2^*}$	908.7	$L \cdot mol^{-1} \cdot s^{-1}$

Comparing Table 8.4 and Table 8.8, one can observe that $k_{p12} < k_{p11}$; that is, the propagation rate constant for ethylene is higher than for propagation with diene, which is expected since ethylene is a more reactive monomer (CHUNG, 2002). It must be emphasized that the real propagation rate constant for diene incorporation is $\frac{k_{p12}}{2}$, because a diene molecule has two vinyl groups, so that incorporation can take place through either one of the two available vinyl groups. The confidence region, obtained with particle swarm optimization, is illustrated in Figure 8.15. The final pair (k_{p12}, k_b) from Table 8.8 is highlighted in the figure as a white circle.

Figure 8.15 shows that the confidence region is not elliptical, indicating the importance of using a method like PSO for determining parameter uncertainties in cases where elliptical approximations fail. Similar behavior has also been observed elsewhere for other nonlinear models (SCHWAAB et al., 2008).
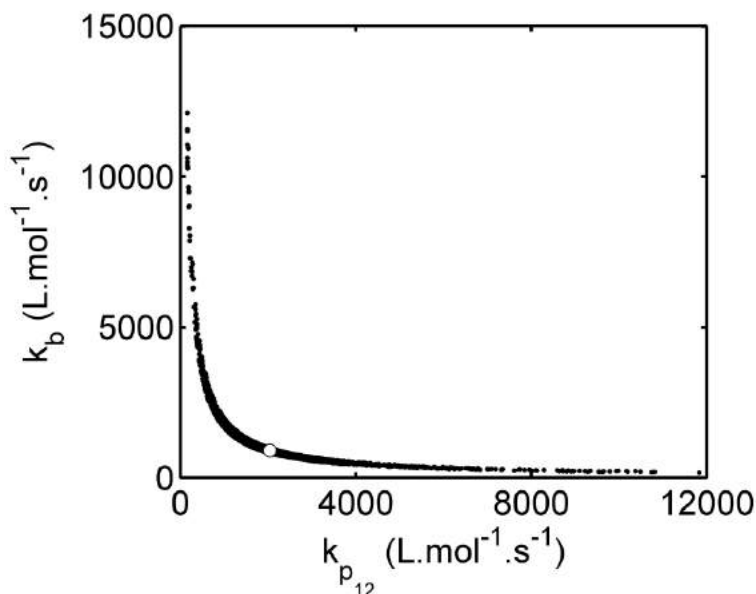
Figure 8.15 – Confidence regions for parameters k_{p12} and k_b obtained with Particle Swarm Optimization.

Again, it must be emphasized that this procedure does not consider the full uncertainty, since other parameters were kept constant during the estimation procedure. As a consequence, Figure 8.15 just presents the uncertainty of this subset of parameters in the scenario where the others do not change.

8.3.2 Model Predictions and Statistical Evaluation

Figures 8.17 to 8.20 compare experimental data and model predictions for copolymer average molecular weights. Observing these figures, it is possible to notice, with the exception of two experimental points (Figure 8.16.b and Figure 8.17.b), that all measured M_n and M_w values were well represented by the model, given the experimental and prediction uncertainties.

As one can see in Figure 8.16, increasing the amount of diene, M_n and M_w also increased. The higher the amount of diene, the higher is the probability of the diene being incorporated into the growing chains and, consequently, the higher is the probability of forming more macromonomer with pendant unsaturations which increases the probability of those chains being reincorporating; generating LCBs. Branched polymers have higher average molecular weights than non-branched polymers of the same type.
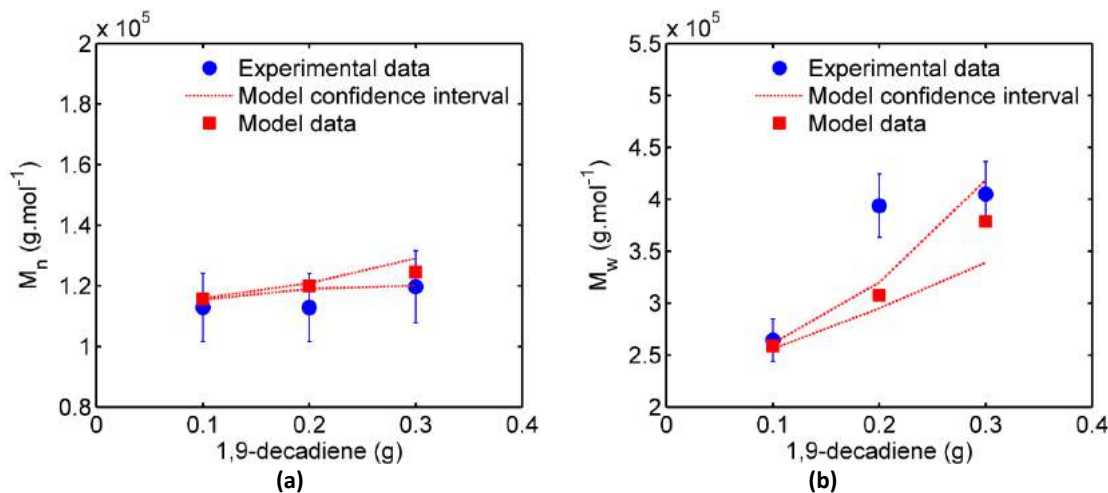
Figure 8.16 – Experimental data and model predictions for (a) number average molecular weights and (b) weight average molecular weights. Conditions D1, E1 and F1 from Figure 8.11.

Observing Figures 8.18 and 8.19, one can conclude that the average molecular weights increased with increasing reaction time. This occurred because at short reactions the propagation and LCB reincorporation reactions occurred less than longer reactions, having less time for the polymer to grow when the reaction was shorter.
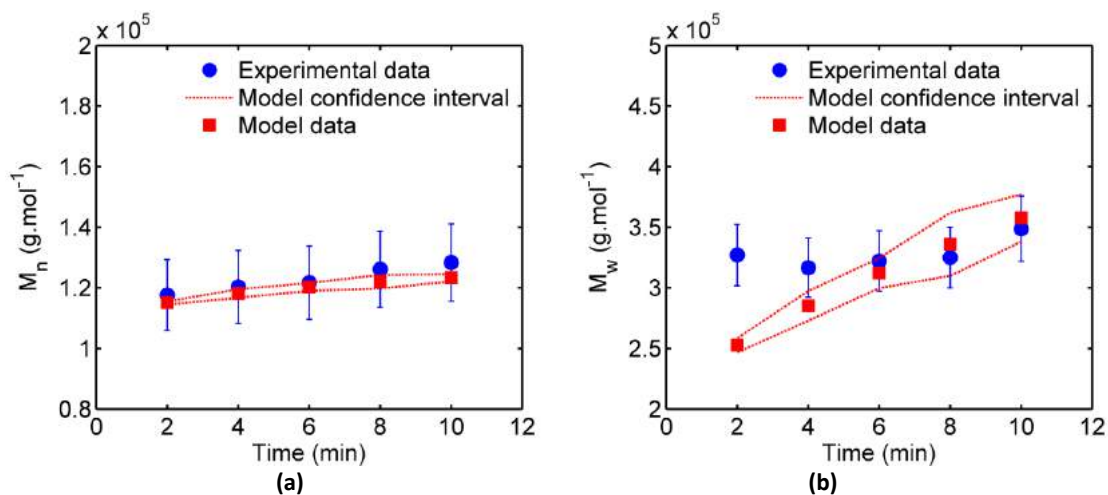
Figure 8.17 – Experimental data and model predictions for (a) number average molecular weights and (b) weight average molecular weights. Conditions G1, G2, G3, G4 and G5 from Figure 8.11.

152
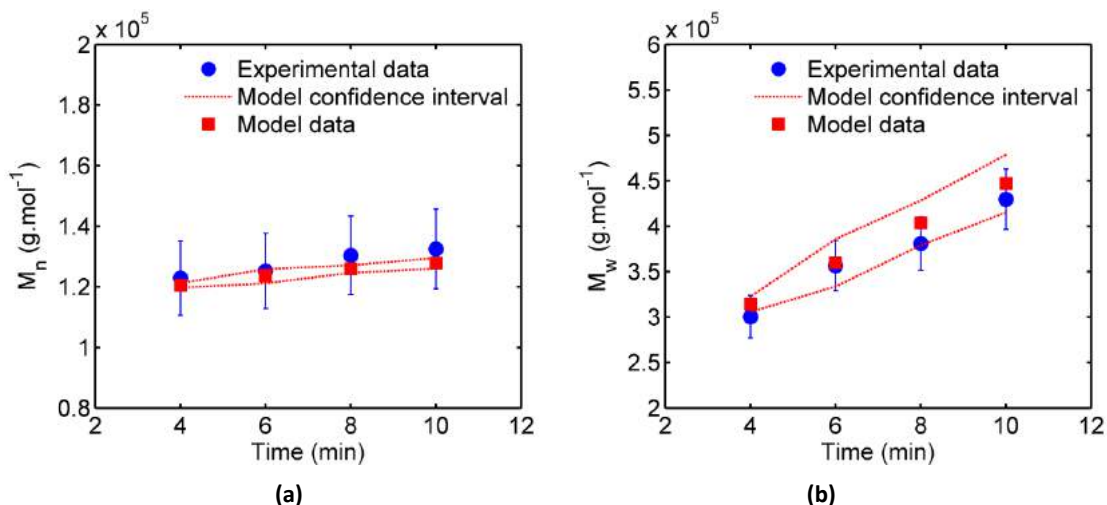
Figure 8.18 – Experimental data and model predictions for (a) number average molecular weights and (b) weight average molecular weights. Conditions H1, H2, H3 and H4 from Figure 8.11.

Analyzing Figure 8.19, increasing the amount of catalyst led to an increase in the catalytic activity which affected directly in the increase of average molecular weights of the copolymer. More catalyst in the system consumes more monomer and comonomer and, consequently, more reactions are processed during the same time.
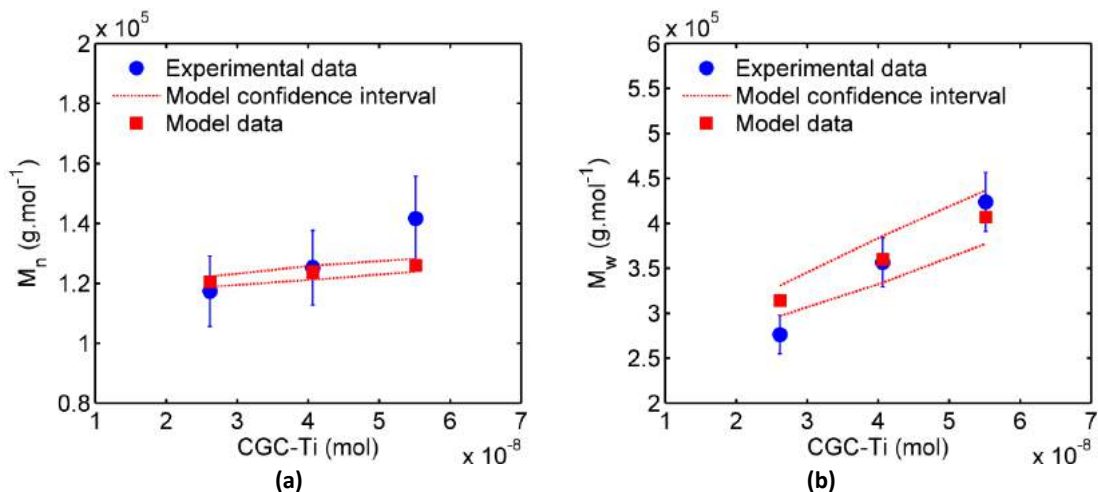
Figure 8.19 – Experimental data and model predictions for (a) number average molecular weights and (b) weight average molecular weights. Conditions H2, I2 and I2 from Figure 8.11.

As mentioned previously, it was assumed that the ethylene feed flow rate was approximately equal to ethylene polymerization rate, since ethylene was supplied to maintain the reactor pressure constant throughout the polymerization. For estimation of the copolymerization parameters, ethylene feed flow rate data were not taken into

account, but such data could be used to confirm the accuracy of the model predictions. Figure 8.20 compares, for different diene and catalyst concentrations, measured and predicted ethylene feed flow rates.

(a)   (b)

(c)   (d)
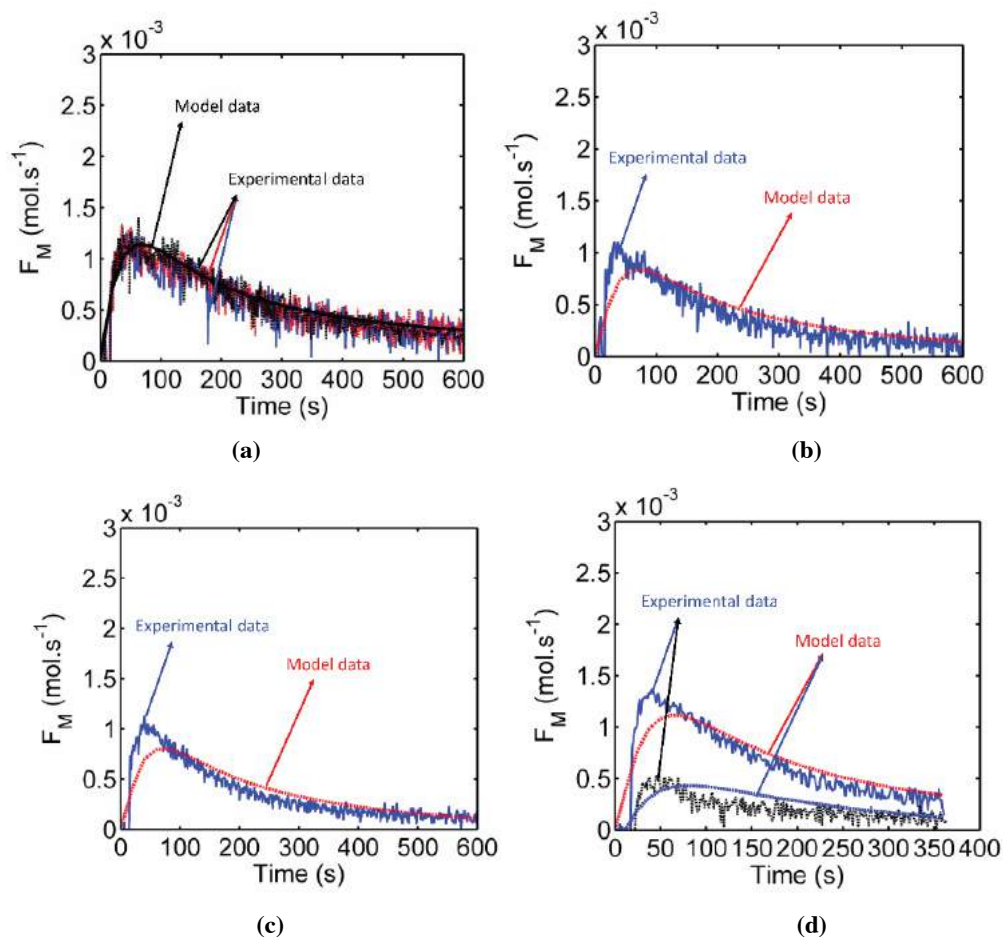
Figure 8.20 – Ethylene feed flow rates measured experimentally and simulated using the method of moments. Conditions: a) D1, E1, F1; b) G5; c) H4; d) I1 (upper curve) and I2 (lower curve).

The modification of the diene content apparently do not affect the ethylene feed flow rate, since the simulated and measured profiles for $\dot{F}_M$ were similar for copolymer samples containing 0.1, 0.2 and 0.3 g of 1,9-decadiene (Figure 8.20.a). Figure 8.20.d clearly shows the influence of catalyst concentration on the ethylene flow rate: the increase of the CGC concentration leads to higher polymerization rates, as expected. Figure 8.20 shows that the model can predict ethylene flow rates (and polymerization rates) well for the analyzed conditions.

154

Figure 8.21 shows the 1,9-decadiene and ethylene ratios throughout the reaction for distinct experimental conditions. It can be noticed that for all experimental conditions shown, the 1,9-decadiene and ethylene ratio does not vary significantly from the beginning to the end of the reaction as it was expected. All the changes in the ratio values were lower than 0.007 and, considering the model uncertainties, these changes can be despised.
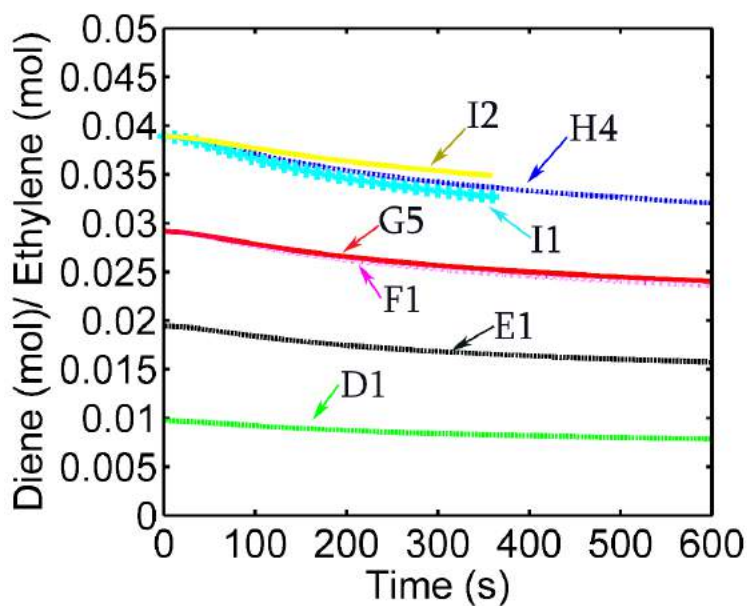
Figure 8.21 – Simulated diene (mol)/ ethylene (mol) over reaction time for different experimental conditions.

Although the Monte Carlo method was not used to estimate the model parameters, it was used to simulate the ethylene/diene copolymerizations using the experimental conditions presented in Figure 8.11. The used parameter values were the ones presented in Table 8.8. The results of these simulations are summarized in Table 8.9.

Table 8.9. Average molecular weights predicted by Monte-Carlo simulation for different polymerization conditions and experimental lower and upper bounds.

Exp. Cond.	1,9-$C_{10}H_{18}$ (g)	Time (min)	M_n[a] (g.mol^{-1})	L. & U. M_n[b] Lim. (g.mol^{-1})	M_w[a] (g.mol^{-1})	L. & U. M_w[b] Lim. (g.mol^{-1})
D1	0.1	10	115579	101649; 124106	263370	243943; 284876
E1	0.2	10	120420	101593; 124037	319030	363392; 424369
F1	0.3	10	118000	107773; 131582	402214	373650; 436349
G1	0.3	2	116454	105914; 129313	266474	301733; 352364
G2	0.3	4	120036	108333; 132266	307103	292100; 341115
G3	0.3	6	121774	109587; 133797	331214	297101; 346954
G4	0.3	8	122697	113574; 138665	345055	299884; 350205
G5	0.3	10	123632	115559; 141088	360850	321748; 375737
H1	0.4	4	122968	110659; 135106	351062	277125; 323626
H2	0.4	6	125329	112758; 137669	382047	328971; 384172
H3	0.4	8	126958	117385; 143318	428900	351546; 410535
H4	0.4	10	127497	119310; 145668	441776	396356; 462865
I1	0.4	6	130489	127562; 155743	455605	391044; 456661
I2	0.4	6	120325	105669; 129014	292932	255057; 297856

[a] Simulated values. [b] Experimental confidence interval

As shown in Table 8.9, the Monte Carlo model provided molecular weight averages within modeling and experimental uncertainty limits, with exception of samples E1 and G1.

Figure 8.22 compares measured and predicted molecular weight averages. Experimental and model errors were also included in the figure. The Monte Carlo confidence intervals for M_w were obtained considering 95% as confidence interval and 5 replicates, according to the t-Student distribution,

$$M_w \pm \frac{t_{Student}\sigma_{M_w}}{\sqrt{N_r}} \tag{8.9}$$

where N_r is the number of replicates and σ_{M_w} is the M_w standard deviation.

The method of moments and the Monte Carlo simulations were used to quantify the LCB frequency in the copolymer. The method of moments calculates the average frequencies of LCB per 1000 carbon atoms and average LCB per chain as a function of polymerization time. The Monte Carlo simulations provide the average frequency of LCB/1000 C and LCB/chain as functions of the polymer molecular weight (MW).

Figure 8.23 to Figure 8.26 illustrate the results of these simulations.
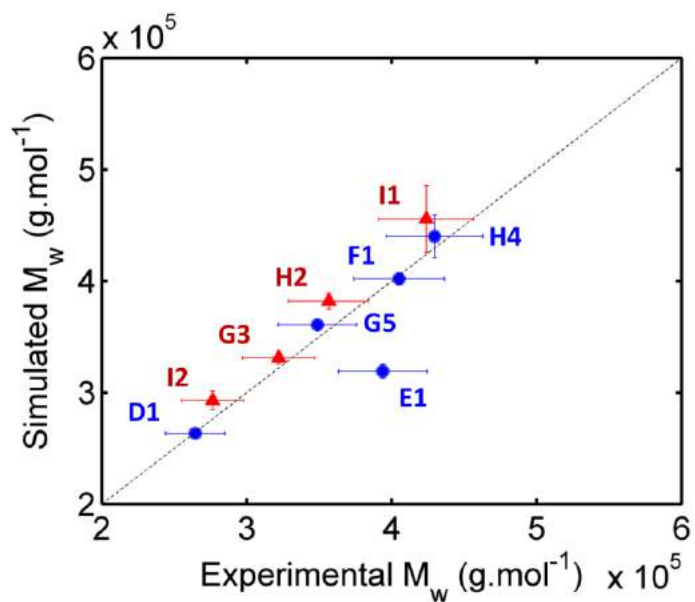
Figure 8.22 – Comparison between experimental and simulated M_w data for the copolymerization using MC simulations.
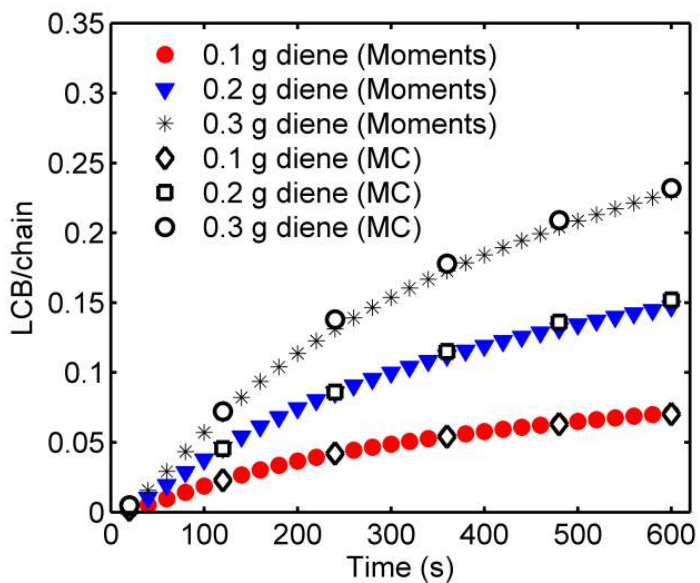
Figure 8.23 – LCB per chain as a function of polymerization time simulated by the method of moments and MC (Simulation conditions: D1, E1 and F1 from Figure 8.11).
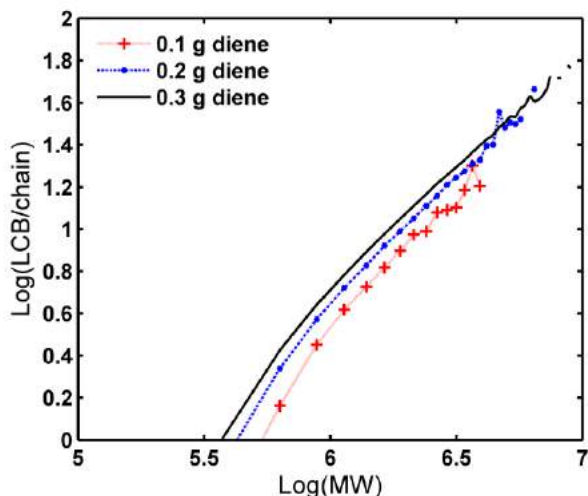
Figure 8.24 – LCB frequency simulated with the MC model for different diene concentrations after 10 minutes of polymerization as function of the molecular weight (Simulation conditions: D1, E1 and F1 from Figure 8.11).

Figure 8.23 to Figure 8.26 show that the increase of the diene concentration cause the increase of the number of LCBs in the copolymer, in agreement with the experimental results shown in Figure 8.12 and Figure 8.13. An interesting result from the Monte Carlo simulations is that LCBs were formed significantly only in chains with high molecular weights; for low and medium molecular weights, the LCB frequency is practically nil. This is in accordance with previously published material (GUZMÁN et al., 2010), which indicates that copolymerizations performed with 1,9-decadiene can eventually lead to production of polymer chains of very high molecular weights and gel, if the chain branching frequency is sufficiently high. This also explains why deviations from linearity are more important at high molecular weights, when the intrinsic viscosity plots are analyzed as functions of the molecular weight.

158
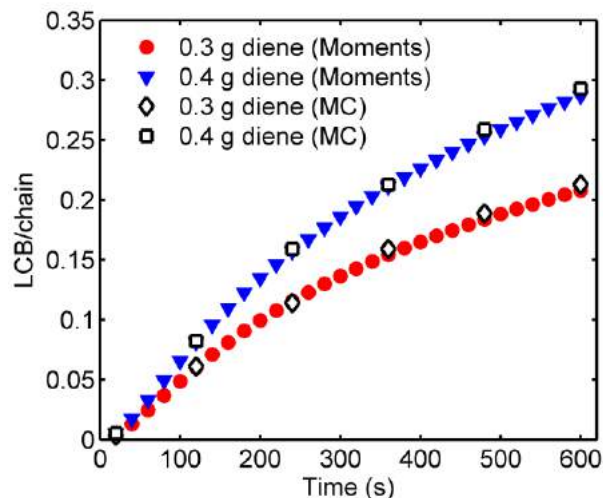
Figure 8.25 – LCB per chain as a function of polymerization time simulated by the method of moments and MC (Simulation conditions: G5 and H4 from Figure 8.11).
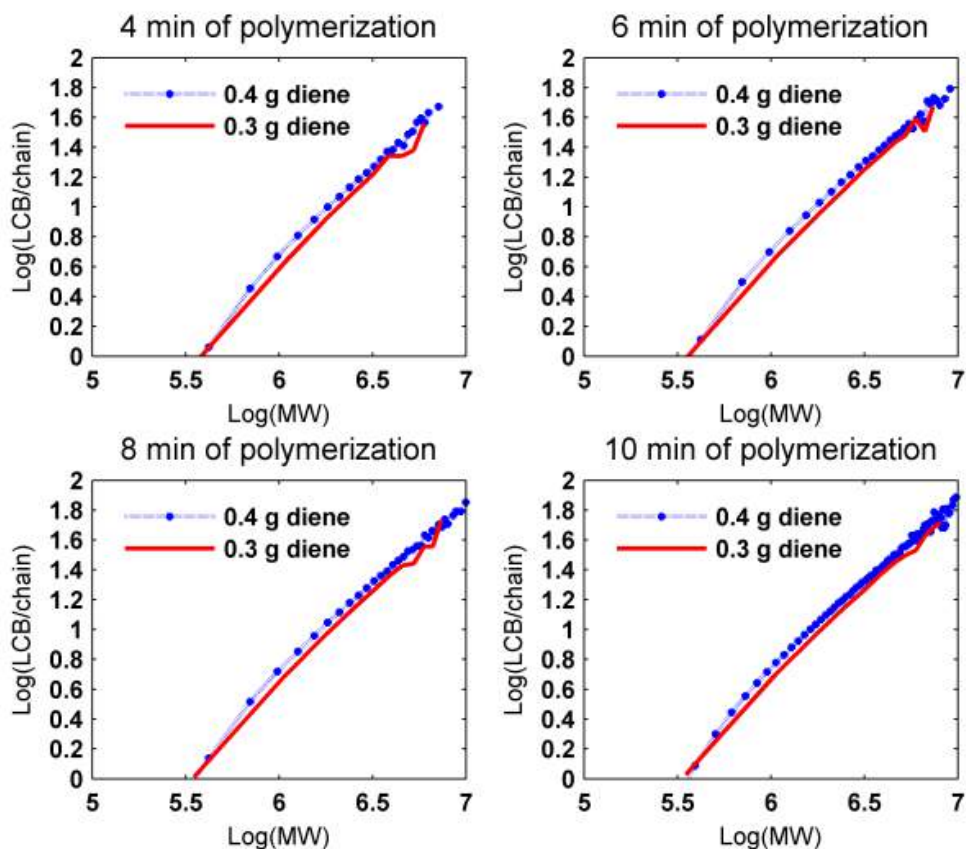
Figure 8.26 – LCB per chain as a function of polymer molecular weight simulated by MC model for different diene concentrations (Simulation conditions: G5 and H4 from Figure 8.11).

Figures 8.27 and 8.28 show the influence of catalyst concentration on the formation of LCBs. Both methods agree that when the CGC concentration is increased, more LCBs are generated, which agrees with experimental observations. Table 8.10 compares the average frequencies of long branches per 1000 carbon atoms and per chain, as simulated by both analyzed methods.
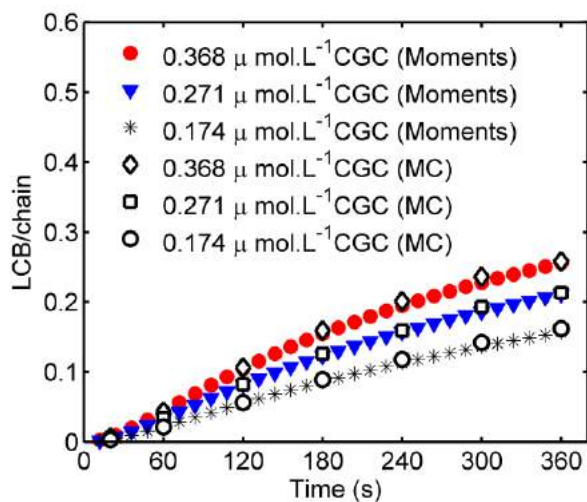
Figure 8.27 – **Frequency of LCB per chain versus polymerization time simulated by the method of moments and MC (Simulation conditions: G3, I1 and I2 from Figure 8.11).**
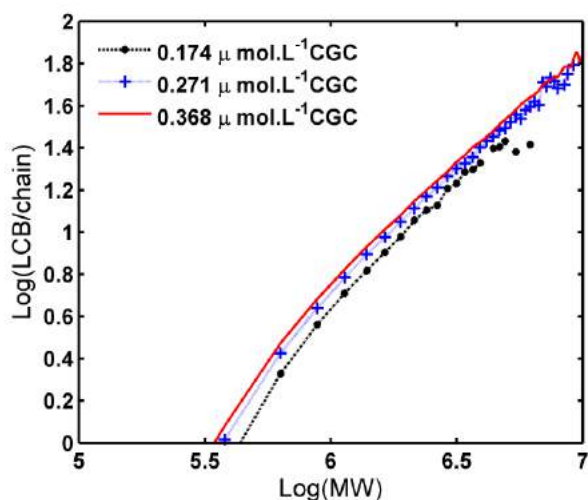
Figure 8.28 – **Frequency of LCB per chain as a function of polymer molecular weight simulated by the MC model after 6 minutes of polymerization (Simulation conditions: G3, I1 and I2 from Figure 8.11).**

160

Table 8.10. Frequencies of LCB/chain and LCB/1000 C atoms predicted by MC method and the method of moments for different polymerization conditions.

Exp. Cond.	1,9-Decadiene (g)	Time (min)	LCB/1000 C atoms (MC)	LCB/1000 C atoms (Moments)	LCB/chain (MC)	LCB/chain (Moments)
D1	0.1	10	0.009	0.009	0.070	0.071
E1	0.2	10	0.018	0.017	0.152	0.147
F1	0.3	10	0.026	0.026	0.232	0.229
G1	0.3	2	0.007	0.007	0.061	0.060
G2	0.3	4	0.014	0.014	0.114	0.116
G3	0.3	6	0.019	0.018	0.159	0.154
G4	0.3	8	0.022	0.021	0.189	0.184
G5	0.3	10	0.025	0.024	0.213	0.208
H1	0.4	4	0.019	0.018	0.159	0.157
H2	0.4	6	0.024	0.024	0.213	0.211
H3	0.4	8	0.029	0.028	0.259	0.253
H4	0.4	10	0.033	0.032	0.293	0.287
I1	0.4	6	0.029	0.029	0.258	0.256
I2	0.4	6	0.019	0.018	0.162	0.157

8.4   Concluding Remarks

A mathematical framework, including the method of moments and Monte Carlo simulation, was proposed to describe polymerization reactions between ethylene and 1,9-decadiene using a CGC catalyst, including an ethylene/diene macromonomer reincorporation steps through pendant vinyl groups. The model was validated using experimental data for the copolymerization of ethylene and 1,9-decadiene with a constrained geometry catalyst in a solution polymerization reactor operated in semi-batch mode. Experimental data included ethylene rates of consumption and average molecular weights of polymer samples.

The method of Moments and the Monte Carlo method predicted very well available average molecular weights and ethylene feed flow rates for the experimental conditions discussed. Furthermore, both methods predicted the average frequencies of LCB per chain and per 1000 carbon atoms as a function of polymerization time for all experimental conditions. In addition, the Monte Carlo method provided additional information on long chain branching frequencies, such as the average number of LCB as a function of the polymer chain size, showing that LCBs are formed mainly at high tail of the molecular weight distribution.

It is important to highlight that the kinetic mechanism proposed herein successfully describes all the collected experimental data and that alternative models have not been found in the literature for similar olefin/ diene polymerization systems.

Despite the encouraging results, it must be recognized though that the experimental evidences for LCB formation, as predicted by the model, are weak. However, given the significant effect of LCB formation on the MWDs, and particularly on the high molecular weight tail of the distribution, there are incentives for more involving modeling of the MWD, as performed in the next chapter.

9 Prediction of Molecular Weight Distributions

9.1 Summary

In the present chapter, the experimental molecular weight distributions of pure PE are compared with the predicted MWDs with the help of the method of polynomial approximation, based on the moments of distributions. Then, the experimental MWDs of the copolymers are compared with the simulated MWDs, as obtained by complete adaptive orthogonal collocation (CAOC) and Monte Carlo (MC) simulations. The advantages and drawbacks of each method are commented. Finally, it is proposed that the rate of macromonomer reincorporation is dependent on the number of pendant double bonds in the macromonomer, as an attempt to approximate the experimental and predicted MWDs.

9.2 Ethylene Homopolymerization

As commented in Chapter 5, the molecular weight distributions for the PE homopolymer were simulated using polynomial approximation based on the moments of the distributions. The Monte Carlo method was also used to simulate the MWDs for the PE produced at 120, 130 and 140 °C with the experimental conditions shown in Figure 8.1. Figure 9.1 shows the MWDs obtained using both techniques.

Observing Figure 9.1, it is possible to conclude that when 4 moments are used the polynomial approximation method converges suitably since the MC method provides results exactly similar to the distribution curves provided by the deterministic approach. When 5 moments are used, the deterministic method presents oscillatory modes, as one can see in Figure 9.2. As discussed by PINTO and BISCAIA (1996), oscillatory behavior of polynomial approximations can be obtained when the number of collocation points is excessively large and can be different for odd and even polynomial degrees. For this reason, in order to compare the simulated MWDs with the experimental ones, 4 moments were considered for all experimental conditions (with verification to assure that no distorted MWD had been generated).
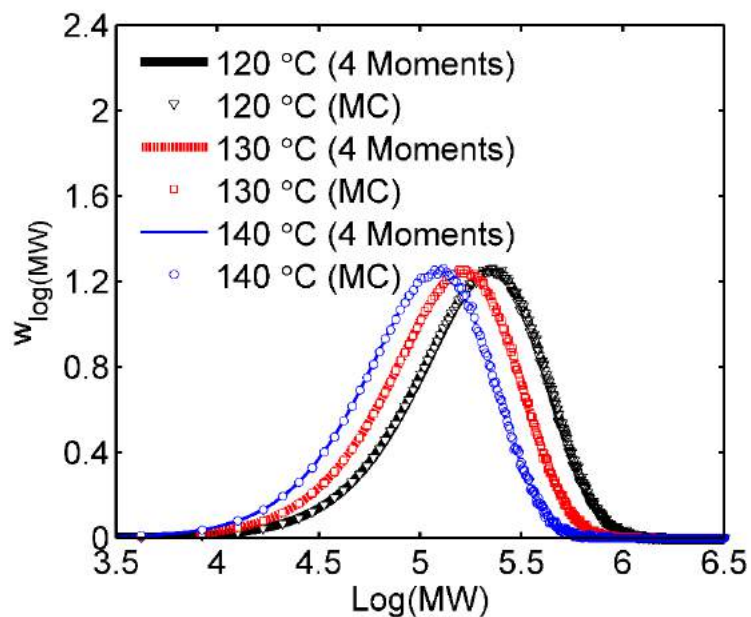
Figure 9.1 – Molecular weight distributions obtained with polynomial approximation with 4 moments and with Monte Carlo method using a control volume of $5 \cdot 10^{-15}$ L for different homopolymerization conditions.
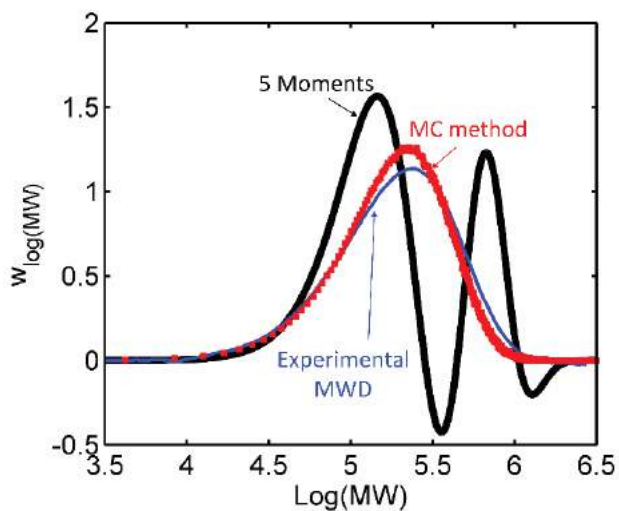
Figure 9.2 – Molecular weight distributions obtained with polynomial approximation with 5 moments and with Monte Carlo method using a control volume of $5 \cdot 10^{-15}$ L and experimental MWD (polymerization conducted at 120 °C).
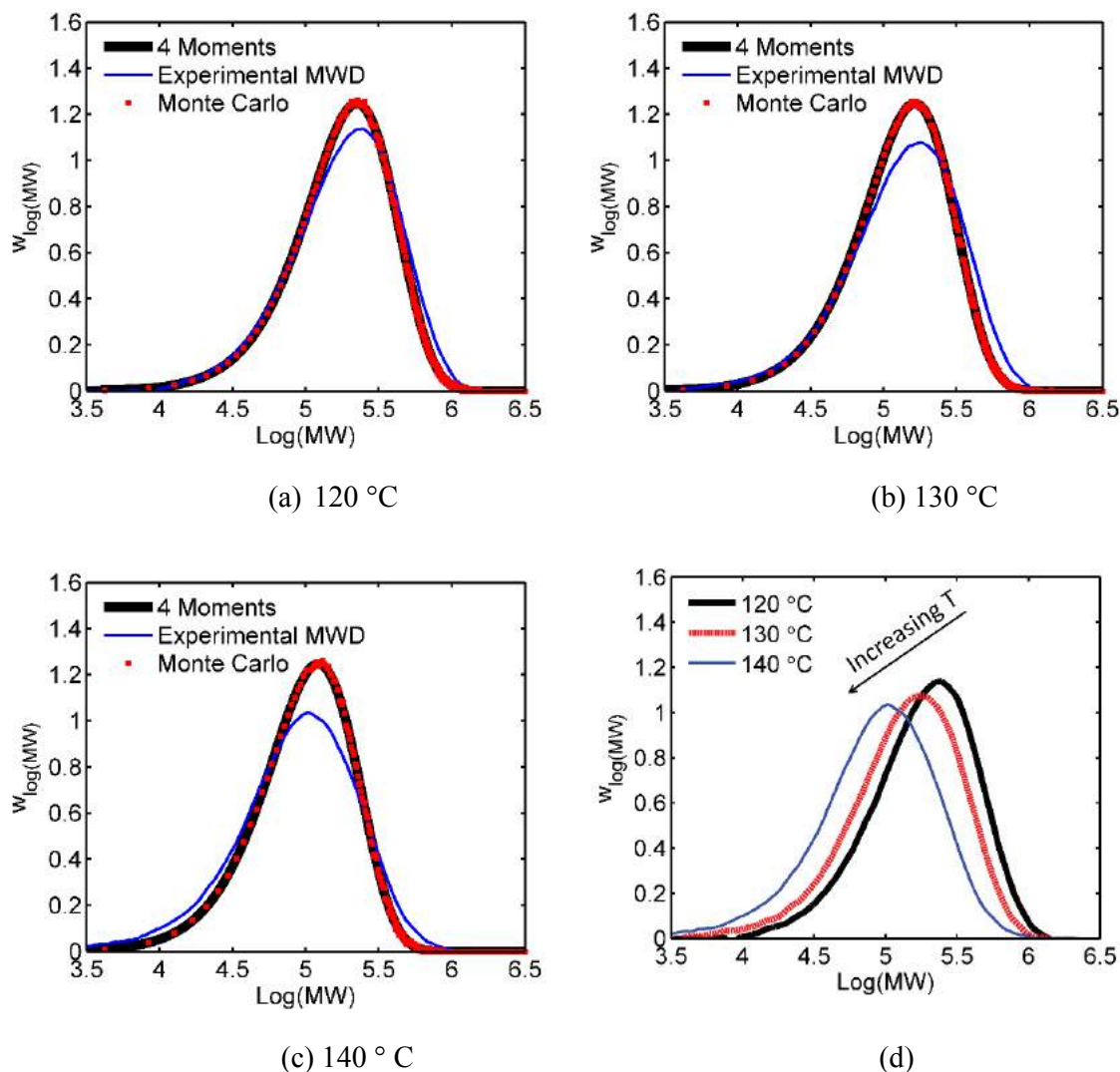
Figure 9.3 – Molecular weight distributions obtained with polynomial approximation with 4 moments and with Monte Carlo method using a control volume of $5 \cdot 10^{-15}$ L for different homopolymerization conditions: (a) 120 °C, (b) 130 °C, (c) 140 °C and (d) all experimental MWDs.

As one can see in Figure 9.3, the simulated MWDs could represent well the experimental MWDs obtained at 120 °C and 130 °C. However, at 140 °C, the predicted distributions were less closer to the experimental ones. Although the temperature varied less than 1 °C during the reaction time, this scenario probably occurred because at 140 °C it was harder to maintain the experimental conditions constant throughout the reaction, which caused the enlargement of the molecular weight distribution. At 120 °C, it is easier to keep experimental conditions almost unchangeable during all executed reactions. In spite of that, fair agreement can be observed in all cases, especially if one considers the intrinsic limitation of the GPC technique.

9.3 Copolymerization of Ethylene and 1,9-decadiene

9.3.1 Applying Monte Carlo to Predict Average Branching Frequency and MWD

Using the Monte Carlo model presented in Section 7.5.4, with the experimental conditions G5 and H4 from Figure 8.11, the MWDs of the final copolymers and the average LCB/chain as function of the molecular weight could be simulated as shown in Figure 9.4 and Figure 9.5.

Evaluating Figure 9.4 and Figure 9.5, it is possible to conclude that the MWD simulated using higher diene concentration is wider than the distribution predicted using lower diene concentration. This is in agreement with the results shown in Table 8.9, as the PI provided by the MC at these conditions are 2.9 and 3.4, respectively. A more detailed discussion about the MWDs is presented in the following sections.
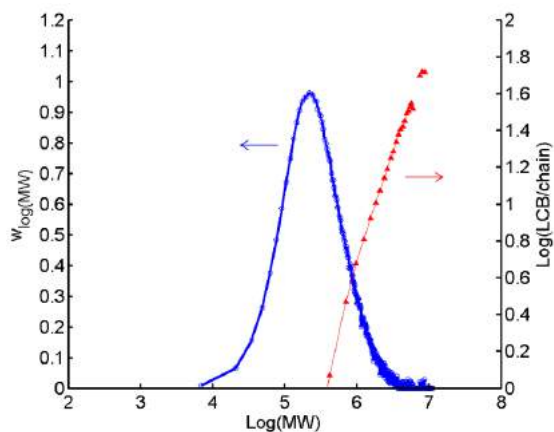
Figure 9.4 – MWD and average LCB/chain as simulated by the MC model for 0.3 g of diene (Simulation condition: G5 from Figure 8.11, control volume 2·10⁻¹⁴ L).
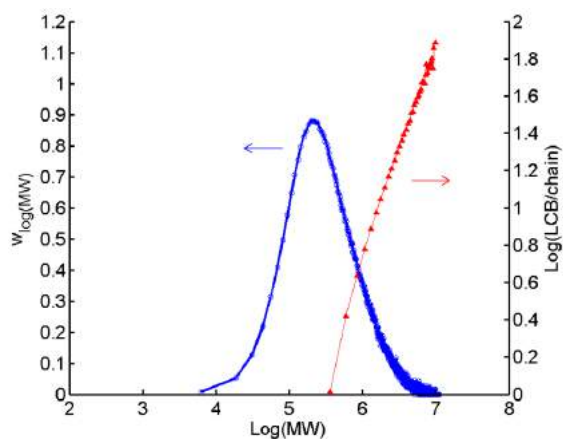
Figure 9.5 – MWD and average LCB/chain as simulated by the MC model for 0.4 g of diene (Simulation condition: H4 from Figure 8.11, control volume 2·10⁻¹⁴ L).

166

The experimental average branching frequency of polyolefins can be estimated through GPC/VISC (with viscosity detector) analysis. This is a relatively simple approach and consists of the following steps (SOARES and MCKENNA, 2012):

1. From the intrinsic viscosity versus molecular weight plot, it is possible to calculate the viscosity branching index g' at each molecular weight as:

$$g' = \frac{[\eta]_b}{[\eta]_l} \qquad (9.1)$$

where $[\eta]_l$ and $[\eta]_b$ are the intrinsic viscosities of linear and branched polymers with the same molecular weight, respectively.

2. Then, it is possible to calculate the branching index g at each molecular weight as:

$$g' = g^\varepsilon \qquad (9.2)$$

where ε depends on the LCB topology, solvent and polymer type. It has been reported that the value of ε is within the interval $0.5 - 1.5$ (SOARES and MCKENNA, 2012). The exponent ε also depends on the molecular weight, which makes the use of Equation (9.2) more complex, since it is assumed here that the exponent is the same for all molecular weights.

3. Then, it is possible to estimate the number of LCBs per chain (n) at each molecular weight using one of the following equations:

$$g = \left[\left(1 + \frac{n}{7}\right)^{0.5} + \frac{4n}{9\pi} \right]^{-0.5} \qquad (9.3)$$

$$g = \frac{6}{n_w} \left\{ 0.5 \left(\frac{2 + n_w}{n_w}\right)^{0.5} \ln\left[\frac{(2 + n_w)^{0.5} + n_w^{0.5}}{(2 + n_w)^{0.5} - n_w^{0.5}}\right] - 1 \right\} \qquad (9.4)$$

where n_w is the weight average number of LCBs per chain $(n = n_w/MM)$ (MM is the molecular weight of the monomeric unit).

167

ZIMM and STOCKMAYER (1949) proposed Equations (9.3) and (9.4) for branching index g and the number of LCBs per chain n. Equation (9.3) assumes that chains are trifunctional, randomly branched, monodisperse, while Equation (9.4) assumes that chains are trifunctional, randomly branched and polydisperse.

A drawback of the GPC/VISC method described above is the value of the exponent ε, which must be known accurately. However, this is not feasible, due to the dependency of ε in respect to the LCB topology and molecular weight. The use of the GPC-MALLS (GPC triple-detector system) constitutes an alternative technique, since the addition of a MALLS detector allows the direct use of the Zimm-Stockmayer expression (Equation (9.3) and Equation (9.4)), as the radius of gyration of the chains eluting from the columns can be determined during the analysis (SOARES and MACKENNA, 2012). Thus, instead of using Equation (9.2), the following expression can be used to calculate the branching index:

$$ g = \frac{\langle R_g^2 \rangle_b}{\langle R_g^2 \rangle_l} \tag{9.5} $$

where $\langle R_g^2 \rangle_l$ and $\langle R_g^2 \rangle_b$ are the squared radius of linear and branched chains of the same molecular weight, respectively.

Figures 9.6 and 9.7 illustrate the average branching frequencies for the copolymer produced using experimental condition G5 from Figure 8.11 and also the simulated LCB/chain and MWD using the MC method. These branching frequencies were calculated using the two relations derived by Zimm and Stockmayer (ZIMM and STOCKMAYER, 1949).

Unexpectedly, the relation derived for monodisperse polymers (Equation (9.3)) seems to fit better the simulated data predicted by the MC method (Figure 9.6) than the relation derived for polydisperse polymers (Figure 9.7). These results also depend on the value selected for the exponent ε, which in the present case was chosen by simple observation of the final graphic. On the other hand, these figures indicate that the Monte Carlo method was able to predict branching frequencies and simultaneously provide better fits for the experimental MWDs.
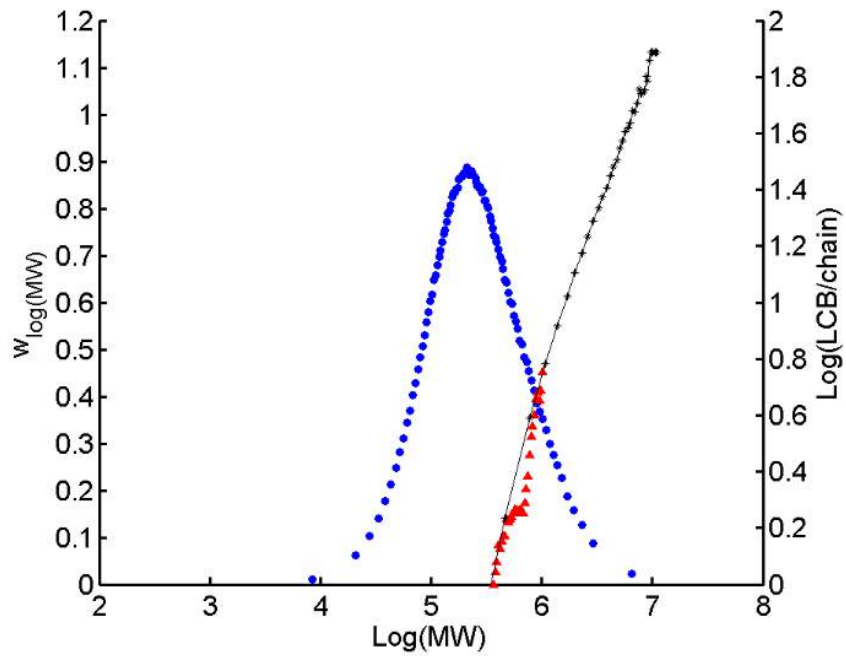
(a) ε = 1.0 (Δ **: experimental data**, -+- **: model prediction for log(LCB/chain)**, o **: model prediction for MWD**)

(b) ε = 0.90 (Δ **: experimental data**, -+- **: model prediction for log(LCB/chain)**, o **: model prediction for MWD**)

169
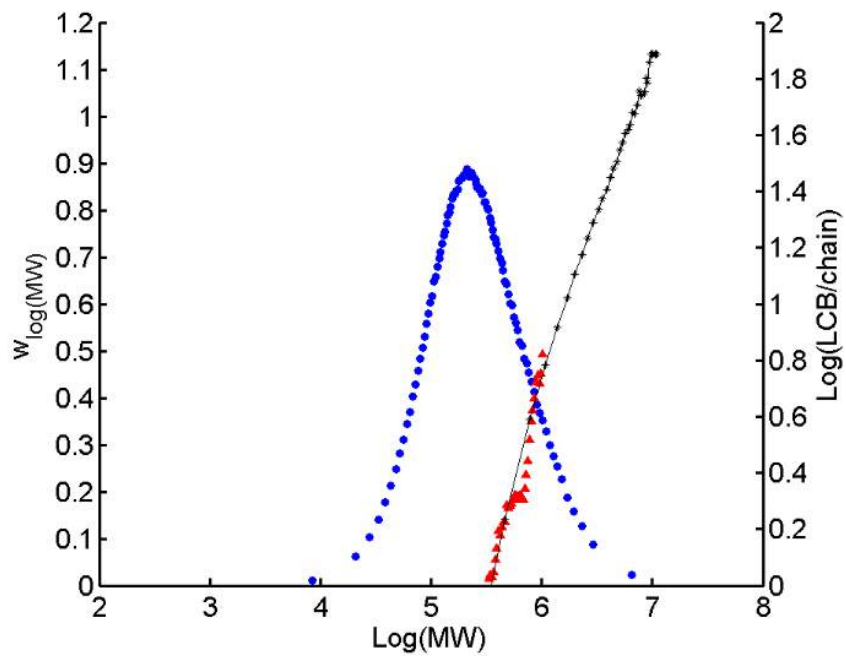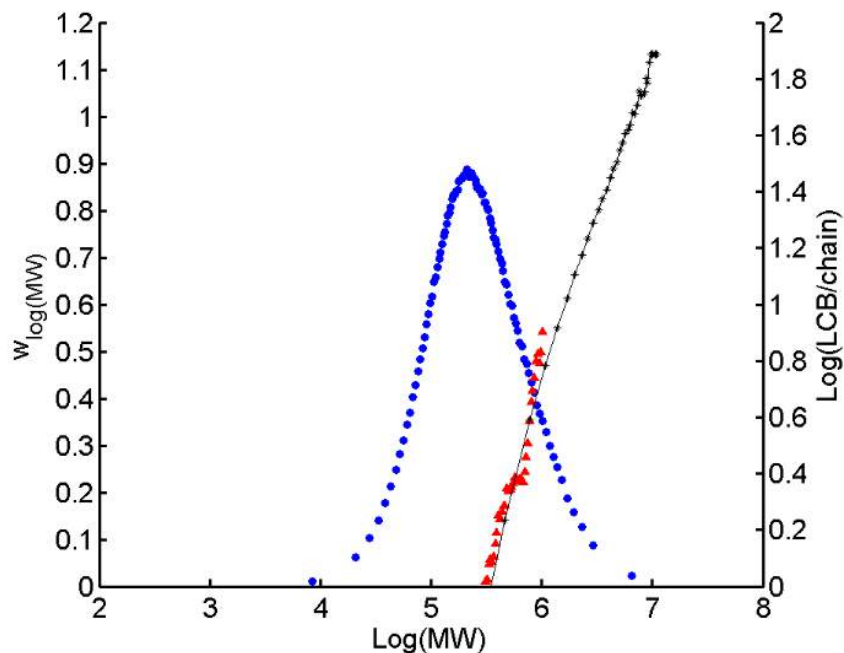
(c) ε = 0.8 (∆ : experimental data, -+- : model prediction for log(LCB/chain), o : model prediction for MWD)
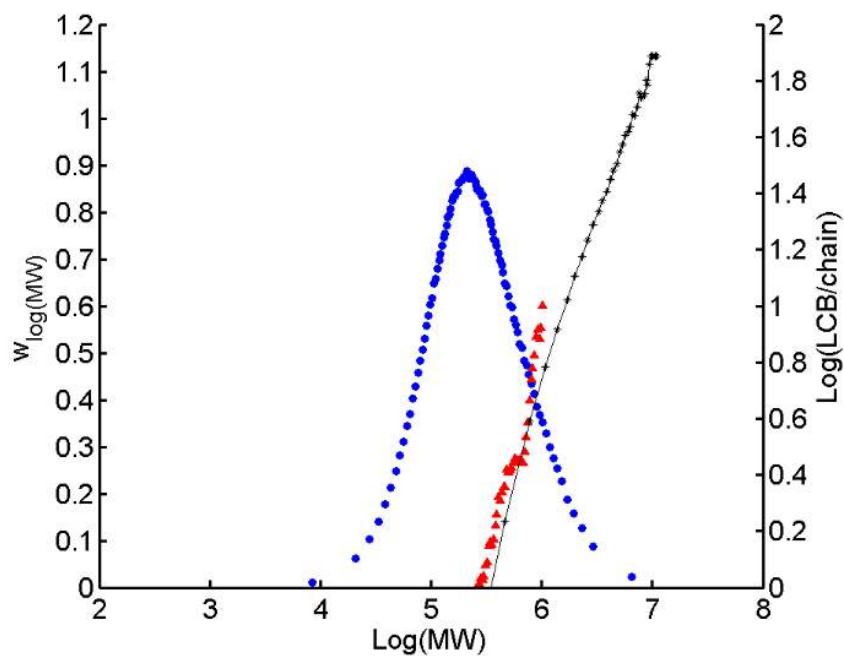
(d) ε = 0.7 (∆ : experimental data, -+- : model prediction for log(LCB/chain), o : model prediction for MWD)

Figure 9.6 – MWD and experimental and simulated average LCB/chain for 0.4 of diene (condition G5 from Figure 8.11) using Equation (9.3) and different values for ε.
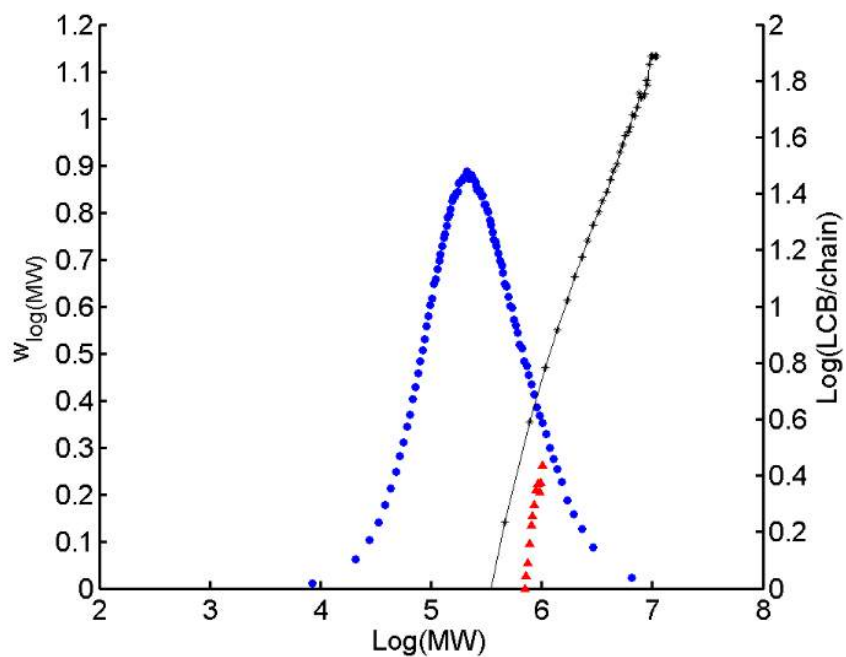
(a) ε = 1.0 (Δ : experimental data, -+- : model prediction for log(LCB/chain), o : model prediction for MWD)
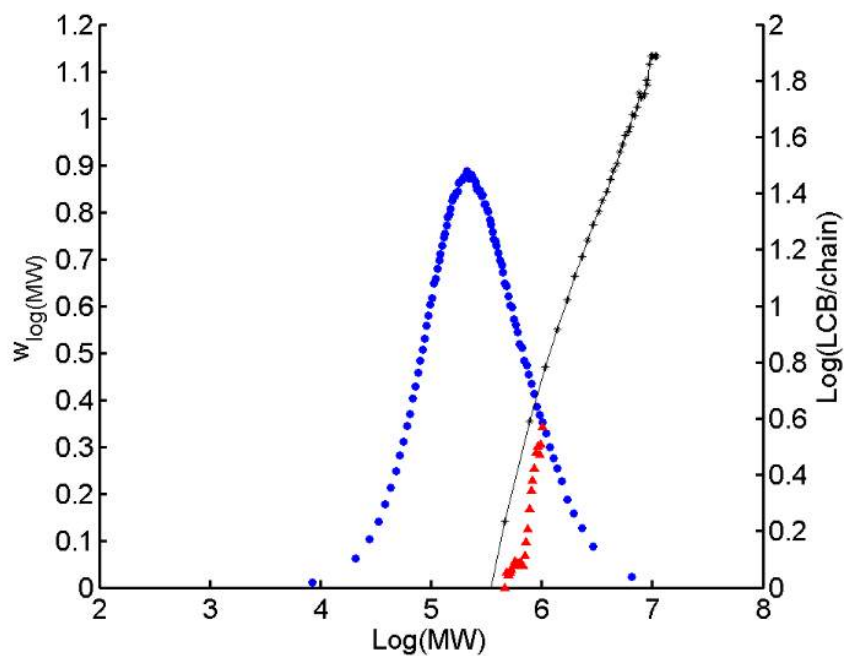
(b) ε = 0.80 (Δ : experimental data, -+- : model prediction for log(LCB/chain), o : model prediction for MWD)
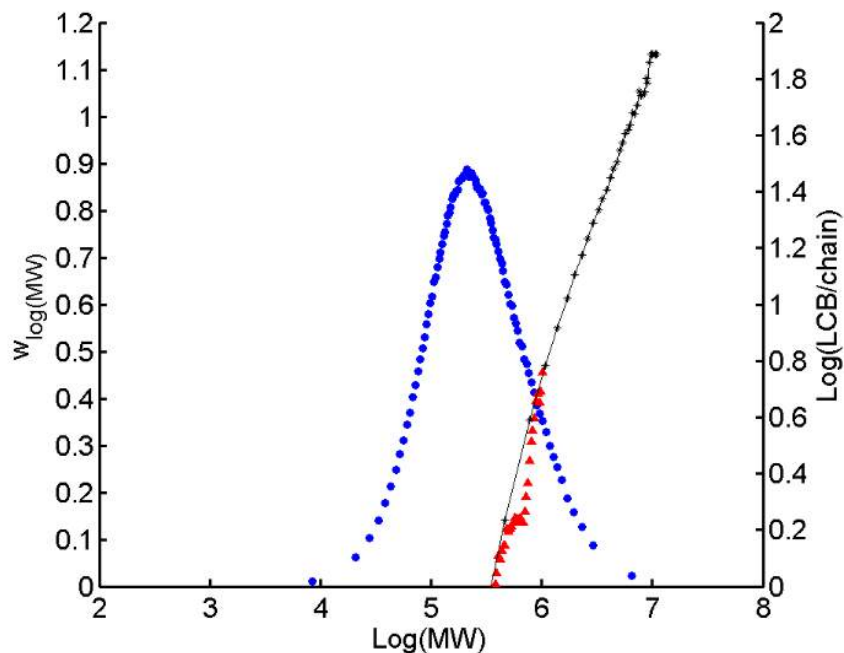
(c) ε = 0.6 (Δ **: experimental data**, **-+- : model prediction for log(LCB/chain),** o **: model prediction for MWD**)
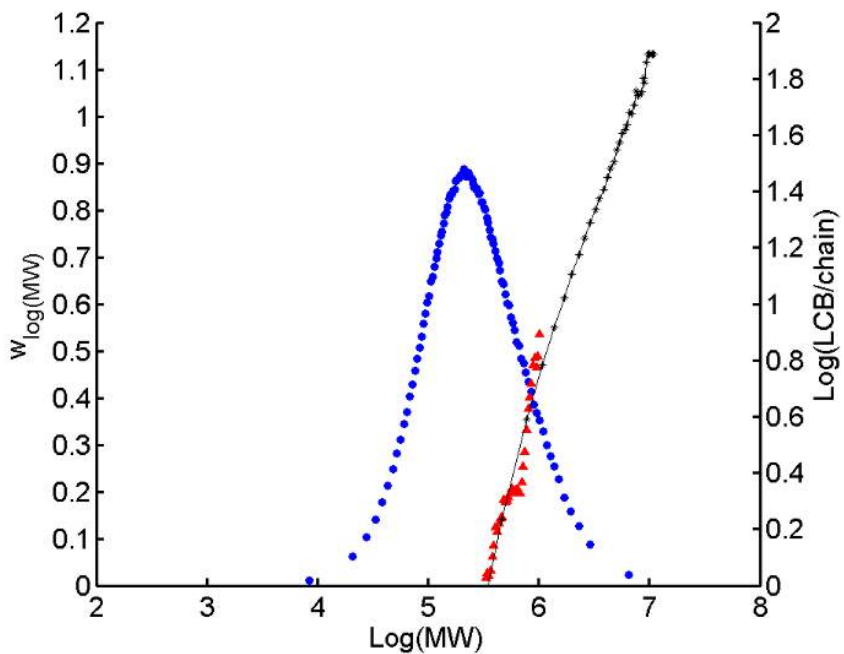
(d) ε = 0.50 (Δ **: experimental data**, **-+- : model prediction for log(LCB/chain),** o **: model prediction for MWD**)

Figure 9.7 – MWD and experimental and simulated average LCB/chain for 0.4 of diene (condition G5 from Figure 8.11) using Equation (9.4) and different values for ε.

172

The results shown in Figures 9.6 and 9.7 are really important since they show very good agreement between experimental and simulated average LCB/chain even considering all uncertainties around the values for ε as commented previously. Moreover, the developed MC model can be used to simulate other copolymerization systems and, after the model validation, it can be used to predict the average LCB/chain when there is no available GPC/VISC.

In the next sections, it will be presented all discussion related to the MWDs of the copolymers. It will be shown that the presence of LCBs directly affects the widening of the molecular weight distributions. However, as a first step, it will be shown the numerical aspects of both techniques employed in the present thesis to build the MWDs (CAOC and MC).

9.3.2 Numerical Aspects of the Adaptive Orthogonal Collocation Method (CAOC)

In order to investigate some numerical aspects of the orthogonal collocation method, the experimental condition H4 (0.4 g of 1,9-decadiene and 10 minutes of reaction) was selected for additional studies. Some simulations were performed, following the procedure shown in Figure 3.1 and applying different numbers of collocation points and integral step sizes.

In Figure 9.8, the MWD calculated with the CAOC is presented for different time steps, with 4 collocation points. Figure 9.9 presents the evolution of collocation points as functions of the simulation time.
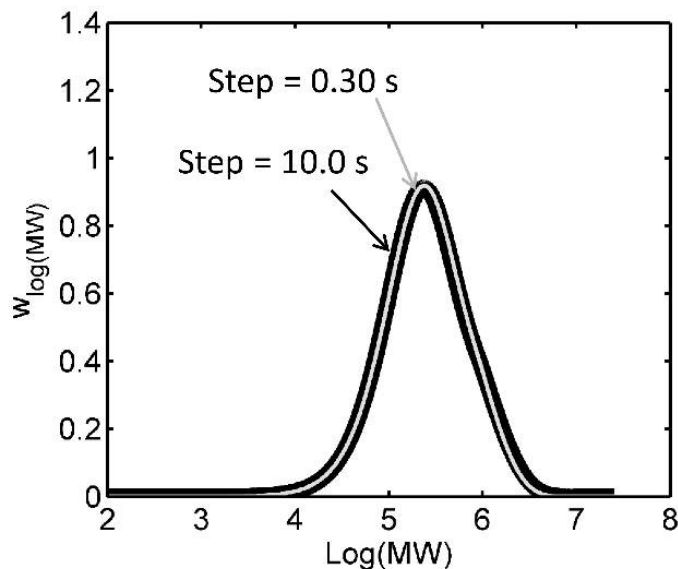
Figure 9.8 – MWD from the complete adaptive orthogonal collocation method using 4 collocation points.

As one can see in Figure 9.8, the profile obtained was unimodal, as expected. The evolution of time points was slightly noisy, especially for the last point in the first instants of reaction. All points stabilized after some time. Analyzing the evolution of the calculated orthogonal collocation points, the reader cannot see much difference in the orthogonal collocation points obtained when 0.30 s is used as the integral step size and compared to those calculated with a step size of 10.0 s. This indicates that for 4 collocation points, it is advantageous to use a larger integration step size which can lead to faster simulations.

Figure 9.10 presents the MWD distributions calculated with the CAOC for different time steps, with 5 collocation points. Figure 9.11 presents the evolution of the collocation points during the time of the simulation.
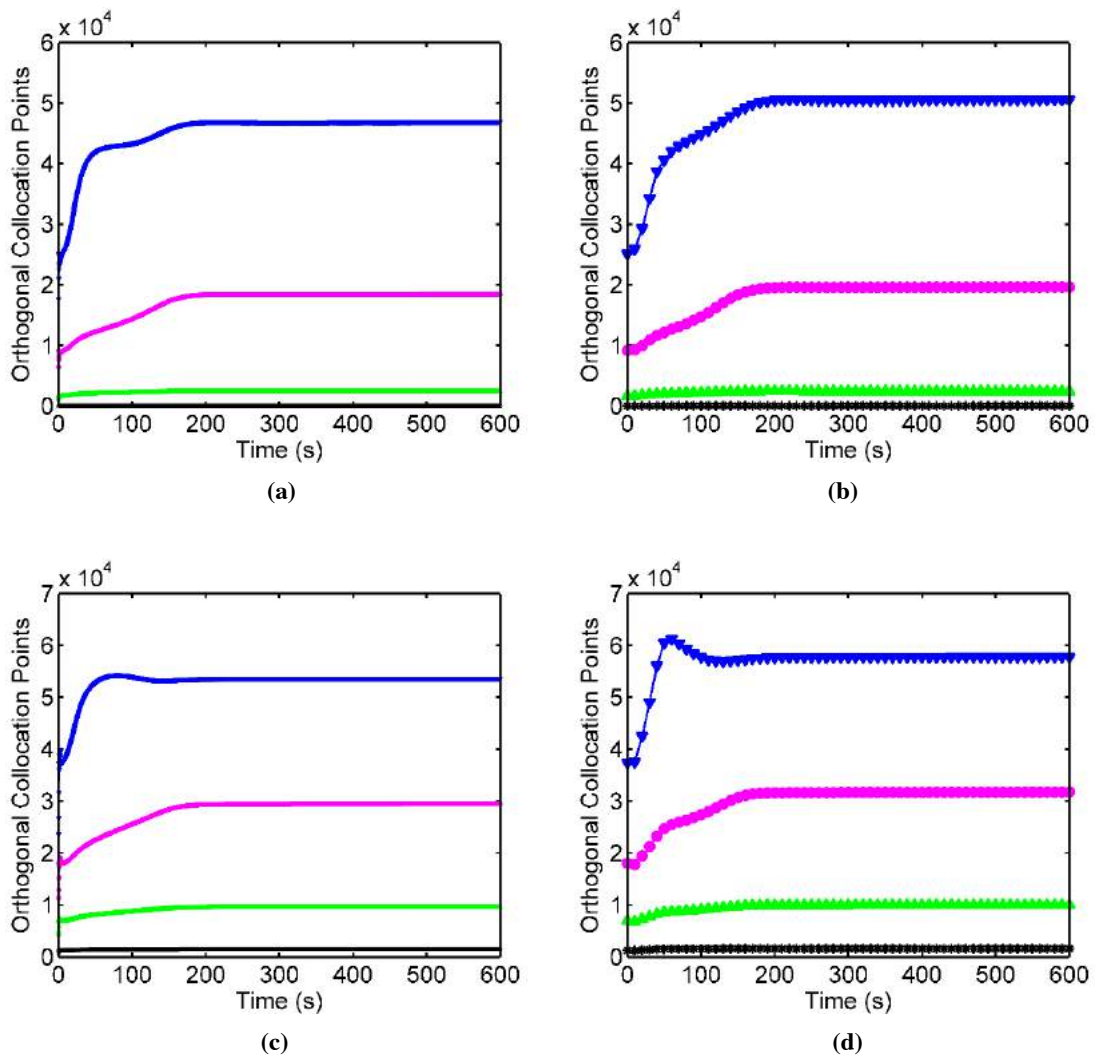
Figure 9.9 – Evolution of the collocation points during time for the living polymers considering (a) 0.30 s and (b) 10.0 s as integration step sizes and for the dead polymers considering (c) 0.30 s and (d) 10.0 s as integration step sizes, using 4 collocation points.
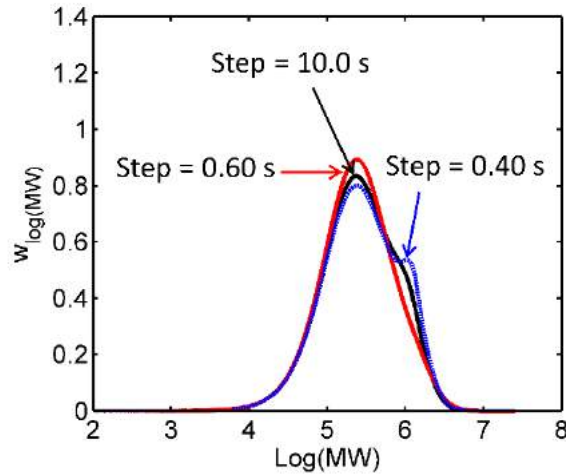
Figure 9.10 – MWD from the complete adaptive orthogonal collocation method using 5 collocation points.
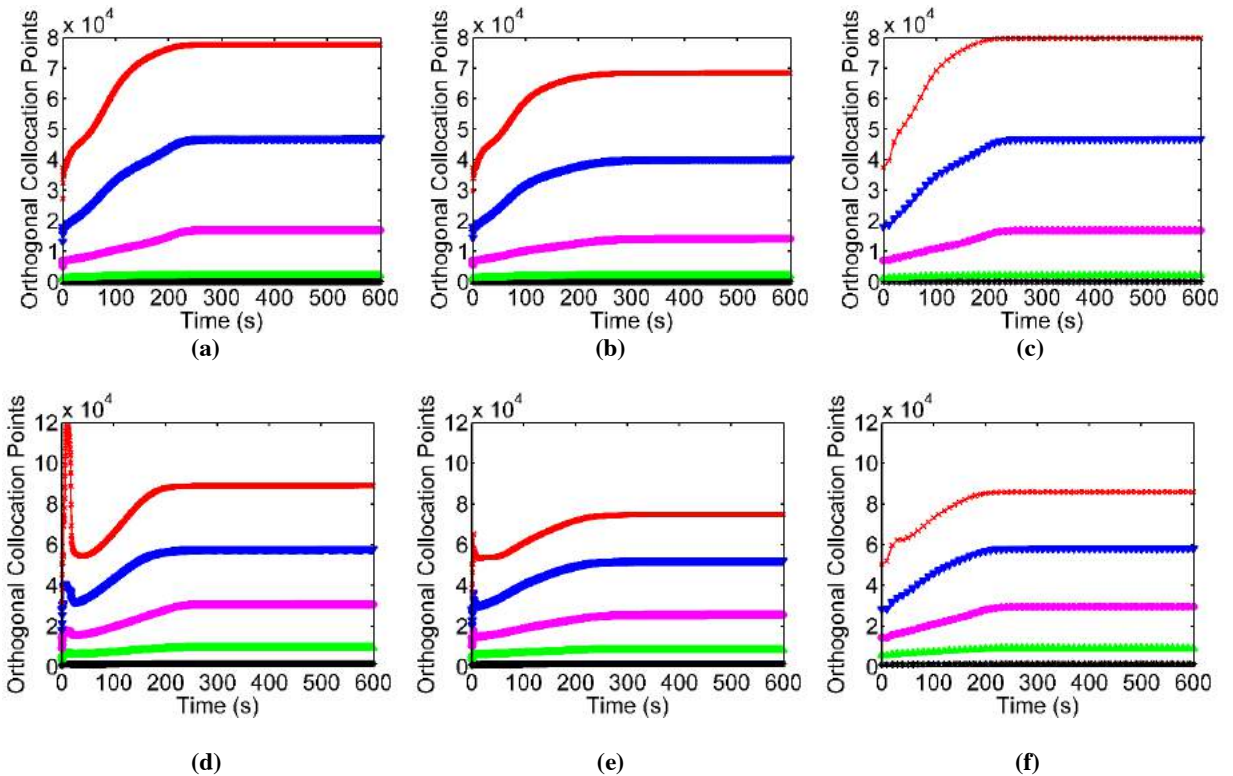
Figure 9.11 – Evolution of the collocation points during time for the living polymers considering (a) 0.40 s, (b) 0.60 s and (c) 10.0 s as integration step sizes and for the dead polymers considering (d) 0.40 s, (e) 0.60 s and (f) 10.0 s as the integration step sizes, using five collocation points.

Surprisingly, Figure 9.10 shows that the MWD obtained with 5 collocation points diverge significantly, depending on the applied integration step size. The best choice for time interval seemed to be 0.6 s. Generally, the lower the step size, the more

176

precise the method is; however, for step size of 0.4 s, an unexpected behavior was observed. Figure 9.11 indicates that all curves presented a clear tendency and low noise in the behavior of the nodal points; with exception of Figure 9.11d, associated with the dead polymer chains for step size of 0.4 s of time integration. For 0.40 s, at the first 25 s of simulation, the collocation points for the dead chains exploded, reaching 120000; then, in last than 10 s, they returned to values around 80000. Figure 9.12 shows how the MWD changed during simulation using 5 collocation points and 0.4 as the step size of integration. The distribution starts to become bimodal at reaction time corresponding 215 s. When the integral step size of 0.60 s was used, all the collocation points calculated for living and dead points were smaller than those calculated with step sizes of 0.4 s and 10.0 s. Thus, these results suggest that convergence tests are highly recommended to achieve trustable results with this numerical technique. From the distributions shown in Figure 9.10, convergence could be obtained using 0.6 s as the integration step size, but when the step size of integration was diminished to 0.4 s, an oscillatory behavior appeared at the high molecular weight region.
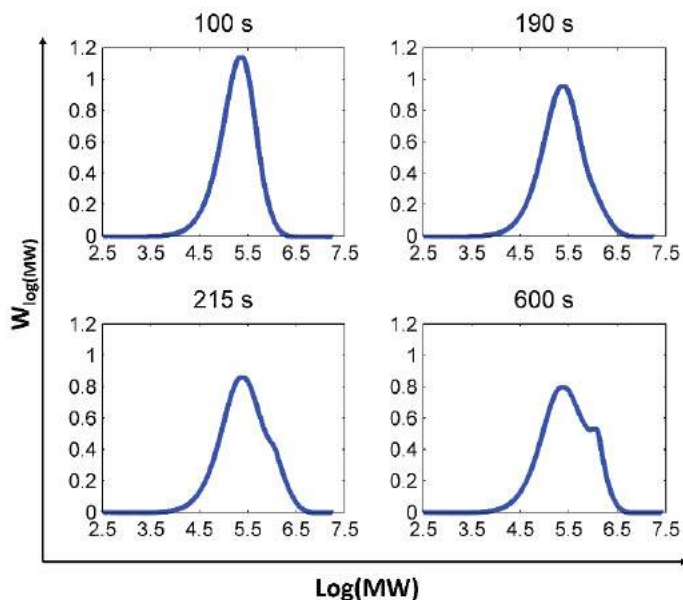
Figure 9.12 – MWDs from the complete adaptive orthogonal collocation method using 5 collocation points and 0.4 s as integral step at polymerization times of 100, 190, 215 and 600 s.

As a matter of fact, as observed through many simulations, the numerical computation of the collocation points is very sensitive to numerical tolerances. This suggests that detailed numerical tuning of tolerances must be carried out prior to use of the discretized model, when collocation procedures are used.

Finally, Figure 9.13 shows the MWD as calculated with 6 collocation points (the curves of 4 and 5 collocation points are also presented for comparison). Figure 9.14 shows the evolution of the collocation points for 6 collocation points. As one can see in Figure 9.13, simulations are in good agreement and no unexpected behavior can be observed for these conditions. Figure 9.14 shows that the evolution of collocation points presented a clear trend, without unexpected growth.
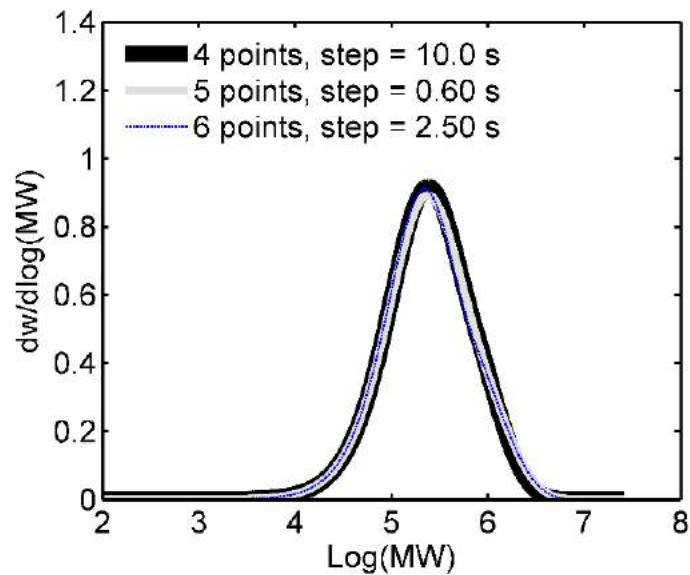
Figure 9.13 – MWD as calculated with the complete adaptive orthogonal collocation method using 4, 5 and 6 collocation points.
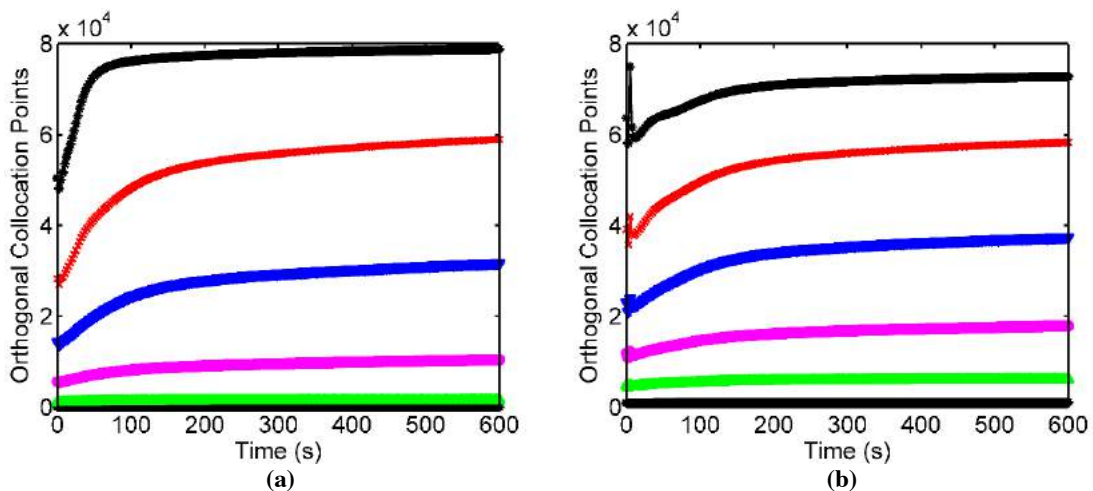
Figure 9.14 – Evolution of the collocation points during time for the (a) living and (b) dead polymers considering 2.50 s as the integration step size, applying six collocation points.

178

It is important to mention that during all the simulations, when 3 s was reached, the procedure initiated the complete adaptive orthogonal collocation procedure, using Flory distribution as reference before this point. Obviously, when the integration step sizes were larger than 3 s, the procedure started the complete adaptation procedure after the analyzed step size.

For condition H4, the method requires only 4 collocation points to converge, which is an advantage when compared to other techniques, given the fast simulation times. On the other hand, it is necessary to confirm the convergence by varying step sizes and number of collocation points. Appendix E presents more details regarding the selection of the number of collocation points and the size of the integration steps, as required for all experimental conditions considered in the present work.

9.3.3 Numerical Aspects of the Monte Carlo Method

In the Monte Carlo method, MWD approximations are not required and all mechanistic polymerization steps can be simulated as assumed. The MC convergence depends only on the control volume, as one can see in Figure 9.15.

The MWD predicted with volume of $1.0 \cdot 10^{-16}$ L is very noisy and is not adequate for an accurate representation of the MWD. On the other hand, the MWDs predicted with volumes of $5.0 \cdot 10^{-15}$, $1.0 \cdot 10^{-14}$ and $4.5 \cdot 10^{-14}$ L are similar to each other, although significant differences can be observed for the computational time. The bigger is the control volume, the longer is the CPU time required to run the simulation. The MWD obtained with volume of $5.0 \cdot 10^{-15}$ L is sufficient to provide accurate results for the experimental condition in analysis.
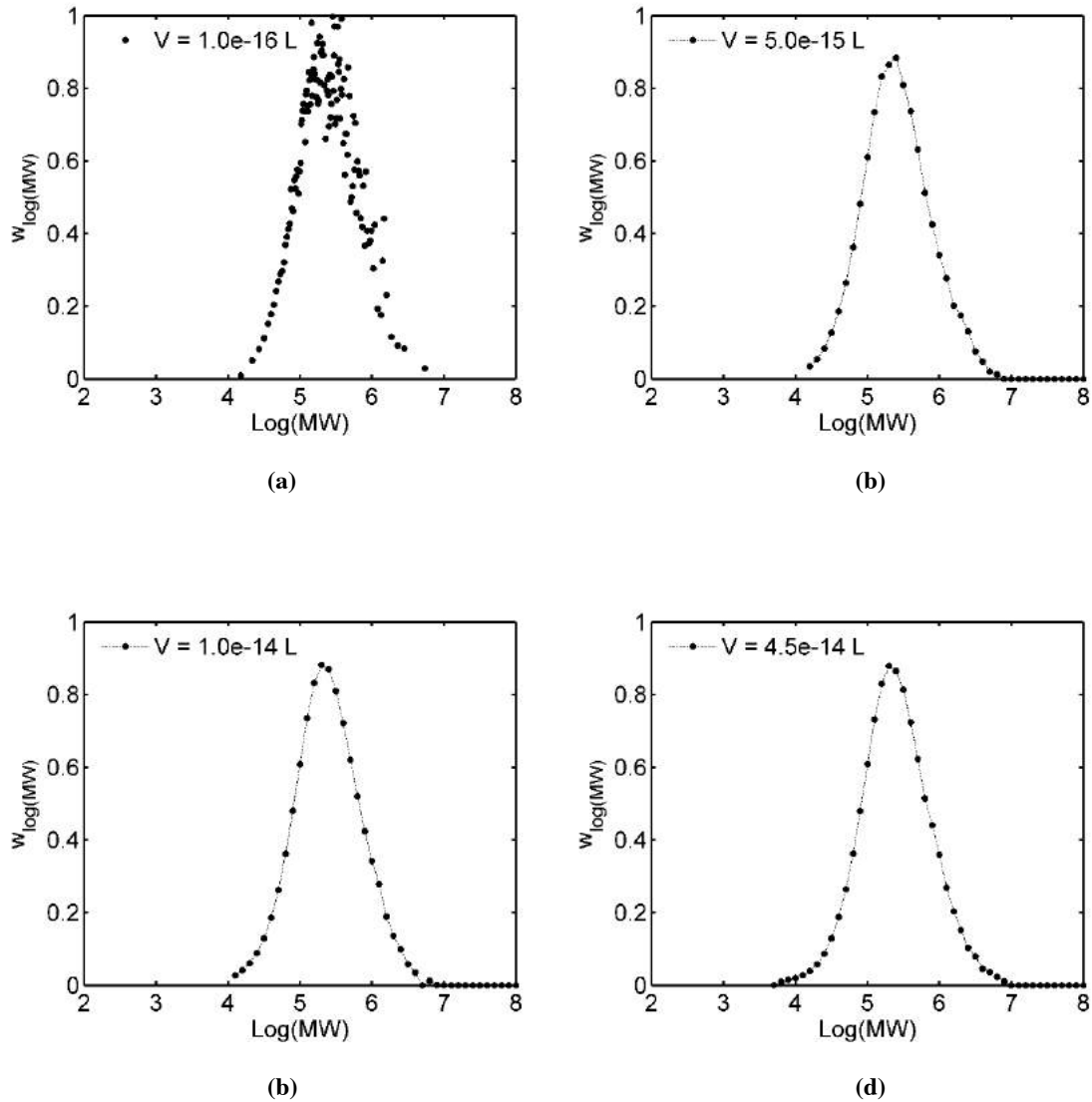
Figure 9.15 – MWD obtained after 10 min of polymerization using condition H4 from Figure 8.11 for different control volumes.

9.3.4 Comparison of Predicted and Experimental MWD

The MWDs were obtained with four collocation points for experimental conditions F1, G2-G5, H1-H4 and I1 from Figure 8.11 using the complete adaptive orthogonal collocation method. From the first iteration until 3.0 s of polymerization, the reference function was considered equivalent to the Flory distribution. After this time, the complete adaptation was adopted. The same experimental conditions were simulated using the Monte Carlo technique. Figures 9.16 to 9.18 illustrate the simulated and predicted MWDs using both numeric methods.
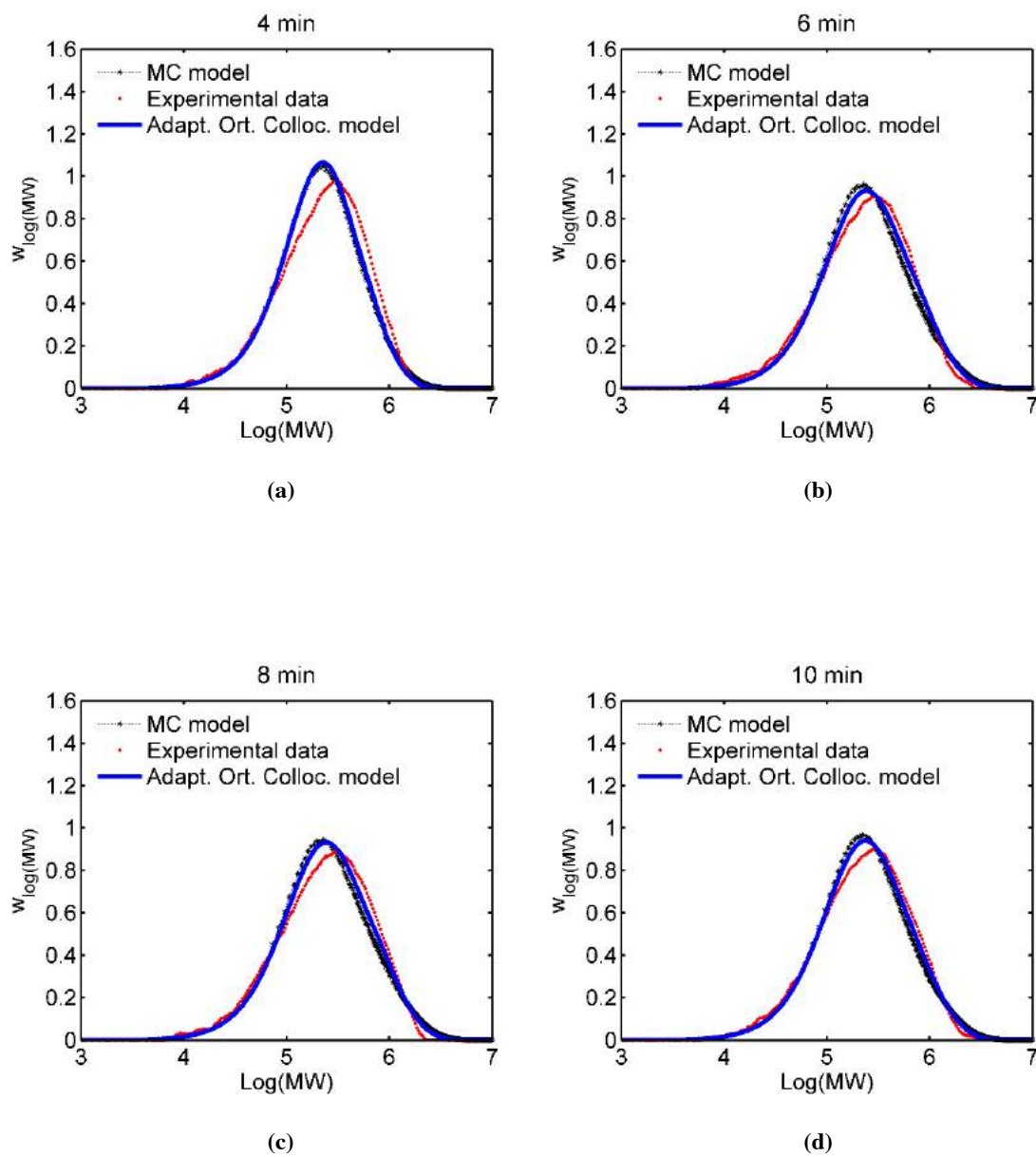
Figure 9.16 – Experimental and simulated MWD of copolymer samples produced after (a) 4, (b) 6, (c) 8 and (d) 10 minutes (Experiment condition: G2 to G5 from Figure 8.11).

181
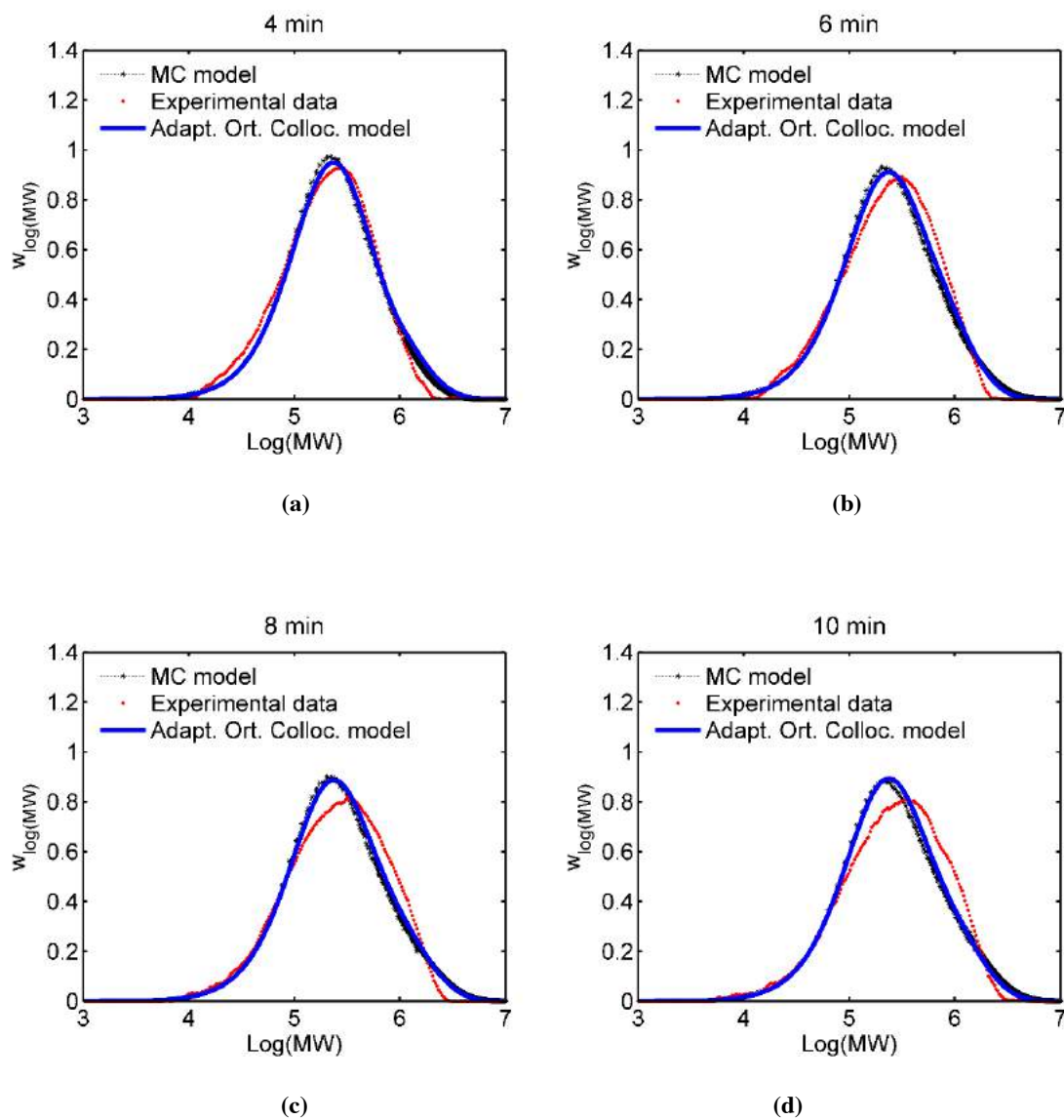
Figure 9.17 – Experimental and simulated MWD of copolymer samples produced after (a) 4, (b) 6, (c) 8 and (d) 10 minutes (Experiment condition: H1 to H4 from Figure 8.11).

(a)

(b)

(c)

(d)
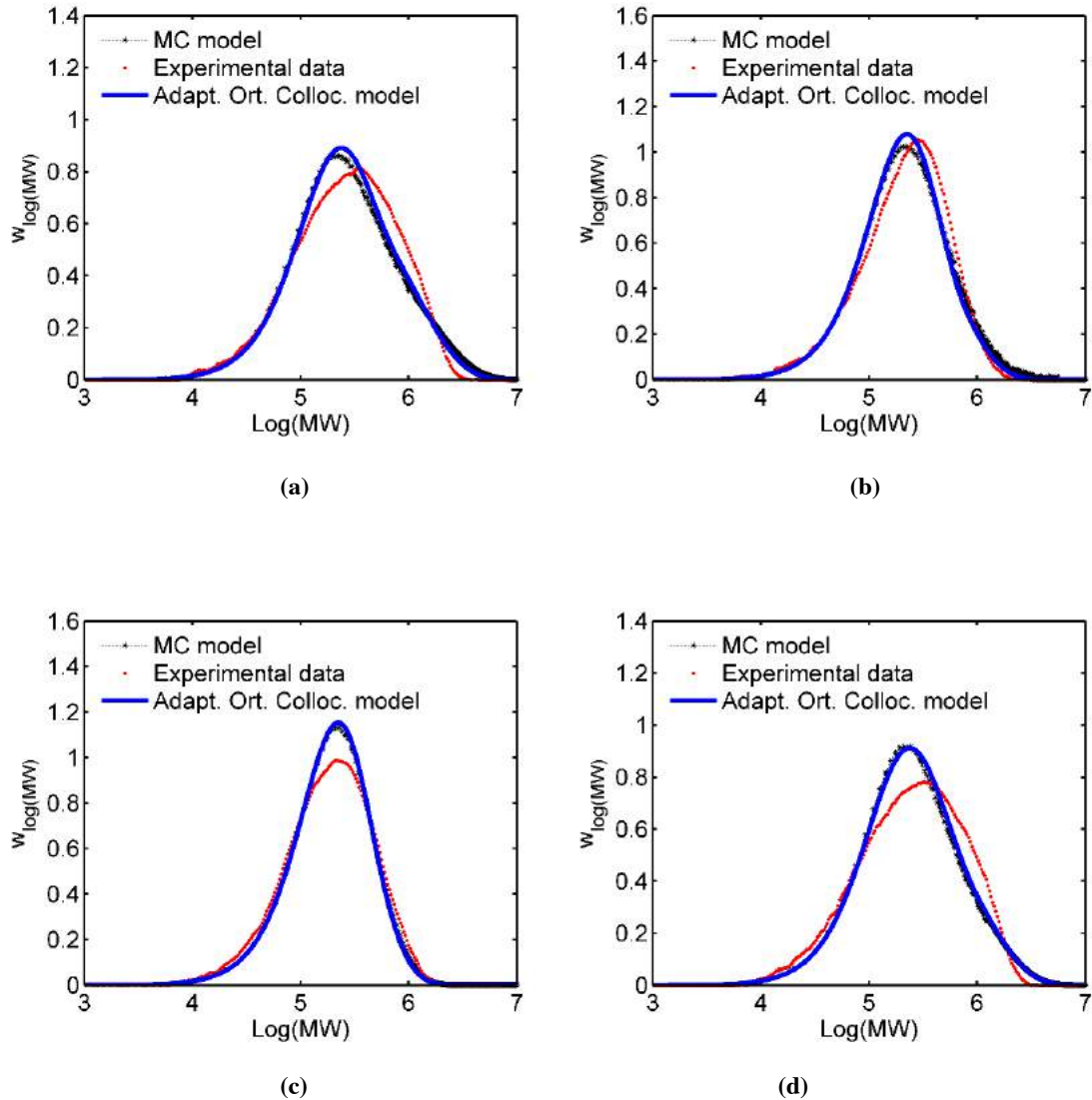
Figure 9.18 – Experimental and simulated MWD of copolymer samples produced after (a) 6 min (Experiment condition: I1), (b) 6 min (Experiment condition: I2), (c) 10 min (Experiment condition: D1) and (d) 10 min (Experiment condition: F1).

In all cases, the Monte Carlo simulations are in very good agreement with the MWD predicted by the complete adaptive orthogonal collocation technique, which seems to validate both implementations. In all analyzed experimental conditions, both methods converged to the same final distribution; minor differences could be observed in conditions I2 and I1, but these differences can be regarded as acceptable, since they are within the numerical accuracy. Thus, the MC method can be used to validate if the MWD obtained with the orthogonal collocation method, instead of repeating the

simulation with additional collocation points, considering the fact that wrong MWDs can be obtained because of numerical instabilities.

The CPU time required to run the simulations using Monte Carlo, applying different control volumes, and using Complete Adaptive Orthogonal Collocation method with different collocation points and integration step sizes were compared and these results are shown in Figure 9.19 and Table 9.1. As can be seen in Table 9.1, the CPU time depends on the number of collocation points used and also on the integration step chosen. In the case for experimental condition D1, it was possible to obtain a fastest simulation with 6 collocation points and 10 s as integration step than when it was used 5 collocation points and 0.59 s as integration step. Thus, besides the convergence analysis, the consumption time required to run the model has also to be evaluated in order to select the most appropriate combination of the number of collocation points and integration step size. Comparing Figure 9.19 and Table 9.1, it is possible to conclude that for the experimental conditions investigated, the CAOC method required almost the same CPU time than the MC method, since to obtain good representation of the MWDs using MC method, a control volume of $5 \cdot 10^{-15}$ L was used and for this volume the CPU times were around 0.8 to 1.2 hours, while the CAOC method required computation times around 0.64 to 1.19 hours.
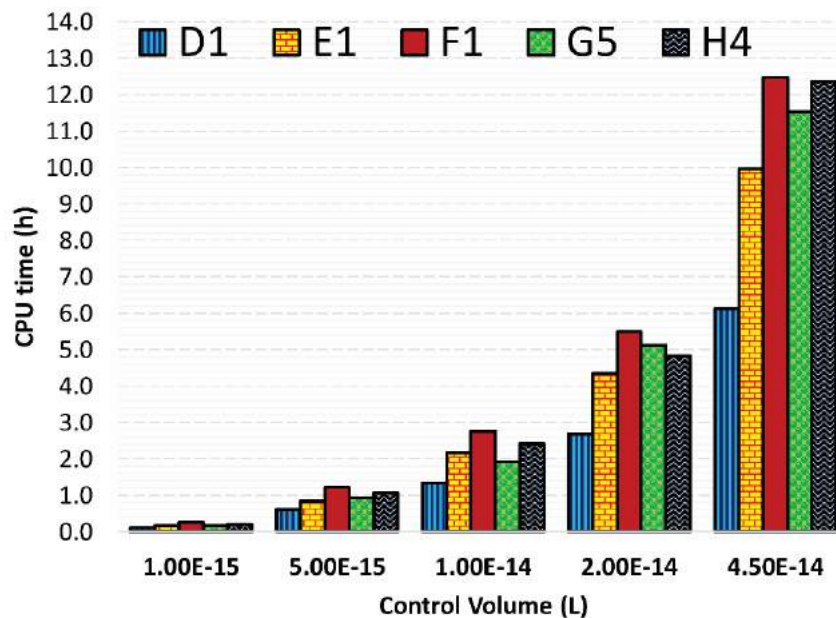
Figure 9.19 – CPU time required to run the Monte Carlo models for different control volumes.

Table 9.1. CPU time required to run the Adaptive Orthogonal Collocation Models for different number of collocation points and integration steps.

Experimental Condition	Collocation Points	Integration Step (s)	CPU Time (h)
	4	0.30	6.34
	4	10	0.64
H4	5	0.60	7.29
	6	2.5	6.18
	4	0.59	3.97
	4	0.98	3.11
G5	4	10.00	0.64
	5	0.59	8.64
F1	4	60.00	0.64
	5	0.59	8.19
E1	4	10	0.65
	6	10	2.17
	5	0.59	6.40
D1	5	10.00	1.19
	6	10.00	1.58

By evaluating Figures 9.16 to 9.18, it becomes possible to conclude that the simulated MWDs reach bigger molecular weights than the experimental distributions, with the only exception of condition D1 (0.1 g of decadiene, the lowest amount of diene used experimentally). According to the adopted mechanism, the reaction channel responsible to form LCB (Equation (7.7)) depends on the average frequency of pendant double bonds in the macromonomer. So, the macromonomer with larger size has higher probability of being incorporated than the macromonomer with smaller size, due to the higher number of pendant double bonds in the chain length. Although this hypothesis seems reasonable, it does not seem to be entirely true since the experimental MWD does not reach so higher molecular weights. Apparently, what defines the probability of a macromonomer being incorporated is the amount of pendant unsaturations that it contains and also its size. Bigger macromonomers may suffer from steric hindrance around the catalyst site, so that they cannot be incorporated into the growing chains so efficiently as a smaller chain. If the macromonomer chain length is also taken into account to calculate the probability of macromonomer incorporation, then the appearance of high molecular weights in the simulated distributions will not be so frequent. For this reason, in the present thesis it is proposed that the reincorporation rate constant can depend on the chain size.

Based on the new hypothesis, the reaction rates for macromonomer reincorporation must be redefined as

$$a_7(\boldsymbol{X}) = R_7^{MC} = k_b^{MC} X_6 \sum_{w=1}^{X_7} \left(j_{from\ L_{i,j,k}} \cdot F(i) \right) \qquad (9.6)$$

where w is a counter and $F(i)$ is a function that depends on the chain length. Figure 9.20 shows how the summation of Equation (9.6) must be performed when the rate constant depends on the chain size.

$$\sum_{w=1}^{X_7} \left[j_{from\ L_{i,j,k}} \cdot F(i) \right] = \left[j \cdot F(i) \right]_{w=1} + \cdots + \left[j \cdot F(i) \right]_{w=X_7}$$
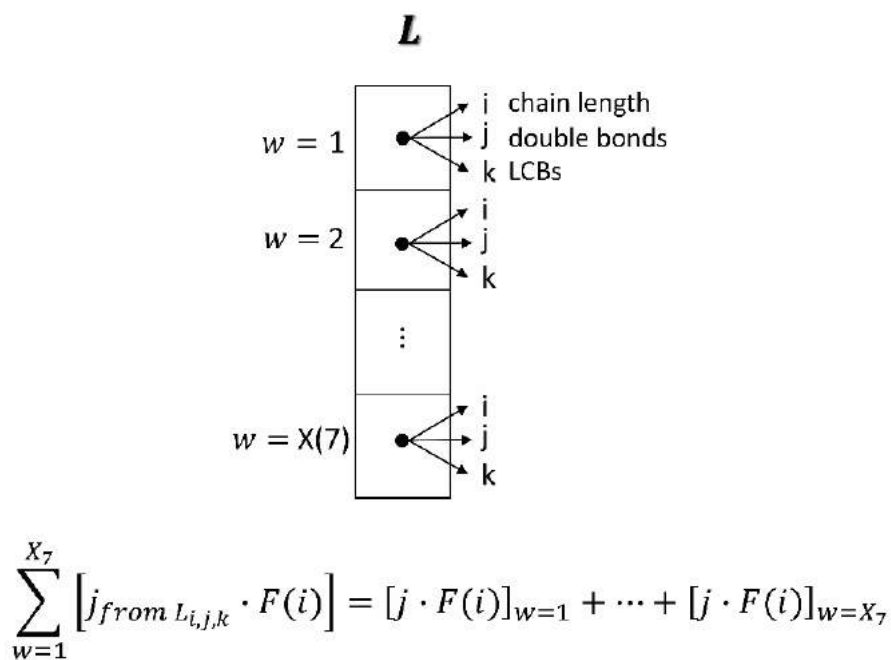
Figure 9.20 – Procedure used to solve the summation of Equation (9.6).

Because function $F(i)$ has to indicate how the macromonomer chain length affects its incorporation into the growing chain, three different expressions were proposed and considered for $F(i)$ (the parameter values were obtained through estimation, considering the available experimental MWD data):

➲ Sigmoid function:

$$F(i) = 1 - \frac{1}{1 + \varphi \cdot exp(-\beta i)} \qquad (9.7)$$

where $\varphi = 7.389$ and $\beta = 0.0001$.[7]

➲ Exponential function:

$$F(i) = \varphi \cdot exp(-\beta \cdot i); \varphi = exp(\beta) \qquad (9.8)$$

where $\beta = 5.61 \cdot 10^{-5}$.[8]

➲ Radius of gyration expression:

$$F(i) = \frac{area}{volume} = \frac{1}{R_g} = \frac{1}{K_s(i \cdot MW)^{\alpha_s}} \qquad (9.9)$$

where MW is the molecular weight of the monomeric unit. Equation (9.9) was presented previously by SUN et al. (2001) to represent other reacting systems, including 1-octene and ethene copolymer samples $(K_s = 0.0208$ and $\alpha_s = 0.587)$.

New simulations for experimental conditions F1, G5, H4 and I1 from Figure 8.11 were performed with the MC method, applying Equation (9.6) and using a control volume of $1.0 \cdot 10^{-14}$ L. Figure 9.21 shows the experimental and simulated MWD considering $F(i)$ as an exponential function. Figures 9.21 and 9.22 compare the experimental and simulated MWD taken into account $F(i)$ as a sigmoid function and a radius of gyration expression respectively.

---

[7] Parameter estimated by induction.
[8] Parameter estimated by induction.
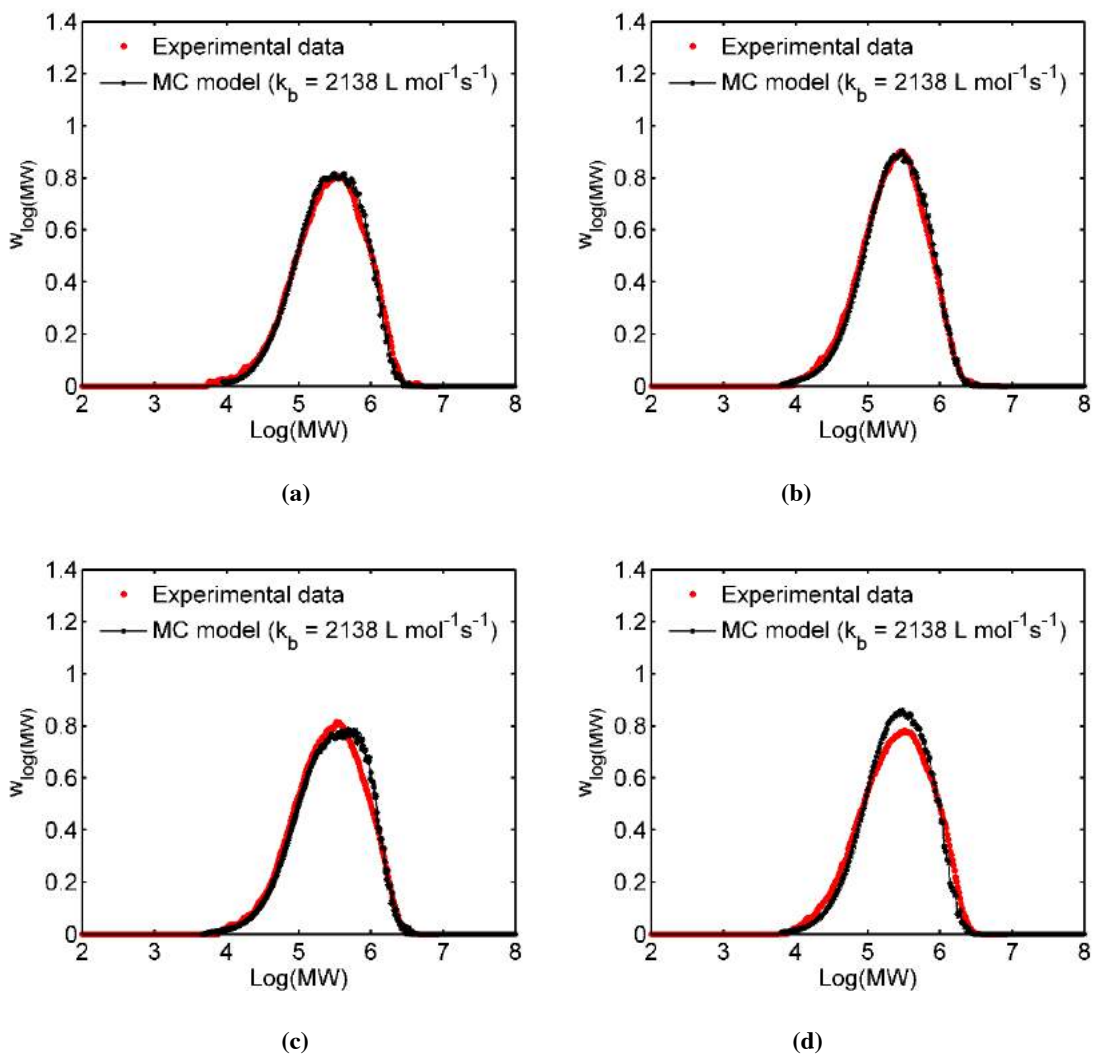
Figure 9.21 – Experimental and simulated MWD of copolymer samples produced with experiment conditions (a) H4, (b) G5, (c) I1 and (d) F1 from Figure 8.11 considering F(i) an exponential function.
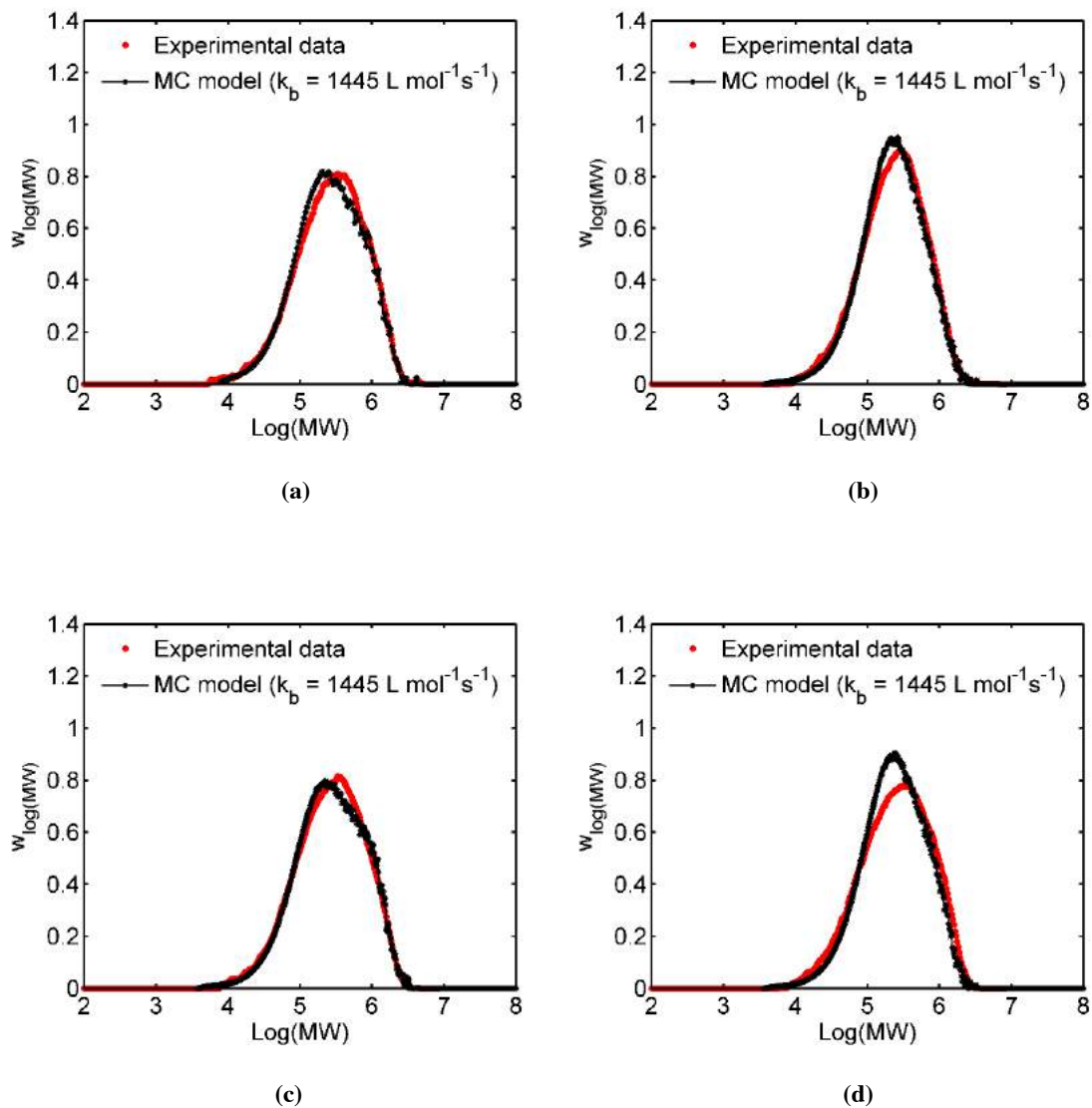
Figure 9.22 – Experimental and simulated MWD of copolymer samples produced with experiment conditions (a) H4, (b) G5, (c) I1 and (d) F1 from Figure 8.11 considering F(i) a sigmoid function.
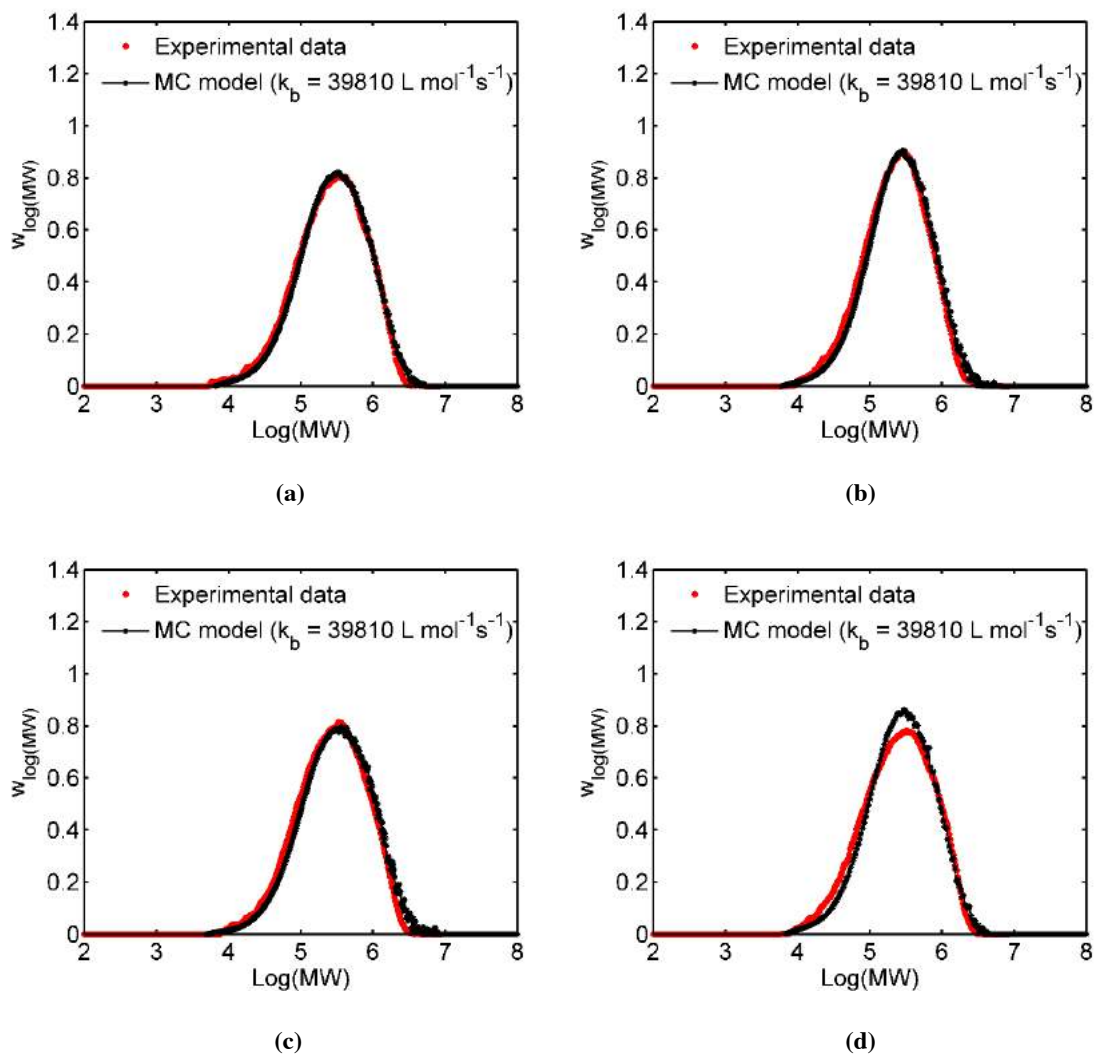
Figure 9.23 – Experimental and simulated MWD of copolymer samples produced with experiment conditions (a) H4, (b) G5, (c) I1 and (d) F1 from Figure 8.11 considering F(i) an expression of the radius of gyration.

According to Figures 9.20 to 9.22, all proposed functions succeeded in representing the molecular weight distributions of the analyzed copolymers, strengthening the hypothesis that the macromonomer reincorporation does not depend only on the amount of pendant unsaturations in the chain, but also on the chain length. All proposed functions consider that small macromonomer chains present higher chances to be incorporated than bigger chains. Apparently through the observation and comparison of Figures 9.20 to 9.22, the exponential function provided MWDs that were closer to the experimental MWDs. For a better view of how these three functions behave during all simulation for experimental conditions H4, G5, I1 and F1, Figures

9.23 and 9.24 were built. In these figures, the $k_b^{MC} \eta$ were plotted against time, where $\eta = \sum_{w=1}^{X_7} \left(j_{from\ L_{i,j,k}} \cdot F(i) \right)$ (Figure 9.20). Then, $k_b^{MC} \eta$ indicates the propensity function for reincorporation of macromonomers, already considering the correcting function $F(i)$.
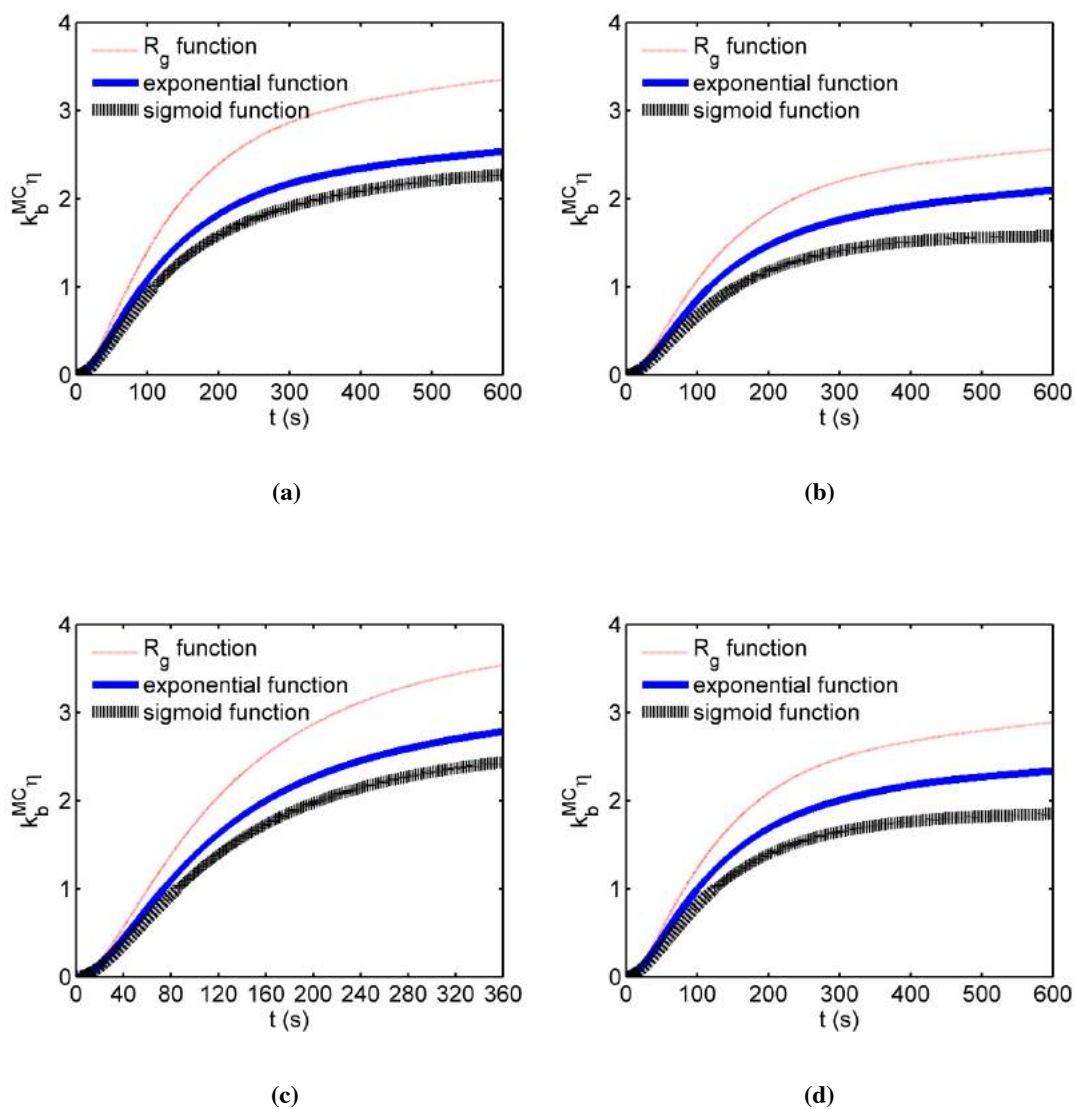
Figure 9.24 – Evolution of $k_b^{MC} \eta$ for experimental conditions (a) H4, (b) G5, (c) I1 and (d) F1 from Figure 8.11.
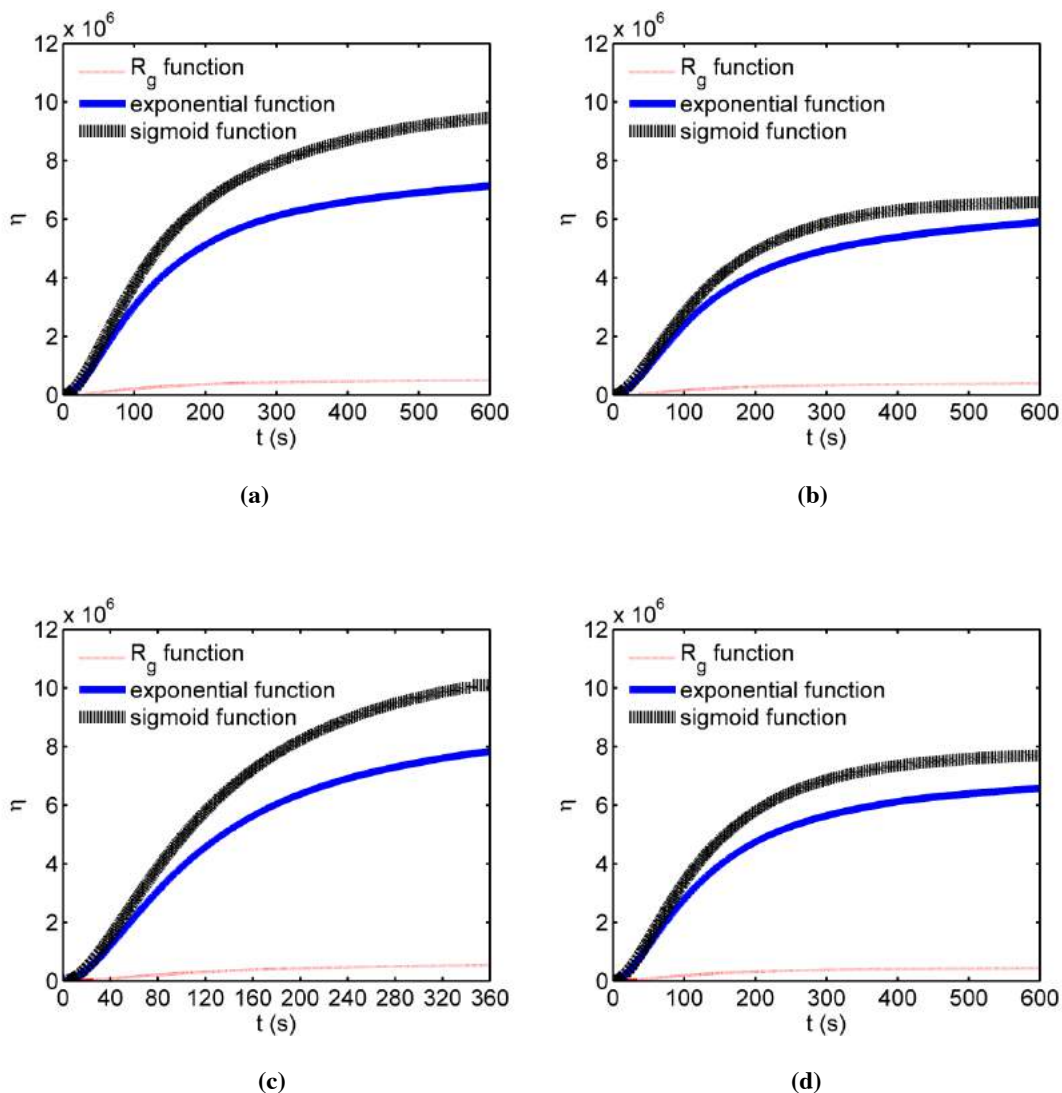
Figure 9.25 – Evolution of η for experimental conditions (a) H4, (b) G5, (c) I1 and (d) F1 from Figure 8.11.

Observing Figures 9.23 and 9.24, it becomes clear that η approaches a limiting value after some time and that this time depends on the function $F(i)$ that is being used. The fact that η tends assintopticaly to a constant value suggests that longer dead chains are being formed but their contribution to the reaction rates are reduced by the function $F(i)$. All three proposed functions (exponential, sigmoid and radius of gyration expressions) get closer to zero for longer chains.

In order to compare the three proposed functions (exponential, sigmoid and radius of gyration), the mean square error Đ, were computed as:

$$\text{Đ} = \sqrt{\frac{\sum_{i=1}^{N}(z_i - y_i)^2}{N - 1}} \qquad (9.10)$$

where z_i is a experimental point that belongs to the experimental MWD data set and y_i is the simulated point that belongs to the MWD data set produced using exponential, sigmoid or radius of gyration expressions for function $F(i)$. So, small Đ values mean that the simulated MWDs are closer to the experimental distributions. Figure 9.26 shows the comparison of the calculated Đ for different F functions. As one can see in this figure, the exponential function achieves the lowest Đ for all the experimental conditions analyzed.
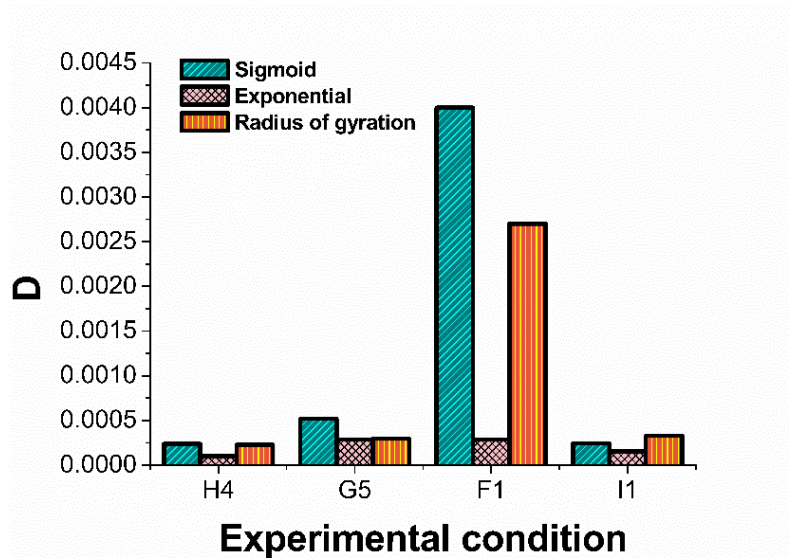
Figure 9.26 – Đ calculated values for experimental conditions H4, G5, I1 and F1 from Figure 8.11.

Although the exponential function presented the lowest Đ for all experimental conditions analyzed, it is unfair to not consider that the radius of gyration expression presented very good performances in building the MWDs. The only exception was for experimental condition F1. However, the parameters of exponential and sigmoid functions (Equations (9.7) and (9.8)) were estimated by induction, while both parameters of the radius of gyration function (K_s and α_s) were taken from the work of SUN et al. (2001) for other copolymer type (1-octene and ethane copolymer). Thus, if K_s and α_s would be estimated by induction, probably the radius of gyration expression would present the lowest Đ.

9.4   Concluding Remarks

Both MC and CAOC methods provided similar MWDs for the analyzed experimental conditions tested. It was shown that the MC method was more efficient to test the consistency of the CAOC than searching if the last model converged by comparing MWDs obtained with different number of collocation points. However, it is important to observe that the kinetic model considered in the current study is simple and that the computation time required to run one simulation of 10 or 15 min with the MC is low, which highlights the advantages of this stochastic method. On the other hand, if the polymerization problem involves longer reaction times, the MC method starts to collide into some numerical barriers, the computational time and CPU memory. In this last case, probably the use of CAOC methods becomes more advantageous.

The presence of LCB was responsible for widening the molecular weight distributions. It was shown that this widening accentuated when the amount of diene and catalyst concentration were increased. Additionally, the formation of LCB did not occur indiscriminately, the obtained results suggest that the incorporation of macromonomers does not only depend on the amount of pendant unsaturations in the chain, but also on the chain length. This dependency was shown to be non linear, but could be described well by an exponential function. A sigmoidal function and a correlation with the radius of gyration and the macromonomer length were also tested, and they also resulted in acceptable distributions, sufficient close to the experimental MWDs. In addition, the radius of gyration expression is probably the best function to be considered if its parameters were estimated by induction.

10 Comparison of Different Dynamic Monte Carlo Methods for the Simulation of Olefin Polymerization

10.1 Summary

In this chapter, different Monte Carlo methods are used to simulate olefin polymerization reactions promoted by coordination catalysts: the Direct method (DM), the First Reaction method (FRM), the Next Reaction method (NRM) and the τ-Leaping method. The first three methods are exact stochastic simulation algorithms (SSA), while the τ-leaping is an approximate method that leads to faster computation times. The four analyzed methods predict similar polymer microstructures, but require significantly different computation times. The efficiency of the methods vary according with the polymerization system under investigation.

10.2 Monte Carlo Simulation Procedures

Methods for dynamic MC simulations include stochastic simulation algorithms (SSA), extensions of SSA, hybrid methods, τ-leaping methods, among others. The performances of some of these MC methods are evaluated in the following sections based on case studies that involve catalyzed polymerization mechanisms.

Five different coordination polymerization systems were selected for comparison of the performances of four different MC methods: DM, FRM, NRM and the τ-Leaping method. All routines were implemented in Fortran. Simulations were performed in a computer Intel(R) Core(TM) i7-4850HQ CPU 2.30GHz, running under Windows.

10.2.1 Case Study I

Case study I is the model represented in Table 4.4. In order to facilitate reading, the mechanism is rewritten in Table 10.1. It is considered that activation of active sites takes place instantaneously $\left(k_i \gg k_p \right)$ and that molar concentrations of monomer and chain transfer agent are constant.

Table 10.1. Polymerization mechanism for Case Study I.

Elementary Step	Chemical Equations [a]	Reaction number
Initiation	$C^* + M \overset{k_i}{\rightarrow} P_1$	Reaction 1 (R1)
Propagation	$P_r + M \overset{k_p}{\rightarrow} P_{r+1}$	Reaction 2 (R2)
Transfer	$P_r + CTA \overset{k_t}{\rightarrow} C^* + D_r$	Reaction 3 (R3)

[a]C^*: catalyst, P_r: living chain with length r, D_r: dead chain with length r, M: monomer, CTA: chain transfer agent.

The chain length distribution (CLD) of living polymer chains produced with a single-site catalyst was simulated with the DM, FRM, NRM and the τ-Leaping method. Figure 10.1 shows that the CLD predicted by all methods were very similar to the original analytical CLD reported by SOARES and HAMIELEC (2007), as shown in Figure 4.12. According to SOARES and HAMIELEC (2007), the concentrations of living chains of different lengths change from the beginning of the polymerization until achieving the steady-state Flory distribution. In this case study, it takes around 2.5 s to reach the steady-state response, as can be seen in Figure 10.1. The CLDs simulated with the τ-Leaping method for very short polymerization times (0.5 and 1.0 s) were slightly different from the others, but this difference became negligible after 1.5 s. Figure 10.2 shows the evolution of average molecular weights and polydispersity with the polymerization reaction time. As one can see, all models predict similar trajectories for M_w, M_n and PI.
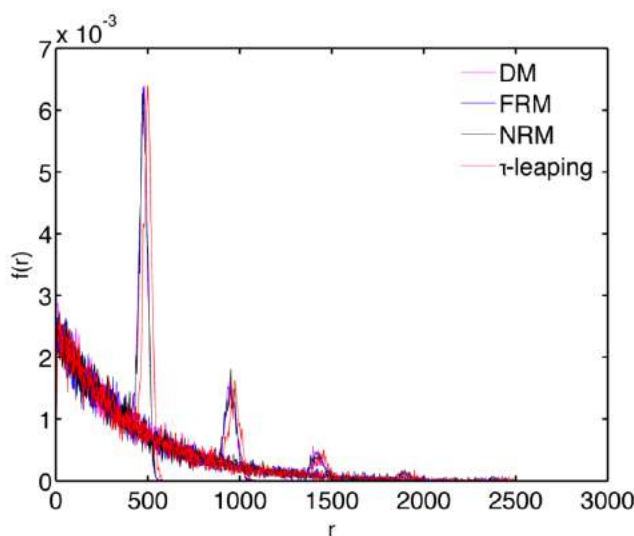
Figure 10.1 – Chain length distribution for living polymer made at 0.5, 1.0, 1.5, 2.0 and 2.5 s (from left to right) using Direct Method (DM), First Reaction Method (FRM), Next Reaction Method (NRM) and τ-leaping (number of molecules of growing chain (P) = $1 \cdot 10^4$, k_p = 3800 L·mol^{-1}·s^{-1}, k_t[CTA] = 2.3 s^{-1}, [M] = 0.25 mol·L^{-1})
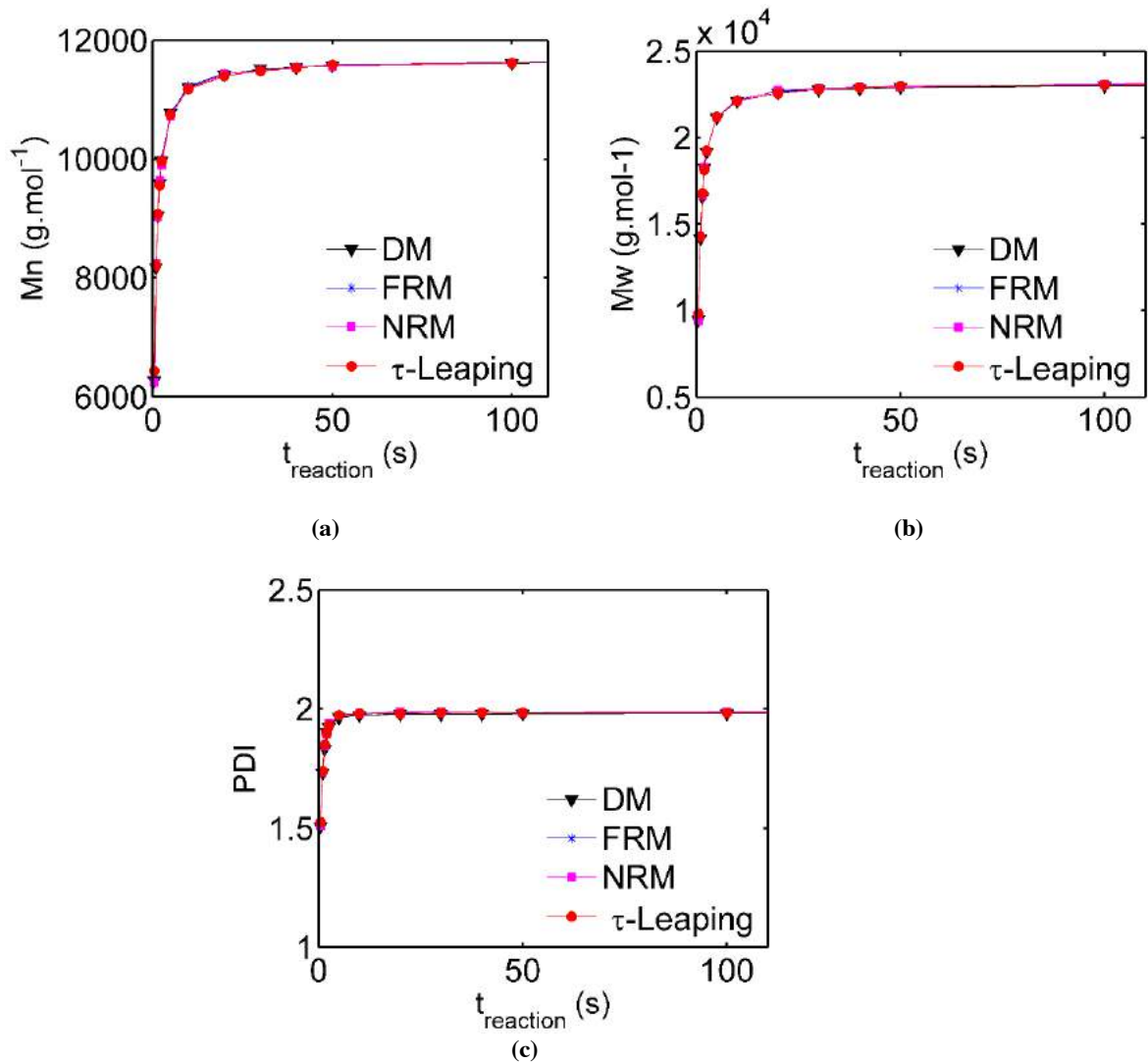
Figure 10.2 – a) M_n, b) M_w, and c) PI for polymer chains produced at different polymerization times using Direct Method (DM), First Reaction Method (FRM), Next Reaction Method (NRM) and τ-leaping (Model parameters: see Figure 10.1).

The required computational times, average molecular weights and polydispersity indexes predicted by each method are compared in Table 10.3. In order to calculate the statistical uncertainties, 10 simulations were performed for each polymerization time. The confidence intervals for the means of M_n, M_w, PI and CPU time were obtained considering the confidence level of 95 %, according to the t-Student distribution. Thus, the confidence intervals were calculated as (SCHWAAB and PINTO, 2007):

$$\bar{x} \pm \frac{t_{Student}\sigma_x}{\sqrt{N_{exp}}} \tag{10.1}$$

where $\bar{x}$ is the sample mean, σ_x is the sample standard deviation, $t_{Student}$ is obtained from the t-Student distribution and N_{exp} is the number of replicates (in this case, 10).

It can be noticed in Table 10.3 that the τ-Leaping method is the fastest one, followed by the NRM. The NRM is faster than the DM because it generates only one random number of each step (see step 13 from Figure 4.22), whereas the DM generates two random numbers (r_1 and r_2 in Equations (4.7) and (4.8)). Additionally, the NMR only updates the indexed priority queue, while the DM updates all propensity functions (MC reaction rates), even those that do not change, spending time unnecessarily, calculates the time interval with $\tau = \frac{1}{a_0(X)} \ln\left(\frac{1}{r_1}\right)$, and searches for reaction R_j using $\sum_{j'=1}^{j} a_{j'}(X) \geq r_2 a_0(X)$. The FRM demands longer computational times than the DM because the FRM eliminates (M-1) time reactions at each step. The time required to generate a random number and to select a propensity function in the DM is shorter than the time needed for the FRM to generate M time steps, choose the lowest time step (whose index corresponds to the next reaction) and discard the other time steps which is in accordance with CAO et al. (2006).

10.2.2 Case Study II

Case study II investigates the copolymerization of ethylene and diene with a single-site catalyst. The mechanism for this polymerization is listed in Table 10.2.

Table 10.2. Copolymerization mechanism for Case Study II.[a]

Propagation	$P_{r,j} + M_1 \xrightarrow{k_{p11}} P_{r+1,j}$ $P_{r,j} + M_2 \xrightarrow{k_{p12}} W_{r+1,j+1}$ $W_{r,j} + M_1 \xrightarrow{k_{p21}} P_{r+1,j}$ $W_{r,j} + M_2 \xrightarrow{k_{p22}} W_{r+1,j+1}$
Spontaneous Transfer	$P_{r,j} \xrightarrow{k_{\beta 1}} P_{1,0} + D_{r,j+1}$ $W_{r,j} \xrightarrow{k_{\beta 2}} P_{1,0} + D_{r,j+1}$
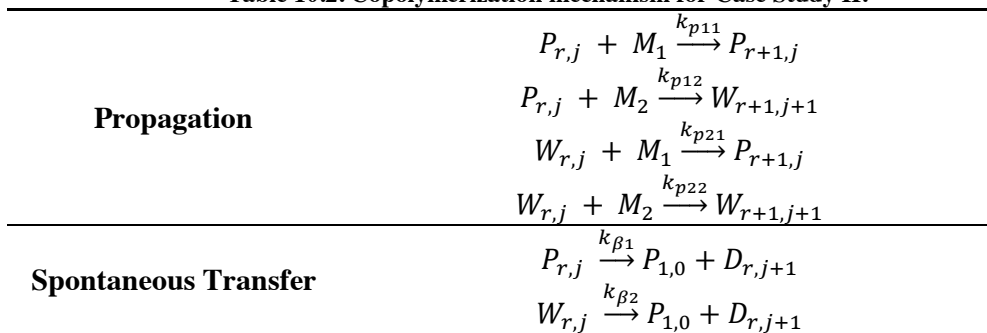
[a] M_1: ethylene, M_2: diene, $P_{r,j}$: growing chain with length r and j double bonds terminated in an ethylene molecule, $W_{r,j}$: growing chain with length r and j double bonds terminated in a diene molecule, $D_{r,j}$: dead chain with length r and j double bonds, k_{pij}: propagation rate constants; $k_{\beta i}$: spontaneous transfer rate constants.

Reac.	DM				NRM			
Time	M_n	M_w	PI	CPU time	M_n	M_w	PI	CPU time
(s)	(g.mol^{-1})	(g.mol^{-1})		(s)	(g.mol^{-1})	(g.mol^{-1})		(s)
0.5	6228 ± 8	9446 ± 12	1.517 ± 0.002	0.441 ± 0.007	6191 ± 26	9409 ± 26	1.520 ± 0.004	0.360 ± 0.010
1.0	8099 ± 24	14157 ± 43	1.748 ± 0.002	0.874 ± 0.007	8119 ± 30	14175 ± 67	1.746 ± 0.002	0.715 ± 0.007
1.5	9011 ± 21	16707 ± 37	1.854 ± 0.004	1.300 ± 0.014	8994 ± 22	16673 ± 48	1.854 ± 0.004	1.066 ± 0.007
2.0	9557 ± 14	18218 ± 44	1.906 ± 0.003	1.744 ± 0.011	9551 ± 25	18248 ± 55	1.911 ± 0.004	1.428 ± 0.08
2.5	9893 ± 27	19162 ± 71	1.937 ± 0.006	2.161 ± 0.006	9883 ± 24	19178 ± 53	1.941 ± 0.002	1.785 ± 0.010
5.0	10696 ± 14	21158 ± 55	1.978 ± 0.004	4.332 ± 0.015	10695 ± 21	21171 ± 51	1.980 ± 0.002	3.546 ± 0.006
10.0	11133 ± 10	22169 ± 41	1.991 ± 0.003	8.675 ± 0.013	11129 ± 16	22202 ± 57	1.995 ± 0.003	7.142 ± 0.029
20.0	11368 ± 7	22648 ± 29	1.992 ± 0.002	17.427 ± 0.044	11380 ± 10	22719 ± 27	1.996 ± 0.002	14.268 ± 0.025
30.0	11448 ± 6	22825 ± 19	1.994 ± 0.001	26.073 ± 0.020	11444 ± 8	22861 ± 21	1.998 ± 0.001	21.474 ± 0.012
40.0	11491 ± 7	22911 ± 14	1.994 ± 0.001	34.815 ± 0.027	11489 ± 6	22949 ± 32	1.997 ± 0.002	28.493 ± 0.060
50.0	11511 ± 5	22957 ± 12	1.994 ± 0.001	43.446 ± 0.022	11523 ± 8	23008 ± 20	1.997 ± 0.001	35.712 ± 0.032
100.0	11562 ± 3	23055 ± 12	1.994 ± 0.001	86.902 ± 0.034	11564 ± 4	23092 ± 17	1.997 ± 0.001	71.271 ± 0.045
Reac.	FRM				τ-Leaping			
Time	M_n	M_w	PI	CPU time	M_n	M_w	PI	CPU time
(s)	(g.mol^{-1})	(g.mol^{-1})		(s)	(g.mol^{-1})	(g.mol^{-1})		(s)
0.5	6240 ± 17	9461 ± 12	1.516 ± 0.003	0.532 ± 0.006	6366 ± 22	9754 ± 27	1.532 ± 0.004	0.205 ± 0.003
1.0	8107 ± 20	14140 ± 28	1.744 ± 0.004	1.067 ± 0.011	8150 ± 22	14287 ± 27	1.753 ± 0.004	0.406 ± 0.003
1.5	9033 ± 22	16710 ± 57	1.850 ± 0.005	1.590 ± 0.010	9041 ± 24	16749 ± 47	1.853 ± 0.004	0.593 ± 0.005
2.0	9543 ± 26	18198 ± 61	1.907 ± 0.005	2.111 ± 0.009	9557 ± 22	18235 ± 57	1.908 ± 0.006	0.785 ± 0.006
2.5	9909 ± 19	19137 ± 52	1.931 ± 0.003	2.636 ± 0.009	9910 ± 16	19206 ± 64	1.938 ± 0.005	0.985 ± 0.003
5.0	10685 ± 28	21146 ± 92	1.979 ± 0.005	5.262 ± 0.008	10695 ± 16	21153 ± 65	1.978 ± 0.005	1.950 ± 0.001
10.0	11141 ± 10	22172 ± 39	1.990 ± 0.002	10.547 ± 0.011	11140 ± 25	22182 ± 65	1.991 ± 0.003	4.017 ± 0.006
20.0	11368 ± 10	22645 ± 26	1.992 ± 0.002	21.041 ± 0.026	11373 ± 16	22650 ± 51	1.991 ± 0.002	8.034 ± 0.012
30.0	11451 ± 9	22827 ± 13	1.993 ± 0.001	31.590 ± 0.038	11448 ± 8	22841 ± 18	1.995 ± 0.001	12.056 ± 0.020
40.0	11493 ± 8	22915 ± 11	1.994 ± 0.001	42.098 ± 0.034	11492 ± 6	22927 ± 23	1.995 ± 0.002	16.023 ± 0.019
50.0	11513 ± 8	22962 ± 15	1.994 ± 0.001	52.610 ± 0.029	11519 ± 8	22983 ± 20	1.995 ± 0.002	20.065 ± 0.034
100.0	11623 ± 5	23065 ± 5	1.984 ± 0.001	103.948 ± 0.071	11565 ± 5	23072 ± 12	1.995 ± 0.001	40.050 ± 0.023

Figure 10.3 illustrates how the CLD of living copolymer chains calculated with the DM and FRM changes with the polymerization reaction time, showing that they are equally suited to represent this copolymerization system. Figure 10.4 shows that the DM is more efficient than the FRM. The generation of one random number per reaction and the search for the minimum step time consumes more computational time than the generation of one random number that satisfies $\sum_{j'=1}^{j} a_{j'}(X) \geq r_2 a_0(X)$. Until about 50

s of polymerization, the computation times required by both methods were similar, but the DM was evidently more efficient than the FRM for longer polymerization times.
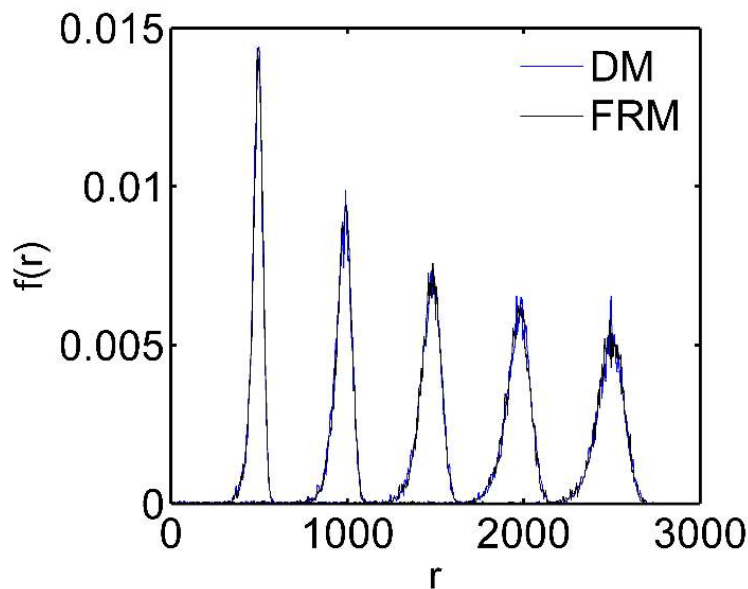
Figure 10.3 – CLD of living copolymer chains produced at times 0.5, 1.0, 1.5, 2.0 and 2.5 s from left to right (0.5% molar of diene, $[CGC]_0 = 1 \cdot 10^{-6}$ mol·L^{-1}, [ethylene]$_0$ = 1 mol·L^{-1}, kp_{11} = 1000 L·mol^{-1}·s^{-1}, r_1 = 7, r_2 = 0.1, kp_{22} = 4 L·mol^{-1}·s^{-1}(NELE et al., 2003), $k_{\beta 1}$ = 0.01 s^{-1} (BEIGHZADEH et al., 1999), $k_{\beta 2} = k_{\beta 1}$, V = 7·10^{-15} L).
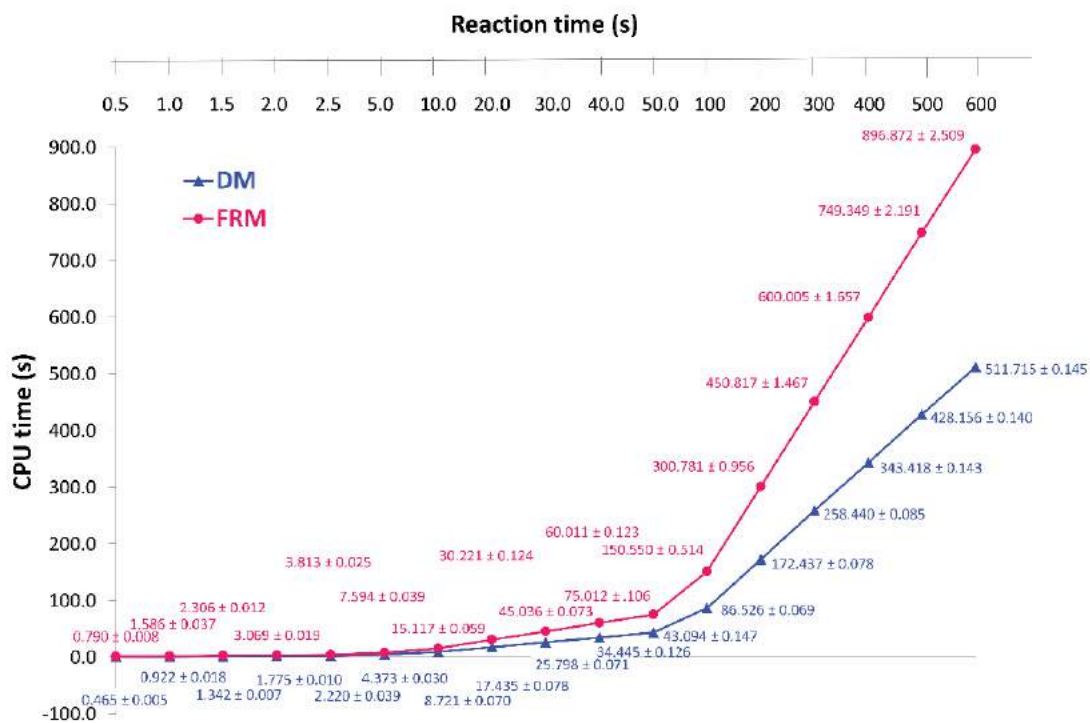
Figure 10.4 - Simulation times for distinct Monte Carlo methods for ethylene/diene copolymerization (Table 10.2, Model parameters: see Figure 10.3).

10.2.3 Case Study III

Case study III describes the copolymerization of ethylene and a diene with long-chain branching formation (Table 10.4).

Table 10.4. Copolymerization mechanism with LCB formation for Case Study III.

Propagation	$P_{r,j,k} + M_1 \xrightarrow{k_{p11}} P_{r+1,j,k}$ $P_{r,j,k} + M_2 \xrightarrow{k_{p12}} W_{r+1,j+1,k}$ $W_{r,j,k} + M_1 \xrightarrow{k_{p21}} P_{r+1,j,k}$ $W_{r,j,k} + M_2 \xrightarrow{k_{p22}} W_{r+1,j+1,k}$
Spontaneous Transfer	$P_{r,j,k} \xrightarrow{k_{t\beta1}} P_{1,0,0} + D_{r,j+1,k}$ $W_{r,j,k} \xrightarrow{k_{t\beta2}} P_{1,0,0} + D_{r,j+1,k}$
Reincorporation via terminal bond	$P_{r,j,k} + D_{l,m,n} \xrightarrow{k_{b1}} W_{r+l,j+m-1,k+n+1}$ $W_{r,j,k} + D_{l,m,n} \xrightarrow{k_{b2}} W_{r+l,j+m-1,k+n+1}$

M_1: ethylene, M_2: diene, $P_{r,j,k}$: growing chain with length r, j double bonds and k LCBs terminated in an ethylene molecule, $W_{r,j,k}$: growing chain with length r, j double bonds and k LCBs terminated in a diene molecule, $D_{r,j,k}$: dead chain with length r, j double bonds and k LCBs, k_{pij}: propagation rate constants; $k_{t\beta i}$: spontaneous transfer rate constants, k_b: reincorporation rate constant.

For Case Study III, the τ-Leaping method was selected as the most efficient one. The mechanism in Case Study III is considerably more complex than those of Case Studies I and II because it involves the formation of branched species, resulting from the polymerization of pendant double bonds formed by the diene copolymerization. Figure 10.5 compares the CPU time required for the DM and τ-Leaping method to simulate the copolymerization presented in Table 10.4, using two different control volume values. Diferently from Case Study I, the time needed to simulate Case Study III by the τ-Leaping method was not much lower than the time needed to simulate the same system using the DM, as one can observe in Figures 10.5a and 10.5b. Although the τ-Leaping method was still faster than the DM, it is significantly more efficient when longer polymerization times are considered. With short polymerization times, between 10 to 60 s, the CPU time consumed by both methods differs no more than 20 s. But, as the polymerization evolves, this difference increases. When a bigger volume was used, the CPU time required by both methods was also bigger when compared with the CPU times consumed when the smaller control volume was chosen.

The relationship between the two methods was not much affected by the change in the control volume and the τ-Leaping method remained more efficient than the DM. The only change observed was in the CPU time difference between the methods: with V = $7 \cdot 10^{-15}$ L, at 10 min of polymerization, τ-Leaping method was 111 s faster than the DM, with V = $9 \cdot 10^{-15}$ L, this difference increased to 217 s approximately.
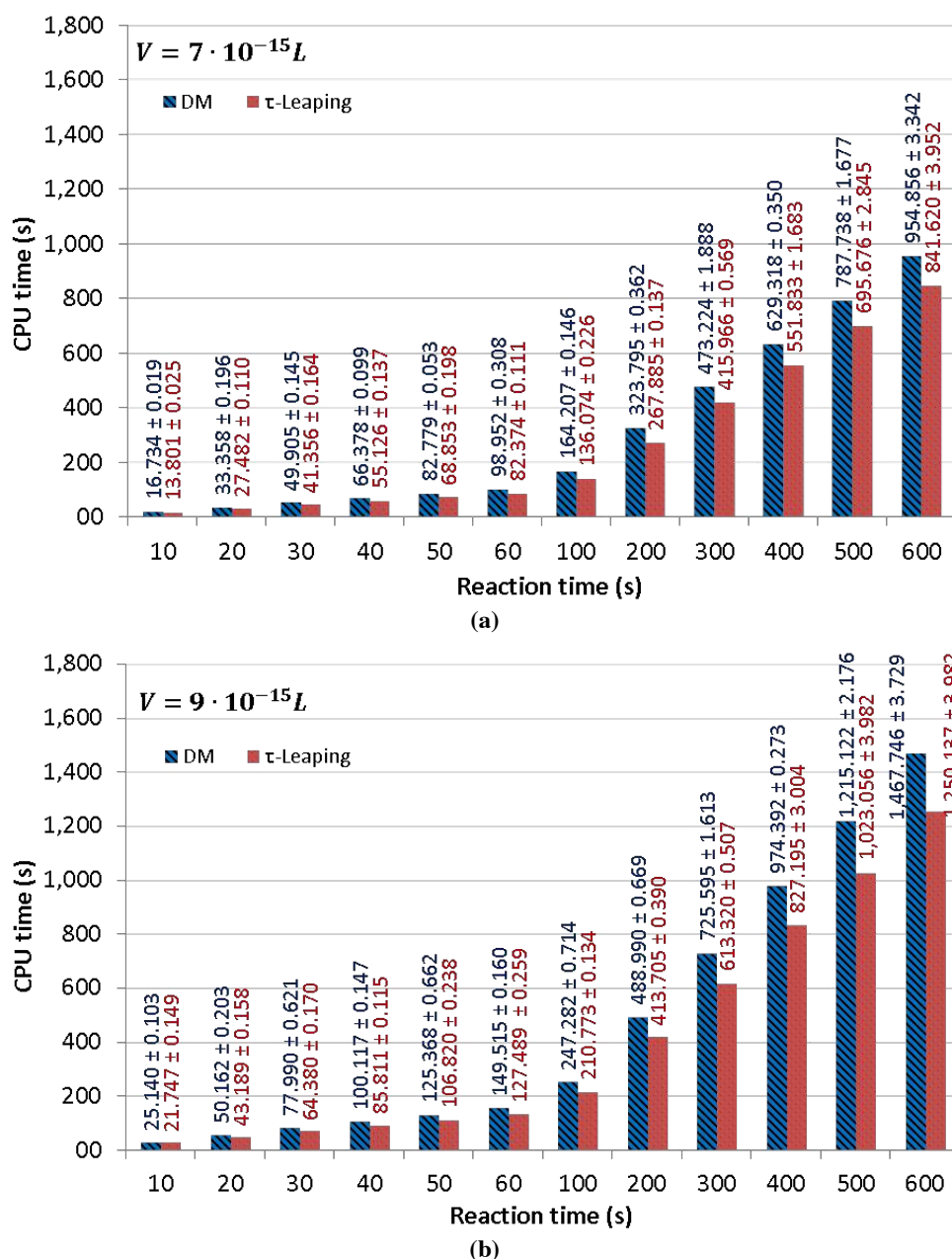
Figure 10.5 – Comparison of the CPU time required for the DM and τ-Leaping method to simulate 10 min of reaction with V equals to $7 \cdot 10^{-15}$ (a) and $9 \cdot 10^{-15}$ L (b). (0.5% molar of diene, $[CGC]_0 = 1 \cdot 10^{-6}$ mol·L^{-1}, $[ethylene]_0 = 1$ mol·L^{-1}, $kp_{11} = 1500$ L·mol^{-1}·s^{-1}, $r_1 = 4$, $r_2 = 0.1$(NELE et al., 2003), $kp_{22} = 40$ L·mol^{-1}·s^{-1}, $k_{\beta 1} = 0.25$ s^{-1}, $k_{\beta 2} = 0.75$, $k_{b1} = kp_{12}/1.2$, $k_{b2} = kp_{21}/1.2$).

Figure 10.6 compares the computational time required to simulate a polymerization reaction that lasts 10 minutes with different control volumes using the τ-Leaping method. Differences in the MWDs produced with different control volumes are also shown. The MWD predicted with the smallest control volume was very noisy and, consequently, not adequate for the accurate representation of MWD. The MWDs predicted with the two largest control volumes differ slightly from each other, providing smooth and similar MWDs. This result is in accordance with the work of AL-HARTHI et al. (2006). Thus, it is intesting to select a control volume that compromises accurate results with reasonable computational times. In the present case study, an appropriate control volume is $7 \cdot 10^{-15}$ L; higher volumes will not improve results significantly.

These results are important to evaluate the accuracy and efficiency of the investigated methods when simulating LCBs/network formation in copolymers of ethylene and diene, showing that the τ-Leaping method seems to be more efficient to describe complex polymerization systems.
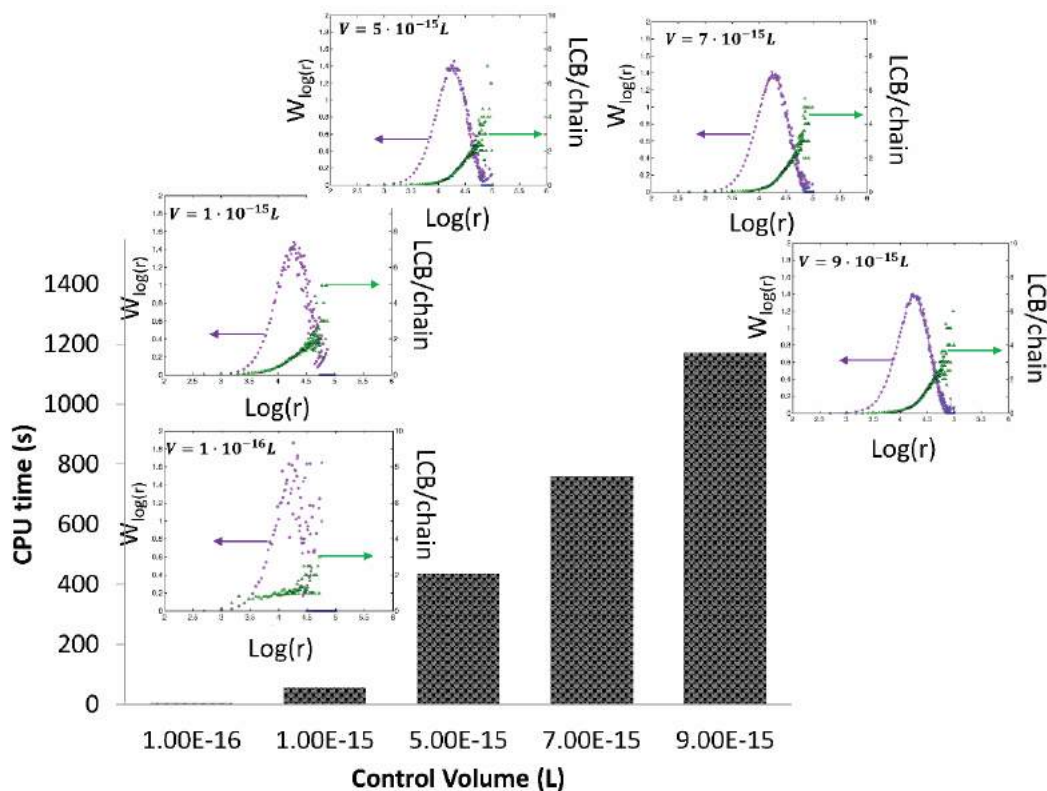
Figure 10.6 - Comparison of the CPU time required for different control volumes and MWD for the dead polymer population and average number of LCB per chain produced at 10 min of polymerization. (10 min of polymerization, 0.5% molar of diene, $[CGC]_0 = 1 \cdot 10^{-6}$ mol·L^{-1}, $[\text{ethylene}]_0 = 1$ mol·L^{-1}, $kp_{11} = 1500$ L·mol^{-1}·s^{-1}, $r_1 = 4$, $r_2 = 0.1$ (NELE et al., 2003), $kp_{22} = 40$ L·mol^{-1}·s^{-1}, $k_{\beta1} = 0.25$ s^{-1}, $k_{\beta2} = 0.75$, $k_{b1} = k_{p12}/1.2$, $k_{b2} = k_{p21}/1.2$).

10.2.4 Case Study IV

This case study simulates the homopolymerization of ethylene with a CGC and using a semi-batch reactor. The kinetic mechanism adopted to represent this polymerization system is the same mechanism proposed in this thesis (Section 7.3) and it is rewritten again in Table 10.5.

Table 10.5. Ethylene polymerization mechanism of Case Study IV using a CGC catalyst.

Catalyst activation	$C \xrightarrow{k_a} C^*$
Initiation	$C^* + M \xrightarrow{k_{p11}} P_1^*$
Propagation (Ethylene)	$P_i^* + M \xrightarrow{k_{p11}} P_{i+1}^*$
Transfer to monomer and β-hydride elimination	$P_i^* \xrightarrow{k_t} L_i^= + C^*$
Living chain deactivation	$P_i^* + P_j^* \xrightarrow{k_{dP}} L_i + L_j + 2DC$

The kinetic rate constants used in the simulations were the same determined in the present thesis with help of parameters estimation and parameter identifiability procedures, as already explained in Chapter 6.

The four Monte Carlo methods, DM, FRM, NRM and τ-Leaping method were used to simulate this polymerization problem considering constant temperature (T = 120 °C) and constant monomer concentration throughout the polymerization. For all simulations, a control volume of $1 \cdot 10^{-14}$ L was adopted. The initial simulation conditions adopted are described in Table 10.6.

Table 10.6. Simulation conditions employed in the Case Study IV.

Catalyst (μmol L^{-1})	0.271
Temperature (°C)	120
Monomer concentration (mol L^{-1})	0.49472
Polymerization times (min)	2, 4, 6, 8, 10

Figure 10.7 illustrates the M_w and M_n profiles during polymerization time predicted by the four MC methods tested and also the CPU time required for each method to run all the simulations.

(a)

(b)
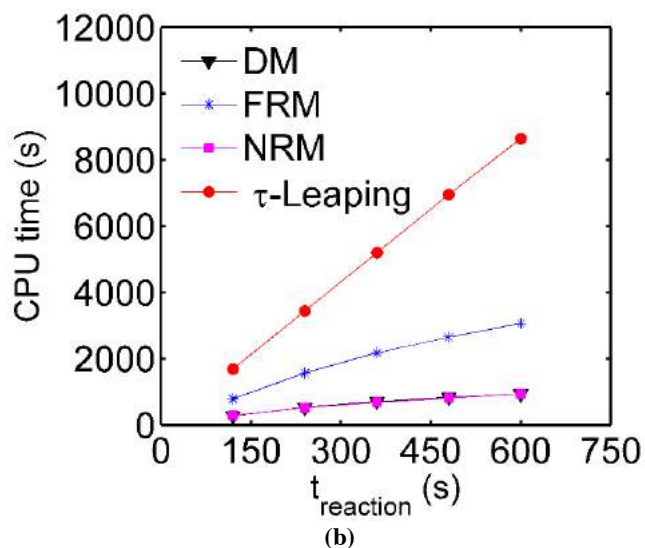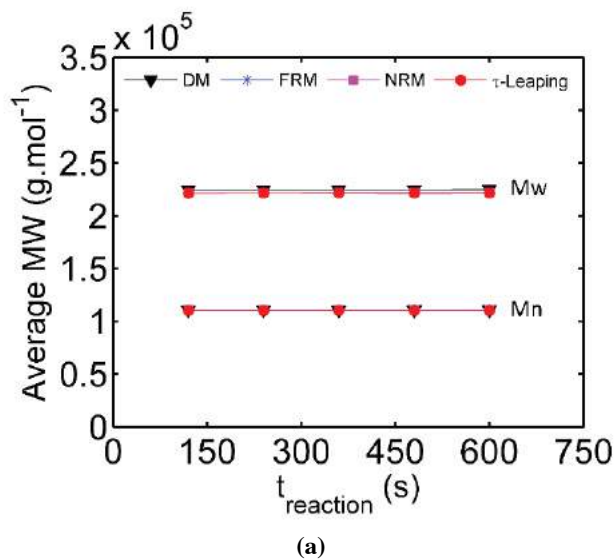
Figure 10.7 – a) Mn and Mw for polymer produced and b) CPU time required to run the simulations at different polymerization times using DM, FRM, NRM and τ-Leaping (Model parameters: k_a = 0.02847 s^{-1}, k_{p11} = 67736.5 L.(mol.s)$^{-1}$, k_t = 8.5 s^{-1} and k_{dP} = 25456.3 L.(mol.s)$^{-1}$).

As one can see in Figure 10.7.a, all MC method predicted similar average molecular weights, as already expected. Each polymerization time was simulated four times by each MC method. The average result from these simulations is the value plotted in Figure 10.7.a for each polymerization time (2, 4, 6, 8 and 10 min). Surprisingly, for this study case, the τ-Leaping method was the slowest among all methods and the NRM was the fastest one, although the DM reached almost the same CPU times consumed by the NRM. The main reason why the τ-Leaping method applied

for this reaction mechanism was less efficient than when the same method was used to simulate the mechanism proposed in Case Study III was the kinetic parameter values. For Case Study III, the largest parameter was kp_{11} = 1500 L·mol^{-1}·s^{-1}, whereas the lowest parameter was $k_{\beta1}$ = 0.25 s^{-1}. Thus, kp_{11} was 6000 bigger than $k_{\beta1}$. In Case Study IV, the largest parameter was also kp_{11} = 67736.5 L·(mol·s)$^{-1}$ and the lowest one was k_a = 0.02847 s^{-1}. So, kp_{11}, this time, was 2,379,224 bigger than k_a. The size of the time step τ was restricted by the timescale of the fastest reaction in the system; so if one reaction is much faster than the others, τ will assume very low values, which turns the τ-Leaping method not so efficient for these cases. Additionally, since the τ-Leaping method was being applied to a polymerization system, if the interval leap was not big enough to compensate the time required to run the direct method to update the chain lengths, this method would consume more time to run the simulation than the time consumed by the DM, for example. This is exactly what happened in the current case study. However, it is important to point out that the statistical uncertainties calculated with Equation (10.1) were very different for the different methods, indicating that parameter scaling maybe of fundamental importance for numerical performance of the analyzed Monte Carlo methods. Figure 10.8 shows these differences more clearly. According to Figure 10.8, the NRM presented the largest statistical uncertainties among the analyzed other methods. However, these uncertainties were not big enough to compromise the final average molecular weights predicted by the NRM. Thus, it can be said that all the MC methods tested here are reliable.
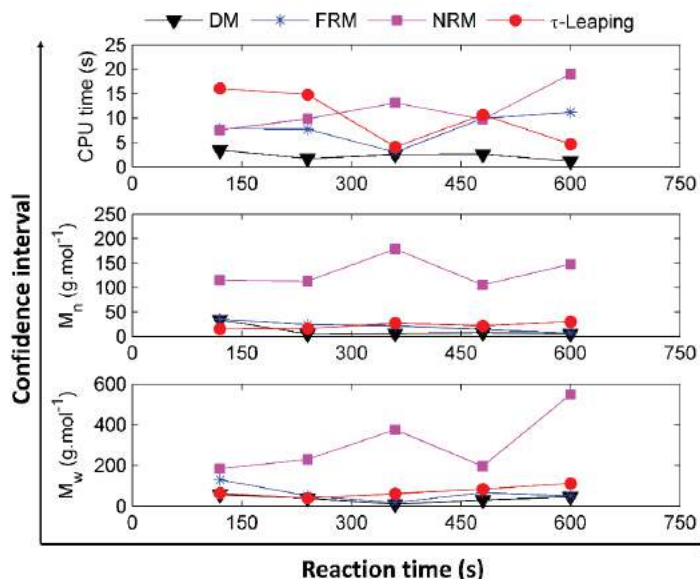
Figure 10.8 – Statistical uncertainties calculated for each Monte Carlo method for CPU time and Mn and Mw considering confidence level of 95 %.

10.2.5 Case Study V

The fifth case study simulates the copolymerization of ethylene with 1,9-decadiene using CGC in a semi-batch reactor. The kinetic mechanism adopted to represent this polymerization is the same mechanism proposed in this thesis (Section 7.5.4) and is rewritten in Table 10.7.

Table 10.7. Ethylene and diene copolymerization mechanism using a CGC catalyst used in Case Study V.[a)]

Catalyst activation	$C \xrightarrow{k_a} C^*$
Initiation	$C^* + M \xrightarrow{k_{p11}} P_{1,0,0}^*$
Propagation (Ethylene)	$P_{i,j,k}^* + M \xrightarrow{k_{p11}} P_{i+1,j,k}^*$
Propagation (Diene)	$P_{i,j,k}^* + D \xrightarrow{k_{p12}} P_{i+1,j+1,k}^*$
Transfer to monomer and β-hydride elimination	$P_{i,j,k}^* \xrightarrow{k_t} L_{i,j,k}^= + C^*$
Living chain deactivation	$P_{i,m,b}^* + P_{j,n,z}^* \xrightarrow{k_{dP}} L_{i,m,b} + L_{j,n,z} + 2DC$
Macromonomer reincorporation	$P_{i,m,b}^* + LL_{j,n,z} \xrightarrow{k_b} P_{i+j,m+n-1,b+z+2}^*$

a) $LL_{j,n,z}$ can be a dead chain with terminal unsaturation $\left(L_{j,n,z}^=\right)$ or not $\left(L_{j,n,z}\right)$.

It was considered that both the macromonomer chain length and the amount of unsaturations affect the probability of macromonomer reincorporation into a growing chain. Thus, the MC reaction rate for macromonomer reincorporation used in this case study was written as Equation (9.6), which assumes the following form:

$$a(X) = k_b^{MC} X_P \sum_{w=1}^{X_{LL}} \left[n_{\epsilon \, LL_{j,n,z}} \cdot e^\beta e^{(-\beta j)} \right] \tag{10.2}$$

where $\beta = 5.61 \cdot 10^{-5}$, n is the amount of double bonds in the macromonomer chain and j is the macromonomer chain length.

The kinetic parameter rate constants used in these simulations were the same ones determined in the present thesis through parameter estimation and after application of parameter identifiability procedures, as presented in Chapter 6.

The two most efficient Monte Carlo methods in Case Study IV, DM and NRM, were selected to simulate this polymerization problem considering constant temperature (T = 120 °C) and constant monomer concentration throughout all polymerization. For all simulations, a control volume of $1 \cdot 10^{-14}$ L was adopted. The initial simulation conditions adopted were the same conditions shown in Table 10.6, adding 0.4 g of 1,9-decadiene (experimental conditions H2 to H4 in Figure 8.11). Each method simulated each polymerization reaction four times, so that the total number of simulation trials was equal to 20 for each MC method. Figure 10.9 illustrates the mean values predicted for each polymerization time by the analyzed MC methods for average molecular weights and long-chain branching frequencies.
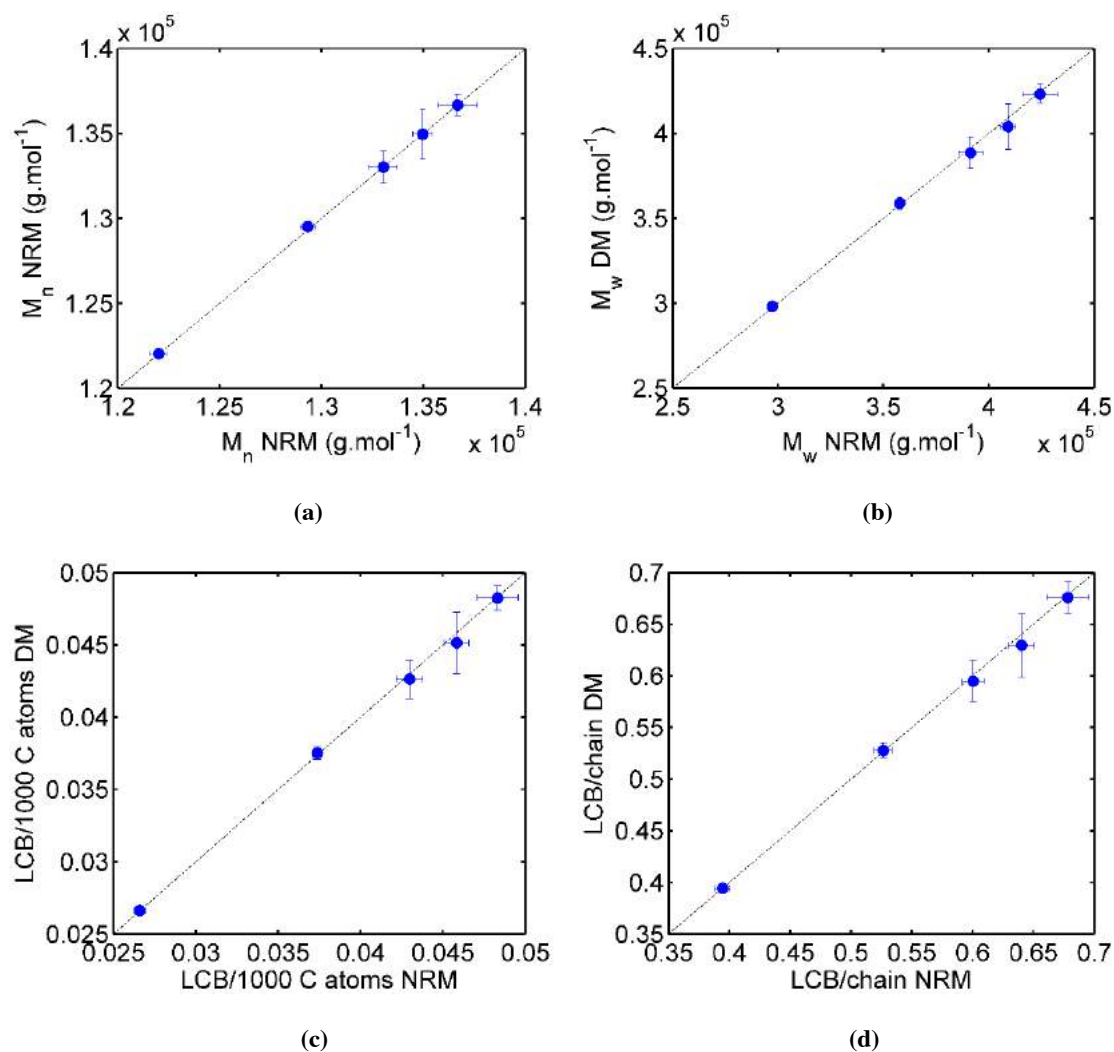
Figure 10.9 – a) Mn, b) Mw, c) LCB/1000 C atoms and d) LCB/chain for copolymers produced at 2, 4, 6, 8 and 10 min (from left to right) using DM and NRM (Model parameters: k_a = 0.02847 s^{-1}, k_{p11} = 67736.5 L.(mol.s)$^{-1}$, k_t = 8.5 s^{-1}, k_{dP} = 25456.3 L.(mol.s)$^{-1}$, k_{p12} = 2039.8 L.(mol.s)$^{-1}$ and k_b = 2138 L.(mol.s)$^{-1}$).

208

As one can see in Figure 10.9, both methods predicted the same average molecular weights and branching frequencies, as already expected. It can also be observed that the statistical uncertainties for both methods were small and not significant to affect the reliability of the predicted values. Figure 10.10 shows the CPU time required by each method to perform the simulations.

Observing Figure 10.10, one can conclude it took the same time for both methods to simulate this case study for all reaction times tested, indicating that their efficiencies were nearly the same.
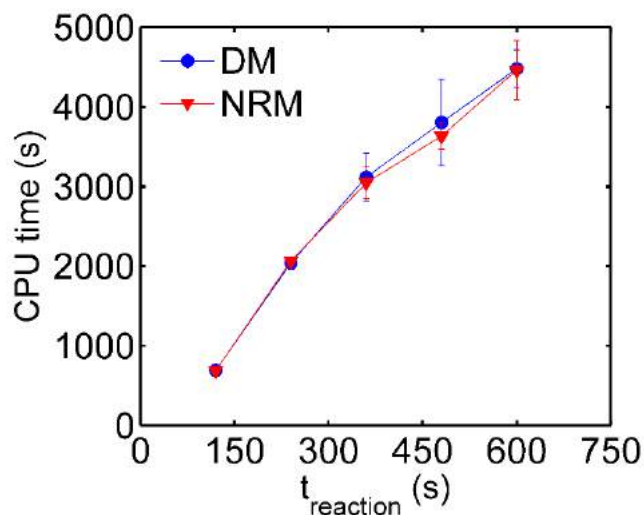
Figure 10.10 – Simulation times for DM and NRM for ethylene/diene copolymerization and their respective uncertainties (Model parameters: see Figure 10.9).

10.3 Concluding Remarks

As observed through many examples, the τ-leaping method is the fastest MC method, being recommended when complex polymerization mechanisms are under investigation, except when the highest reaction rate constant significantly differs from the lowest reaction rate constant. For example, in Case Study III, when the largest kinetic parameter was 6000 times larger than the smallest parameter, the τ-leaping method was the most efficient analyzed MC method. On the other hand, in Case Study IV, when this difference was larger than 2,000,000 times, the τ-leaping method was the slowest analyzed MC method, whereas the NRM, because of its intelligent data storage

and handling approach, presented better performance when compared to the τ-leaping method and the FRM. Nevertheless, the DM at Case Studies IV and V presented efficiencies that were similar to the efficiencies of the NRM.

11 Conclusions

Based on GPC analyses, it was shown that the ethylene/1,9-decadiene copolymer synthesized with CGC in a semi-batch reactor presents long-chain branches. The presence of LCBs in the copolymer was confirmed through the comparison of the intrinsic viscosities of the copolymer samples with the one of the PE without diene. When the plot of the intrinsic viscosity as a function of the logarithm of molecular weight deviates, at the region of higher molecular weights, of the correspondent plot of the homopolymer, LCBs are present in the polymer chains. This deviation was observed for all analyzed copolymer samples and it was more accentuated as longer was the copolymerization reaction and as higher amounts of diene and catalyst were used.

Using the Zimm-Stockmayer expression and the experimental intrinsic viscosity measured with GPC/VISC, it was possible to determine the average LCB/chain as a function of the logarithm of the molecular weight. The MC model simulated very similar values for average LCB/chain than the ones determined experimentally for the analyzed experimental condition. Moreover, the developed MC model can be used to simulate other copolymerization systems and, after the model validation, it can be used to predict the average LCB/chain when there is no available GPC/VISC.

The developed model for ethylene and 1,9-decadiene copolymerization using a CGC catalyst in a semi-batch reactor fitted suitably to experimental data comprising feed-flow rates, average molecular weights, molecular weight distributions and LCB/chain distributions. Based on the experimental results, the reincorporation of macromonomer by its terminal unsaturation was shown not to occur at significant rates, so that this reaction step could be ignored in the developed model.

The method of moments constituted an efficient tool to be used in the parameter estimation process to predict average properties, since it is simple and fast to solve. The parameters identifiability analysis was shown to constitute a proper tool for selection of estimable parameters during estimation procedure, since polymerization kinetics naturally leads to a great number of model parameters and probably ill-posed problems for determination of the parameter values and respective uncertainties. The method of particle swarm optimization was shown to constitute an important tool to build

confidence regions of the estimable parameters, since it naturally performs a high number of objective function evaluations. The confidence regions showed that the parameters values can contain high uncertainty when only a subset of parameters are estimated while others are kept on fixed values. However, characterizing the full uncertainty of all parameters can be inaccessible or make the problems intractable.

Monte Carlo methods provided additional information on long chain branching frequencies, such as the average number of LCB as a function of the molecular weight distribution, showing that LCBs are formed mainly at higher molecular weights. Additionally, for the copolymerization system under study, it did not take long times to simulate the overall polymerizations by stochastic procedures, which were shown to constitute excellent tools to build the MWDs.

The method of moments and the Monte Carlo method predicted average molecular weights and ethylene feed flow rates with good accuracy for the discussed experimental conditions. Furthermore, both methods provided good fits for the average frequencies of LCB per chain and per 1000 carbon atoms as functions of the polymerization time for all experimental conditions.

Both MC and CAOC methods provided very similar MWDs for the analyzed experimental condition. Comparing the MWDs predicted by the MC method with the experimental MWDs, it was shown that the incorporation of the macromonomer does not only depend on the amount of pendant unsaturations in the chain, but also on the chain length. This dependency was shown to be not linear, but it could be well described by an exponential law. A sigmoidal function and a correlation with the radius of gyration and the macromonomer length were also tested, also resulting in acceptable calculated distributions, close to the experimental MWDs, although performances obtained with the exponential law were always better. However, the parameters of exponential and sigmoidal functions were estimated by induction, while both parameters of the radius of gyration function (K_s and α_s) were taken from the literature and belong of other copolymer type (1-octene and ethane copolymer). Thus, if K_s and α_s would be estimated by induction, probably the radius of gyration expression would present the lowest Đ.

For the polymerization problems investigated in the present thesis, Monte Carlo methods can be successfully applied to predict the MWDs calculated by the CAOC

method. Thus, the use of MC methods can be proposed to test the convergence of the CAOC, being more efficient than checking if CAOC convergence is attained through simulations performed with additional collocation points and with different time integration steps. However, it is expected that for more complex polymerization problems, containing additional reaction steps, the MC may not constitute a feasible simulation method, given the CPU time required to run the simulation. In this case, the CAOC may become a much more attractive method for modeling and simulation of olefin polymerizations.

The CAOC simulation results of the present thesis showed that some aspects related to calculation of the collocation points (the roots of the orthogonal polynomial) must be improved. It is not clear if the source of numerical difficulties is related to the weighing function, the variable domain, numerical precision of the root finding procedure or a combination of these factors. This must be investigated in the near future in order to enhance the robustness of the CAOC technique.

11.1 Suggestions for Future Work

It would be interesting to conduct similar kinetic investigations with other dienes, such as nonadiene, hexadiene, octadiene, to check if the dependency on the macromonomer size will also affect the macromonomer reincorporation reaction rate, as observed with the decadiene.

Another subject that needs to be investigated is the acceleration of Monte Carlo method, in order to use this technique in the parameter estimation process. Then, distribution data could also be used to estimate the parameters. To achieve this goal, parallel MC programming can be employed. Thus, instead simulating a unique reaction during one iteration, many reactions can be simulated simultaneously, saving CPU time.

It is important to comprehend the source of the numerical difficulties that appear running the CAOC method. Simulations must be conduct to identify the source of these problems in order to improve the robustness of the CAOC technique.

Perform parameter estimation by induction for the two parameters K_s and α_s of the radius of gyration function in order to enhance the prediction of the MWDs, approximating them to the experimental MWDs measured with GPC.

12 References

ALBERTON, A.L., 2010. *Estimação de parâmetros e planejamento de experimentos: Estudo de incertezas e funções de informação*. Rio de Janeiro: Universidade Federal do Rio de Janeiro.

ALBERTON, K. P. F., 2013, "*Identificabilidade de Parâmetros: Aspectos Conceituais e Desenvolvimento de Novos Procedimentos*". PhD thesis, PEQ/COPPE/UFRJ, Rio de Janeiro, Brasil.

ALBERTON, K. P. F., ALBERTON, A. L., MAGGIO, J. A. D., DÍAZ, M. S., SECCHI, A. R., 2013, "Accelerating the Parameters Identifiability Procedure: Set by Set Selection", *Comput. Chem. Eng.*, v. 55, pp. 181 – 197.

AL-HARTHI, M., SOARES, J. B. P., SIMON, L. C., 2006, "Dynamic Monte Carlo Simulation of Atom-Transfer Radical Polymerization", *Macromol. Mater. Eng.*, v. 291, pp. 993 – 1003.

ALOBAIDI, F., YE, Z., ZHU, S., 2003, "Ethylene Polymerization with Silica-Supported Nickel-Diimine Catalyst: Effect of Support and Polymerization Conditions on Catalyst Activity and Polymer Properties", *Macromol. Chem. Phys.*, v. 204, pp. 1653–1659.

ALOBAIDI, F., YE, Z., ZHU, S., 2004, "Ethylene polymerization with homogeneous nickel–diimine catalysts: effects of catalyst structure and polymerization conditions on catalyst activity and polymer properties", *Polymer*, v. 45, pp. 6823–6829.

ALSHAIBAN, A., SOARES, J. B. P., 2009, "Simulation of Propylene Polymerizationin Industrial Reactors Using Ziegler-Natta Catalysts in the Presence of Electron Donors", *Macromol. Symp.*, v. 285, pp. 8 – 22.

ALSHAIBAN, A., SOARES, J. B. P., 2011, "Mathematical Modeling of the Microstructure of Poly(propylene) Made with Ziegler-Natta Catalysts in the Presence of Electron Donors", *Macromol. React. Eng.*, v. 5, pp. 96 – 116.

ALT, H. G., 1999, "The Heterogenization of Homogeneous Metallocene Catalysts for Olefin Polymerization", *J. Chem. Soc., Dalton Trans.*, pp. 1703 – 1709.

ALVAREZ, J., ALVAREZ, J., 1987, "Solution of Summation-Difference Equations by Collocation Techniques", *Chem. Engng. Sci.*, v. 42, pp. 2883 – 2898.

ALVAREZ, J., ALVAREZ, J., 1989, "Solution of Dynamic Summation-Difference Equations by Adaptive Collocation", *Chem. Engng. Sci.*, v. 44, pp. 1161 – 1174.

ANANTAWARASKUL, S., SOMNUKGUANDE, P., SOARES, J. B. P., 2012, "Monte Carlo Simulation of the Microstructure of Linear Olefin Block Copolymers", *Macromol. Symp.*, v. 312, pp. 167 – 173.

ANDERSON, T., ABRAMS, D., GRENS II, E., 1978, "Evaluation of Parameters for Nonlinear Thermodynamic Models", *AlChE Journal*, v. 24, pp. 20 – 29.

BANNISTER, I., BILLINGHAM, N. C., ARMES, S. P., 2009, "Monte Carlo Modelling of Living Branching Copolymerisation of Monovinyl and Divinyl Monomers: Comparison of Simulated and Experimental Data for ATRP Copolymerisation of Methacrylic Monomers", *Soft Matter*, v. 5, pp. 3495 – 3504.

BARD, Y., 1974, Nonlinear Parameter Estimation. San Diego, Academic Press Inc. USA.

BEIGZADEH, D., SOARES, J. B. P., DUEVER, T. A., HAMIELEC, A. E., 1999, "Analysis of Branching Structure in Polyethylene Resins Synthesized with Constrained – Geometry Catalyst Systems, Using Monte Carlo Simulation", *Polym. React. Eng. J.*, v. 7, pp. 195 – 205.

BEIGZADEH, D., SOARES, J. B. P., DUEVER, T. A., 1999, "Combined Metallocene Catalysts: An Efficient technique to manipulate Long-Chain Branching Frequency of Polyethylene", *Macromol. Rapid. Commun.*, v. 20, pp. 541 – 545.

BEIGZADEH, D., SOARES, J. B. P., DUEVER, T. A., 2001, "Production of Polyolefins with Controlled Long Chain Branching and Molecular Weight Distributions Using Mixed Metallocene Catalysts", *Macromol. Symp.*, v. 173, pp. 179 – 194.

BEIGZADEH, D., SOARES, J. B. P., DUEVER, T. A., 1999a, "Analysis of Branching Structure in Polyethylene Resins Synthesized with Constrained-Geometry Catalyst Systems, Using Monte Carlo Simulation", *Polym. Reac, Eng.*, v. 7, pp. 195 – 205.

BEIGZADEH, D., SOARES, J. B. P., HAMIELEC, A. E., 1999b, "Recipes for Synthesizing Polyolefins with Tailor-Made Molecular Weight, Polydispersity Index, Long-Chain Branching Frequencies, and Chemical Composition Using Combined Metallocene Catalyst Systems in a CSTR at Steady State", *J. Appl. Polym. Sci.*, v. 71, pp. 1753 – 1770.

BEIGZADEH, D., SOARES, J. B. P., DUEVER, T. A., 2001, "Modeling of Fractionation in CRYSTAF Using Monte Carlo Simulation of Crystallizable Sequence Lengths: Ethylene/1-Octene Copolymers Synthesized with Single-Site-Type Catalysts", *J. Appl. Polym. Sci.*, v. 80, pp. 2200 – 2206.

BEIGZADEH, D., 2003, "Monte Carlo Simulation of Long-Chain Branched Polyethylene Chains Synthesized with Dual-Site-Type Catalyst Systems", *Macromol. Theor. Simul.*, v. 12, pp. 174 – 183.

BRANDÃO, A. L. T., SOARES, J. B. P., PINTO, J. C., ALBERTON, A. L., 2015, "When Polymer Reaction Engineers Play Dice: Applications of Monte Carlo Models in PRE", *Macromol. React. Eng.*, v. 9, pp. 141 – 185.

BRANDÃO, A. L. T., SOARES, J. B. P., PINTO, J. C., ALBERTON, A. L., 2016, "Comparison of Different Dynamic Monte Carlo Methods for the Simulation of Olefin Polymerization", *Macromol. Symp.*, v. 360, pp. 160 – 178.

BRANDOLIN, A., SARMORIA, C., FAILLA, M. D., VALLÉS E. M., 2007, "Mathematical Modeling of the Reactive Modification of High-Density Polyethylene. Effect of Vinyl Content", *Ind. Eng. Chem. Res.*, v. 46, pp. 7561 – 7570.

BRAUN, D., CHERDRON, H., REHAHN, M., RITTER, H., VOIT, B., 2012, *Polymer Synthesis: Theory and Practice, Fundamentals, Methods, Experiments*, Springer, Science & Business Media.

BRESLOW, D., NEWBURG, N., 1957, "Bis-(Cyclopentadienyl)-titanium Dichloride – Alkylaluminum Complexes as Catalysts for the Polymerization of Ethylene", *J. Am. Chem. Soc.*, v. 79, pp. 5071 – 5073.

BRESLOW, D., NEWBURG, N., 1959, "Bis-(Cyclopentadienyl)-titanium Dichloride – Alkylaluminum Complexes as Soluble Catalysts for the Polymerization of Ethylene", *J. Am. Chem. Soc.*, v. 81, pp. 81 – 86.

BRITOVSEK, G. J. P., GIBSON, V. C., HOARAU, O. L., SPITZMESSER, S. K., WHITE, A. J. P., WILLIAMS, D. J., 2003, "Iron and Cobalt Ethylene Polymerization Catalysts: Variation on the Central Donor", *Inorg. Chem.*, v. 42, pp. 3454 – 3465.

CAO, Y., GILLESPIE, D. T., PETZOLD, L. R., 2006, "Efficient Step Size Selection for the Tau-Leaping Simulation Method", *J. Chem. Phys.*, v. 124, pp. 044109.

CAO, Y., LI, H., PETZOLD, L., 2004, "Efficient Formulation of the Stochastic Simulation Algorithm for Chemically Reacting Systems", *J. Chem. Phys.*, v. 121, pp. 4059.

CANU, P., RAY, W. H., 1991, "Discrete Weighted Residual Methods Applied to Polymerization Reactions", *Computers Chem. Engng.*, v. 15, pp. 549 – 564.

CARELLA, J. M., GOTRO, J. T., GRAESSLEY, W. W., 1986, "Thermorheological Effects on Long-Chain Branching in Entangled Polymer Melts", *Macromolecules*, v. 19, pp. 659 – 667.

CARTWRIGHT, J. H. E., PIRO, O., 1992, "The Dynamics of Runge-Kutta Methods", *Int. J. Bifurcation Chaos*, v. 2, pp. 427 – 449.

CERRUTI, L., 1999, "Historical and Philisophical Remarks on Ziegler-Natta Catalysts", *An International Journal for the Philosophy of Chemistry*, v. 5, pp. 3–41.

CHAFFEY-MILLAR, H., STEWART, D., CHAKRAVARTY, M. M. T., KELLER, G., BARNER-KOWOLLIK, C., 2007, "A Parallelised High Performance Monte Carlo Simulation Approach for Complex Polymerisation Kinetics", *Macromol. Theor. Simul.*, v. 16, pp. 575 – 592.

CHEMWEEK, 2016, disponível em: http://www.chemweek.com/lab/PEPP-2016-The-global-polyolefins-industry-has-a-bright-future_79771.html. Visited: October 21, 2016.

CHO, K. S., AHN, K. H., LEE, S. J., 2004, "Simple Method for Determining the Critical Molecular Weight form the Loss Modulus", *J. Polym. Sci. Part B: Polym. Phys.*, v. 42, pp. 2724 – 2729.

CHUM, P. S., KUPER, W. J., GUEST, M. J., 2000, "Materials Properties Derived from INSITE Metallocene Catalysts", *Adv. Matter*, v. 12, pp. 1759 – 1767.

CHUM, P. S., SWOGGER, K. W., 2008, "Olefin Polymer Technologies—History and Recent Progress at The Dow Chemical Company", *Prog. Polym. Sci.*, v. 33, pp. 797–819.

CHUNG, T. C., 2002, *Functionalization of Polyolefins*, Academic Press.

CIHLÁŘ, J., MEJZLÍK, J., HAMŘÍK, O., 1978, "Influence of water on ethylene polymerization catalyzed by titanocene systems", *Makromol. Chem.*, v. 179, pp. 2553–2558.

CIHLÁŘ, J., MEJZLÍK, J., HAMŘÍK, O., HUDEC, P., MAJER, J., 1980, "Polymerization of ethylene catalyzed by titanocene systems, 1. Catalytic systems Cp2TiEtCl/AlEtCl2 and Cp2TiEtCl/(AlEtCl2 + H2O)", *Makromol. Chem.*, v. 181, pp. 2549–2561.

COLLMAN, J. P., HEGEDUS, L. S., NORTON, J. R., FINKE, R. G., 1987, *Principles and Applications of Organotransition Metal Chemistry*, Mill Valey, University Science Books.

COSTEUX, S., WOOD-ADAMS, P. M., BEIGZADEH, D., 2002, "Molecular Structure of Metallocene-Catalyzed Polyethylene: Rheologically Relevant Representation of Branching Architecture in Single Site Catalyst and Blended Systems", *Macromolecules*, v. 35, pp. 2514 – 2528.

COSTEUX, S., ANANTAWARASKUL, S., WOOD-ADAMS, P. M., SOARES, J. B. P., 2002, "Distribution of the Longest Ethylene Sequence in Ethylene/α-Olefin

Copolymers Synthesized with Single-Site-Type Catalysts", *Macromol. Theor. Simul.*, v. 11, pp. 326 – 341.

COSTEUX, S., 2003, "Statistical Modeling of Randomly Branched Polymers Produced by Combination of Several Single-Site Catalysts: Toward Optimization of Melt Properties", *Macromolecules*, v. 36, pp. 4168 – 4187.

COSTEUX, S., WOOD-ADAMS, P. M., BEIGZADEH, D., 2002, "Molecular Structure of Metallocene-Catalyzed Polyethylene: Rheologically Relevant Representation of Branching Architecture in Single Site Catalyst and Blended Systems", *Macromolecules*, v. 35, pp. 2514 – 2528.

COUTINHO, F. M. B., MELLO, I. L., MARIA, L. C. S., 2003, "Polietileno: Principais Tipos, Propriedades e Aplicações", *Polímeros*, v. 13, pp. 1-13.

DIAS, R. C. S., COSTA, M. R. P. F. N., 2010, "Branching and Crosslinking in Coordination Terpolymerizations", *Macromol. React. Eng.*, v. 1, pp. 440 – 467.

DONG, Z., YE, Z., 2012, "Hyperbranched Polyethylenes by Chain Walking Polymerization: Synthesis, Properties, Functionalization, and Applications", *Polymer Chemistry*, v. 3, pp. 286–301.

DRACHE, M., SCHIMIDT-NAAKE, G., BUBACKB, M., VANA, P., 2005, "Modeling RAFT polymerization Kinetics via Monte Carlo Methods: Cumyl Dithiobenzoate Mediated Methyl Acrylate Polymerization", *Polymer*, v. 46, pp. 8483 – 8493.

DRACHE, M., SCHIMIDT-NAAKE, 2007, "RAFT Polymerization – Investigation of the Initialization Period and Determination of the Transfer Coefficients", *Macromol. Symp.*, v. 259, pp. 397 – 405.

DRACHE, M., SCHIMIDT-NAAKE, 2008, "Initialization of RAFT Agents with Different Leaving Groups – Determination of the Transfer Coefficients", *Macromol. Symp.*, v. 271, pp. 129 – 136.

DRAWERT, B., LAWSON, M. J., PETZOLD, L., KHAMMASH, M., 2010, "The Diffusive Finite State Projection Algorithm for Efficient Simulation of the

Stochastic Reaction-Diffusion Master Equation", *J. Chem. Phys.*, v. 132, pp. 74101-1 – 74101-12.

ESPIE, D. M., MACCHIETTO, S., 1988, "Nonlinear Transformations for Parameter Estimation", *Ind. Eng. Chem. Res.*, v. 27, pp. 2175 – 2179.

FERREIRA JR., L. C., NELE, M., COSTA, M. A. S., PINTO, J. C., 2010, "Mathematical Modeling of MWD and CBD in Polymerizations with Macromonomer Reincorporation and Chain Running", *Macromol. Theory Simul.*, v. 19, pp. 496 – 513.

FINLAYSON, B. A., 1981a, *The Method of Weighted Residuals and Variational Principles*, Academic Press, New York, USA.

FINLAYSON, B. A., 1981b, *Nonlinear analysis in Chemical Engineering*, McGraw-Hill, New York, USA.

FLORES, T. M., 2006, *Modelagem da Copolimerização de Olefinas: Estudo da Aplicabilida de Dados em Fase Líquida para a Fase Gás*. Tese de M.Sc., Universidade Federal do Rio Grande do Sul, Porto Alegre, Brasil.

FLORY, P. J., 1946, "Fundamental Principles of Condensation Polymerization", *Chem. Rev*, v. 39, pp. 137 – 197.

FRIEBE, L., WERNER, N., OBRECHT, W., 2006, "Neodymium-Based Ziegler/Natta Catalysts and their Application in Diene Polymerization", *Adv. Polym. Sci.*, v. 204, pp. 1–154.

GABORIEAU, M., CASTIGNOLLES, P., 2011, "Size-exclusion Chromatography (SEC) of Branched Polymers and Polysaccharides", *Analytical and bioanalytical chemistry*, v. 399, n. 4, pp. 1413–23.

GALIMBERTI, M., MASCELLANI, N., PIEMONTESI, F., CAMURATI, I., 1999, "Random Ethene/ Propene Copolymerization from a Catalyst System based on a "Constrained Geometry" Half-Sandwich Complex", *Macromol. Rapid. Commun.*, v. 20, pp. 214 – 218.

GALVAN, R., TIRRELL, M., 1986, "Molecular Distribution Predictions for Ziegler-Natta Polymerization Using a Two-Site Model", *Chem. Engng. Sci.*, v. 41, pp. 2385 – 2393.

GHIOTTO, F., PATERAKI, C., TANSKANEN, J., SEVERN, J., LUEHMANN, N., KUSMIN, A., STELLBRINK, J., LINNOLAHTI, M., BOCHMANN, M., 2013, "Probing the Structure of Methylaluminoxane (MAO) by a Combined Chemical, Spectroscopic, Neutron Scattering, and Computational Approach", *Organometallics*, v. 32, pp. 3354 – 3362.

GIBSON, M. A., BRUCK, J., 2000, "Efficient Exact Stochastic Simulation of Chemical Systems with Many Species and Many Channels", *J. Phys. Chem. A*, v. 104, pp. 1876 – 1889.

GILLESPIE, D. T., 1976, "A General Method for Numerically Simulating the Stochastic Time Evolution of Coupled Chemical Reactions", *J. Comput. Phys.*, v. 22, pp. 403 – 434.

GILLESPIE, D. T., 1977, "Exact Stochastic Simulation of Coupled Chemical Reactions", *J. Phys. Chem.*, v. 81, pp. 2340 – 2361.

GILLESPIE, D. T., 1992, "A Rigorous Derivation of the Chemical Master Equation", *Physica A*, v. 188, pp. 404 – 425.

GILLESPIE, D. T., 2001, "Approximate Accelerated Stochastic Simulation of Chemically Reacting Systems", *J. Phys. Chem.*, v. 115, pp. 1716 – 1733.

GILLESPIE, D. T., PETZOLD, L. R., 2003, "Improved Leap-Size Selection for Accelerated Stochastic Simulation", *J. Chem. Phys.*, v. 119, pp. 8229 – 8234.

GILLESPIE, D. T., 2007, "Stochastic Simulation of Chemical Kinetics", *Annu. Rev. Phys. Chem.*, v. 58, pp. 35 – 55.

GILLESPIE, D. T., 2008, *Formal Methods for Computational Systems Biology*, (Eds: M. Bernardo, P. Degano, G. Zavattaro), Springer, Germany, Part I/p. 125.

GNANOU, Y., FONTANILLE, M., 2008, *Organic and physical chemistry of polymers*. Hoboken, John Wiley & Sons, Inc.

GUZMÁN, J. D., ARRIOLA, D. J., KARJALA, T., GAUBERT, J., KOLTHAMMER, B. W. S., 2010, "Simple Model to Predict Gel Formation in Olefin-Diene Copolymerizations Catalyzed by Constrained-Geometry Complexes", *AlChE Journal*, v. 56, pp. 1325 – 1333.

HAAG, M. C., SIMON, L. C., SOARES, J. B. P., 2003, "Comparing Strategies for the Synthesis of Polyolefinic Thermoplastic Elastomers via Macromonomer Incorporation", *Macromol. Theor. Simul.*, v. 12, pp. 142 – 152.

HAMIELEC, A. E., SOARES, J. B. P., 1996, "Polymerization Reaction Engineering- Metallocene Catalysts", *Prog. Polym. Sci.*, v. 21, pp. 651–706.

HAMIELEC, A. E., SOARES, J. B. P., 1997, "The Chemical Composition Component of the Distribution of Chain Length and Long Chain Branching for Copolymerization of Olefins and Polyolefin Chains Containing Terminal Double-Bonds", *Macromol. Theory Simul.*, v. 6, pp. 591 - 596.

HICKS, F. A., BROOKHART, M., 2001, "A Highly Active Anilinotropone-Based Neutral Nickel (II) Catalyst for Ethylene Polymerization", *Organometallics*, v. 20, pp. 3217–3219.

HIGHAM, D. J., 2008, "Modeling and Simulating Chemical Reactions", *SIAM Rev.*, v. 50, pp. 347 – 368.

HINES, W., MONTGOMERY, D. C., GOLDSMAN, D. M., BORROR, C. M., 2003, *Probability and Statistics in Engineering*. 4 ed., John Wiley & Sons.

HUANG, J., REMPEL, G. L., 1995, "Ziegler-Natta Catalyst for Olefin Polymerization: Mechanistic Insights from Metallocene Systems", *Prog. Polym. Sci.*, v. 20, pp. 459–526.

HULBURT, H. M., KATZ, S., 1964, "Some Problems in Particle Technology. A Statistical Mechanical Formulation", *Chem. Engng. Sci.*, v. 19, pp. 555 – 574.

IEDEMA, P. D., HOEFSLOOT, H. C. J., 2002, "Molecular-Weight-Distribution Modelling of Radical Polymerization in Batch and Continuous Reactors with Transfer to Polymer Leading to Gel Formation", *Macromol. Theory Simul.*, v. 11, pp. 410 – 428.

IEDEMA, P., D., HOEFSLOOT, H. C. J., SMIT, J., 2004a, "Predicting the Molecular Weight Distribution of Polyethylene for Mixed Systems with a Constrained-Geometry Metallocene Catalyst in a Semibatch Reactor", *Ind*. *Eng*. *Chem*. *Res*., v. 43, pp. 36 – 50.

IEDEMA, P., D., HOEFSLOOT, H. C. J., 2004b, "A Conditional Monte Carlo Method to Predict Branched Architectures from Molecular Weight and Degree of Branching Distribution of Polyethylene for Single and Mixed Systems with a Constrained Geometry Metallocene Catalyst in Continuous Reactors", *Polymer*, v. 45, pp. 6071 – 6082.

KAMINSKY, W., 2013, *Polyolefins: 50 years after Ziegler and Natta I: Polyethylene and Polypropylene*. Springer.

KARAK, N., 2009, *Fundamentals Of Polymers: Raw Materials To Finish Products*. New Delhi, PHI Learning Pvt. Ltd.

KEALEY, T. J., PAULSON, P. L., 1951, "A New Type of Organo-Iron Compound", *Nature*, v. 168, 1039 – 1040.

KENNEDY, J., EBERHART, R., 1995, "Particle Swarm Optimization", *Proc IEEE International Conference on Neural Networks*, pp. 1942 – 1948.

KHORASANI, M. M., SAEB, M. R., MOHAMMADI, Y., AHMADI, M., 2014, "The Evolutionary Development of Chain Microstructure During Tandem Polymerization of Ethylene: A Monte Carlo Simulation Study", *Chem*. *Eng*. *Sci*., v. 111, pp. 211 – 219.

KOKKO, E., 2002, *Metallocene-Catalyzed Ethene Polymerization: Long-Chain Branched Polyethene*, Msc. Thesis, Helsinki University of Technology, Espoo, Finland.

KOKKO, E., MALMBERG, A., LEHMUS, P., LÖFGREN, B., SEPPÄLÄ J. V., 2000, "Influence of the Catalyst and Polymerization Conditions on the Long-Chain Branching of Metallocene-Catalyzed Polyethenes", *J*. *Polym*. *Sci*., *Part A: Polym*. *Chem*., v. 38, pp. 376 – 388.

KOKKO, E., PIETIKINEN, P., KOIVUNEN, J., SEPPÄLÄ, J. V., 2001, "Long-Chain-Branched Polyethylene by the Copolymerization of Ethene and Nonconjugated α,ω-Dienes", *J. Polym. Sci., Part A: Polym. Chem.*, v. 39, pp. 3805 – 3817.

KOLODKA, E., WANG, W.-J., ZHU, S., HAMIELEC, A. E., 2002, "Copolymerization of Propylene with Poly(ethylene-co-propylene) Macromonomer and Branch Chain-Length Dependence of Rheological Properties", *Macromolecules*, v. 35, pp. 10062 – 10070.

KOLODKA, E., WANG, W.-J., ZHU, S., HAMIELEC, A. E., 2003, "Synthesis and Characterization of Long-Chain-Branched with Metallocene Catalysts: Copolymerization of Ethylene with Poly(ethylene-co-propylene)", *Macromol. Rapid Commun*, v. 24, pp. 311 – 315.

KONSTANTINOV, I., VILLA, C., KARJALA, T., JAIN, P., 2016, "Dual Catalyst Model Describing the Effect of Branching on the Molecular Architecture of Polyolefins", *Macromol. React. Eng.*, v. 10, pp. 140 – 150.

KOU, B., MCAULEY, K. B., HSU, C. C., BACON, D. W., 2005, "Mathematical Model and Parameter Estimation for Gas-Phase Ethylene Homopolymerization with Supported Metallocene Catalyst", *Macromol. Mater. Eng.*, v. 290, pp. 537 – 557.

KRESSER, T. O. J., 1969, *Polyolefin Plastics*. 1st edition. New York, Van Nostrand Reinhold Company.

KREYZSIG, E., 1989, *Introductory Functional Analysis with Applications*. USA, John Wiley & Sons.

KURAN, W., 2001, *Principles of Coordination Polymerisation*, New York, John Wiley & Sons.

LAI, S. Y., WILSON, J. R., KNIGHT, G. W., STEVENS, J. C., CHUM, P. W. S., 1993a, *Elastic Substantially Linear Olefin Polymers*. US Patent 5,272,236.

LAI, S. Y., WILSON, J. R., KNIGHT, G. W., STEVENS, J. C., CHUM, P. W. S., 1993b, *Elastic Substantially Linear Olefin Polymers*. US Patent application 93/08221.

LAURENCE, R. L., GALVAN, R., TIRREL, M. V., 1994, "Mathematical Modeling of Poymerization Kinetics". In: *Polymer Reactor Engineering*, C. McGreavy, Ed., VCH Publishers, New York, pp. 87 – 124.

LAW, V., BAILEY, R., 1963, "A Method for the Determination of Approximate System Transfer Functions", *Chem. Engng. Sci.,* v. 18, pp. 189 – 202.

LIU, P., LIU, W., WANG, W-J., LI, B-G., ZHU, S., 2016, "A Comprehensive Review on Controlled Synthesis of Long-Chain Branched Polyolefins: Part 1, Single Catalysts Systems", *Macromol. React. Eng.*, v. 10, pp. 156 - 179.

LUCAS, E. F., SOARES, B. G., MONTEIRO, E., 2001, *Caracterização de Polímeros. Determinação de Peso Molecular e Análise Térmica*. 1ª ed. Rio de Janeiro, Brasil, E-papers. Capítulo 1.

MAAFA, I. M., SOARES, J. B. P., ELKAMEL, A., 2007, "Prediction of Chain Length Distribution of Polystyrene Made in Batch Reactors with Bifunctional Free-Radical Initiators Using Dynamic Monte Carlo Simulation", *Macromol. React. Eng.*, v. 1, pp. 364 – 383.

MACHADO, F., PINTO, J. C., 2011, "Uma Revisão sobre Polimerização de Olefinas Usando Catalisadores Ziegler-Natta Heterogêneos", *Polímeros*, v. 21, pp. 321–334.

MACQUARRIE, D. A., 1967, "Stochastic Approach to Chemical Kinetics", *J. Appl. Probab.*, v. 4, pp. 413 – 478.

MADKOUR, T. M., MARK, J. E., 1995, "Monte Carlo Simulations on the Stereoregularity, Crystallinity, and Related Physical Properties of Poly[methyl(3,3,3-trifluoropropyl)siloxane]", *Macromolecules*, v. 28, pp. 6865 – 6870.

MADKOUR, T. M., MARK, J. E., 1997, "Modeling of the Crystallization of Isotactic Polypropylene Chains", *J. Polym. Sci., Part B: Polym. Phys.*, v. 35, pp. 2757 – 2764.

MADKOUR, T. M., MARK, J. E., 1998, "Simulations on Crystallization in stereoblock Poly(propylene). Idealized Structures Showing the Effects of Atactic Block Length", *Macromol. Theory Simul.*, v. 7, pp. 69 – 77.

MAIER, C., CALAFUT, T., 2008, *Polypropylene: The Definitive User's Guide and Databook*. Elsevier Science, USA.

MANDAL, B. M., 2013, *Fundamentals of Polymerization*. World Scientific: Hackensack, NJ, USA.

MARQUES, M. D. F. V., JUNIOR, P. A. A. C., GUIMARÃES, M. J. C., COUTINHO, F. M. B., 1998, "Catalisadores Metalocênicos: Aspectos Gerais e Heterogeneização", *Polímeros: Ciência e Tecnologia*, v. 8, pp. 26 – 40.

MCCOLLUM, J. M., PETERSON, G. D., COX, C. D., SIMPSON, M. L., SAMATOVA, N. F., 2006, "The Sorting Direct Method for Stochastic Simulation of Biochemical Systems with Varying Reaction Execution Behavior", *Comput. Biol. Chem.*, v. 30, pp. 39 – 49.

MCCORD, E. F., MCLAIN, S. J., NELSON, L. T. J., et al., 2001, "13 C and 2D NMR Analysis of Propylene Polymers Made with a-Diimine Late Metal Cataysts", *Macromolecules*, v. 34, pp. 362–371.

MCLEAN, K. A. P., WU, S., MCAULEY, K. B., 2012, "Mean-Squared-Error Methods for Selecting Optimal Parameter Subsets for Estimation", *Ind. Eng. Chem. Res.*, v. 51, pp. 6105 – 6115.

MEHDIABADI, S., SOARES, J. B. P., 2008, "Production of Long-Chain Branched Polyolefins with Two Single-Site Catalysts: Comparing CSTR and Semi-Batch Performance", *Macromol. React. Eng.*, v. 2, pp. 529 – 550.

MEHDIABADI, S., 2011, *Synthesis, Characterization and Polymerization Kinetic Study of Long Chain Branched Polyolefins Made with Two Single-Site Catalysts*. PhD. Thesis, University of Waterloo, Waterloo, Canada, pp. 147.

MEHDIABADI, S., SOARES, J. B. P., 2009, "Influence of Metallocene Type on the Order of Ethylene Polymerization and Catalyst Deactivation Rate in a Solution Reactor", *Macromol. Symp.*, v. 285, pp. 101 – 114.

MEHDIABADI, S., SOARES, J. B. P., 2011, "Production of Ethylene/ α-Olefin/ 1,9-Decadiene Copolymers with Complex Microstructures Using a Two-Stage Polymerization Process", *Macromolecules*, v. 44, pp. 7926 – 7939.

MEHDIABADI, S., SOARES, J. B. P., 2012, "Ethylene Homopolymerization Kinetics with a Constrained Geometry Catalyst in a Solution Reactor", *Macromolecules*, v. 45, pp. 1777 – 1791.

MEIMAROGLOU, D., KIPARISSIDES, C., 2014, "Review of Monte Carlo Methods for the Prediction of Distributed Molecular and Morphological Polymer Properties", *Ind. Eng. Res.*, v. 53, pp. 8963 – 8979.

MILLER, S. A., TEBBOTH, J. A., TREMAINE, J. F., 1952, "Dicyclopentadienyliron" , *J. Chem. Soc.*, pp. 632 – 635.

MOGILICHARLA, A., MITRA, K., MAJUMDAR, S., 2014, "Modeling of Propylene Polymerization with Long Chain Branching", *Chem. Eng. J.,* v. 246, pp. 175 – 183.

MOHAMMADI, Y., NAJAFI, M., HADDADI-ASL, V., 2005, "Comprehensive Study of Free Radical Copolymerization Using Monte Carlo Simulation Method, 1 Both Reactivity Ratios Less than Unity", *Macromol. Theor. Simul.*, v. 14, pp. 325 – 336.

MONJI, M., ABEDI, S., POURMAHDIAN, S., TAROMI, F. A., 2009, "Effect of Prepolymerization on Propylene Polymerization", *J. Appl. Polym. Sci.*, v. 112, pp. 1863–1867.

NAGA, N., IMANISHI, Y., 2002, "Copolymerization of Ethylene and 1,7-Octadiene, 1,9-Decadiene with Zirconocene Catalysts", *Macromol. Chem. Phys.*, v. 203, pp. 2155 - 2162.

NAGA, N., TOYOTA, A., 2004, "Unique Insertion Mode of 1,7-Octadiene in Copolymerization with Ethylene by a Constrained-Geometry Catalyst", *Macromol. Rapid. Commun.*, v. 25, pp. 1623 – 1627.

NAJAFI, M., HADDADI-ASL, V., MOHAMMADI, Y., 2007, "Application of the Monte Carlo Simulation Method to the Investigation of Peculiar Free-Radical Copolymerization Reactions: Systems with Both Reactivity Ratios Greater than Unity", *J. Appl. Polym. Sci.*, v. 106, pp. 4138 – 4147.

NELE, M., COLLINS, S., DIAS, M. L., PINTO, J. C., LIN, S., WAYMOUTH, R. M., 2000, "Two-State Models for Olefin Polymerization Using Metallocene Catalysts. 1. Application to Fluxional Metallocene Catalyst Systems", *Macromolecules*, v. 33, pp. 7249 – 7260.

NELE, M., MOHAMMED, M., XIN, S., COLLINS, S., DIAS, M. L., PINTO, J. C., 2001, "Two-State Models for Propylene Polymerization Using Metallocene Catalysts. 2. Application to ansa-Metallocene Catalyst Systems", *Macromolecules*, v. 34, pp. 3830 – 3841.

NELE, M., SAYER, C., PINTO, J. C., 1999, "Computation of Molecular Weight Distributions by Polynomial Approximation with Complete Adaptation Procedures", *Macromol. Theory Simul.*, v. 8, pp. 199 – 213.

NELE, M., SOARES, J. B. P., PINTO, J. C., 2003, "Evolution of Molecular Weight and Long Chain Branch Distributions in Olefin-Diene Copolymerization", *Macromol. Theory Simul.*, v. 12, pp. 582 – 592.

NELE, M., SOARES, J. B. P., 2003, "Molecular Weight and Long Chain Branch Distributions of Branch-Block Olefinic Thermoplastic Elastomers", *Macromol. Theory Simul.*, v. 12, pp. 386 – 400.

ODIAN, G., 2004, *Principles of Polymerization*. 4 ed. New Jersey, John Wiley & Sons.

228

PARODI, S., NOCCI, R., GIANNINI, U., BARBÈ P. C., SCATA, U., 1982, *Components and Catalysts for the Polymerization of Olefins*. European Patent 45,977, to Montedison.

PATER, J. T. M., WEICKERT, G., SWAAIJ, W. P. M. V., 2002, "Polymerization of Liquid Propylene With a 4th Generation Ziegler – Natta Catalyst – Influence of Temperature, Hydrogen and Monomer Concentration and Prepolymerization Method on Polymerization Kinetics", *Chem. Eng. Sci.*, v. 57, pp. 3461–3477.

PAUL, HOWARD, "Polyolefins Process Advances and Metallocene Catalysis". *APE International, Polyolefins Conference, a Forum for New Ideas and Innovation*, Houston, TX, USA, 2015.

PETZOLD, L. R., 1982, "*A Description of DASSL: A Differentia/Algebraic System Solver*". , IMACS World Congress, Montreal.

PIETIKÄINEN, P., VÄÄNÄNEN, T, SEPPÄLÄ, J. V., 1999, "Copolymerization of Ethylene and Non-Conjugated Dienes with Cp_2ZrCl_2/MAO Catalyst System", *Eur. Polym. J.*, v. 35, pp. 1047 – 1055.

PINTO, J. C., BISCAIA Jr., E. C., 1988, "Order Reduction Strategies for Models of Staged Separation Systems", *Comput. Chem. Engng.*, v. 12, pp. 821 – 831.

PINTO, J. C., BISCAIA Jr., E. C., 1996, "An Adaptive Orthogonal Collocation Technique for Discrete Distributions on Infinite Domains", *Latin Am. Appl. Res.*, v. 26, pp. 1 – 20.

PINTO, J.C., LOBAO, M.W., ALBERTON, A.L., et al., 2011, "Critical Analysis of Kinetic Modeling Procedures". In: *International Journal of Chemical Reactor Engineering*. v. 9.

PLADIS, P., KIPARISSIDES, C., 1998, "A Comprehensive Model for the Calculation of Molecular Weight-Long-Chain Branching Distribution in Free-Radical Polymerizations", *Chem. Engng. Sci.*, v. 53, pp. 3315 – 3333.

POLYMEREXPERT, 2002, available in: <http://www.polymerexpert.fr/ en/

presentation/ histoire-des-polymeres />. Visited: October 17, 2016.

PREISHUBER-PFLUGL, P., BROOKHART, M., 2002, "Highly Active Supported Nickel Diimine Catalysts for Polymerization of Ethylene", *Macromolecules*, v. 35, pp. 6074–6076.

REICHERT, K., MEYER, K., 1973, "Zur Kinetik der Niederdruckpolymerisation von Athylen mit loslichen Ziegler-Katalysatoren", *Makromol. Chem.*, v. 169, pp. 163 – 176.

RIBEIRO, L. D., SECCHI, A. R., BISCAIA Jr., E. C., 2015, "Highly-accurate model order reduction technique on a discrete domain", *Braz. J. Chem. Eng.*, v. 32, pp. 767 – 779.

RICE, J. R., 1966, "Experiments on Gram-Schmidt Orthogonalization", *Mathematics of Computation*, v. 20, pp. 325 – 328.

SALAMI-KALAJAHI, M., NAJAFI, M., HADDADI-ASL, V., 2009, "Application of Monte Carlo Simulation Method to Polymerization Kinetics over Ziegler-Natta Catalysts", *Int. J. Chem. Kinet.*, v. 41, pp. 45 – 56.

SANTOS, J. P. L., CASTIER, M., MELO, P. A., 2007, "Polymerization of 1-Hexene using α-Diimine Nickel Catalysts: Stochastic Simulation of Branch Distribution", *Polymer*, v. 48, pp. 5152 – 5160.

SARZOTTI, D. M., NARAYAN, A., WHITNEY, P. M., SIMON, L. C., SOARES, J. B. P., 2005, "Microstructural Characterization of Molecular Weight Fractions of Ethylene/ 1,7-Octadiene Copolymers Made with a Constrained Geometry Catalyst", *Macromol. Mater. Eng.*, v. 290, pp. 584 – 591.

SAYER, C., ARAUJO, P. H. H., ARZAMENDI, G., ASUA, J. M., LIMA, E. L., PINTO, J. C., 2001, "Modeling Molecular Weight Distribution in Emulsion Polymerization Reactions with Transfer to Polymer", *J. Polym. Sci. A Polym. Chem.*, v. 39, pp. 3513 – 3528.

SCHWAAB, M., 2005, *Avaliação de Algoritmos Heurísticos de Otimização em Problemas de Estimação de Parâmetros*. PhD thesis, PEQ/COPPE/UFRJ, Rio de Janeiro, Brasil.

SCHWAAB, M., PINTO, J. C., 2007, *Análise de Dados Experimentais I, Fundamentos de Estatística e Estimação de Parâmetros*. Rio de Janeiro, E-papers Serviços Editoriais Ltda. ISBN: 8576500884.

SCHWAAB, M., BISCAIA Jr., E. C., MONTEIRO, J. L., PINTO, J. C., 2008, "Nonlinear Parameter Estimation trough Particle Swarm Optimization*", Chem. Engng. Sci.*, v. 63, pp. 1542 – 1552.

SCHWAAB, M., LEMOS, L. P., PINTO, J. C., 2008, "Optimum Reference Temperature for Reparameterization of the Arrhenius Equation. Part 2: Problems Involving Multiple Reparameterizations", *Chem. Engng. Sci.*, v. 63, pp. 2895 – 2906.

SCHWAAB, M., PINTO, J.C., 2007, "Optimum reference temperature for reparameterization of the Arrhenius equation. Part 1: Problems involving one kinetic constant". In: *Chemical Engineering Science*. v. 62, pp. 2750–2764.

SERNETZ, F. G., MÜLHAUPT, R., WAYMOUTH, R. M., 1997, "Homo-, Co- and Terpolymerization of 1,5-Hexadiene Using a Methylalumoxane Activated Mono-Cp-Amido-Complex", *Polymer Bulletin*, v. 38, pp. 141 – 148.

SEVERN, J. R., CHADWICK, J. C., DUCHATEAU, R., et al., 2005, ""Bound but Not Gagged- Immobilizing Single-Site Alpha-Olefin Polymerization Catalysts", *Chemical reviews*, v. 105, n. 11, pp. 4073–4147.

SEYMOUR, R. B., CHENG, T., 1986, *The History of Polyolefins*. Massachusetts, Kluwer Academic Publishers.

SIMON, L., SOARES, J. B. P., 2002, "Polyethylene Made with Combinations of Single-Site-Type Catalysts: Monte Carlo Simulation of Long-Chain Branch Formation", *Macromol. Theory Simul.*, v. 11, pp. 222 – 232.

SINN, H., KAMINSKY, W., 1980, "Ziegler – Natta Catalysis", *Adv. Org. Chem.*, v. 18, pp. 99 – 149.

SMALL, B. L., BROOKHART, M., 1998, "Iron-Based Catalysts with Exceptional High Activities and Selectivities for Oligomerization of Ethylene to Linear α-Olefins", *J. Am. Chem. Soc.*, v. 120, pp. 7143 – 7144.

SOARES, J., 2002, "Mathematical Modeling of the Long-Chain Branch Structure of Polyolefins Made with Two Metallocene Catalysts: An Algebraic Solution" ,*Macromol. Theory Simul.*, v. 11, pp. 184 – 198.

SOARES, J. B. P., 2004, "Polyolefins With Long Chain Branches Made With Single-Site Coordination Catalysts: A Review of Mathematical Modeling Techniques for Polymer Microstructure", *Macromolecular Materials and Engineering*, v. 289, pp. 70 – 87.

SOARES, J. B. P., MCKENNA, T. F. L., 2012, "*Polyolefin Reaction Engineering*", Wiley, Weinheim, Germany, pp. 19,135.

SOARES, J., HAMIELEC, A. E., 1996, "Bivariate Chain Length and Long Chain Branching Distribution for Copolymerization of Olefins and Polyolefin Chains containing Terminal Double-Bonds", *Macromol. Theory Simul.*, v. 5, pp. 547 – 572.

SOARES, J. B. P., ANANTAWARASKUL, S., 2005, "Crystallization Analysis Fractionation", *J. Polym. Sci. Part B: Polym. Phys.*, v. 43, pp. 1557 – 1570.

SOARES, J. B. P., MCKENNA, T. F. L., 2013, *Polyolefin Reaction Engineering*. John Wiley & Sons.

SIMON, L. C., SOARES, J. B. P., SOUZA, R. F., 2002, "Monte-Carlo Simulation of Branching Distribution in Ni-Diimine Catalyzed Polyethylene", *AlChE Journal*, v. 46, pp. 1234 – 1240.

SIMON, L. C., SOARES, J. B. P., 2002, "Polyethylene Made with Combinations of Single-Site-Type Catalysts: Monte Carlo Simulation of Long-Chain Branch Formation", *Macromol. Theor. Simul.*, v. 11, pp. 222 – 232.

SIMON, L. C., SOARES, J. B. P., 2005, "Monte Carlo Simulation of Long-Chain Branched Polyolefins Made with Dual Catalysts: A Classification of Chain

Structures in Topological Branching Families", *Ind. Eng. Chem. Res.* 2005, v. 44, pp. 2461 – 2468.

SOARES, J. B. P., HAMIELEC, A. E., 1996, "Bivariate Chain Length and Long Chain Branching Distribution for Copolymerization of Olefins and Polyolefin Chains Containing Terminal Double – Bonds", *Macromol. Theor. Simul.*, v. 5, pp. 547 – 572.

SOARES, J. B. P., HAMIELEC, A. E., 1997, "The Chemical Composition Component of the Distribution of Chain Length and Long Chain Branching for Copolymerization of Olefins and Polyolefin Chains Containing Terminal Double-Bonds", *Macromol. Theor. Simul.*, v. 6, pp. 591 – 596.

SOARES, J. B. P., HAMIELEC, A. E., 2007, "Chain Length Distributions of Polyolefins Made with Coordination Catalysts at Very Short Polymerization Times – Analytical Solution and Monte Carlo Simulation", *Macromol. React. Eng.*, v. 1, pp. 53 – 67.

SOARES, J. B. P., HAMIELEC, A. E., 2008, "Chain Length Distributions of Polyolefins Made in Stopped-Flow Reactors for Non-Instantaneous Site Activation", *Macromol. Reac. Eng.*, v. 2, pp. 115 – 125.

SOARES, J. B. P., NGUYEN, T., 2007, "Dynamic Monte Carlo Simulation of Olefin Polymerization in Stopped Flow Reactors", *Macromol. Symp.*, v. 260, pp. 189 – 196.

SOGA, K., PARK, J. R., SHIONO, T., 1991, "Copolymerization of Ethylene and Propylene with a CpTiCl3/SiO2-MAO Catalyst System", *Polym. Commun.*, v. 32, pp. 310 – 313.

SOGA, K., UOZUMI, T., SAITO, M., SHIONO, T., 1994, "Structure of Polypropene and Poly(ethylene-co-propene) Produced with an Alumina-Supported CpTiCl3/common Alkylaluminium Catalyst System", *Macromol. Chem. Phys.*, v. 195, pp. 1503 – 1515.

SOGA, K., UOZUMI, T., NAKAMURA, S., TONERI, T., TERANISHI, T., SANO, T., ARAI, T., 1996, "Structures of Polyethylene and Copolymers of Ethylene

with 1-Octene and Oligoethylene Produced with the Cp2ZrCl2 and [(C5Me4)SiMe2N(t-Bu)]TiCl2 Catalysts", *Macromol. Chem. Phys.*, v. 197, pp. 4237 – 4251.

SOGA, K., SHIONO, T., 1997, "Ziegler-Natta Catalysts for Olefin polymerizations", *Prog. Polym. Sci.*, v. 22, pp. 1503–1546.

STADLER, F. J., PIEL, C., KAMINSKY, W., Munstedt, H., 2006, "Rheological Characterization of Long-Chain Branched Polyethylenes and Comparison with Classical Analytical Methods", *Macromol. Symp.*, v. 236, pp. 209 – 218.

STEVENS, J. C., VANDERLENDE, D. D., 2005, *Isotatic Propylene Copolymers, Their Preparation and Use*. US Patent 6,960,635.

STEWART, W. E., LEVIEN, K. L., MORARI, M., 1985, "Simulation of Fractionation by Orthogonal Collocation", *Chem. Engng. Sci.*, v. 40, pp. 409 – 421.

SUGAWARA, M., 1994, *Branching Structure and Performances of Metallocene-Based Copolymers*. Proceedings of the 4th International Business Forum on Specialty Polyolefins, Houston, Texas, USA, 37.

SUN, T., BRANT, P., CHANCE, R. R., GRAESSLEY, W. W., 2001, "Effect of Short Chain Branching on the Coil Dimensions of Polyolefins in Dilute Solution" *Macromolecules*, v. 34, pp. 6812 – 6820.

SWALLOWE, G. M., 1999, *Mechanical Properties and Testing of Polymers, An A-Z Reference*, Springer.

SWOGGER, K. W., KAO, C. I., 1993, Process Technology for Unique Polymer Design Using Dow Constrained Geometry Catalyst. In "*Polyolefins VIII*", Technical Paper, Reg. Tech. Conf. – Soc. Plast. Eng., pp. 13 – 20.

TAU, L. M., CHUM, P. S., KARANDE, S., BOSNYAK, C., 2005, *Blends and sealant compositions comprising isotactic propylene copolymers*. US Patent 6,919,407.

TEYMOUR, F., CAMPBELL, J. D., 1994, "Analysis of the Dynamics in Gelation in Polymerization Reactors Using the "Numerical Fractionation" Technique", *Macromolecules*, v. 27, pp. 2460 – 2469.

THOMPSON, D. E., MCAULEY, K. B., MCLELLAN, P. L., 2009, "Parameter Estimation in a Simplified MWD Model for HDPE Produced by a Ziegler-Natta Catalyst", *Macromol. React. Eng.*, v. 3, pp. 160 – 177.

TONGTUMMACHAT, T., ANANTAWARASKUL, S., SOARES, J. B. P., 2016, "Understanding the Formation of Linear Olefin Block Copolymers with Dynamic Monte Carlo Simulation", *Macromol. React. Eng.*, DOI: 10.1002/mren.201600002.

TOREKI, R., 2015, Organometallic Hypertextbook, available at: http://www.ilpi.com/organomet/alkene.html, visited: October 24th, 2016.

TRIEBE, K., SAUNDERS, G., MEISS NER, R., 2006, "Characterization of Branched Polyolefins by High Temperature GPC Utilizing Function Specific Detectors Branching in Polyolefins", *Macromol. Symp.*, v. 236, pp. 228–234.

UEYAMA, N., ARAKI, T., TANI, H., 1974, "Behaviour of the $R_2AlOAlR_2$ Catalyst in the Polymerization of Propylene Oxide", *Macromolecules*, v. 7, pp. 153 – 160.

UOZUMI, T., TIAN, G., AHN, C. H., JIN, H., TSUBAKI, S., SANO, T., SOGA, K., 2000, "Synthesis of Functionalized Alternating Olefin Copolymer and Modification to Graft Copolymer by Hydrosilylation", *J. Polm. Sci. Part A.*, v. 38, pp. 1844 – 1847.

VILLADSEN, J., MICHELSEN, L. M., 1978, *Solution of Differential Equation Models by Polynomial approximation*, Prentice-Hall, Englewood Cliffs, NJ, USA.

WANG, S., TAIT, P. J., MARSDEN, C. E., 1991, "Phillips-Type Polymerization Catalysts: Kinetic Behaviour and Active Centre Determination", *J. Mol. Catal.*, v. 65, pp. 237–252.

WANG, W-J., YAN, D., ZHU, S., HAMIELEC, A., 1998, "Kinetics of Long Chain Branching in Continuous Solution Polymerization of Ethylene Using Constrained Geometry Metallocene", *Macromolecules*, v. 31, pp. 8677 – 8683.

WANG, W. -J., ZHU, S., 2000, "Structural Analysis of Ethylene/Propylene Copolymers Synthesized with a Constrained Geometry Catalyst", *Macromolecules*, v. 33, pp. 1157 – 1162.

WANG, W. -J., ZHU, S., PARK, S.-J., 2000, "Long Chain Branching in Ethylene/Propylene Solution Polymerization Using Constrained Geometry Catalyst", *Macromolecules*, v. 33, pp. 5770 – 5776.

WANG, W-J., KHARCHENKO, S., MIGLER, K., ZHU, S., 2004, "Triple-detector GPC Characterization and Processing Behavior of Long-Chain-Branched Polyethylene Prepared by Solution Polymerization with Constrained Geometry Catalyst", *Polymer*, v. 45, pp. 6495 – 6505.

WANG, W-J., YE, Z., FAN, H., LI, B.-G., K., ZHU, S., 2004, "Dynamic Mechanical and Rheological Properties of Metallocene-Catalyzed Long-Chain-Branched Ethylene/Propylene Copolymers", *Polymer*, v. 45, pp. 5497 – 5504.

WANG, L., YU, H.-J., MA, Z.-L., JIANG, S., FENG, L.-F., GU, X.-P., 2006, "Preparation of Novel MgCl2-Adduct Supported Spherical Ziegler-Natta Catalyst for a-Olefin Polymerization", *J. Appl. Polym. Sci.*, v. 99, pp. 945–948.

WECKHUYSEN, B. M., SCHOONHEYDT, R. A., 1999, "Olefin Polymerization Over Supported Chromium Oxide Catalysts", *Catal. Today*, v. 51, pp. 215–221.

WILKINSON, G., ROSENBLUM, M., WHITING, M. C., WOODWARD, R. B., 1952, "The Structure of Iron Bis-Cyclopentadienyl", *J. Am. Chem. Soc.*, v. 74, pp. 2125 – 2126.

WONG, K. T., LUUS, R., 1980, "Model Reduction of High–Order Multistage Systems by the Method of Orthogonal Collocation", *Can. J. Chem. Engng.*, v. 58, pp. 382 – 388.

WOO, T. K., MARGL, P. M., ZIEGLER, T., BLOECHL, P. E., 1997, "Static and ab Initio Molecular Dynamics Study of the Titanium (IV)-Constrained Geometry Catalyst $(CpSiH_2NH)Ti-R^+$. 2. Chain Termination and Long Chain Branching", *Organometallics*, v. 16, pp. 3454 – 3468.

XU, G., RUCKENSTEIN, 1998, "Ethylene Copolymerization with 1-Octene Using a 2-Methylbenz[e]indenyl-Based ansa-Monocyclopentadienylamido Complex and Methylaluminoxanes Catalyst", *Macromolecules*, v. 31, pp. 4724 – 4729.

YANG, Q., JENSEN, M. D., McDANIEL, M. P., 2010, "Alternative View of Long Chain Branch Formation by Metallocene Catalysts", *Macromolecules*, v. 43, pp. 8836 – 8852.

YAO, K. Z., SHAW, B. M., KOU, B., MCAULEY, K. B., BACON, D., 2003, "Modeling Ethylene/ Butene Copolymerization with Multi-site Catalysts: Parameter Estimability and Experimental Design", *Polym. React. Eng.*, v. 11, pp. 563 – 588.

YIANNOULAKIS, H., YIAGOPOULOS, A., PLADIS, P., KIPARISSIDES, C., 2000, "Comprehensive Dynamic Model for the Calculation of the Molecular Weight and Long Chain Branching Distributions in Metallocene-Catalyzed Ethylene Polymerization Reactors", *Macromolecules*, v. 33, pp. 2757 – 2766.

YOSHINO, K., UEDA, A., DEMURA, T., KURAHASHI, K., MATSUDA, Y., 2003, "Property of Syndiotactic Polypropylene and Its Application to Insulation of Electric Power Cable – Property, Manufacturing and Characteristics", *Proceedings of the 7th International Conference of Properties and Applications of Dielectric Materials*, pp. 175 – 178.

YOUNG, M.-J., MA, C.-C. M., 2002, "Polymerization Kinetics and Modeling of Solution PE Process with Metallocene Catalysts", *J. Polym. Eng.*, v. 22, pp. 75 – 93.

ZHANG, J., FAN, H., LI, B. G., ZHU, Sh., 2008, "Modeling and Kinetics of Tandem Polymerization of Ethylene Catalyzed by Bis(2-dodecylsulfanyl-ethyl)amine-CrCl$_3$ and Et(Ind)$_2$ZrCl$_2$", *Chem. Eng. Sci.*, v. 63, pp. 2057 – 2065.

ZHENGHONG, L., ZHIKAI, C., YAOTANG, S., 2006, "Monte Carlo Simulation of Propylene Polymerization (I) Effects of Impurity on Propylene Polymerization", *Chinese J. Chem. Eng.*, v. 14, pp. 194 – 199.

ZIMM, B. H., STOCKMAYER, W. H., 1949, "The Dimensions of Chain Molecules Branches and Rings", *J. Chem. Phys.*, v. 17, pp. 1301 – 1314.
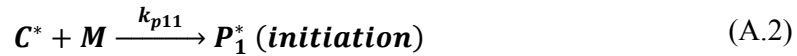
Appendix A

Supplementary Material for Chapter 3

A.1. Summary

Herein, the supplementary material is presented for Chapter 3 that describes the deterministic methods employed in the present PhD thesis.

A.2. Polymerization Example

A simple polymerization mechanism was proposed to make the comprehension of the deterministic methods easier. The mechanism can be written as:

$$C \xrightarrow{k_a} C^* \; (\boldsymbol{activation}) \tag{A.1}$$

$$C^* + M \xrightarrow{k_{p11}} P_1^* \; (\boldsymbol{initiation}) \tag{A.2}$$

$$P_i^* + M \xrightarrow{k_{p11}} P_{i+1}^* \;\; (\boldsymbol{propagation}) \tag{A.3}$$

A.2.1. Material Balances

The material balances for all species present in the polymerization system are presented in the following equations.

$$C = C(0) \cdot \exp(-k_a \cdot t) \tag{A.4}$$

$$C^* = C(0) \cdot (1 - \exp(-k_a \cdot t)) \tag{A.5}$$

$$\frac{dM}{dt} = 0 \tag{A.6}$$

$$\frac{dP_1^*}{dt} = k_{p11} \cdot \frac{M}{V} \cdot V \left(\frac{C^*}{V} - \frac{P_1^*}{V} \right) \tag{A.7}$$

$$\frac{dP_i^*}{dt} = k_{p11} \cdot \frac{M}{V} \cdot V \cdot \left(\frac{P_{i-1}^*}{V} - \frac{P_i^*}{V} \right) \tag{A.8}$$

Based on the moments definition, as described in Section 3.2, one can derive the moments equations for the living chains:

$$\frac{dP_1^*}{dt} + \sum_{i=2}^{\infty} i^k \cdot \left(\frac{dP_i^*}{dt}\right) = \sum_{i=1}^{\infty} \frac{d(i^k \cdot P_i^*)}{dt}$$
$$= k_{p11} \frac{M}{V}\left[\frac{C^*}{V} - \sum_{i=1}^{\infty} \frac{i^k P_i^*}{V} + \sum_{i=2}^{\infty} \frac{i^k P_{i-1}^*}{V}\right] V \tag{A.9}$$

The last term on the right-hand size of Equation (A.9) must be changed in order for the summation to start at 1, instead of chain size 2. This can be done by expanding the summation term according with:

$$\sum_{i=2}^{\infty} \frac{i^k P_{i-1}^*}{V} = \frac{2^k P_1^*}{V} + \frac{3^k P_2^*}{V} + \frac{4^k P_3^*}{V} + \cdots + \frac{n^k P_{n-1}^*}{V} + \cdots = \sum_{i=1}^{\infty} \frac{(i+1)^k P_i^*}{V} \tag{A.10}$$

Thus, Equation (A.9) can be rewritten as:

$$\sum_{i=1}^{\infty} \frac{d(i^k \cdot P_i^*)}{dt} = \frac{\mu_k}{dt} = k_{p11} \frac{M}{V}\left[\frac{C^*}{V} - \sum_{i=1}^{\infty} \frac{i^k P_i^*}{V} + \sum_{i=1}^{\infty} \frac{(i+1)^k P_i^*}{V}\right] V \tag{A.11}$$

From Equation (A.11) all moment expressions can be determined.

A.3. Roots Calculation Procedure in the Orthogonal Collocation Method

The N collocation points are calculated with help of the following iterative numerical procedure, as illustrated in Figure A.1. The quadrature weights were calculated as shown in Figure A.2.
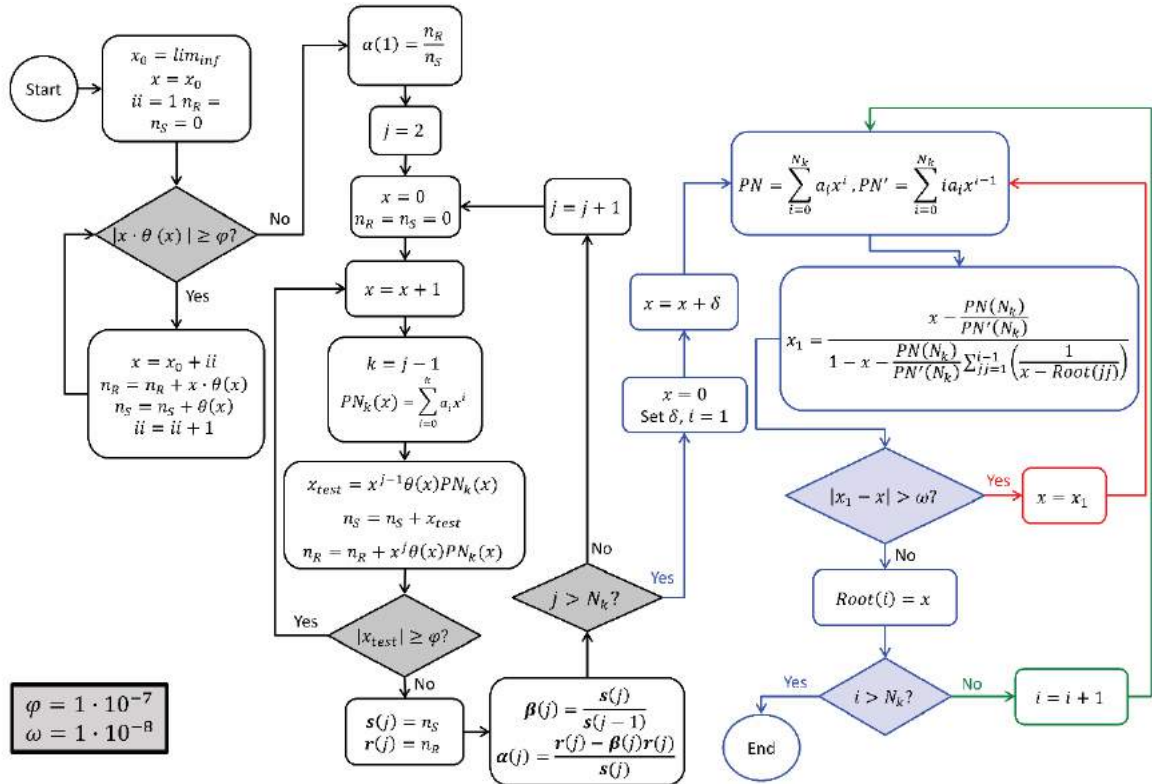
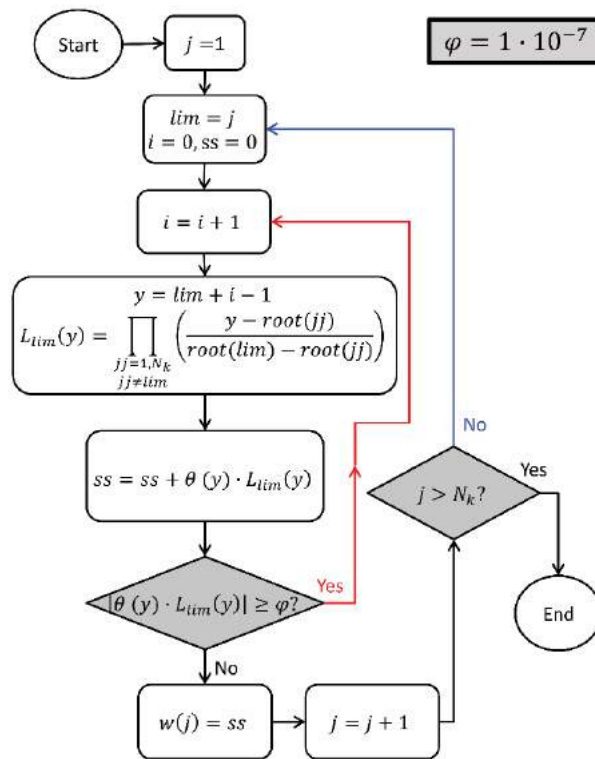**Figure A.1 - Flowchart of the iterative procedure used to calculate the collocation points.**

Figure A.2 - Flowchart of the iterative procedure used to calculate the quadrature weights.

240

Appendix B

Supplementary Material for Chapter 5

B.1 Summary

The present section describes the supplementary material of Chapter 5 dedicated to describe the experimental methodology employed in the present work.

B.2 Detailed Experimental Apparatus

All experimental apparatuses used to perform the experiments are listed below:

o 20 mL glass sampling cylinders

- Employed to store reagent solutions prepared in the glovebox.

o Molecular sieves

- Used to absorb moisture present in some reagents.

o CuO/Al_2O_3 packed beds

- Employed to collect dissolved oxygen and water in ethylene and nitrogen gases.

o Metal Cannulas

- Used to transfer the reagents into the reactor.

o Rubber septum

- Used to seal the cylinder which contained the clean toluene.

o Rubber hoses

o PVC tubings

o 1 L Beakers

- Used to collect the reactor content.

o Aluminum foil

- Used to cover the 1-L beaker where the reactor contents were dumped into after being blow out from the reactor. The aluminum foil avoided the solution contents to spill out of the beaker after hitting its base.

o Magnetic stir plates and spinbar magnetic stir bars

- Used to keep the reactor contents in ethanol overnight in a beaker under constant stirring.

o Plastic funnels and filter papers

- Used to separate the polymer material from toluene and ethanol.
  o Weighing scale
    - Used to measure the obtained polymer weight.

B.3 Control System

As mentioned in Chapter 5, the temperature of the reactor was controlled by two independent proportional-integral derivative controllers as illustrated in Figure B.1. The reactor pressure was adjusted by an in-line pressure regulator installed in the ethylene feed line.
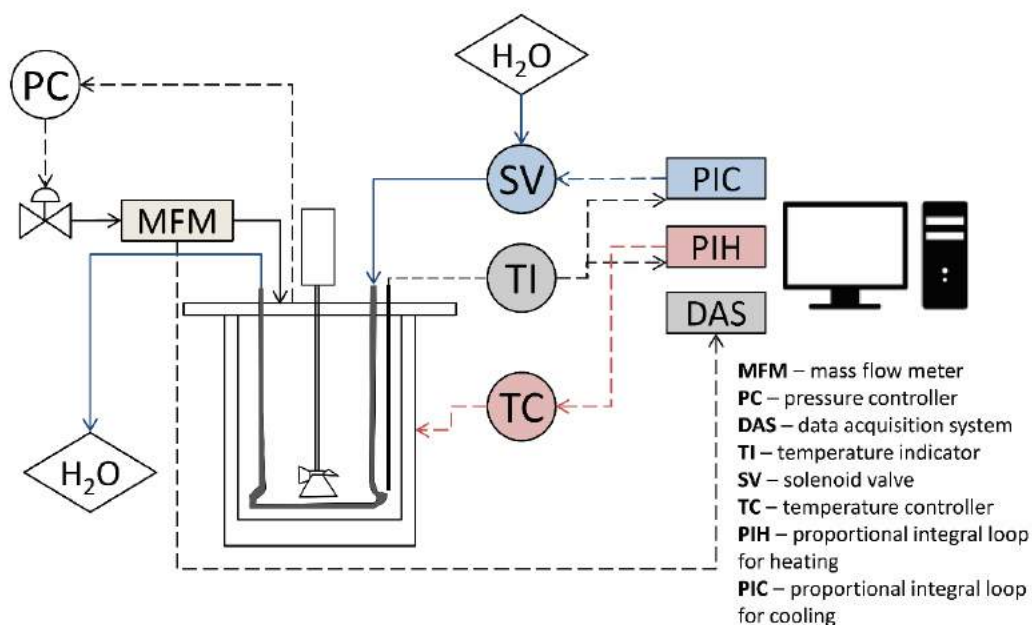

MFM – mass flow meter
PC – pressure controller
DAS – data acquisition system
TI – temperature indicator
SV – solenoid valve
TC – temperature controller
PIH – proportional integral loop for heating
PIC – proportional integral loop for cooling

Figure B.1 – Control system illustration.

Appendix C

Derivation of the Objective Function

After performing NE experiments, each one with NY output variables, one will obtain the vector of output variables $\boldsymbol{y^e}$, containing $NE \cdot NY$ elements. Admitting that the errors ε_k of variables y_k^e follow the normal distribution, then, the probability density distribution for ε_k becomes:

$$\wp(\varepsilon_k) = \frac{1}{\sqrt{2 \cdot \pi \cdot \sigma_{y_k}^2}} \cdot \exp\left(-\frac{1}{2} \cdot \frac{\varepsilon_k^2}{\sigma_{y_k}^2}\right) \tag{C.1}$$

Admitting that experiments are independent[9], the probability density of the whole set of measured errors $\boldsymbol{\varepsilon} = \{\varepsilon_1, \varepsilon_2, \dots\}$ can be written as:

$$\wp(\boldsymbol{\varepsilon}) = \prod_{k=1}^{NE \cdot NY} \frac{1}{\sqrt{2 \cdot \pi \cdot \sigma_{y_k}^2}} \cdot \exp\left(-\frac{1}{2} \cdot \frac{\varepsilon_k^2}{\sigma_{y_k}^2}\right) \tag{C.2}$$

where $\sigma_{y_k}^2$ is the variance of y_k^e. Admitting that the model is perfect, with the true value given by the model $y_k^m(\boldsymbol{\theta}, \boldsymbol{x_k})$, where $\boldsymbol{\theta}$ is the set of model parameters and $\boldsymbol{x_k}$ are the inlet variables for the experimental point k, then the error can be written as:

$$\varepsilon_k = y_k^e - y_k^m \tag{C.3}$$

With all the previous assumptions, the probability density $\wp(\boldsymbol{\varepsilon})$ can be rearranged as:

---

[9] The probability density of independent events is the multiplication of the individual probabilities

$$\wp(\boldsymbol{\varepsilon}) = \frac{1}{\sqrt{(2 \cdot \pi)^{NE \cdot NY} \cdot \prod_{k=1}^{NE \cdot NY} \sigma_{y_k}^2}} \cdot \exp\left(-\frac{1}{2} \cdot \sum_{k=1}^{NE \cdot NY} \frac{\left(y_k^e - y_k^m(\boldsymbol{\theta}, \boldsymbol{x}_k)\right)^2}{\sigma_{y_k}^2}\right) \qquad \text{(C.4)}$$

Finally, if the experiment is well done, which means that the experimental data y_k^e were obtained with minimum unavoidable difference in respect to the true value y_k^m, $\wp(\boldsymbol{\varepsilon})$ must be the point of maximum for that set of experiments. However, since one do not know the true value y_k^m, as the model parameters are unknown, one can estimate the parameters by maximizing $\wp(\boldsymbol{\varepsilon})$:

$$\boldsymbol{\theta}^{est} = \arg\max_{\boldsymbol{\theta}} \wp(\boldsymbol{\varepsilon}) = \arg\min_{\boldsymbol{\theta}} \sum_{k=1}^{NE \cdot NY} \frac{\left(y_k^e - y_k^m(\boldsymbol{\theta}, \boldsymbol{x}_k)\right)^2}{\sigma_{y_k}^2} \qquad \text{(C.5)}$$

This defines the objective function as the weighted least-squares function (BARD, 1974), which is:

$$F_{obj} = \sum_{i=1}^{NE} \sum_{j=1}^{NY} \frac{\left[y_{ij}^e - y_{ij}^m(\boldsymbol{x}_i^e, \boldsymbol{\theta})\right]^2}{\sigma_{y_{ij}}^2} \qquad \text{(C.6)}$$

One must note that the $\sum_{k=1}^{NE \cdot NY}(\cdot)$ can be replaced by the sum in experiments and output variables of each experiment, i.e., $\sum_{k=1}^{NE \cdot NY}(\cdot) = \sum_{i=1}^{NE} \sum_{j=1}^{NY}(\cdot)$ (for example, y_{ij}^e represents the output j from experiment i).

Appendix D

Derivation of the Moments Equation

D.1 Summary

In the present Appendix, the moments equations used to describe the copolymerization of ethylene and 1,9-decadiene with CGC in semi-batch reactor are derived.

D.2 Balance Equations

As already presented in Chapter 7, the balance equations for the living and dead chains can be written as:

For living polymer chains with size one P_1^*

$$\frac{dP_1^*}{dt} = k_{p11}\left(\frac{C^*}{V}\right)\left(\frac{M}{V}\right)V - k_{p11}\left(\frac{P_1^*}{V}\right)\left(\frac{M}{V}\right)V - k_{dP}\left(\frac{P_1^*}{V}\right)\sum_{i=1}^{\infty}\left(\frac{P_i^*}{V}\right)V$$

$$- k_t\left(\frac{P_1^*}{V}\right)V - k_b\varphi\left(\frac{P_1^*}{V}\right)\sum_{j=1}^{\infty}j\left(\frac{L_j^=}{V}\right)V - k_{p12}\left(\frac{P_1^*}{V}\right)\left(\frac{D}{V}\right)V \tag{D.1}$$

For living polymer chainswith size greater than one $P_i^*, i \in (2,\infty)$

$$\frac{dP_i^*}{dt} = -k_{p11}\left(\frac{P_i^*}{V}\right)\left(\frac{M}{V}\right)V + k_{p11}\left(\frac{P_{i-1}^*}{V}\right)\left(\frac{M}{V}\right)V + k_{p12}\left(\frac{P_{i-1}^*}{V}\right)\left(\frac{D}{V}\right)V$$

$$- k_{dP}\left(\frac{P_i^*}{V}\right)\sum_{j=1}^{\infty}\left(\frac{P_j^*}{V}\right)V - k_t\left(\frac{P_i^*}{V}\right)V - k_{p12}\left(\frac{P_i^*}{V}\right)\left(\frac{D}{V}\right)V \tag{D.2}$$

$$- k_b\varphi\left(\frac{P_i^*}{V}\right)\sum_{j=1}^{\infty}j\left(\frac{L_j^=}{V}\right)V + k_b\varphi\sum_{j=1}^{i-1}j\left(\frac{P_{i-j}^*}{V}\right)\left(\frac{L_j^=}{V}\right)V$$

For dead polymer chains $LL_i, i \in (1,\infty)$

$$\frac{dLL_i}{dt} = k_t\left(\frac{P_i^*}{V}\right)V + k_{dP}\left(\frac{P_i^*}{V}\right)\sum_{j=1}^{\infty}\left(\frac{P_j^*}{V}\right)V - k_b\varphi i\left(\frac{L_i^=}{V}\right)\sum_{j=1}^{\infty}\left(\frac{P_j^*}{V}\right)V \tag{D.3}$$

Applying the moments definition, as:

Living chain moments: $\mu_k = \sum_{i=1}^{\infty} i^k P_i^*$

Dead chains moments: $\lambda_k = \sum_{i=1}^{\infty} i^k LL_i$

the balance equations for living chains (Equations (D.1) and (D.2)) can be represented in terms of the living moments, according with the following procedure:

$$\frac{dP_1^*}{dt} + \frac{d\sum_{i=2}^{\infty} i^k P_i^*}{dt} = \frac{d\mu_k}{dt}$$

$$
\begin{aligned}
\frac{d\mu_k}{dt} = & \; k_{p11}\left(\frac{C^*}{V}\right)\left(\frac{M}{V}\right)V - k_{p11}\sum_{i=1}^{\infty} i^k \left(\frac{P_i^*}{V}\right)\left(\frac{M}{V}\right)V \\
& - k_{dP}\sum_{i=1}^{\infty} i^k \left(\frac{P_i^*}{V}\right)\sum_{i=1}^{\infty}\left(\frac{P_i^*}{V}\right)V - k_t \sum_{i=1}^{\infty} i^k \left(\frac{P_i^*}{V}\right)V \\
& - k_b\varphi \sum_{i=1}^{\infty} i^k \left(\frac{P_i^*}{V}\right)\sum_{j=1}^{\infty} j\left(\frac{L_j^=}{V}\right)V - k_{p12}\sum_{i=1}^{\infty} i^k \left(\frac{P_i^*}{V}\right)\left(\frac{D}{V}\right)V \\
& + k_{p11}\sum_{i=2}^{\infty} i^k \left(\frac{P_{i-1}^*}{V}\right)\left(\frac{M}{V}\right)V + k_{p12}\sum_{i=2}^{\infty} i^k \left(\frac{P_{i-1}^*}{V}\right)\left(\frac{D}{V}\right)V \\
& + k_b\varphi \sum_{i=2}^{\infty}\sum_{j=1}^{i-1} i^k j \left(\frac{P_{i-j}^*}{V}\right)\left(\frac{L_j^=}{V}\right)V
\end{aligned}
\tag{D.4}
$$

Using the moments definition presented previously, Equation (D.4) can be simplified to:

$$
\begin{aligned}
\frac{d\mu_k}{dt} = & \; k_{p11}\left(\frac{C^*}{V}\right)\left(\frac{M}{V}\right)V - k_{p11}\left(\frac{\mu_k}{V}\right)\left(\frac{M}{V}\right)V - k_{dP}\left(\frac{\mu_k}{V}\right)\left(\frac{\mu_0}{V}\right)V - k_t\left(\frac{\mu_k}{V}\right)V \\
& - k_b\varphi\left(\frac{\mu_k}{V}\right)\left(\frac{\lambda_1}{V}\right)V - k_{p12}\left(\frac{\mu_k}{V}\right)\left(\frac{D}{V}\right)V \\
& + k_{p11}\sum_{i=2}^{\infty} i^k \left(\frac{P_{i-1}^*}{V}\right)\left(\frac{M}{V}\right)V + k_{p12}\sum_{i=2}^{\infty} i^k \left(\frac{P_{i-1}^*}{V}\right)\left(\frac{D}{V}\right)V \\
& + k_b\varphi \sum_{i=2}^{\infty}\sum_{j=1}^{i-1} i^k j \left(\frac{P_{i-j}^*}{V}\right)\left(\frac{L_j^=}{V}\right)V
\end{aligned}
\tag{D.5}
$$

The three last terms on the right-hand side of Equation (D.5) can be modified as:

$$
k_{p11}\sum_{i=2}^{\infty} i^k \left(\frac{P_{i-1}^*}{V}\right)\left(\frac{M}{V}\right)V = k_{p11}\sum_{i=1}^{\infty}(i+1)^k \left(\frac{P_i^*}{V}\right)\left(\frac{M}{V}\right)V
\tag{D.6}
$$

$$k_{p12} \sum_{i=2}^{\infty} i^k \left(\frac{P_{i-1}^*}{V}\right)\left(\frac{D}{V}\right) V = k_{p12} \sum_{i=1}^{\infty} (i+1)^k \left(\frac{P_i^*}{V}\right)\left(\frac{D}{V}\right) V \tag{D.7}$$

$$k_{b1}\varphi \sum_{i=2}^{\infty} \sum_{j=1}^{i-1} i^k j \left(\frac{P_{i-j}^*}{V}\right)\left(\frac{L_j^=}{V}\right) V = k_{b1}\varphi \sum_{i=i}^{\infty} \sum_{j=1}^{\infty} (i+j)^k j \left(\frac{P_i^*}{V}\right)\left(\frac{L_j^=}{V}\right) V \tag{D.8}$$

Finally, the general living moments balance equation can be obtained:

$$\begin{aligned}
\frac{d\mu_k}{dt} = {} & k_{p11} \left(\frac{C^*}{V}\right)\left(\frac{M}{V}\right) V - k_{p11}\left(\frac{\mu_k}{V}\right)\left(\frac{M}{V}\right) V - k_{dP}\left(\frac{\mu_k}{V}\right)\left(\frac{\mu_0}{V}\right) V - k_t \left(\frac{\mu_k}{V}\right) V \\
& - k_b\varphi \left(\frac{\mu_k}{V}\right)\left(\frac{\lambda_1}{V}\right) V - k_{p12}\left(\frac{\mu_k}{V}\right)\left(\frac{D}{V}\right) V \\
& + k_{p11} \sum_{i=1}^{\infty} (i+1)^k \left(\frac{P_i^*}{V}\right)\left(\frac{M}{V}\right) V + k_{p12} \sum_{i=1}^{\infty} (i+1)^k \left(\frac{P_i^*}{V}\right)\left(\frac{D}{V}\right) V \\
& + k_{b1}\varphi \sum_{i=i}^{\infty} \sum_{j=1}^{\infty} (i+j)^k j \left(\frac{P_i^*}{V}\right)\left(\frac{L_j^=}{V}\right) V
\end{aligned} \tag{D.9}$$

From Equation (D.9), the zeroth, first and second living moments balance equations can be derived, as shown in Chapter 7 (Equations (7.21) to (7.23)).

Now, if the same methodology is applied for the dead polymer chains,

$$\frac{d \sum_{i=1}^{\infty} i^k LL_i}{dt} = \frac{d\lambda_k}{dt}$$

one can derive the general dead moments balance equation:

$$\frac{d\lambda_k}{dt} = k_t \left(\frac{\mu_k}{V}\right) V + k_{dP}\left(\frac{\mu_k}{V}\right)\left(\frac{\mu_0}{V}\right) V - k_b\varphi \sum_{i=1}^{\infty} i^{k+1}\left(\frac{L_i^=}{V}\right)\left(\frac{\mu_0}{V}\right) \tag{D.10}$$

From Equation (D.10), one can derive the zeroth, first and second dead moments balance equations, as shown in Chapter 7 (Equations (7.24) to (7.26)).

Appendix E

Convergence Analyses of Adaptive Orthogonal Collocation Method

E.1 Summary

Convergence analyses of the complete adaptive orthogonal collocation method dis carried out for all experimental conditions discussed previously. For the majority of the cases, the method converged using only 4 orthogonal collocation points. The evolution of the collocation points for living and dead polymer chains are also presented.

It is important to comment that many previous simulations were carried out, although only the results that can be used to explain more clearly the features of the procedure adopted in the present work are shown in this section.

E.2 Experimental Condition G5 (0.3 g of 1,9-decadiene, 0.271 μmol L^{-1} of CGC and 10 minutes of reaction)

Figure E.1 illustrates the MWD obtained when the same integration step size was applied (δ = 0.6 s) and 3, 4 and 5 collocation points were used. It is possible to observe that the method converged for 4 and 5 collocation points, whereas with 3 collocation points, the MWD simulated presents a very narrow PI that cannot characterize the analyzed copolymer. Figure E.2 shows the collocation points for living and dead polymer chains calculated during the polymerization reaction time.

In Figures E.2.a and E.2.d, the last collocation point converged for relatively low values, when compared with values obtained when 4 and 5 collocation points were considered. Perhaps this explains why 3 collocation points lead to narrow MWD, since longer lengths cannot be described.
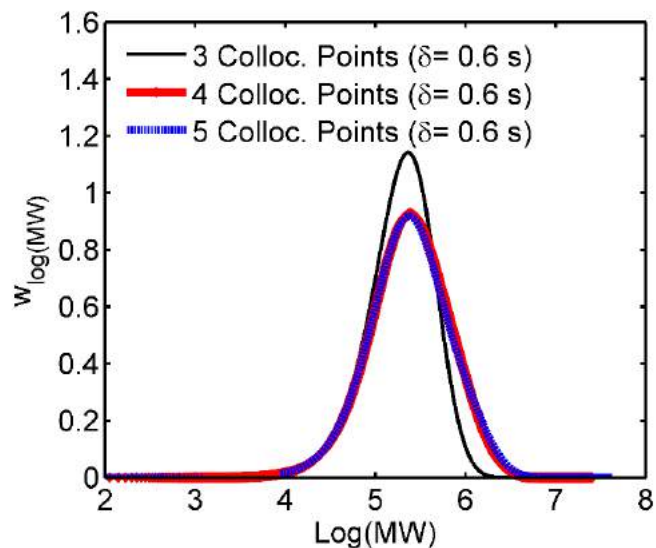
Figure E. 1 – MWD obtained with the complete adaptive orthogonal collocation method using 3, 4 and 5 collocation points (experimental condition G5).

(a)   (b)   (c)
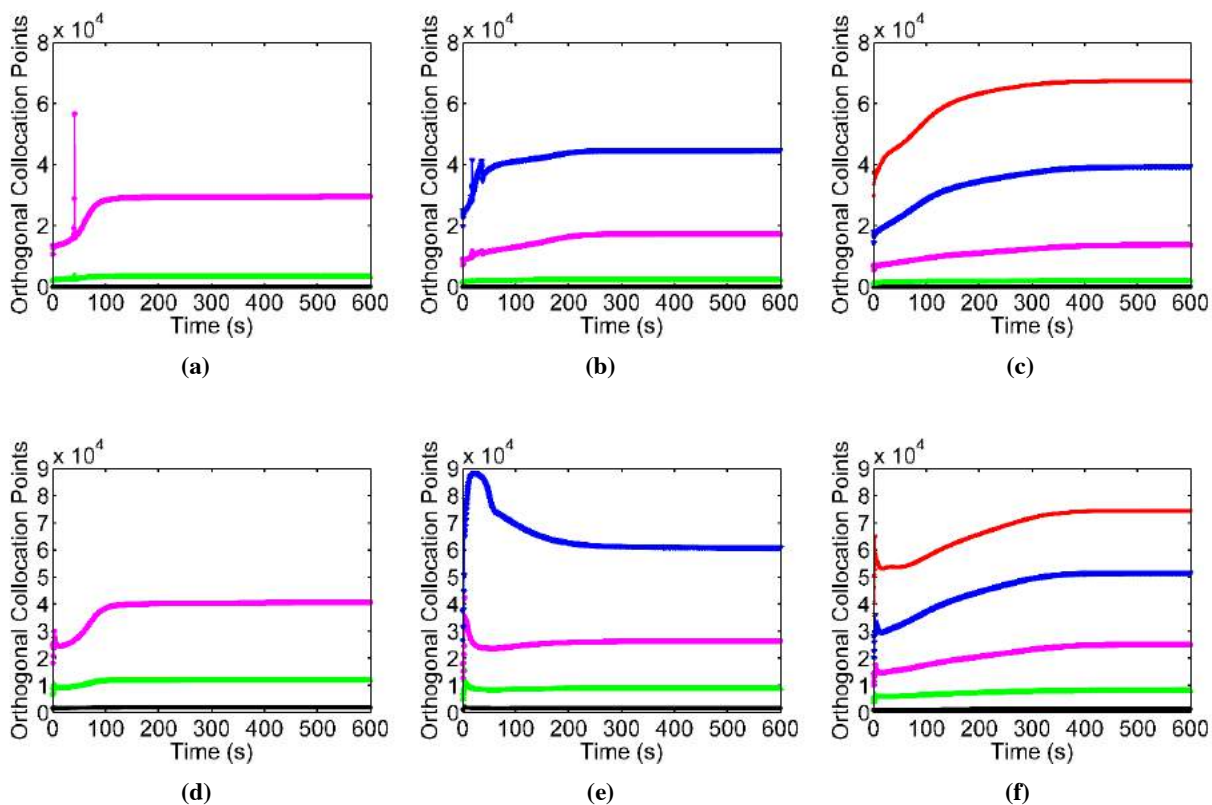
(d)   (e)   (f)

Figure E. 2 – Evolution of the collocation points during time for the living polymers using (a) 3, (b) 4 and (c) 5 collocation points and for the dead polymers considering (d) 3, (e) 4 and (f) 5 collocation points and 0.6 s as integration steps.

249

E.3 Experimental Condition I1 (0.4 g of 1,9-decadiene, 0.368 μmol L^{-1} of CGC and 6 minutes of reaction)

Figure E.3 illustrates the MWD obtained when the different integration step sizes were applied and four collocation points were used.
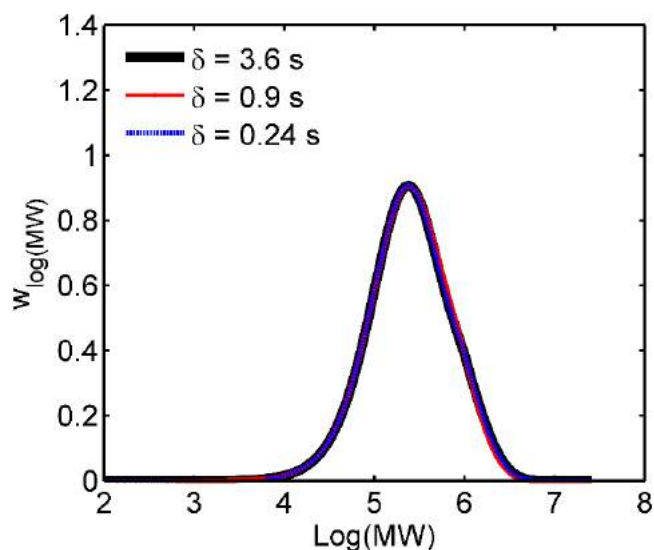
Figure E. 3 – MWD obtained with the complete adaptive orthogonal collocation method using 4 orthogonal collocation points and different integration step sizes (experimental condition I1).

As one can see in Figure E.3, the method converged for 4 orthogonal collocation points and variation of the integration step size leads to equivalent numerical results. Figure E.4 shows the dynamic collocation point profiles for this case study.

It is possible to analyze in Figure E.4 that the evolution of the orthogonal collocation points for the living polymer chains was similar for the three studied cases (Figure E.4.a to E.4.c). On the other hand, when an integration step size of 0.24 s was used, the method struggled to calculate the proper values for the collocation points during the first 50 s of reaction. Then, it succeeded in reaching final collocation points that allow the method to converge, producing MWDs that were equivalent to the ones predicted when step sizes of 0.9 and 3.6 s were applied. Applying five collocation points and an integration step of 0.24 s, the method did not converge, producing a bimodal distribution as one can see in Figure E.5. Figure E.6 illustrates the collocation points calculated during the simulation when 5 collocation points were employed.
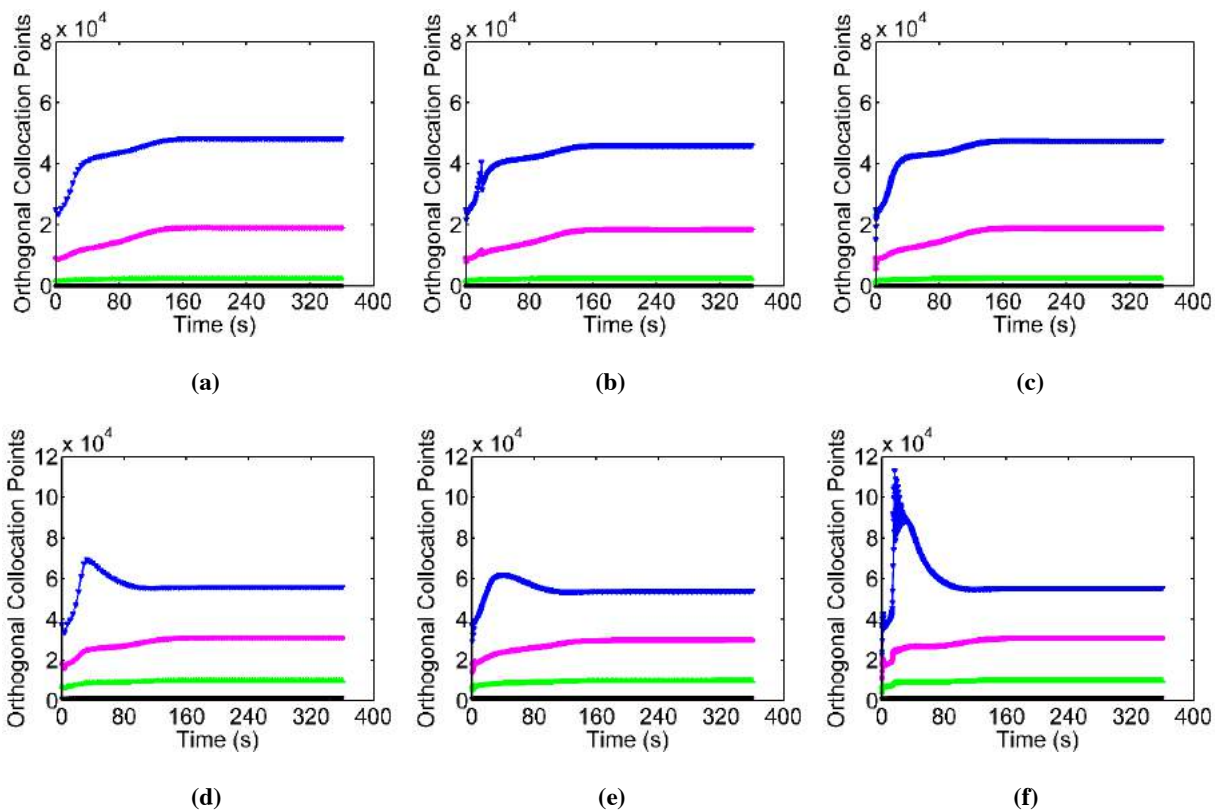
Figure E. 4 – Evolution of the collocation points during time for the living polymers using (a) 3.6, (b) 0.9 and (c) 0.24 s of integration step sizes and for the dead polymers considering (d) 3.6, (e) 0.9 and (f) 0.24 s of integration step sizes and 4 collocation points.
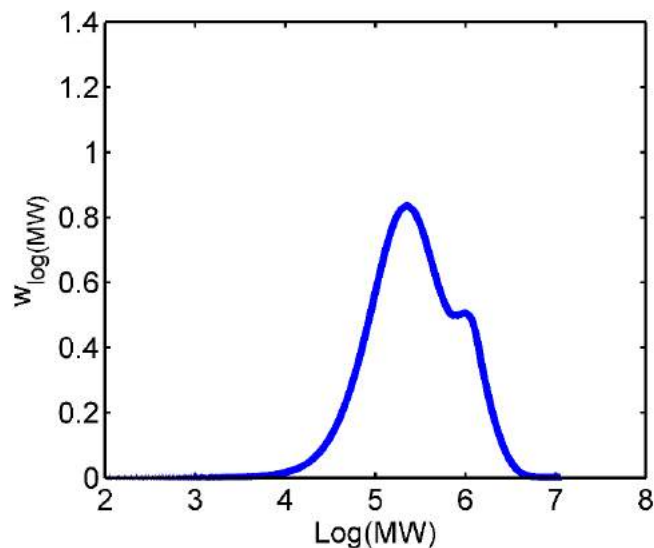

Figure E. 5 – MWD obtained with the complete adaptive orthogonal collocation method using 5 orthogonal collocation points and 0.24 s of integration step size (experimental condition I1).
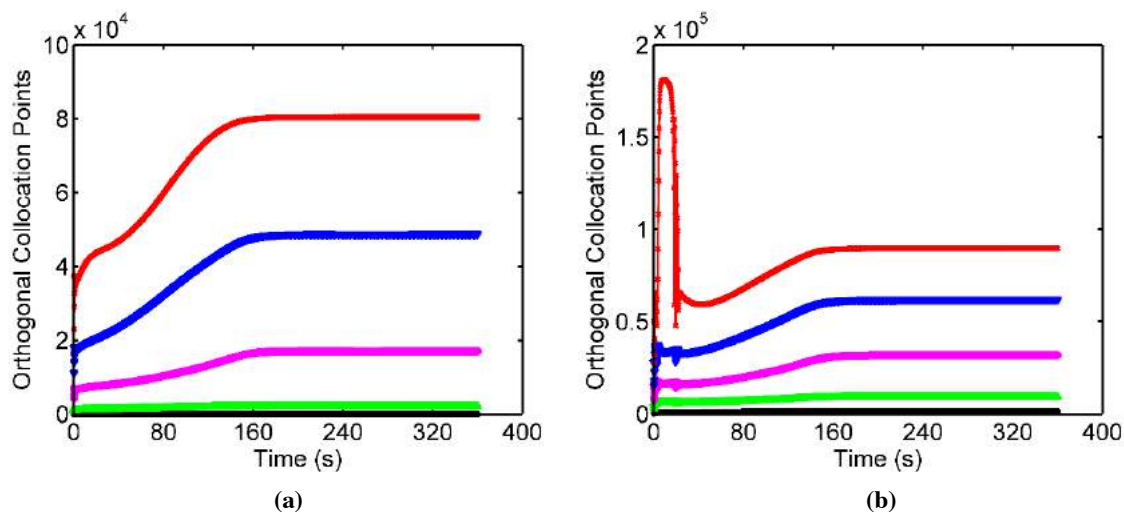
Figure E. 6 – Evolution of the collocation points during time for the (a) living and (b) dead polymers using 0.24 s as integration step sizes and 5 collocation points.

The CAOC calculated collocation points for the dead chains, during the first 50 s, that were very high and these values probably affected all the calculations performed afterwards, since the process is adaptive and the current data depends on the data calculated in the last iteration. Consequently, the MWD produced presented bimodality, which do not agree with the MWDs provided when 4 collocation points were applied and also with the experimental distribution of condition I1. This type of numerical instability can be the result of bad initialization of the weighing function or bad numerical performance of the routine used for calculation of the collocation points.

E.4 Experimental Condition I2 (0.4 g of 1,9-decadiene, 0.174 μmol L^{-1} of CGC and 6 minutes of reaction)

Figure E.7 illustrates the MWD obtained when 4 and 5 collocation points were employed. For 4 points, the method successfully converged even when the integration step size was modified. However, for 5 collocation points, the distribution diverged from the MWD obtained when 4 collocation points were used. Figure E.8 illustrates the calculated collocation points during the simulation for different integration step sizes and total of collocation points used.

Observing Figure E.8.c and Figure E.8.f it seems that the last collocation point did not converge, but it continued to grow until the simulation was interrupted. Maybe this explains why when 5 collocation points and an integration step size of 0.24 s were applied the method did not converge to the right MWD.
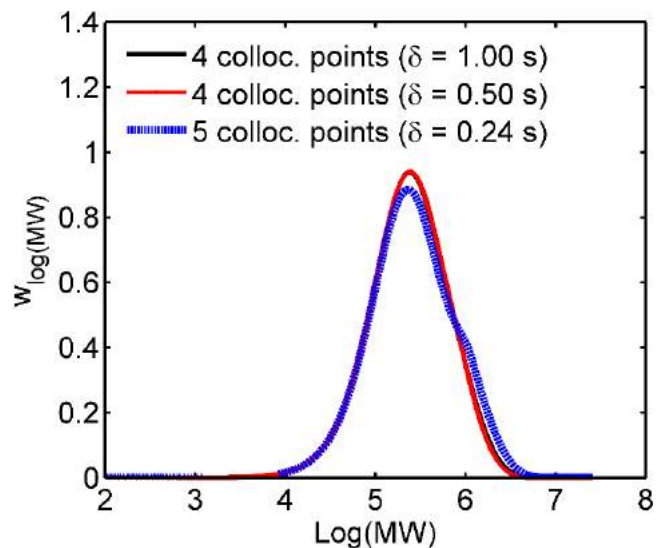
Figure E.7 – MWD obtained with the complete adaptive orthogonal collocation method using 4 and 5 orthogonal collocation points and different integration step sizes for experimental condition I2.
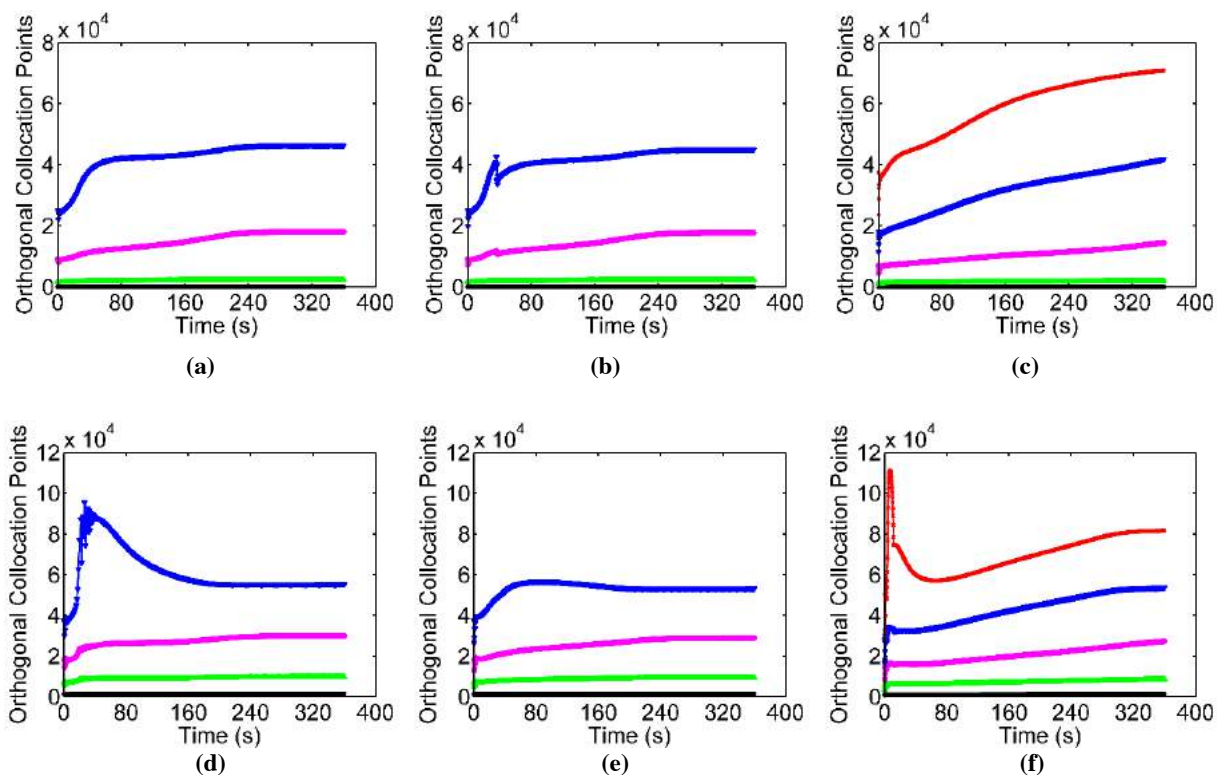

Figure E.8 – Evolution of the collocation points during time for the living polymers using (a) 1.0 and (b) 0.5 s of integration step sizes and 4 collocation points and (c) 0.24 s of integration step sizes and 5 collocation points and for the dead polymers considering (d) 1.0 and (e) 0.5 s of integration step sizes and 4 collocation points and (f) 0.24 s of integration step sizes and 5 collocation points.

E.5 Experimental Condition D1 (0.1 g of 1,9-decadiene, 0.325 μmol L^{-1} of CGC and 10 minutes of reaction)

For this experimental condition, simulations were carried out using 4, 5 and 6 collocation points. The method converged when 5 and 6 collocation points were applied. For 4 points, the calculated MWD presented larger PI than the PI of the MWDs predicted with additional orthogonal collocation points. Figure E.9 shows this result and Figure E.10 illustrates the evolution of the orthogonal collocation points during reaction time for the living and dead polymer chains.
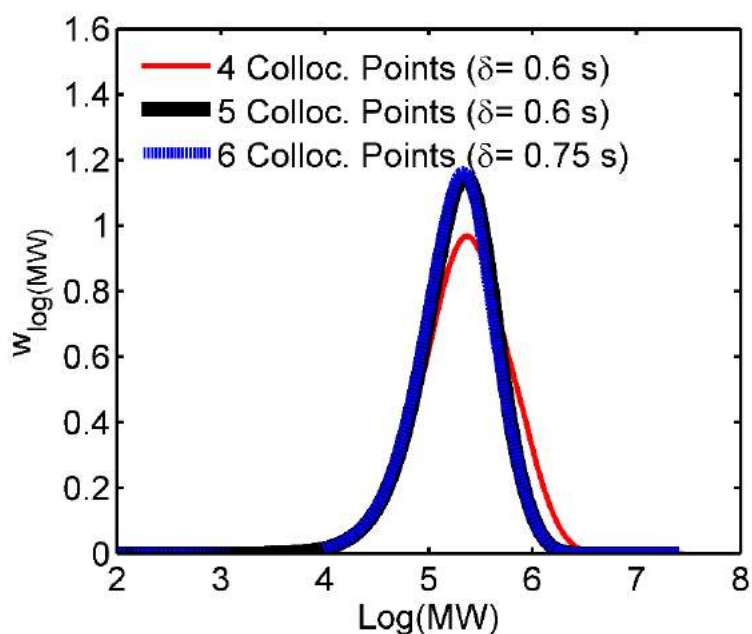

Figure E. 9 – MWD obtained with the complete adaptive orthogonal collocation method using 4, 5 and 6 orthogonal collocation points and 0.6 s and 0.75 s as integration step sizes for experimental condition D1.
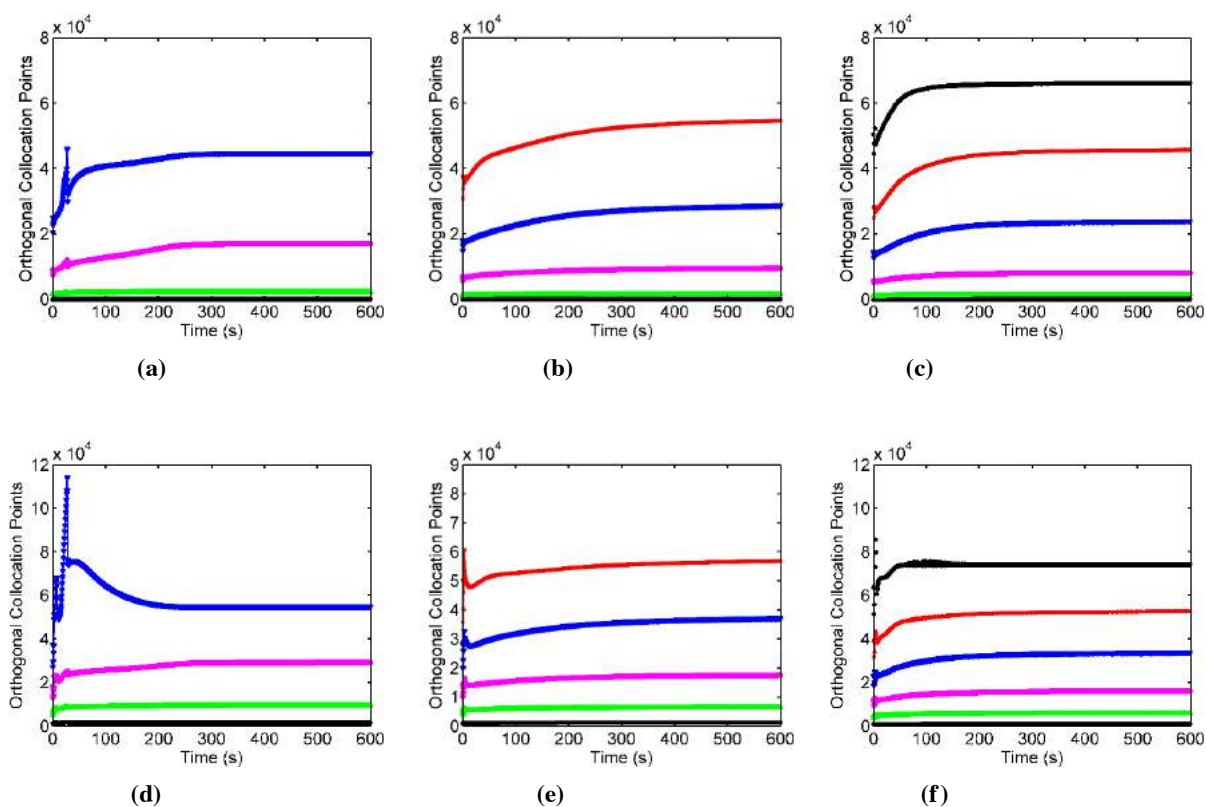
Figure E. 10 – Evolution of the collocation points during time for the living polymers using (a) 4, (b) 5 and (c) 6 collocation points and for dead polymers using (d) 4, (e) 5 and (f) 6 collocation points (experimental condition: D1).

E.6 Experimental Condition E1 (0.2 g of 1,9-decadiene, 0.325 μmol L^{-1} of CGC and 10 minutes of reaction)

The MWDs obtained when four and five collocation points with integration step sizes of 0.3 and 0.6 s were used are shown in Figure E.11. The collocation point values for the living and dead polymer chains calculated during the simulations for these cases are presented in Figure E.12.

The CAOC method converged for 4 collocation points using an integration step size of 0.3 s and for 5 collocation points using 0.6 s as the integration step. When 0.3 s was applied as the integration step, the obtained distribution presented bimodality, indicating the poor numerical performance during the integration. Figure E.12.c shows that the last collocation point ended the simulation with a value that was much bigger than the one obtained when the same number of collocation points was applied and 0.6 s was used as the integration step size, as one can see in Figure E.12.b. This clearly indicates that the collocation points must be bounded by some sort of maximum limit.
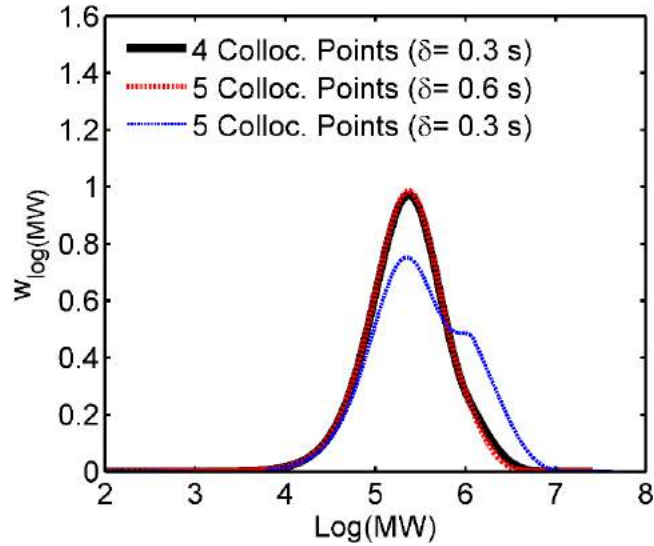
255

Figure E. 11 – MWD obtained with the complete adaptive orthogonal collocation method using 4 and 5 orthogonal collocation points and different integration step sizes (experimental condition E1).
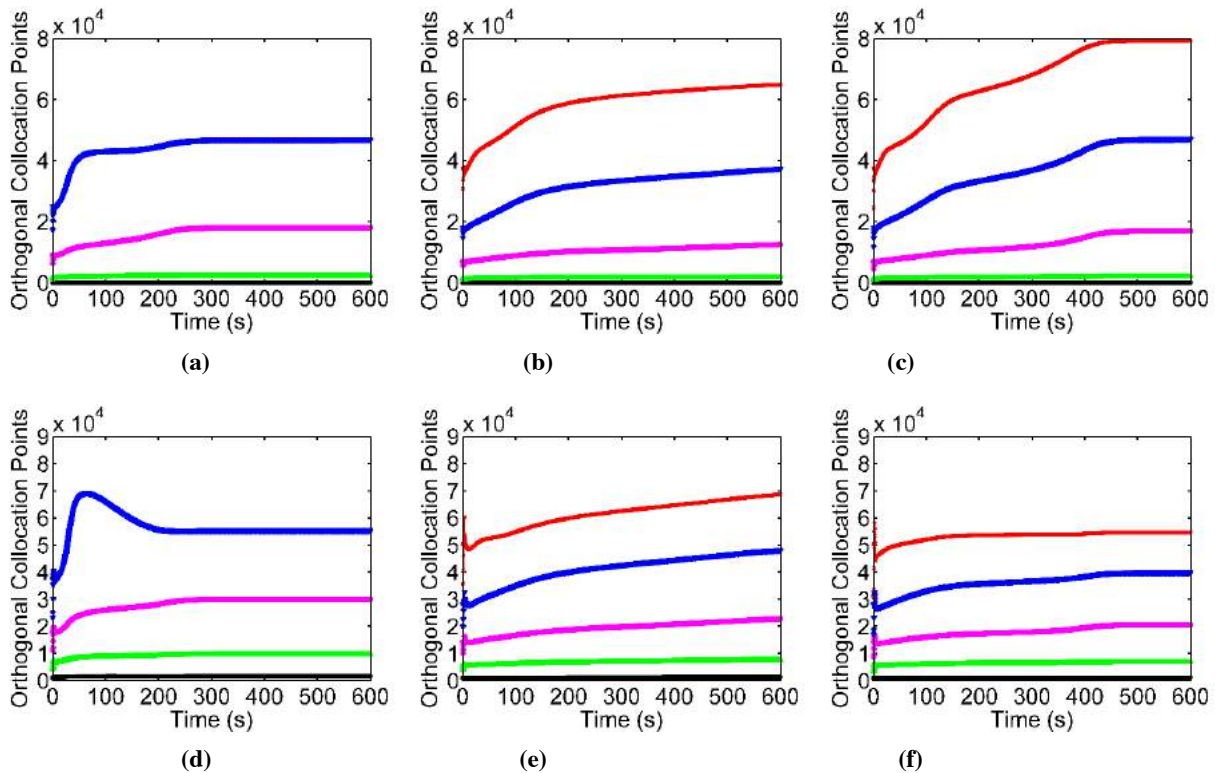

Figure E. 12 – Evolution of the collocation points during time for the living polymers using (a) 0.3 s of integration step size and 4 collocation points and (b) 0.6 and (c) 0.3 s of integration step sizes and 5 collocation points and for the dead polymers using (d) 0.3 s of integration step size and 4 collocation points and (e) 0.6 and (f) 0.3 s of integration step sizes and 5 collocation points.

E.7 Experimental Condition F1 (0.3 g of 1,9-decadiene, 0.325 μmol L^{-1} of CGC and 10 minutes of reaction)

The MWDs predicted by the CAOC method applying 4 and 5 collocation points are illustrated in Figure E.13. The method converged for 4 collocation points, as the distribution obtained with 5 points matches with the distribution produced with four points using the same integration step size. Figure E.14 illustrates the evolution of the collocation point values during polymerization time for living and dead polymers.
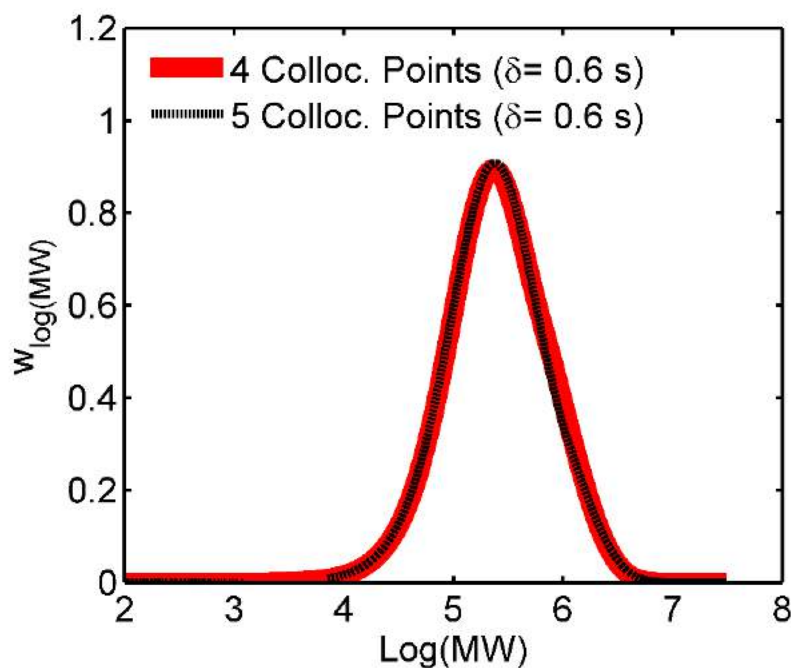

Figure E. 13 – MWD obtained with the complete adaptive orthogonal collocation method using 4 and 5 orthogonal collocation points and 0.6 s as integration step sizes (experimental condition F1).
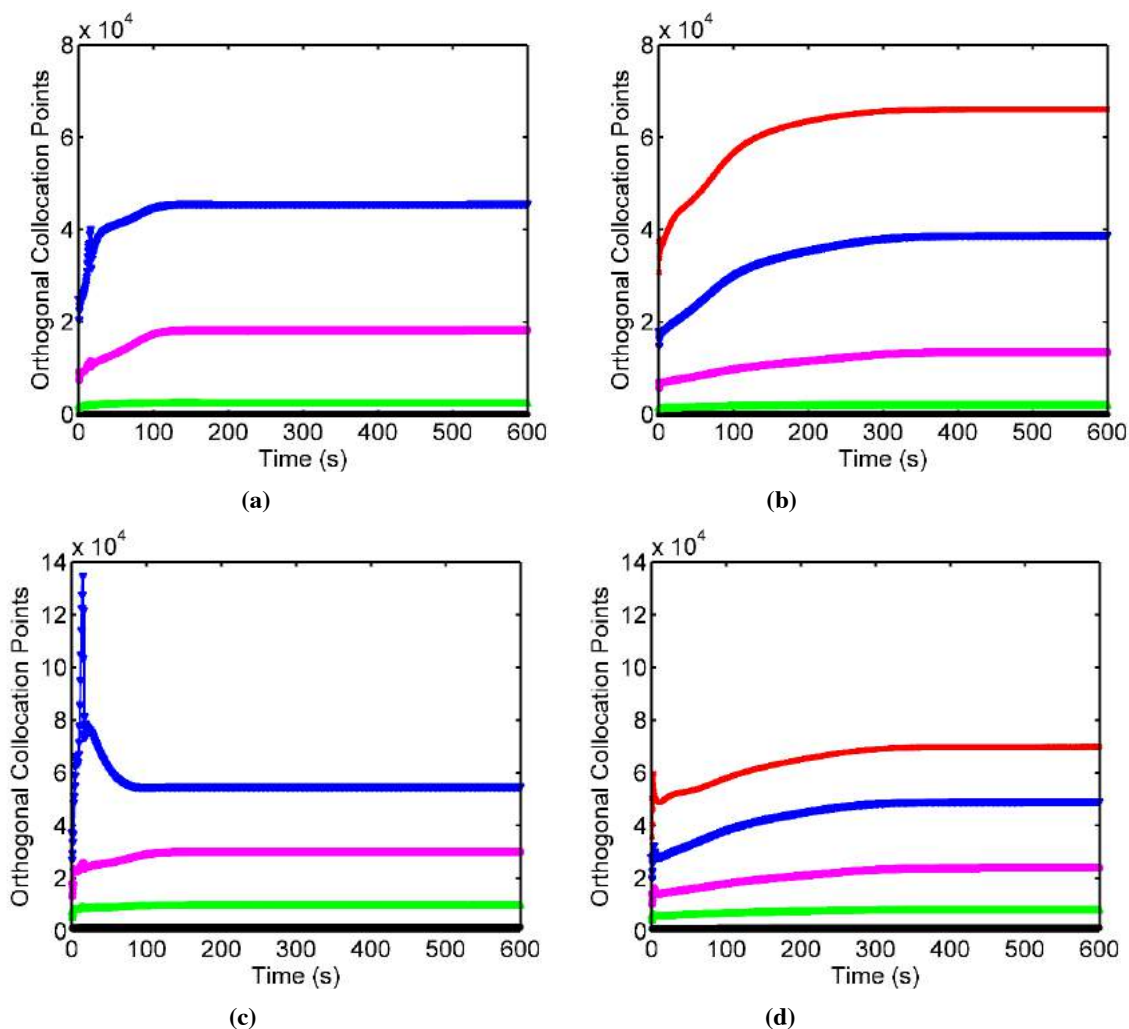
Figure E. 14 – Evolution of the collocation points during time for the living chains using (a) 4 and (b) 5 collocation points and for the dead polymers using (c) 4 and (d) 5 points and 0.6 s as the integration step sizes (experimental condition: F1).

As one can see in Figure E.14.c, the method almost exploded the values for the dead collocation points in the first 10 s of simulation, but it succeeded in decreasing those values afterwards, achieving convergence for the dead collocation points approximately after 80 s of polymerization time. When five collocation points were applied, for the living and dead collocation points (Figures E.14.b and E.14.d), it took longer times to achieve convergence for these points than the time required to read convergence when four collocation points were used.

These results show that some aspects related to calculation of the collocation points (the roots of the orthogonal polynomial) must be improved. It is not clear whether the source of numerical difficulties is related to the weighing function, the variable domain, numerical precision of the root finding procedure or a combination of

these factors. This must be investigated in the near future in order to enhance the robustness of the technique.